VOLUME 104 NUMBER 3

THE ASTROPHYSICAL JOURNAL

AN INTERNATIONAL REVIEW OF SPECTROSCOPY AND ASTRONOMICAL PHYSICS

Founded in 1895 by GEORGE E. HALE *and* JAMES E. KEELER

Edited by

OTTO STRUVE
Managing Editor

S. CHANDRASEKHAR
Associate Managing Editor

Yerkes Observatory of the University of Chicago

PAUL W. MERRILL
Mount Wilson Observatory of the Carnegie Institution of Washington

HARLOW SHAPLEY
Harvard College Observatory
Cambridge, Massachusetts

N. U. MAYALL
Lick Observatory
University of California

NOVEMBER 1946

THE UNIVERSITY OF CHICAGO PRESS
CHICAGO, ILLINOIS, U.S.A.

November 1946 Vol. 104, No. 3

THE ASTROPHYSICAL JOURNAL

AN INTERNATIONAL REVIEW OF SPECTROSCOPY AND ASTRONOMICAL PHYSICS

The Astrophysical Journal is published bimonthly by the University of Chicago at the University of Chicago Press, 5750 Ellis Avenue, Chicago, Illinois, during July, September, November, January, March, and May. ¶The subscription price is $10.00 a year; the price of single copies is $2.00. Orders for service of less than a full year will be charged at the single-copy rate. ¶Postage is prepaid by the publishers on all orders from the United States and its possessions, Argentina, Bolivia, Brazil, Chile, Colombia, Costa Rica, Cuba, Dominican Republic, Ecuador, Guatemala, Haiti, Republic of Honduras, Mexico, Morocco (Spanish Zone), Nicaragua, Panama, Paraguay, Peru, Rio de Oro, El Salvador, Spain (including Balearic Islands, Canary Islands, and the Spanish Offices in Northern Africa; Andorra), Spanish Guinea, Uruguay, and Venezuela. ¶Postage is charged extra as follows: for Canada and Newfoundland, 42 cents on annual subscriptions (total $10.42); on single copies, 7 cents (total $2.07); for all other countries in the Postal Union, 96 cents on annual subscriptions (total $10.96), on single copies 16 cents (total $2.16). ¶Patrons are requested to make all remittances payable to The University of Chicago Press, in United States currency or its equivalent by postal or express money orders or bank drafts.

The following are authorized agents:

For the British Empire, except North America, India, and Australasia: The Cambridge University Press, Bentley House, 200 Euston Road, London, N.W. 1, England. Prices of yearly subscriptions and of single copies may be had on application.

Claims for missing numbers should be made within the month following the regular month of publication. The publishers expect to supply missing numbers free only when losses have been sustained in transit, and when the reserve stock will permit.

Business correspondence should be addressed to The University of Chicago Press, Chicago 37, Illinois.

Communications for the editors and manuscripts should be addressed to: Otto Struve, Editor of THE ASTROPHYSICAL JOURNAL, Yerkes Observatory, Williams Bay, Wisconsin.

Line drawings and photographs should be made by the author, and all marginal notes such as co-ordinates, wave lengths, etc., should be included in the cuts. It will not be possible to set up such material in type.

One copy of the corrected galley proof should be returned as soon as possible to the editor, Yerkes Observatory, Williams Bay, Wisconsin. Authors should take notice that the manuscript will not be sent to them with the proof.

The cable address is "Observatory, Williamsbay, Wisconsin."

The articles in this journal are indexed in the *International Index to Periodicals*, New York, N.Y.

Applications for permission to quote from this journal should be addressed to The University of Chicago Press, and will be freely granted.

Entered as second-class matter, July 31, 1940, at the Post-Office at Chicago, Ill., under the act of March 3, 1879.
Acceptance for mailing at special rate of postage provided for in United States Postal Act of October 3, 1917, Section 1103, amended February 28, 1925.

[PRINTED IN U.S.A.]

THE ASTROPHYSICAL JOURNAL

AN INTERNATIONAL REVIEW OF SPECTROSCOPY AND ASTRONOMICAL PHYSICS

VOLUME 104 NOVEMBER 1946 NUMBER 3

ON THE DYNAMICAL STABILITY OF STARS

P. LEDOUX*

Yerkes Observatory

Received July 12, 1946

ABSTRACT

It is well known that if the ratio of specific heats, Γ, in a star is a constant and smaller than $\frac{4}{3}$, the star is dynamically unstable. In this paper the case in which Γ is variable in the star is discussed in some detail, especially for the homogeneous and standard models. It is shown that if Γ becomes smaller than $\frac{4}{3}$ in a part of the star, that part has to be very extensive to render the star unstable. For example, if $\Gamma = \frac{5}{3}$ in the central part of a star and is as small as 1 in the outer part, this has to extend to a depth at which the temperature is of the order of half the central temperature. Peculiar forms of $\Gamma(r)$ could increase the instability considerably, but it is doubtful whether any of these could be of physical importance.

1. *General considerations.*—It has been known for a long time[1] that a star with a constant ratio of specific heats, Γ, smaller than $\frac{4}{3}$ is dynamically unstable. If Γ is variable, this should apply to a certain mean value of Γ.[2] This becomes clearer if we consider a formula such as the one given by the author in a recent paper.[3] For a small radial adiabatic deformation, such that

$$\frac{\delta r}{r_0} = \xi\,(r_0)\; e^{i\sigma t},$$

σ^2 is given by

$$\sigma^2 = -\frac{\int_0^R (3\Gamma - 4)\,\xi\, d\Omega_0 + 3\int_0^R \frac{P_0}{\rho_0}\,\xi\, r_0\,\frac{d\Gamma}{d r_0}\, dm}{\int_0^R \xi\, dI_0}, \qquad (1)$$

* Fellow of the Belgian-American Educational Foundation, at the Yerkes Observatory.

[1] Ritter, *Anwendungen des mechanisches Wärmetheorie auf kosmologische Probleme*, 1879. The result derived there concerns a homogeneous star. For a more general result see, e.g., S. Rosseland, *Pub. Oslo U. Obs.*, No. 1, p. 20; or S. Chandrasekhar, *An Introduction to the Study of Stellar Structure*, 1939, p. 52, and references given there.

[2] Cf. L. Biermann and T. G. Cowling, *Zs. f. Ap.*, **19**, 1, 1939 (first part of the paper, where a formula of type [1], except for the term in $d\Gamma/dr_0$, is used).

[3] P. Ledoux, *Ap. J.*, **102**, 56, 1945.

where the suffix zero refers to equilibrium values. Furthermore,

$$\Omega_0 = -\int_0^R \frac{Gm\,(r)\,dm}{r_0} = -3\int_0^R P_0 dV_0 \qquad \text{and} \qquad I_0 = \int_0^R r_0^2 dm$$

represent, respectively, the gravitational potential energy and the moment of inertia with respect to the origin, and ξ is the solution of the differential equation

$$\frac{d^2\xi}{dr_0^2} + \left[\frac{4-\mu}{r_0} + \frac{1}{\Gamma}\frac{d\Gamma}{dr_0}\right]\frac{d\xi}{dr_0} + \left[\frac{\sigma^2\rho_0}{\Gamma P_0} - \frac{\mu}{r_0^2}\left(3-\frac{4}{\Gamma}\right) + \frac{3}{\Gamma r_0}\frac{d\Gamma}{dr_0}\right]\xi = 0\,, \qquad (2)$$

satisfying the boundary conditions

$$\xi r_0 = 0 \qquad \text{at} \qquad r_0 = 0 \qquad (3)$$

and

$$\delta P = -\Gamma P_0\left[3\xi + r_0\frac{d\xi}{dr_0}\right] = 0 \qquad \text{at} \qquad r_0 = R\,. \qquad (4)$$

In equation (2), $\mu = Gm(r)\rho_0/r_0P_0$, and Γ is the general adiabatic exponent defined by $dQ = dU - Pd\rho/\rho^2 = 0$, where the variation of the internal energy dU is expressed in terms of P and ρ. In a star, Γ is, in general, a function of the ratio of the pressure of radiation to the total pressure $(1-\beta)$, of the degree of ionization, and of the number of degrees of freedom of the particles.[4]

Equation (2) reduces to Eddington's equation for small radial pulsations if Γ is constant. Formula (1) can also be written as

$$\sigma^2 = \frac{9\int_0^R \xi\Gamma P_0 dV_0 + 4\int_0^R \xi\, d\Omega_0 + 3\int_0^R \Gamma P_0 r_0 \frac{d\xi}{dr_0}\, dV_0}{\int_0^R \xi\, dI_0}\,, \qquad (5)$$

if we integrate the last term of the numerator by parts.

If σ^2, as given by equation (1) or equation (5), is positive, a small radial oscillation will result, which will be damped out or not according to the condition of vibrational stability.[5] But if σ^2 is negative, the star will be violently unstable, as the small disturbance considered will grow exponentially with the time.

Cases have been considered in which, because of a very small abundance of hydrogen and helium, Γ becomes smaller than $\frac{4}{3}$ in an appreciable part of the star.[6] The stability of these models has been investigated[2] by a general method, using the minimal property of the total available energy of the star in case of stability. However, the rigorous application of such a condition is rather difficult, and it seems worth while to re-examine the problem from the point of view of the sign of σ^2.

If Γ is a constant and if ξ is the amplitude of the fundamental mode, then it readily follows from equation (1) that the star is unstable for this mode if Γ is smaller than $\frac{4}{3}$.

The case of the harmonics, however, is not so simple. If Γ_c^n denotes the critical value of Γ for the harmonic of order n, then, on the basis of the general theory of equations of type (2), we can expect that Γ_c^n will be smaller, the higher the order n of the harmonic considered. We shall see that this is true in the examples which have so far been discussed in some detail. Thus, in general, we may expect that if Γ is a constant for the whole

[4] R. H. Fowler and E. A. Guggenheim, *M.N.*, **85**, 961, 1925.

[5] Cf., e.g., T. G. Cowling, *M.N.*, **94**, 768, 1934; **96**, 42, 1935; **98**, 528, 1938; and P. Ledoux, *Ap. J.*, **94**, 537, 1941.

[6] L. Biermann, *Zs. f. Ap.*, **18**, table on 356, 1939; also n. 2.

star, it is through the fundamental mode that the stability of the star will first be endangered when we go along a series of models with decreasing Γ.

Considering, next, the general case of variable Γ, we shall first re-write equation (2) in the form

$$\frac{d}{dr_0}\left(p\,\frac{d\xi}{dr_0}\right) - q\xi + \sigma^2 r_0^4 \rho_0 \xi = 0\,, \tag{2'}$$

where

$$p = \Gamma P_0 r_0^4 \qquad \text{and} \qquad q = \left[\,(3\Gamma - 4)\,Gm\,(r)\,r_0\rho_0 - 3\,r_0^3 P_0\,\frac{d\Gamma}{dr_0}\right].$$

Now let Γ_m be the minimum value of Γ along r. Denoting by a suffix m the values corresponding to Γ_m, we have $p_m \leqslant p$ and, if $d\Gamma/dr_0$ is everywhere negative or zero, $q_m \leqslant q$. Hence $\sigma_n^2 \geqslant (\sigma_n^2)_m$.

If $d\Gamma/dr_0$ is positive in some regions of the star, we cannot say anything rigorous about the relative values of q and q_m. But, in general, the second term in q is small compared to the first one, and we can expect that in most cases the preceding inequalities will hold. Thus if Γ_m is greater than Γ_c^n, the star will be stable toward the harmonics of order n or greater, and the fundamental mode remains the most dangerous one for the stability of the star. Since $\Gamma_c^0 = \frac{4}{3}$, the star will be stable if Γ is greater than $\frac{4}{3}$ all over the star.

However, there might be exceptions; for, writing equation (1) in the form

$$\sigma^2 \int_0^R \xi\, dI_0 = -\int_0^R 4\pi\xi\, r_0^3\, \frac{d}{dr_0}\left[\,(3\Gamma - 4)\,P_0\right] dr_0\,, \tag{1'}$$

let us consider again the fundamental mode. The pressure P is essentially positive and decreases from the center to the surface, where it can be taken as being zero. If $(3\Gamma - 4)$ is everywhere positive ($\Gamma > \frac{4}{3}$), the star will certainly be stable if $(3\Gamma - 4)P_0$ decreases everywhere with increasing r.

But if $(3\Gamma - 4)P_0$, for instance, remains constant, then $\sigma^2 = 0$, and the star is on the verge of instability, although Γ is greater than $\frac{4}{3}$ everywhere. Of course, this particular case implies an infinite Γ at the surface, and physically it has no meaning.

In fact, if $(3\Gamma - 4)$ is everywhere positive, we can admit for physical reasons only the range of Γ, $0 < 3\Gamma - 4 \leqslant 1$; and $(3\Gamma - 4)P_0$ will be an oscillating function in r, each oscillation corresponding to the ionization of a new shell of electrons of some fairly abundant element. If $(3\Gamma - 4)P_0$ starts at the center with its maximum value (this is likely as long as the central temperature remains high), these oscillations will be superposed on a generally decreasing curve. And if there should be n regions of increasing $(3\Gamma - 4)P_0$, there will be $(n + 1)$ regions of decreasing $(3\Gamma - 4)P_0$—and one of them just near the surface. Starting from the surface, we can associate them by pairs (decreasing, increasing), and the decreasing one will have a greater weight than the increasing one, as the corresponding r and ξ will be greater.

Therefore, on this account, the right-hand member of equation (1′) will tend to be positive; but, furthermore, we are still left with a region of decreasing $(3\Gamma - 4)P_0$ at the center. Thus it is very unlikely that this case could lead to instability.

If $(3\Gamma - 4)P_0$ starts by increasing at the center, then we shall have as many regions in which $(3\Gamma - 4)P_0$ increases as regions where it decreases. The same reasoning would apply, but in this case the argument loses some of its force, as we have no extra region of decreasing $(3\Gamma - 4)P_0$ near the center. Thus cases in which an important ionization takes place just at the center might require a more careful analysis.

However, for the time being, we shall assume that the fundamental mode is the most dangerous for the stability of the star and that it is stable if Γ is everywhere greater than $\frac{4}{3}$.

2. *Approximate formula for* σ^2.—Now we shall consider the case in which Γ becomes smaller than $\frac{4}{3}$ in some part of the star. For the fundamental mode of pulsation one usually gets quite a good approximation[3] for σ^2 by assuming ξ to be a constant in formula (5). In that case, equation (5) becomes

$$\sigma^2 = -\frac{(3\bar{\Gamma} - 4)\,\Omega_0}{I_0}, \tag{6}$$

where

$$\bar{\Gamma} = \frac{\int_0^R \Gamma P_0 dV_0}{\int_0^R P_0 dV_0}. \tag{7}$$

Thus in a first approximation the sign of σ^2 and consequently the stability or instability of the star will be determined by the value of Γ, averaged with respect to $\int_0^{r_0} P_0 dV_0$ over the whole star. As the pressure P decreases rapidly with increasing r, the external layers, where Γ is most likely to become smaller than $\frac{4}{3}$, will have to be very extensive to influence $\bar{\Gamma}$ appreciably.

3. *Applications of formula* (6).—As examples we shall consider the cases of the homogeneous and standard models, and for the sake of simplicity we shall further divide the star into two parts: a central region, where $\Gamma_i = \frac{5}{3}$, and an outer part, where $\Gamma_e = 1$, an extreme case very favorable to instability.

If r_c is the radius of the sphere separating the two regions, we know that, for $r_c = R$, σ^2 is positive and the star is stable; for $r_c = 0$, σ^2 is negative and the star is unstable. As σ^2 is an eigen-value of equation (2), which is of the Sturm-Liouville type, it will vary continuously with the coefficients of equation (2), and when r_c decreases from R to zero, σ^2 will decrease continuously, passing through the value zero and becoming negative. Thus σ^2 will have one zero in the interval $0 < r < R$, which will separate the stable from the unstable configurations.

In a first approximation we can determine the critical value r_c corresponding to $\sigma^2 = 0$ from a formula of the type (6), which in this case can be written as

$$I_0\sigma^2 = 0 = 9\Gamma_i \int_0^{r_c} P_0 dV_0 + 9\Gamma_e \int_{r_c}^R P_0 dV_0 + 4\Omega_0. \tag{8}$$

In the case of the homogeneous model,

$$\Omega_0 = -\tfrac{6}{15}\,\pi^2 G\rho^2 R^5 \quad \text{and} \quad P = \frac{2\pi G}{3}\,\rho^2 (R^2 - r^2)\,; \tag{9}$$

and our condition becomes, after introducing the numerical values of Γ_i and Γ_e,

$$\frac{2}{5}\left(\frac{r_c}{R}\right)^5 - \frac{2}{3}\left(\frac{r_c}{R}\right)^3 + \tfrac{2}{15} = 0.$$

This equation has one root in the interval $0 \leqslant r_c/R \leqslant 1$. We find

$$\frac{r_c}{R} = 0.64,$$

or, in terms of mass or temperature,

$$\frac{m_c}{M} \simeq 0.26 \quad \text{and} \quad \frac{T_c}{T_0} \simeq 0.6$$

if T_0 is the central temperature (small masses).

For the standard model $\Omega_0 = -3GM^2/2R$, and in Emden's variables the condition is

$$(3\Gamma_e - 4) + \frac{3}{2}\frac{6.8969}{(2.018)^2}(\Gamma_i - \Gamma_e)\int_0^{z_c} u^4 z^2 dz = 0. \tag{10}$$

We find that equation (10) leads to the following values:

$$z_c \simeq 1.6 \quad \text{or} \quad \frac{r_c}{R} \simeq 0.23, \quad \frac{m_c}{M} \simeq 0.35, \quad \frac{T_c}{T_0} \simeq 0.7.$$

Thus in both cases we see that, even with a Γ as small as 1 in the outer part, this must be very extensive before the stability of the star is endangered; in fact, the outer part contains appreciably more than half the mass.

However, our approximation ξ = constant, on which equation (8) is based, is rather crude. If we go back to equation (5), we see that if ξ increases with r, the mean value of Γ should, in fact, be smaller than the one defined by equation (7), and this would increase the instability of the star. But, on the other hand, the third term of the numerator would be positive and contribute to the stability.

To gain a definite idea as to the magnitude of these effects a rigorous method of treating the problem will be developed in the following section and applied to the two cases considered here.

4. *Rigorous treatment in the case of a discontinuity of* Γ.—We shall consider again a star composed of two parts, separated by a surface of discontinuity of Γ (sphere r_c), and we shall distinguish by the suffixes i and e the values relating to the internal and the external parts, respectively.

We have to solve equation (2); but in this case, apart from the boundary conditions (3) and (4), we shall have two more conditions at the surface of discontinuity of Γ: a kinematical condition which reduces to

$$A\,(\xi_i)_{r_c} = B\,(\xi_e)_{r_c} \tag{11}$$

and a dynamical condition,

$$(\delta P_i)_{r_c} = (\delta P_e)_{r_c},$$

or, explicitly,

$$A\Gamma_i\left(3\xi_i + r\frac{d\xi_i}{dr}\right)_{r_c} = B\Gamma_e\left(3\xi_e + r\frac{d\xi_e}{dr}\right)_{r_c}, \tag{12}$$

where ξ_i and ξ_e already satisfy equations (3) and (4), respectively.

The condition that the homogeneous system (11) and (12) admits solutions other than the trivial ones $A = B = 0$ is that its determinant vanish. We must have

$$\left|\begin{array}{cc} \xi_i & \xi_e \\ \Gamma_i\left(3\xi_i + r\dfrac{d\xi_i}{dr}\right) & \Gamma_e\left(3\xi_e + r\dfrac{d\xi_e}{dr}\right) \end{array}\right|_{r=r_c} = 0. \tag{13}$$

As ξ_i and ξ_e are functions of σ^2, equation (13) provides us with an equation to determine its value. However, in general, equation (2) does not admit of analytical solutions which are explicit in σ^2.

The direct procedure would then be for a given value of r_c to choose a value of σ^2, compute by numerical integration the corresponding values of ξ_i and ξ_e, and determine whether they satisfy condition (13). Repeat this until a correct value of σ^2 has been found. If it is positive, move r_c toward the center and start all over again, and so on

until a critical value of r_c, r_c', is found such that, for $r_c > r_c'$, $\sigma^2 > 0$, and, for $r_c < r_c'$, $\sigma^2 < 0$. This would be a very arduous task.

However, as we are mainly interested in the critical value of r_c, we can obtain it much more simply by putting $\sigma^2 = 0$ in equation (2) and treating r_c as a parameter, which can then be determined by equation (13). In this way only one numerical integration will be required.

a) The homogeneous model.—Writing $x = r/R$ and using relation (9), we can write equation (2) as[7]

$$\frac{d^2\xi}{dx^2} + \frac{4 - 6x^2}{x\,(1 - x^2)}\frac{d\xi}{dx} + J\xi = 0\,, \tag{14}$$

where

$$J = \frac{3\sigma^2}{2\pi G\rho\Gamma} - 2a \qquad \text{and} \qquad a = \left(3 - \frac{4}{\Gamma}\right).$$

If we suppose that $\sigma^2 = 0$, then

$$J = -2a\,. \tag{15}$$

Equation (14) has two regular singularities, one at $r = 0$ ($x = 0$) and one at $r = R$ ($x = 1$). The roots of the indicial equation at $x = 0$ are 0 and -3. The general solution would then have the form

$$\xi_i = A\lambda_i(x) + A'x^{-3}[\phi_i + \lambda_i(x)\, lg\, x]\,, \tag{16}$$

where $\lambda_i(x)$ is holomorphic and ϕ_i regular in the vicinity of $x = 0$. As the solution (16) must satisfy the boundary condition (3), we must take $A' = 0$, and we are left with

$$\xi_i = A\lambda_i(x)\,.$$

T. E. Sterne, in the paper we have already referred to, has shown that $\lambda_i(x)$ is of the form

$$\lambda_i(x) = \sum_{k=0}^{\infty} a_{2k}x^{2k}\,, \tag{17}$$

where the coefficients are determined in accordance with the relations

$$a_0 = 1 \qquad \text{and} \qquad a_{2k+2} = a_{2k}\frac{2k\,(2k+5) - J}{(2k+2)\,(2k+5)}\,. \tag{18}$$

If Γ is a constant over the whole star, then this solution should also satisfy condition (4), which is possible only if J has one of the values

$$J_k = 2k\,(2k+5)\,; \tag{19}$$

for the series (17) will then terminate with the term $a_{2k}x^{2k}$ and will represent the eigenfunction of order k; the corresponding eigen-value of σ^2 can be deduced from equation (19) and the definition of J. For any other value of J than those given by equation (19) the series does not terminate. However, it is converging for $0 \leqslant x < 1$ and diverging only at $x = 1$.

Another point brought out clearly by Sterne's analysis is that, while the fundamental mode becomes unstable for $\Gamma < \frac{4}{3}$, the higher harmonics continue to be stable. Indeed, as we may directly verify from equation (19), the first harmonic becomes unstable only if $\Gamma < \frac{3}{5}$ and the second one if $\Gamma < \frac{4}{21}$.

[7] T. E. Sterne, *M.N.*, **97**, 582, 1937.

At $r = R$, the indicial equation has the double root 0. We can again, from the boundary condition (4), show that the solution of equation (14) will be of the form $\xi_e = B\lambda_e(x)$; and, expanding $\lambda_e(x)$ as a series in powers of $(1 - x)$, we obtain from equation (14)

$$\lambda_e(x) = \sum_{k=0}^{\infty} b_k (1-x)^k , \tag{20}$$

with the following recurrence formula for the coefficients:

$$k^2 b_k = \tfrac{1}{2}[(k-1)(k+4) - J](b_{k-1} - b_{k-2}) + (k+1)[(k-1)\, b_{k-1} + b_{k-2}] . \tag{21}$$

If we take

$$J = (k-1)(k+4) \tag{22}$$

and if we admit that this value of J also satisfies the relation

$$(k-1)\, b_{k-1} + b_{k-2} = 0 , \tag{23}$$

so that $b_k = 0$, it is easy to prove that b_{k+1} and all the succeeding coefficients also vanish and the series will terminate with the term $b_{k-1}(1-x)^{k-1}$.

However, as we can readily verify with the first few terms, the relation (23) will be satisfied only if k is odd. The series will accordingly terminate with an even power of $(1 - x)$. If Γ is a constant for the whole star, our solution (20) must also satisfy equation (3), and this is possible only if the series terminates, that is, for the values of J given by equation (22) for k odd. One verifies that these J's are identical with those given by equation (19). Thus, starting from the surface, we recover the same eigen-values as those given by Sterne. This is, of course, what we should expect. For any value of J different from the ones given by equation (22), the series (20) converges for $0 < x \leqslant 1$; but it diverges at $x = 0$.

In our case the values of J are fixed by equation (15). With the values $\Gamma_i = \frac{5}{3}$, $\Gamma_e = 1$, which we have already adopted, $J_i = -1.2$ and $J_e = +2$, and the solutions ξ_i and ξ_e will not terminate. However, as our condition (13) has to be applied at a point $0 < x < 1$, we need not be concerned with the possible divergence of the series we have referred to above.

Computing the numerical values of the coefficients a_{2k} and b_k for this particular case and introducing the corresponding solutions (17) and (20) into equation (13), we obtain the following values of x_c or r_c/R:

$$(x_c)_2 = 0.575 , \qquad (x_c)_4 = 0.717 , \qquad (x_c)_6 = 0.725 , \qquad (x_c)_8 = 0.727 ,$$

which correspond, respectively, to approximations limited to terms of degree 2, 4, 6, and 8. These values converge so very rapidly that we may adopt the last value as precise enough for our purpose.

Comparing this value

$$\frac{r_c}{R} = 0.727 \quad \text{or} \quad \frac{m_c}{M} = 0.384 \quad \text{or} \quad \frac{T_c}{T_0} = 0.47$$

with those given by our first approximation, we see that the instability is somewhat greater than is disclosed by equation (6). This corresponds to the fact, illustrated in Figure 1, that ξ increases slightly from the center to the surface, $d\xi/dr$ experiencing a discontinuity when the compressibility changes.

b) The standard model.—The case of the standard model can be treated in the same way, except that we cannot obtain series converging all over the interior of the star. But, before discussing this problem, we shall first determine whether in this case also the gen-

eral proposition on the stability of the star toward its different modes is satisfied. The exact verification would require numerical integrations. However, we can avail ourselves of the method developed in a previous paper.[8] It was shown there that successive approximations for σ^2 can be obtained by solving determinants of order 2, 4, 6, etc. Because of the form given there to those determinants it is evident that in a given approximation (determinant of rank $2j$) the condition for one or more of the roots σ^2 to be zero is that the minor of rank j in the lower left corner be zero. This provides an equation in $a = (3 - 4/\Gamma)$, which enables us to find successive approximations for the critical Γ_c^n.

In this way we obtain for the first harmonic the critical value $\Gamma_c^1 = 0.891$ in a first approximation and $\Gamma_c^1 = 0.922$ in a second approximation. For the second harmonic, the first approximation gives $\Gamma_c^2 = 0.537$. Of course, this does not provide upper limits for the critical Γ_c; but, as the method converges fairly rapidly as far as the values of σ^2 are

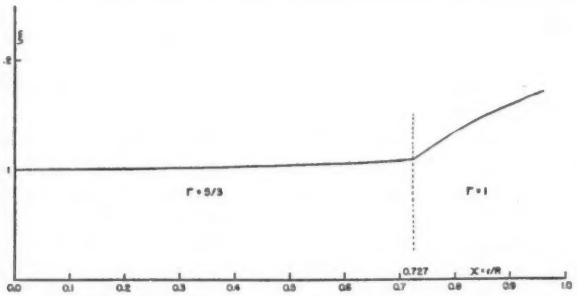

FIG. 1.—Variation of the amplitude with the radius in the homogeneous model for a discontinuity of Γ as indicated.

concerned, we can assume that the same is true of the Γ_c and that their order at least is correct: $\frac{4}{3} > \Gamma_c^1 > \Gamma_c^2$. In the case of Γ_c^1 it is even safe to assume that its real value will be smaller than 1.

Returning to equation (2), we can re-write it in terms of Emden's variables for the case $\sigma^2 = 0$ in the form

$$\frac{d^2\xi}{dz^2} + \frac{d\xi}{dz}\left[\frac{4}{z} + \frac{4}{u}\frac{du}{dz}\right] + \xi\left[\frac{4a}{z}\frac{1}{u}\frac{du}{dz}\right] = 0,$$

where a has the value $a_i = 0.6$ for $z < z_c$ and $a_e = -1$ for $z > z_c$. With the help of well-known series for u, we can obtain series for ξ_i and ξ_e in the neighborhood of $r = 0$ and $r = R$, satisfying conditions (3) and (4), respectively. With these we can start our numerical integrations, one at the center and one at the surface.

The necessary calculations are rather light, as it turns out that the solution which we have to extend furthest is ξ_e. This is the simplest, too, as ξ_e and $d\xi_e/dz$ vary very slowly in a large part of the star. The simplest way to solve equation (13) in this case seems to be to compute its value at different points and then interpolate between its positive and negative values. This shows that the critical value of z_c is of the order of 2.45.

Figure 2 represents the corresponding solution ξ, which exhibits the same peculiarities as the ones discussed in the case of the homogeneous model. However, here ξ in-

[8] P. Ledoux and C. L. Pekeris, *Ap. J.*, **94**, 124, 1941.

creases more rapidly, as should have been expected from the greater central condensation of the standard model. And, owing to this, the correct values,

$$\frac{r_c}{R}\simeq 0.36\,, \qquad \frac{m_c}{M}\simeq 0.66\,, \qquad \text{and} \qquad \frac{T_c}{T_0}\simeq 0.47\,,$$

deviate more from the first approximation than in the case of the homogeneous model.

Of course, a varying Γ may mean also a varying mean molecular weight, $\bar{\mu}$, which would result in a slightly different distribution of density. Also the small value of Γ adopted in the external layers would lead to convection, which would again affect the distribution of mass. However, the results just obtained for two models with widely different central condensations show that small deviations, such as those referred to above,

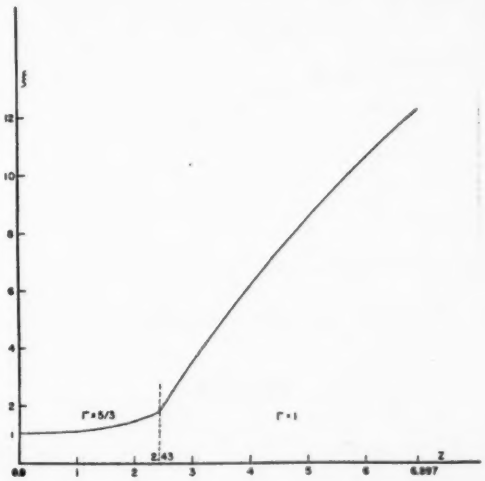

FIG. 2.—Variation of the amplitude with the radius in the standard model for a discontinuity of Γ as indicated.

would affect very little the critical values, especially the critical temperature T_c. Thus we can conclude that, even if Γ_e has its smallest possible value $\Gamma_e = 1$ in the external layers, these layers have to extend to a depth at which the temperature is approximately half the central temperature before the star becomes unstable.

5. *Extension of these results to cases in which* $\Gamma_e \neq 1$.—Of course, Γ_e in practice will not reach such a small value as $\Gamma_e = 1$; and Figure 3 (full curve) shows how the critical ratio, r_c/R, as given by our approximate formula (10), varies with Γ_e for the standard model.

We know the correct critical values for $\Gamma_e = 1$, and another integration in the case of $\Gamma_e = 1.2$ gives

$$\frac{r_c}{R}\simeq 0.22\,, \qquad \frac{m_c}{M}= 0.33\,, \qquad \frac{T_c}{T_0}= 0.71\,.$$

On the other hand, as Γ_e tends toward $\frac{4}{3}$, r_c/R tends toward zero, and ξ tends to become a constant, so that the correct critical values will approach more and more the approximate ones and their variation with Γ_e cannot differ very much from the representation given by the dashed curve. For $\Gamma_e = 1.3$, the external layers have to reach a depth at

which the temperature is of the order of 88 per cent of the central temperature ($r_c/R = 0.13$; $m_c/M = 0.09$) before the star becomes unstable.

6. *Extension to cases in which* $\Gamma_i \neq \frac{5}{3}$.—On the other hand, until now we have always supposed that $\Gamma_i = \frac{5}{3}$, which corresponds to a negligible radiation pressure, $[(M/M_\odot)\bar{\mu}^2 \leqslant 1]$. If the mass increases, Γ_i will decrease and tend toward $\frac{4}{3}$ for very large masses.

With $\Gamma_e = 1$, our approximate equation (10) gives the results summarized in Table 1.

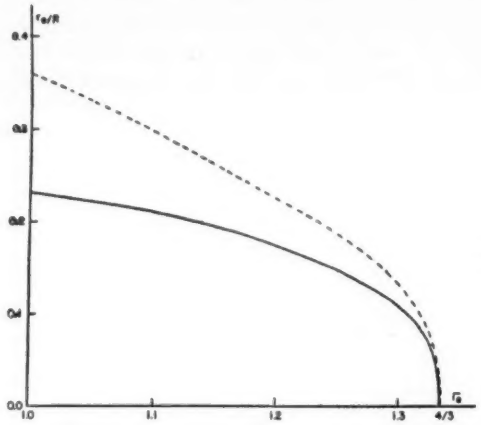

FIG. 3.—Variation of the critical ratio r_c/R with Γ_e in the case of the standard model and $\Gamma_i = 5/3$

TABLE 1

$(M/M_\odot)\bar{\mu}^2$	Γ_i	r_c/R	m_c/M	T_c/T_0	$(M/M_\odot)\bar{\mu}^2$	Γ_i	r_c/R	m_c/M	T_c/T_0
1.....	5/3	0.23	0.35	0.7	220.6.....	1.379	0.41	0.78	0.38
9.14.....	1.538	.27	.46	.62	402.0.....	1.366	.43	.82	.36
18.63.....	1.481	.29	.52	.58	1705.9.....	1.350	0.49	0.88	0.30
47.69.....	1.429	0.33	0.60	0.51					

These results are also plotted in Figure 4 (full curve). Of course, the real critical values will be different; but we know the correct value for $\Gamma_i = \frac{5}{3}$, and another integration for $\Gamma_i = 1.363$ gives

$$\frac{r_c}{R} \simeq 0.49, \qquad \frac{T_c}{T_0} \simeq 0.29, \qquad \text{and} \qquad \frac{m_c}{M} \simeq 0.89.$$

Again the correct and approximate curves should approach one another as Γ_i tends toward $\frac{4}{3}$, so that we can again tentatively draw a dashed curve, as in Figure 4, to represent the real variations of r_c/R.

Thus, even for large masses, the external layers, where Γ_e is as small as 1, must still be very extensive. For instance, if $(M/M_\odot)\bar{\mu}^2 = 400$, we find from the dashed curve in Figure 4 that Γ_e must be equal to 1 as far as

$$r_e \simeq 0.48R, \qquad \text{where} \qquad T_e \simeq 0.31T_0$$

before the star reaches the limit of stability.

7. *Small* Γ*'s in the vicinity of the center.*—In contrast to our discussion in the previous sections, we can contemplate the opposite situation and suppose that $\Gamma_i < \frac{4}{3}$ and $\Gamma_e > \frac{4}{3}$. If we take $\Gamma_i = 1$ and $\Gamma_e = \frac{5}{3}$, the two terms in equation (10) simply change sign, and thus in a first approximation we still get the critical values

$$r_c/R \simeq 0.23 , \qquad m_c/M \simeq 0.35 , \qquad \text{and} \qquad T_c/T_0 \simeq 0.7 .$$

As the integrand of the second term in equation (10) has a well-marked maximum around $z = 1.4$, the Γ's corresponding to that region will have the greatest weight in the evaluation of $\bar{\Gamma}$, and therefore it is in that region that a small Γ could have the greater effect.

If we take $\Gamma = 1$ in an interval between z_1 and z_2, having $z = 1.4$ as its mid-point and $\Gamma = \frac{5}{3}$ everywhere else, we find that the star is on the verge of instability in a first ap-

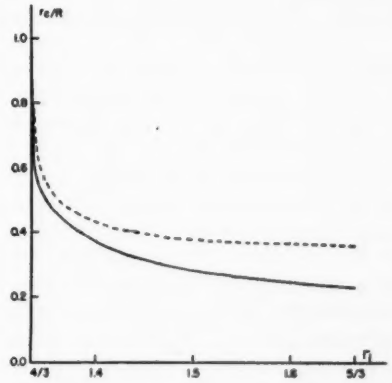

FIG. 4.—Variation of the critical ratio r_c/R with Γ_i in the case of the standard model and $\Gamma_e = 1$

proximation, when $z_1 \simeq 0.9$ and $z_2 \simeq 1.9$. Thus for instability the region of $\Gamma = 1$ must extend from $r/R \simeq 0.13$ to $r/R \simeq 0.28$; accordingly, it occupies a spherical shell of thickness $R/7$ and has a mass of about 0.4 M; the temperatures at its boundaries are, respectively, 88 and 61 per cent of the central temperature.

8. *Numerical applications.*—No detailed application has been carried out, but often the results given in the preceding sections enable one to decide whether a star is stable or not. In general, it appears that the conclusions of L. Biermann and T. G. Cowling[2] will be confirmed.

As an example we shall treat the case of the sun. R. H. Fowler and E. A. Guggenheim[4] have shown that, quite generally in the interior of a star, only two consecutive states of ionization of a given element need be considered at the same time. For a given temperature T and electron concentration N_e, there will be approximately as many atoms in one state as in the other if the difference of ionization energy between them is of the order of ψ, as defined by

$$e^{\psi/kT} = \frac{2\,(2\pi m_e kT)^{3/2}}{h^3 N_e} . \tag{24}$$

Under these circumstances we can also assume, following Biermann, that all the states with ionization potentials $\chi \leqslant \psi - kT$ will be ionized and those with ionization potential $\chi \leqslant \psi + kT$ will be un-ionized.

For the sun the standard model gives a fairly good representation, and, for an abundance of hydrogen by weight X of the order of $\frac{1}{3}$, it leads to a central temperature of 2×10^7 degrees and a central density of the order of 75 gm/cm^3. Under these conditions the ionization will already be well advanced, and in a first approximation one can write

$$N_e = \frac{\rho}{m^H}\left(\frac{1+X}{2}\right). \tag{25}$$

With this value of N_e, equation (24) gives for ψ a value of the order of 4400 ev. at the center of the sun. Looking at a table of ionization potentials, one realizes immediately that no important ionization will set in here. Thus, near the center of the sun, the matter can be considered as behaving like a monatomic gas, and, as the radiation pressure can be neglected, we can take $\Gamma = \frac{5}{3}$.

At the point where the temperature drops to half, its central value ψ is still of the order of 3300 ev., and we can again take $\Gamma = \frac{5}{3}$. But we should require Γ to be equal to 1 here and in the rest of the star to bring it to the verge of instability, and this is obviously impossible.

Even for a vanishing abundance of hydrogen, if we take the following mixture to represent the relative abundance by number of atoms of the other elements: $O:Mg:Fe = 8:3:1$, the same considerations as before show that the sun would still be stable.

These results can easily be extended to the other stars of the main sequence. However, for stars of very large masses the pressure of radiation becomes important; and, as that case was not considered by Biermann and Cowling, we shall treat an example. Let us take an extreme case—the Trumpler stars—and let us consider especially NGC 6871.5, for which $M \simeq 400\ M_\odot$ and $R \simeq 16.6\ R_\odot$. If we suppose that it is built on the standard model and composed of pure hydrogen, the central temperature, T_0, is of the order of 10^8 degrees and the central density of the order of 6.6 gm/cm^3. The ratio β of the gas pressure to the total pressure is 0.375. Under these conditions, since hydrogen is very easily ionized, we can assume that, in an extensive region starting from the center, the adiabatic exponent for the gas is $\frac{5}{3}$ and the combined exponent Γ for the matter and radiation will be 1.4. From Figure 4 we see, then, that for instability Γ should be equal to 1 in a region extending from the surface to $r \simeq 0.43R$, where $T \simeq \frac{1}{3}T_0$. But at this temperature the hydrogen is still completely ionized, and the region where Γ is equal to 1.4 will extend much farther toward the surface. Thus the star is stable.

If the star does not contain any hydrogen, the central conditions remain more or less the same, as the increase of $\bar{\mu}$ is practically compensated by the decrease of β, which becomes $\beta = 0.1$. At the center the gas can again be considered as monatomic, and $\Gamma = 1.35$. With this value of Γ in the central part we see from Figure 4 that, for instability, Γ should be equal to 1 from the surface to a point $r \simeq 0.54R$, where $T \simeq (\frac{1}{4})T_0$. But, for that temperature and the corresponding density, ψ is still of the order of 20,000 ev., and Γ will retain its value 1.35 much further, and the star is still stable.

However, it is known from other evidence[9] that the standard model gives a very poor representation of the internal structure of the Trumpler stars and a homogeneous model probably would be better. The problem is then a little complicated by the fact that, for such a model, β varies with depth; but for pure hydrogen one can again determine that the star is stable.

For vanishing hydrogen content, the central temperature is of the order of 3.2×10^7 degrees, $\beta \simeq 0.06$, and $\psi \simeq 28{,}000$ ev., so that we can still take for Γ the value corresponding to a mixture of monatomic gas and radiation. We find $\Gamma \simeq 1.343$. At the point where $T = \frac{1}{2}T_0$ and $r \simeq 0.96R$, ψ is still of the order of 12,500 ev., and for the mixture considered above we can still neglect ionization and $\Gamma = 1.4$. Computing Γ at

[9] Chandrasekhar, *op. cit.*, p. 313.

different points inside that region, we find that it remains very close to its central value, as far as $r \simeq 0.8R$, so that the average taken with respect to $\int_0^{r_0} PdV$ cannot be very different from it, say $\Gamma = 1.35$. Using equation (6), we find that Γ must be smaller than 1 in the external region to reach instability. However, we know that the instability is somewhat greater than revealed by equation (6); and Γ, although greater than 1, will be fairly small in that external region, so that probably we could not have much greater masses built on such a model except if they contain an appreciable amount of hydrogen.

In that respect it seems that the condition of vibrational stability is more restrictive. It has been shown,[10] for example, that a star built on the standard model, for which Kramer's law of opacity and Bethe's law of generation of energy are valid, would become unstable when the quantity $(M/M_\odot)\bar{\mu}^2$ is somewhat greater than 100. Since in the case of NGC 6871.5, $M/M_\odot$ is of the order of 400, we should have to take an extremely large abundance of hydrogen to avoid instability.

A change of model in the sense of a greater homogeneity would not help, since in that case the amplitude ξ would increase less rapidly from the center to the surface and the stabilizing terms which arise near the surface would have less weight in the integral expressing the condition of vibrational stability.

For stars of very small masses falling in the region of low hydrogen content in the Hertzsprung-Russell diagram, it does not seem either that any instability of the kind considered here will appear. For instance, in the case considered by Biermann[11] in connection with his theory of the nova phenomena, $M \simeq 0.5M_\odot$, $R \simeq \frac{1}{5}R_\odot$, the radiative equilibrium might become unstable from the surface to a point where the temperature is of the order of $10^{6.5}$ degrees to 10^7 degrees. But this is of the order of only one-tenth of the central temperature, which in this case is $T_0 \simeq 10^8$ degrees. From this point to the point where $T = \frac{1}{2}T_0$, Γ is certainly greater than 1. Thus, although the radiative equilibrium can be unstable fairly deep, the star remains dynamically stable, at least for a radial perturbation.

Of course, as Biermann and Cowling[2] have shown, it is for large radius that dynamical instability appears most easily; and past a certain value of the radius (for a given mass) one can determine the minimum abundance of hydrogen necessary to keep the configuration stable. The method developed here could be used to obtain more precise values of the critical radius or of the minimum amount of hydrogen, but it would require detailed computation.

9. *Special cases.*—This discussion has left out some special cases, but it is doubtful whether they have any physical interest. For instance, we limited ourselves to real values of σ^2. But in the case of the Roche's model, T. E. Sterne[7] has shown that all modes are unstable for $\Gamma < \frac{4}{3}$, all the corresponding σ^2 then having an imaginary part.

As the coefficients of equation (2) are essentially real, σ^2 can have only an imaginary part if the same is true of ξ. But we can study ξ in the vicinity of the singularities of equation (2) and see whether, for models having a physical meaning, the appearance of imaginary values is possible. For such models ρ, P, and Γ remain finite and different from zero for $0 \leqslant r < R$. We can also suppose that $d\Gamma/dr$ remains finite in the same interval.

Then equation (2) can have singularities only at $r = 0$ and $r = R$. At $r = 0$, $\mu = Gm(r)\rho/Pr$ tends toward zero as r^2 and $(1/\Gamma)(d\Gamma/dr)$ remains finite. The coefficient of $d\xi/dr$ will therefore tend toward infinity as $4/r$. In the same way the coefficient of ξ will tend toward infinity as $1/r$. Thus $r = 0$ is a regular singularity, and the corresponding indicial equation, $\theta(\theta - 1) + 4\theta = 0$, has real roots only, and the solution will be essentially real near $r = 0$. At $r = R$, the singularities of equation (2) will depend on

[10] P. Ledoux, *Ap. J.*, **94**, 537, 1941.

[11] *Op. cit.*, p. 344.

the behavior of the ratio ρ/P and the quantity $d\Gamma/dr$. As long as we use equation (2), it seems natural in this connection to take the same point of view as the one adopted in the theories of the internal structure of stars, namely, that P, ρ, and T tend toward zero at $r = R$ and that Kramer's law of opacity is valid.

We may then verify[12] that ρ/P will tend toward infinity as $8/(1 - r/R)$ and that $d\Gamma/dr$, which ultimately varies as $d\beta/dr$, remains finite. Thus $r = R$ is also a regular singularity, and the indicial equation, $\theta(\theta - 1) + 8\theta = 0$, can have only real roots. Thus ξ will be real everywhere, and so will σ^2.

Finally, if a star approaches dynamical instability (σ becomes small), there will be a point at which the usual method of perturbation used to obtain the condition of vibrational stability will cease to be applicable, since the perturbation σ' of σ (due to the nonadiabatic processes) will no longer be small compared to σ and the terms in σ'^2 will not be negligible compared to $\sigma\sigma'$ or σ^2.

It would probably be interesting to study the interaction of these two types of instability and try to obtain a more general criterion of stability.

[12] S. Chandrasekhar, *M.N.*, **96**, 647, 1936; also J. Tuominen, *Ann. Acad. Sci. Fenn.*, Ser. A, Vol. **48**, No. 16, 1938.

THE ATMOSPHERE OF 10 LACERTAE*

LAWRENCE H. ALLER
Kirkwood Observatory, Indiana University
Received July 8, 1946

ABSTRACT

Line intensities measured on Mount Wilson coudé plates of 10 Lacertae provide data for an investigation of the atmosphere of this star by Unsöld's method. From the Stark broadening of the hydrogen lines and the ionization equilibrium, the electron pressure, temperature, and surface gravity are estimated: $\log P_e = 2.80$; effective temperature $T = 29{,}600°$ K; and $\log g = 4.44$. Within the large errors of the data, the relative abundances of helium, carbon, nitrogen, oxygen, neon, magnesium, and silicon turn out to be the same as in τ Scorpii. The discrepancy in the computed neon to oxygen ratio between the planetary nebulae and the hot stars remains. Calculations of target areas for collisional excitation of forbidden neon lines, on the one hand, and f-values for the permitted transitions observed in the stars, on the other, are necessary before this question can be clarified.

In a discussion of the continuous spectrum it is shown that the need for a blanketing-effect correction of the type indicated by Unsöld is almost eliminated if the mean value of the stellar absorption coefficient is computed in the manner suggested by Chandrasekhar.

INTRODUCTION

In the course of a photometric investigation of the spectra of the brighter nuclei of the planetary nebulae it became apparent that a representative early-type absorption-line star could serve as a useful comparison object. The electron pressure, effective temperature, and composition of main-sequence stars of about the same temperature as the central stars of the planetaries might provide useful norms for the possibly more complex atmospheres of the latter objects. At least, comparisons between absorption-line O stars and planetary nuclei, on the one hand, and characteristic Wolf-Rayet stars and Wolf-Rayet type nuclei, on the other, may be valuable.

Unsöld's study of τ Scorpii[1] provides us with useful data of the type we are seeking, but it seemed worth while to apply similar methods to at least one other representative main-sequence star. Accordingly, for comparison with the planetary nuclei I have chosen 10 Lacertae, an O-type, main-sequence object, which falls close to the temperature and level of ionization of representative planetary nuclei.

THE OBSERVATIONAL MATERIAL

The data upon which the present discussion is based consist of coudé plates, obtained with the 100-inch reflector at Mount Wilson Observatory. The suitable spectra are given in the accompanying tabulation.

Plate	Date	Exposure	Emulsion	Disp.	Camera	Wave-Length Range (λλ)
Ce 952.....	1937 Sept. 7	120^m	Imp. Ec. Sp.	Prism	"UV"	4900–3500
3939.....	1945 Aug. 25	130	East. 103*a*-0	Grating	114-inch	4140–3500
4063.....	1945 Nov. 22	212	East. 100*a*-0	Grating	114-inch	4140–3500

* This investigation was made possible by a co-operative arrangement with the Mount Wilson Observatory.

[1] *Zs. f. Ap.*, 21, 22, 1941.

Table 1 gives the wave lengths adopted from Struve's measures[2] and my own, the identifications, and the quantity log $W/\lambda + 6$, where W is the equivalent width and λ is the wave length. Log W/λ is the physically significant quantity for curve-of-growth discussions.

For lines to the violet of λ 4143 the tabulated intensities are based upon all three plates; for the longer wave lengths only the Ce 952 data are available. For many of the weaker lines the intensities are very uncertain, and errors of a factor of 2 in W are quite possible. Despite their much greater dispersion, the grating plates show no more lines than the prism plates. A comparison of the hydrogen lines on the prism and the grating plates shows that a correction of about 20 per cent for light scattered by the grating must be applied. The agreement between the corrected intensities derived from the grating plates with those found from the prism plates is satisfactory, considering the weakness of the lines. Many of the lines lie just at the limit of measurability on the coudé plates.

TABLE 1

LINE INTENSITIES IN THE SPECTRUM OF 10 LACERTAE

Line	Identification	log $W/\lambda+6$	Line	Identification	log $W/\lambda+6$	Line	Identification	log $W/\lambda+6$
3587.5....	*He* I	1.62	3998.66...	*N* III, *S* II?	0.99	4275.67...	*O* II	0.54
3613.54...	*He* I	1.30	4003.47...	*N* III	1.32	4303.88...	*O* II	1.25
3634.27...	*He* I	1.61	4009.36...	*He* I	1.48	4317.2....	*O* II	0.20
3664.0....	*Ne* II	1.15	4026.22...	*He* I	2.37	4325.64...	*O* II, *C* III	0.08
3694.24...	*Ne* II	1.32	4056.09...	*C* III	1.15	4345.60...	*O* II	1.25
3695.4....	*O* III	0.74	4060.70...	*O* II	1.20	4347.5....	*O* II	1.19
3699.15...	*O* III	0.92	4062.9....	*O* II	0.70	4349.42...	*O* II	1.42
3703.4....	*O* III	1.18	4067.93...	*C* III	1.31	4351.27...	*O* II	0.86
3705.10...	*He* I	1.70	4069.11...	*C* II, *C* III	1.32	4366.9....	*O* II	0.86
3707.12...	*O* III	1.09	4069.81...	*O* II, *C* III	1.60	4379.15...	.....	0.53
3709.68...	*Ne* II	1.14	4072.18...	*O* II	1.32	4388.0....	*He* I	1.97
3713.03...	*Ne* II, *O* II	1.37	4074.00...	*O* III	1.04	4392.0....	*S* II	1.02
3715.05...	*O* III	1.20	4075.90...	*O* II	1.38	4437.48...	*He* I	0.98
3727.33...	*Ne* II, *O* II	1.52	4078.86...	*O* II	1.02	4465.5....	*O* II	0.87
3750.25...	*O* II	0.76	4081.01...	*O* III	0.90	4471.5....	*He* I	2.22
3754.76...	*N* III, *O* III	1.54	4083.89...	*O* II	0.80	4481.25...	*Mg* II	1.04
3757.26...	*O* III	1.54	4085.20...	*O* II	0.79	4510.94...	*N* III	1.2:*
3759.95...	*O* III	1.71	4088.95...	*Si* IV	1.82	4514.84...	*N* III	1.5:
3762.36...	*O* II, *Si* IV	1.35	4097.32...	*N* III	1.69	4518.00...	.....	0.64
3766.46...	*Ne* II	1.10	4103.40...	*N* III	1.35	4523.5....	*N* III	1.19
3773.32...	*Si* IV	0.91	4116.11...	*Si* IV	1.62	4541.75...	*He* II	1.92
3774.0....	*O* III	1.22	4119.25...	*O* II	1.25	4552.68...	*Si* III	0.54
3776.98...	*Ne* II, *O* II	1.10	4120.82...	*He* I	1.71	4631.18...	*Si* IV	1.16
3791.40...	*O* III, *Si* III	1.44	4143.84...	*He* I	1.70	4634.28...	*N* III	0.90
3803.04...	*O* II	0.80	4152.54...	*C* III	1.19	4638.62...	*O* II	1.05
3805.55...	*He* I	1.02	4153.33...	*O* II, *S* II?	1.01	4641.61...	*N* III, *O* II	1.25
3806.56...	*Si* III	0.95	4156.51...	*O* II, *C* III	1.26	4647.42...	*C* III	1.67
3819.75...	*He* I	2.21	4163.00...	*C* III	1.15	4650.24...	*C* III, *O* II?	1.75
3867.42...	*He* I	1.30	4169.04...	*He* I, *O* II	1.04	4651.46...	*C* III	1.30
3882.2....	*O* II	1.05	4185.5....	*O* II	0.78	4654.41...	*Si* IV	1.30
3911.99...	*O* II	0.75	4186.91...	*C* III	1.33	4658.23...	.....	0.58
3926.74...	*He* I	1.07	4189.85...	*O* II	1.02	4661.85...	*O* II	0.87
3938.82...	*N* III	0.92	4195.77...	*N* III	1.12	4685.80...	*He* II	2.22
3954.37...	*O* II	0.80	4200.....	*He* II, *N* III	1.49	4705.32...	*O* II	1.12
3961.67...	*O* III	1.45	4212.38...	*Si* IV	1.22	4713.11...	*He* I	1.76
3964.88...	*He* I	1.56	4253.80...	*O* II, *S* III?	1.28	4921.93...	*He* I	2.15
3995.00...	*N* II	0.83	4267.19...	*C* II	1.28			

* The colon denotes a line intensity possibly vitiated by a plate defect.

[2] *Ap. J.*, **90**, 722, 1939; see also *ibid.*, **74**, 225, 1931; and **77**, 321, 1933.

The discussions of curve of growth and abundances were carried out some time ago on the basis of the results from Ce 952. Since grating intensities are available for only a portion of the total wave-length range and since the prism intensity system agrees well with the corrected grating intensity system, I have not recomputed the abundances of helium and the heavier elements. Although a few improvements might be obtained, it would seem appropriate to hold new calculations in abeyance until additional homogeneous data are available for the entire spectral range. On the other hand, since the confluence of the Balmer series plays an important role in the calculation of the hydrogen abundance, all data have been utilized for this problem.

In Table 2 the second column gives the central depth of the lines measured in terms of the continuous spectrum as unity, the third gives the logarithm of the equivalent

TABLE 2

THE HYDROGEN LINES IN 10 LACERTAE

Wave Length	Central Depth, R_c	log W	log $N_{0,2}H$	Wave Length	Central Depth, R_c	log W	log $N_{0,2}H$
4861.33.....	0.41	0.39	13.99	3835.38.....	0.40	0.34	15.47
4340.47.....	.48	.40	14.53	3797.92.....	.....	.30	15.58
4101.74.....	.47	.40	14.88	3770.65.....	.....	.20	15.64
3970.06.....	.47	.40	15.14	3750.18.....	.....	.11	15.68
3889.00.....	0.46	0.40	15.33	3734.38.....	.....	−0.10	15.58

width in Angstrom units, and the computed quantity in the last column (see eq. [2]) enables us to estimate the population of the second level in hydrogen. The central depths of the hydrogen lines are not given beyond λ 3835, where the lines begin to overlap seriously, and the true position of the continuum is unknown. The material suggests that the true central intensities of the hydrogen lines are nearly constant, and I have adopted $R_c = 0.47$ as the most probable value.

INTERPRETATION OF THE LINE INTENSITIES

For the estimates of electron pressure, temperature, and composition, I have followed very closely the method given by Unsöld in his τ Scorpii paper. Except for *O* III, where additional line strengths had to be computed, Unsöld's f-values have been used throughout. Both τ Scorpii and 10 Lacertae are main-sequence stars of apparently similar atmospheric structure, and the procedure should suffice to fix the relative compositions of the atmospheres of these two stars, even though the absolute values might be in error. For the purposes of the initial calculations, the assumed temperatures of 31,500° K was taken from Kuiper's scale for an O9 star. Hence we need to correct Unsöld's $\log f/(R_c \Delta\omega_D)$ by only −0.07 in order to apply them to 10 Lacertae. Here f is the Ladenburg "f" or oscillator strength; the Doppler breadth $\Delta\omega_D$ is given by

$$\Delta\omega_D = \frac{2\pi c}{\lambda^2}\Delta\lambda_D = \frac{2\pi c}{\lambda}\sqrt{\frac{2kT}{M}}, \qquad (1)$$

where T is the kinetic temperature and M is the mass of the atom in question.

The total number of hydrogen atoms in the second level above the photosphere, $N_{0,2}H$, may be estimated in three ways:[3]

[3] The ordinary curve-of-growth procedure is not applicable to H, because the effective damping constant, which is determined by the interatomic Stark effect, increases from line to line in the higher members of the series. Hence other procedures for estimating abundances must be employed. For a discussion of the problem of the hydrogen lines in stellar spectra see Unsöld, *Physik der Sternatmosphären*, p. 286; see also Merrill and Wilson, *Ap. J.*, **80**, 19, 1934.

1. On the assumption that the hydrogen lines are formed in an optically thin layer ($N_{0,2}Hf \ll 1$), the equivalent width, W_n, for the $2-n$ transition is related to $N_{0,2}H$ by the expression

$$W_n = \frac{\pi e^2}{m c^2} \lambda_n^2 f N_{0,2} H = 0.886 \times 10^{-12} \lambda_n^2 f N_{0,2} H . \qquad (2)$$

Among the lower members of the series, this relation is certainly not correct, and the computed $N_{0,2}H$ will be too small. Equation (2) approaches validity as we go to higher and higher series members. Near the limit of the series, another difficulty comes in. Because of the overlapping of the line wings, one tends to draw the continuum too low, and the estimates of W_n are consistently too small. A plot of $N_{0,2}H$ against n gives a curve that rises for a time and then levels off and finally dips down as the measured W_n becomes too small. If we extrapolate the rising branch of the curve to a large value of n, in the fashion indicated by Unsöld, we obtain the limiting value for an optically thin layer. In this manner I have obtained $\log N_{0,2}H = 15.72$.

2. One may employ the value of the Balmer discontinuity as measured by Barbier and Chalonge[4] in conjunction with the "thin-layer approximation" to estimate the number of hydrogen atoms in the second hydrogen level. Since $\log D = 0.04$, we obtain

$$1.38 \times 10^{-17} N_{0,2} H = 0.09 , \qquad (3)$$

whence $\log N_{0,2}N = 15.81$.

3. Finally, we may treat the dip in the continuum at the Balmer limit by the interpolation formula more commonly employed in the "finite-layer" treatment of absorption lines.[5]

$$R = \frac{1}{\frac{1}{k_\lambda} + \frac{1}{R_c}} . \qquad (4)$$

Here R is the amount of the depression below the level of the undisturbed continuum, $k_\lambda = 1.38 \times 10^{-17} N_{0,2}H$ is the absorption coefficient at the Balmer limit, and $R_c = 0.47$ for 10 Lacertae. Since $R = 0.09$ from the date of Barbier and Chalonge, $\log N_{0,2}H = 15.90$.

As the most probable value, I have adopted $\log N_{0,2}H = 15.80$, a result very similar to that obtained for τ Scorpii by Unsöld.

One may compute the electron density from the equivalent widths of $H\beta$, $H\gamma$, and $H\delta$ or estimate it from the number of resolvable hydrogen lines on a good plate (Inglis-Teller method[6]).

If N is the number of charged particles effective in broadening a line of equivalent width W_λ, then

$$N = 6.5 \times 10^{12} \frac{W_\lambda^{5/2}}{C_n N_{0,2} H} , \qquad (5)$$

where C_n is a constant for each line. If, following Unsöld, we suppose that $N = 1.5 N_e$, we find

	λ 4861	λ 4340	λ 4101
$\log N_e$.....	13.88	14.18	14.34

The mean value is $\log N_e = 14.13$.

[4] *Ann. d. ap.*, Vol. **3**, No. 2, 1940.

[5] See *Physik der Sternatmosphären*, eq. (69.3), p. 266.

[6] *Ap. J.*, **90**, 439, 1939.

The number of resolvable lines of the Balmer series depends on the Stark broadening and therefore on the ionic density. If the density of the ions is large, as in the atmosphere of a dwarf, the Stark broadening will be large and the resolved Balmer lines will be fewer than in a star of low atmospheric density. If n_m is the principal quantum number of the last resolvable Balmer line, the Inglis-Teller formula gives

$$\log N = 23.26 - 7.5 \log n_m \,. \qquad (6)$$

Struve has listed the Balmer lines up to $n = 14$ in 10 Lacertae; thus we obtain $\log N_e = 14.6$. We cannot be sure, however, on the basis of the present data, that some kind of turbulence does not enter to widen the Balmer lines; hence I have adopted $\log N_e = 14.10$ for further calculations.

From the neutral helium lines and the thin-layer approximation, we can obtain a lower limit to the population of the 2^3P level by the methods indicated by Unsöld. In this way it is found that

$$\log N(2^3P) = 14.5 \pm 0.3 \,.$$

With respect to ionized helium the situation is more favorable for our purposes in 10 Lacertae than in τ Scorpii, since we can measure the intensities of two of the Pickering lines, λ 4541 and λ 4200. If we wish to employ the thin-layer approximation (eq. [2]), as Unsöld suggests, we must reduce the measured profile $R(\lambda)$ by means of equation (4) to obtain k_λ. From the computed k_λ one may then compute the corrected width by means of

$$W'_\lambda = \int k_\lambda \, d\lambda \,.$$

Here W'_λ is the equivalent width reduced to a thin layer. This procedure gives us a lower limit to the NH computed from equation (2). The numerical results are given in the accompanying tabulation. Notice that the N_4 calculated from the 4686 line (reduced

Lower Level	λ	log W	log W'	log $N_n'H$	log N_4H
$n'=3$	4686	−0.11	+0.06	13.14	13.00
4	4541	−0.43	−0.30	14.06	.....
4	4200	−0.9	.....	14.0	.....

from $n' = 3$ to $n' = 4$ with the Boltzmann equation and $T = 31{,}500°$ K) is ten times smaller than that computed from the Pickering lines!

It seems not unlikely that the 4686 line may be affected by incipient emission, while the Pickering lines are little disturbed. In the spectra of certain O-type stars the λ 4686 series is sometimes seen in emission, while the Pickering series appears in absorption. Hence I have adopted $\log N_4H = 14.00$ from the two Pickering lines.

The calculation of the abundances of the other ions—*C* III, *N* II, *N* III, *O* II, *Ne* II, etc.—has been carried out in the manner described by Unsöld, so far as the 10 Lacertae data will permit. In this hotter star the lines are fewer and weaker, and the accidental errors in the intensities are more serious. In particular, the *O* II, *Ne* II, and *N* III lines are much weaker in 10 Lacertae, but the *O* III lines are stronger and more numerous. I have plotted $\log W/(R_c 2\Delta\lambda_D)$ against $\log f/(R_c \Delta\omega_D)$ in the usual way and have obtained the $\log NH$ values by a comparison with the theoretical curve of growth. The material does not suffice to fix the damping constant a; hence, on the basis of Unsöld's work, I have adopted $\log a = -1$.

The columns of Table 3 list, first, the observed ion, the excitation potential of the lower term (or configuration) of the transition involved, subtracted from the ionization potential, viz., $\chi_r - \chi_{r,s}$; the logarithm of the number of atoms in the level s in the rth stage of ionization, $\log N_{r,s}H$; and, finally, $\log N_{r+1}, HP_e$ calculated from the combined Boltzmann and Saha equations for a temperature of 31,500° K ($5040/T = 0.16$) and also 29,500° K ($5040/T = 0.17$). The lines of *O* II enable one to compute the number of *O* III ions; the *O* III lines, in their turn, enable the calculation of the number of *O* IV ions to be made; etc. In other words, the lines arising from an atom in the rth stage of ionization enable us to compute the number of ions in the $(r + 1)$th ionization stage.

TABLE 3

DATA FOR THE CALCULATION OF IONIC ABUNDANCES

Ion	$\chi_r - \chi_{r,s}$	No. of Lines*	$\log N_{r,s}H$	$\log N_{r+1}HP_e$		Adopted Mean
				$\theta = 0.16$	$\theta = 0.17$	
H	3.38	.....	15.80	25.43	25.33	.....
He I	3.61	.....	14.50	24.34	24.24	.....
He II	3.37	2	14.00	23.03	22.93	.....
C III	7.64	1	11.50	20.98	20.80	21.20
	7.92	3	12.80	21.60	21.46	
	18.25	3	13.40	21.40	21.15	
N II	11.09	1	12.30	21.31	21.15	
N III	8.00	1	13.00	22.00	21.72	21.00
	11.77	8	13.10	21.10	20.93	
	16.99	1	12.00	19.67	19.42	
O II	6.17	2	13.40	22.35	22.22	22.00
	9.25	8	13.40	22.10	21.94	
	12.12	6	13.50	22.20	22.00	
O III	21.68	4	14.20	21.70	21.21	20.80
	17.64	4	13.60	20.60	20.42	
Ne II	6.20	1	12.30	21.90	21.80	21.95
	13.82	5	13.90	22.30	22.08	
Mg II	6.14	1	11.88	20.97	20.84	
Si III	14.39	1	12.2	20.8	20.6	
Si IV	8.67	3	12.30	20.70	20.58	20.70
	21.00	2	14.00	21.40	21.13	

* The third column gives the number of good lines available for estimating the abundance of the ion concerned. Lines possibly blended are given half-weight.

If we use $T = 31{,}500°$ K in connection with the Saha equation and the computed ratios, *He* III/*He* II, *N* IV/*N* III, *O* IV/*O* III, *Si* IV/*Si* III, we obtain $\log P_e = 3.20$ and $\log N_e = 14.56$. On the other hand, a temperature of 29,600° K gives $\log N_e = 14.10$, in closer agreement with our previous estimate from the Stark broadening of the hydrogen lines. Quite possibly the true electron density and effective temperature fall between these limits.

For the purposes of an illustrative calculation I have adopted $\log P_e = 2.80$, $T_e = 29{,}600°$ K. Actually, the relative abundances of the constituents are affected only very little by the exact choice one makes here. For example, an electron pressure of 1,600 dynes and $T_e = 31{,}500°$ K give essentially the same relative abundances. Factors to reduce the observed ionic abundances to the relative proportions of the actual elements result in small corrections to the observed ionic densities (Table 4).

The close agreement of the proportions of helium, carbon, nitrogen, oxygen, neon, silicon, and magnesium in the atmospheres of 10 Lacertae and τ Scopii is probably fortuitous in view of the uncertainties accruing from the low line intensities in the hotter star. The apparently greater abundance of hydrogen in 10 Lacertae may be real, but it is more tempting to attribute it to the observational uncertainties, even though the hydrogen abundance should be better established than those of the other elements whose relative proportions agree so well with the τ Scorpii results. Nevertheless, the lines of the heavier elements all seem to be weaker than they should be if the proportion of hydrogen to the total mixture is the same as in τ Scorpii.

In 10 Lacertae as in τ Scorpii, the neon abundance turns out to be about the same as the oxygen abundance, in marked contrast to the results obtained from the planetary nebulae,[7] where the abundance of neon was found to be between 0.1 and 0.01 that of oxygen on the basis of the intensities of the forbidden lines of *Ne* III and *Ne* V and of plausible assumptions concerning the target areas for collisional excitation. Until the

TABLE 4

COMPOSITION OF THE ATMOSPHERE OF 10 LACERTAE

Atom	log NHP_e	Relative Numbers of Atoms	
		10 Lac	τ Sco
H	25.33	1600	1000
He	24.26	134	180
C	21.34	0.16	0.17
N	21.38	0.18	0.38
O	22.02	0.8	1.0
Ne	21.97	0.7	1.1
Si	20.95	0.06[6]	0.06[4]
Mg	20.84	0.05	0.06

target areas are accurately computed, however, we cannot decide whether this apparent discrepancy is real or not. It may be that 10 Lacertae and τ Scorpii are "neon-rich" objects. An example in point in Nova Persei, which showed unusually strong forbidden neon lines. Further analyses of coudé spectra of early-type stars might help here.

The figures given in Table 4 probably represent a lower limit to the ratio of the heavier elements to hydrogen. The *f*-values for many of the transition arrays may be appreciably less than the value of 1, which Unsöld had assumed. Hence the abundances of carbon, nitrogen, oxygen, etc., relative to hydrogen may have to be increased by a factor possibly of the order of 2. An improvement in the abundance ratio can be attained only when the relevant *f*-values have been correctly computed. But it is difficult to see how the oxygen group could contribute as much as 35 per cent of the total mass of the stellar atmosphere, as Biermann,[8] in a recent paper, supposes is the situation for the mean composition of the sun. On the basis of the present results, an oxygen-group concentration in the neighborhood of 3 per cent seems quite possible; but it seems unlikely that the *f*-values could be off by the factor of 20, which the 35 per cent oxygen-group concentration would require.

[7] Aller and Menzel, *Ap. J.*, **102**, 239, 1945.

[8] *Zs. f. Ap.*, **22**, 244, 1943.

REMARKS ON THE THEORY OF THE CONTINUOUS SPECTRUM

The problem of the continuous spectrum of 10 Lacertae and τ Scorpii is essentially the same. Unsöld has discussed this question in detail. Since the lines appear to be formed in accordance with the mechanism of local thermodynamic equlibrium or "absorption," the effective optical depth of the photosphere is

$$t_0 = \frac{1}{1 + \frac{3}{2}\beta_0}, \tag{7}$$

where

$$\beta_0 = \frac{\frac{3}{8}\frac{hc}{\lambda k T_0}}{1 - e^{-hc/\lambda k T}} \frac{\bar{k}}{k_\lambda} \tag{8}$$

and

$$\bar{t}_0 = t_0 \frac{\bar{k}}{k_\lambda} \tag{9}$$

is the effective optical depth in the integrated radiation, while t_0 is the optical depth at the wave length in question. Radiative equlibrium theory requires that

$$R_c = t_0 , \tag{10}$$

where $1 - R_c$ is the central intensity of a strong line. Now $1/(1 - R_c)$ is the ratio of the flux of the total radiation of the star in the neighborhood of the line to the flux in the center of the strong absorption line, i.e., $F_\lambda/F_{\lambda,0}$. Burkhardt[9] has tabulated this quantity as a function of the parameters, $a = hc/\lambda k T_e$ and $\bar{k}/k_\lambda$. At the line center, $k_\lambda(a)$, the line absorption coefficient, is very large; and the emergent radiation corresponds to the boundary temperature, T_0. Given R_c and some estimate of the effective temperature, we can determine $\bar{k}/k_\lambda$ empirically, provided that our assumptions about the increase of temperature with optical depth and the constancy of $\bar{k}/k_\lambda$ with t are fulfilled. In this way Unsöld obtained an empirical estimate of $\bar{k}/k_\lambda$ of the order of 2.5 at λ 4000. Since $R_c = t_0 = 0.45$ at λ 4000 in τ Scorpii, the corresponding optical depth in the integrated radiation is 1.12. Unsöld then calculated $\bar{k}$ and k_λ from the theoretical atomic absorption coefficients and found that the $\bar{k}/k_\lambda$ ratio should be less than 0.5 for λ 4000. From the mass of the material above the photosphere and the computed mean absorption coefficient, he found the mean optical depth to be $t_0 = 0.055$. The twenty-fold discrepancy between the two results was explained by supposing that the large absorption beyond the Lyman and helium series acted like the absorption lines in the solar spectrum to retard the outward flow of radiation and thereby to modify the temperature distribution in the underlying layers. That is, instead of the temperature's being given by the usual expression, $T^4 = T_0^4(1 + 3t/2)$, the rise in temperature with optical depth is much steeper. With this blanketing-effect correction and a mean optical depth of 1.00, Unsöld was able to reconcile the observed features of the continuous spectrum.

In a recent paper[10] Chandrasekhar has pointed out that there is no justification for the use of the Rosseland mean coefficient of absorption in stellar-atmosphere problems and that the proper procedure is to calculate a mean absorption coefficient according to

$$\bar{k} = \int k_\nu \left(\frac{F_\nu^{(1)}}{F}\right) d\nu . \tag{11}$$

[9] *Zs. f. Ap.*, **13**, 56, 1936.

[10] *Ap. J.*, **101**, 328, 1945.

The quantity $(F_\nu^{(1)}/F)$ has been tabulated. Furthermore, if $k_\lambda/\bar{k}$ is independent of the optical depth, the temperature distribution on the gray-body assumption continues to be valid in the second approximation.

I have calculated the continuous absorption coefficient as a function of frequency for an atmosphere with an electron pressure of 630 dynes ($\log P_e = 2.80$) and an effective temperature of 29,600° K. Contributions to the continuous absorption coefficient arise from photoelectric absorption by hydrogen and by helium and from electron scattering. The hydrogenic contribution has been evaluated in the manner indicated by Unsöld, the helium absorption is taken from the work of Greenstein for the excited levels[11] and from Vinti's calculations from the ground state.[12] The electron scattering is computed on the assumption that each atom in the atmosphere supplies one electron. The resultant k_λ is very similar to that depicted by Unsöld; slight differences arise from the lower helium abundance which I have employed and from the slightly different temperature and electron pressure. The adopted effective temperature T_e of 29,600° K corresponds to an optical depth of about 0.7; hence the weighting function $(F_\nu^{(1)}/F)$ chosen is that tabulated by Chandrasekhar for $t = 0.7$. Graphical integration yielded a value of $\bar{k} = 3.0$ per gram of the stellar material. The mean absorption coefficient is relatively insensitive to optical depth; a calculation carried out for $t = 0.10$ with the same k_λ gives $\bar{k} = 2.4$, but I have retained $k = 3.0$ for the present calculations. The variation of $k_\lambda/\bar{k}$ in the observable spectral range is shown in the accompanying table. The straight mean value

λ	k_λ	$k_\lambda/\bar{k}$	λ	k_λ	$k_\lambda/\bar{k}$
6500	3.83	1.30	3650	1.22	0.42
5000	2.32	0.80		2.14	.72
4000	1.49	0.50	3000	1.26	0.42

of R_c is about 0.45. If we take the corresponding value of $F_\nu/F_{\nu,0} = 1.82$ and use $T = 29{,}000°$ K, we find an empirical $\bar{k}/k_\lambda$ of about 3 rather than the theoretical value of 2 at λ 4000 from the above table. Thus there still exists a discrepancy of the sign indicated by Unsöld, but the amount is much reduced.

The mean optical depth, l_0, is given by $l_0 = NHM_0\bar{k}$ or $NH\bar{a}$, i.e., the amount of material above the photosphere multiplied by the absorption coefficient. The number of atoms above the photosphere of 10 Lacertae is 3.7×10^{22}, and the absorption coefficient, $\bar{a}$, per atom is 6.17×10^{-24}; hence $l_0 = 0.228$. We must correct, however, for the fact that we did not take the negative absorptions into account in computing NH. The mean value of $(1 - e^{-hc/\lambda kT_e})$ for λ 4000 is 0.70; hence we must correct HN to 5.3×10^{22}, and we find a mean optical depth t_0 of 0.33. The theoretical l_0 computed from equations (7), (8), and (9) with $\bar{k}/k_\lambda = 2$ for λ 4000 gives $t_0 = 0.5$ and $l_0 = 1.0$. Thus there is a discrepancy of a factor of 3 between the optical depths computed by the two methods and the deviation remains in the direction indicated by Unsöld.

The present calculations, although approximate, do show that, when the mean absorption coefficient is calculated in the fashion suggested by Chandrasekhar, the necessary correction for the blanketing effect is largely eliminated. The discrepancies remaining seem to be of the order of magnitude of those frequently encountered in astrophysical work; and, until detailed numerical integrations for model stellar atmospheres are carried out, we cannot decide whether these discordances arise from errors in our assumptions (e.g., the constancy of $k_\lambda/\bar{k}$ with optical depth) or from the neglect of the blanketing effect. A complete theory of radiative transfer ought to be able to handle large varia-

[11] *Ap. J.*, **95**, 299, 1942.

[12] *Phys. Rev.*, **42**, 632, 1932.

tions of k_λ with λ (such as are encountered in the hotter stars) without invoking additional corrections for a blanketing effect, as least when the atmosphere is in local thermodynamic equilibrium.

It is important to establish the relation between the ultraviolet energy distribution and the energy distribution in the observable range, in connection with the calculations of the temperatures of the planetary nuclei by the Zanstra-Menzel method and for the determination of bolometric corrections.

All atmospheric models that assume uniformly stratified layers provide no mechanism for the release of extra amounts of energy at the stellar surfaces, either through "windows" in the far ultraviolet part of the spectrum or by high-speed particles. The model we have assumed requires that the atmosphere become very opaque in the far ultraviolet because of the ionization of *He* I and, finally, *He* II atoms from the ground level.

In conclusion I should like to express my gratitude to Drs. W. S. Adams and P. W. Merrill for permission to use their plates of 10 Lacertae. Dr. Adams and later Dr. Bowen kindly gave me the opportunity to work at the Mount Wilson Observatory on this problem. Thanks are due to Henry Norris Russell, Jesse Greenstein, Leo Goldberg, D. H. Menzel, S. Chandrasekhar, W. Baade, Olin Wilson, and Paul W. Merrill, who read the manuscript and made numerous valuable suggestions.

THE LIGHT-CURVES OF R AQUARII

CECILIA PAYNE-GAPOSCHKIN AND CONSTANCE BOYD
Harvard College Observatory
Received July 24, 1946

ABSTRACT

The visual and photographic light-curves of R Aquarii are presented and analyzed by separating the "red component" from the "blue component" photometrically. The relative behavior of the two "components" is shown to be closely related to the spectroscopic phenomena observed at the Mount Wilson, Yerkes, and Harvard observatories.

The complex variable star, R Aquarii, consists of a long-period variable ($P = 383$ days), an extensive and peculiar bright-line nebula, and what appears to be a variable stellar component capable of producing high excitation. The purpose of the present paper is to analyze the light-curves of R Aquarii in order to examine the bearing of these data on the physical nature of the system.

The variations of R Aquarii have been studied on plates of the Harvard collection. One of us (Miss Boyd) measured plates made before JD 27000; most of the plates were measured twice. In addition, Miss Boyd determined the magnitudes of comparison stars, selected from the visual sequence, on the International scale; these magnitudes are basic to the present investigation. Some years later R Aquarii was placed on the system-

TABLE 1

COMPARISON STARS FOR R AQUARII

Designation	DM No.	HD	I Pg	Spectrum	Designation	DM No.	HD	I Pg	Spectrum
a	−16°6345	222643	7.17	K2	h	−16°6370	223315	9.31	G5
b	15 6507	222559	7.52	K0	l	15 6345	222861	9.90	F5
c	16 6373	223428	7.63	K0	n	15 6479	.....	10.49	F5
d	15 6505	223542	7.97	K0	o	16 6354	.....	10.78	F5
e	15 6491	223006	8.76	K2	p	16 6350	.....	11.15	F8
g	−16 6363	223306	8.72	F5	q	−16 6355	.....	11.49	.....

atic program for the study of the brighter variable stars, carried out by C. Payne-Gaposchkin and S. Gaposchkin with the aid of a grant from the Milton Fund of Harvard University. The measures were made by S. Gaposchkin, and each plate was measured once. This series of observations overlaps the period covered by Miss Boyd and extends about 3500 days beyond; however, it employs only the small-scale patrol plates, whereas Miss Boyd, by studying all possible early plates, achieved more complete coverage during the early years. All photographic observations have been reduced with Miss Boyd's magnitudes. They are not published in detail but are available to scientific workers at the Harvard Observatory.

In addition to the photographic record, there exists a rather complete and continuous series of visual observations, made by the members of the A.A.V.S.O. and others. Mr. Leon Campbell has generously made available these data, combined into 10-day means.

The light-curves are shown in Figure 1. Visual observations are shown by circles, photographic observations by dots: small dots denote weight 1; medium dots, weight

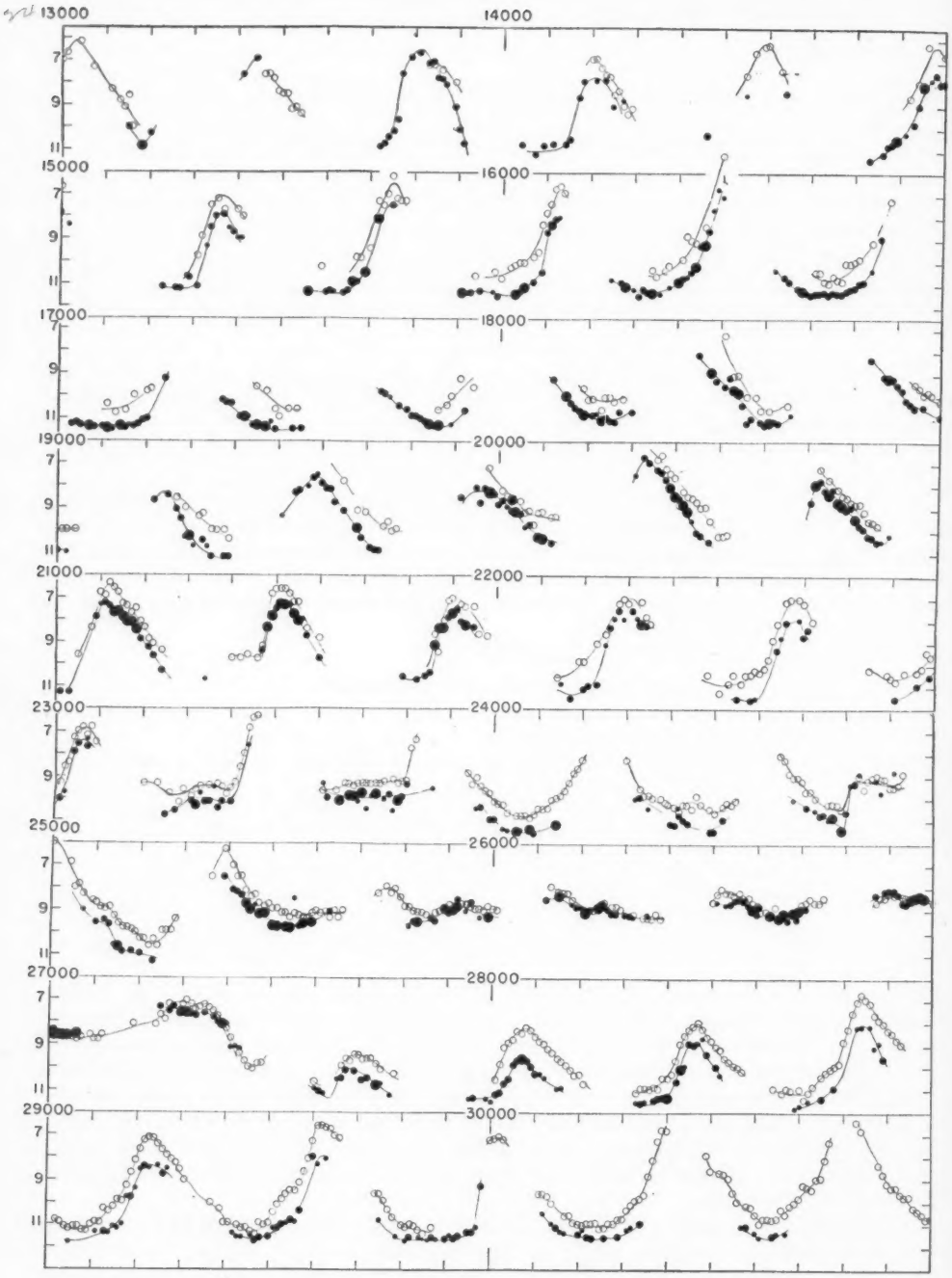

FIG. 1.—Visual (*circles*) and photographic (*dots*) light-curves of R Aquarii

2–9; large dots, weight 10 or more. Each estimate contributes weight 1 to the mean, except doubtful estimates, which contributed weight ½.

The well-known disturbance of the light-curve between JD 24000 and JD 28000, associated with remarkable spectroscopic phenomena, is shown by both visual and photographic curves. The star was evidently bluer than usual during the disturbed interval.

A complex light-curve may be analyzed on the following simple assumptions: (1) Two sources of light are present. (2) These sources, though variable in brightness, are of constant color. (3) In the present case it is assumed that the components resemble a long-period variable (color index 1.3 mag.) and a blue star (color index 0.0 mag.). The apparent color index of an unresolved pair of stars, each of known and constant color, is a function of their difference of magnitude only.

TABLE 2

PHOTOGRAPHIC LIGHT-CURVES OF RED AND BLUE COMPONENTS

JD	Maxima of Integrated Curve		Minima of Integrated Curve		JD	Maxima of Integrated Curve		Minima of Integrated Curve	
	Red Comp.	Blue Comp.	Red Comp.	Blue Comp.		Red Comp.	Blue Comp.	Red Comp.	Blue Comp.
22511	.....	.....	12.99:	11.69:	26748	.....	.....	11.49:	8.89:
22898	.....	.....	12.20:	12.30:	26903	(]12)	8.21	.....	.....
23058	8.76	7.76	.....	.....	27122	.....	.....	12.25:	8.85:
23286	.....	.....	11.99	10.69	27287	10.09	7.49	.....	.....
23678	.....	.....	11.36	10.36	27682	11.11	10.81	.....	.....
24064	.....	.....	12.63	11.98	28062	9.61	]12	.....	.....
24450	.....	.....	12.11	11.81	28300	.....	.....	13.42	11.77
24790	.....	.....	12.13	11.48	28470	9.60	9.70	.....	.....
24810	.....	.....	]12	9.31	28750	.....	.....	12.91	11.91
25222	.....	.....	12.46	11.46	28840	8.11	]12	.....	.....
25388	7.66	9.66	.....	.....	29230	8.41	]12	.....	.....
25609	.....	.....	12.09	9.49	29460	.....	.....	13.80	11.70
25981	.....	.....	11.89	9.29	29620	7.91	]12	.....	.....
26142	9.99	8.69	.....	.....	29850	.....	.....	13.47	11.82
26370	.....	.....	]12	9.31	30230	.....	.....	13.42	11.77
26517	10.19	8.89	.....	.....	30630	.....	.....	12.63	11.98

The light-curves of R Aquarii prove to be difficult to analyze, because the average color index has not remained constant, even during apparently undisturbed intervals. From JD 21000 to JD 23000 the star was bluer throughout its range than it was either before JD 19000 or after JD 28000, when its average color index was 1.3 mag. Possibly the abnormal blueness in the 2500 days that preceded the appearance of the "companion" spectrum is real and physically significant. Peculiarities of the light-curve at the minima near JD 21400 and JD 21800 suggest that the blue component was even then visible; but no colors have been determined at those dates.

After a number of trials it was decided to obtain a color index for the red component from the colors before JD 19000 and after JD 28000, these being the maximum observed values. The analysis was carried out from JD 23000 on, for individual maxima and minima, with the results shown in Table 2 and Figure 2.

It is unnecessary to discuss the spectra in the disturbed interval concurrently with the light-curve, as a very complete spectroscopic discussion through that epoch has been made by Merrill.[1] In Figure 2 of his paper, Merrill analyzes the light-curve into two

[1] *Ap. J.*, **81**, 312, 1934.

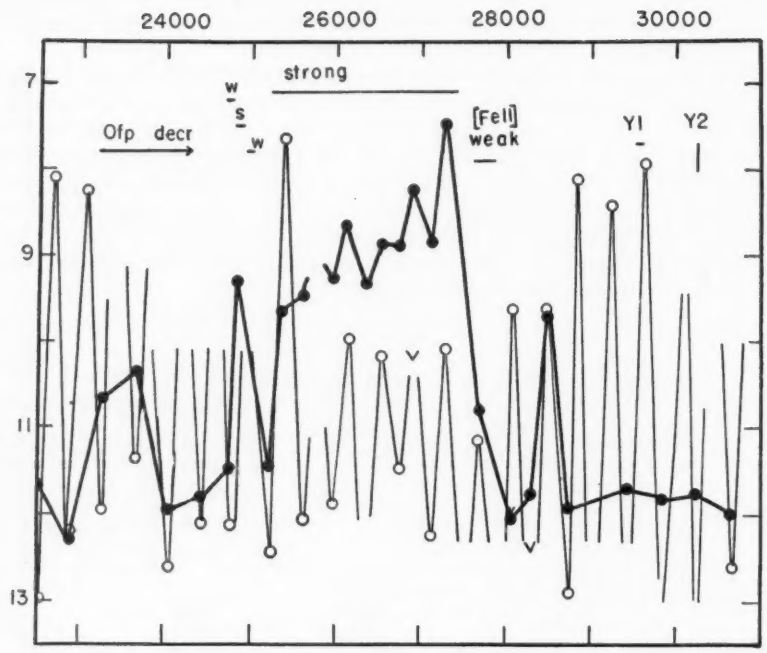

FIG. 2.—Brightness of red and blue components at maxima and minima of long-period variable. Circles and light lines, red component; dots and heavy lines, blue component. Spectroscopic changes are indicated in the figure; the references to the "Ofp" component are from Merrill's paper; w = weak; s = strong.

TABLE 3*

SPECTROSCOPIC OBSERVATIONS OF R AQUARII

JD or Year		Companion	Nebular Lines
1919–1921		Not seen	Outstanding
1922–1925		Type Ofp; decreasing intensity	Outstanding
1926, July, Sept.		Weak	Moderate intensity
1926, Dec.; 1927, Jan.		Strong; type Bep; *Fe* II predominant	Weak
1927		Weak; type Ofp	Moderate intensity
1928–1933		Strong; same type as Dec., 1926	Very weak
1934–1935		Weak; [*Fe* II] and [*S* II] predominant	Very weak
1937–1939		Weak	Increasing intensity
29520–610	Y1	[*O* II] strong; [*O* III] 4363 weak; intensities of N_1, N_2, show effect of occultation by *TiO;* evidence of stratification	
30206–219	Y2	Return to [*Fe* III] stage; [*O* II]	

* *References for table:*
P. W. Merrill, *The Spectra of Long-Period Variable Stars*, p. 84, 1940.
Y1: P. Swings and O. Struve, *ibid.*, **91**, 616, 1940.
Y2: P. Swings and O. Struve, *ibid.*, **95**, 159, 1942.

components; and the close parallel between his results and ours is an indication that our analysis has been carried out on acceptable lines.

Merrill's analysis goes as far as JD 27700, and our curves extend 3000 days further. Swings and Struve have added to the spectroscopic information since the "companion" grew weaker. A summary of the more conspicuous spectroscopic changes is given in Table 3.

The light-curves show that both supposed components of R Aquarii are indeed variable; the large range of the long-period variable is well known, and the blue star also seems to vary, by as much as 5 mag. A striking and significant fact is that the range of

TABLE 4

JD	Blue Component		Red Component		JD	Blue Component		Red Component	
	Average Pg. Mag.	Average Maximum	Average Minimum	Average Range		Average Pg. Mag.	Average Maximum	Average Minimum	Average Range
16000–18600...	11.82	7.86	12.20	4.34	25300–28000...	9.0	9.81	12.05	2.24
21000–23500...	.....	8.64	12.37	3.73	28000–31000...	11.81	8.73	13.28:	4.55:

the long-period variable is suppressed while the blue component is bright. The average behavior of the components is summarized in Table 4.

From Table 4 it may be seen that the early and late ranges are sensibly equal; that in the 2500 days before the disturbed period, both the photographic magnitude of the long-period light-curve at maximum and the range were below normal; and that during the disturbed interval the photographic maximum of the long-period light-curve was depressed by 2 mag. and its range was reduced to 2.25 mag. Since JD 28000 the maximum of the long-period curve has increased progressively.

The present paper is concerned primarily with the analysis of the light-curves; the system is to be discussed in conjunction with other complex systems, such as Z Andromedae and T Coronae Borealis. Apparently, R Aquarii presents a combination of the behavior of a long-period variable and a star subject to recurrent outbursts and allied to the recurrent novae. Whether the two sets of phenomena proceed from a single or a multiple source must be the subject of later discussion.

THE LIGHT-CURVES OF Z ANDROMEDAE AND AX PERSEI

CECILIA PAYNE-GAPOSCHKIN
Harvard College Observatory
Received July 24, 1946

ABSTRACT

The visual and photographic light-curves are compared and analyzed for Z Andromedae. The behavior of the "red component" and the "blue component" is analyzed photometrically and is shown to be closely related to the remarkable spectroscopic variations of the star. The photographic light-curve of AX Persei is shown to bear a strong resemblance to that of Z Andromedae, and the similarity of the spectroscopic phenomena in the two systems suggests that they have a close physical resemblance.

The two stars discussed in the present paper are excellent and similar examples of complex variable stars which appear to consist of a red component and a blue star that is a close relative of the recurrent novae. Both have been studied in the systematic program that was financed by a grant from the Milton Fund of Harvard University.

Miss Virginia Brenton made 1102 observations of Z Andromedae; the star has already been discussed in general terms by Mrs. Greenstein[1] and by Dr. Richard Prager, who

TABLE 1

COMPARISON STARS FOR Z ANDROMEDAE

BD	HD	Spectrum	I Pg	BD	HD	Spectrum	I Pg
+47°4177	221188	A0	7.75	+48°4094	.....	A	10.70
+47 4186	221515	B9	8.57	+48 4088	.....	.....	11.29
+48 4101	221775	B9	9.20	.....	.....	.....	11.90
+48 4090	.....	F8	9.52	.....	.....	.....	13.00

TABLE 2

COMPARISON STARS FOR AX PERSEI

Designation	BD	I Pg	Designation	BD	I Pg
a	+53°342	10.48	e	.....	12.06
b	+53 340	10.97	f	.....	12.31
c	.....	11.67	g	.....	12.70:
d	.....	11.86			

derived a photographic light-curve.[2] Mr. Masaaki Huruhata made estimates of AX Persei, and Miss Frances Wright made 229 more measures on recent plates. An earlier discussion of part of the Harvard material was made by Lindsay.[3] The photographic magnitudes for comparison stars have been redetermined by Miss Frances Wright. They are given in Tables 1 and 2.

The light-curves of Z Andromedae are given in Figure 1, that of AX Persei in Figure 2. In Figure 1 are given visual magnitudes, as published by Mr. Leon Campbell from the

[1] *Harvard Bull.*, No. 906, 1937.

[2] *Pop. Astr.*, **49**, 445, 1941.

[3] *Harvard Bull.*, No. 888, 1932.

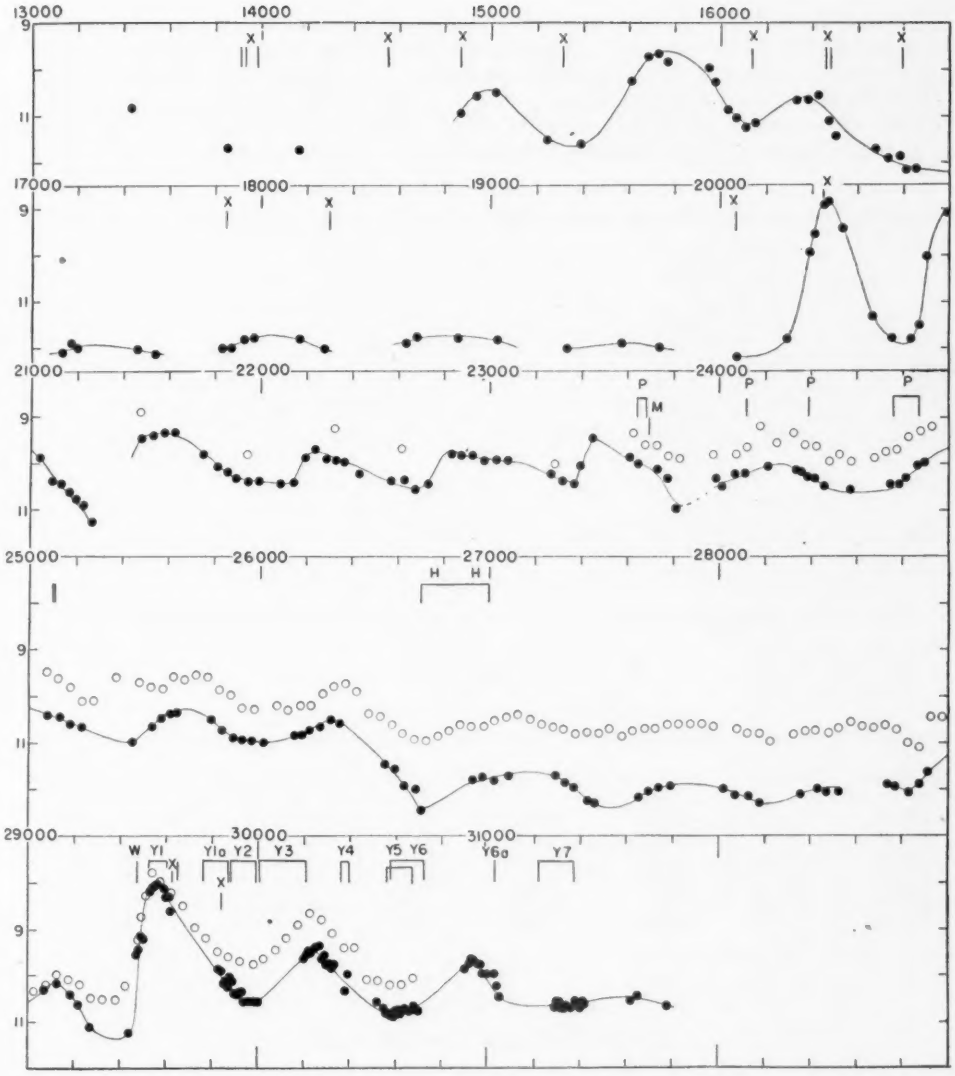

FIG. 1.—Photographic and visual light-curves of Z Andromedae. Harvard spectra are marked by symbol *X*.

observations made by the A.A.V.S.O., combined in 50-day means. The observations are not published here, but are available to scientific workers at the Harvard Observatory.

It is evident from the figures that both stars display a definite periodicity. Maxima of Z Andromedae are tabulated in Table 3; those of AX Persei in Table 4. The lengths of cycles for the two stars are compared in Table 5. The similarity is striking.

The visual and photographic light-curves for Z Andromedae permit the separation of the light-curves of the two stars by the method described in an earlier paper.[4] The results are given in Figure 3. Unfortunately, no visual light-curve is available for AX Persei.

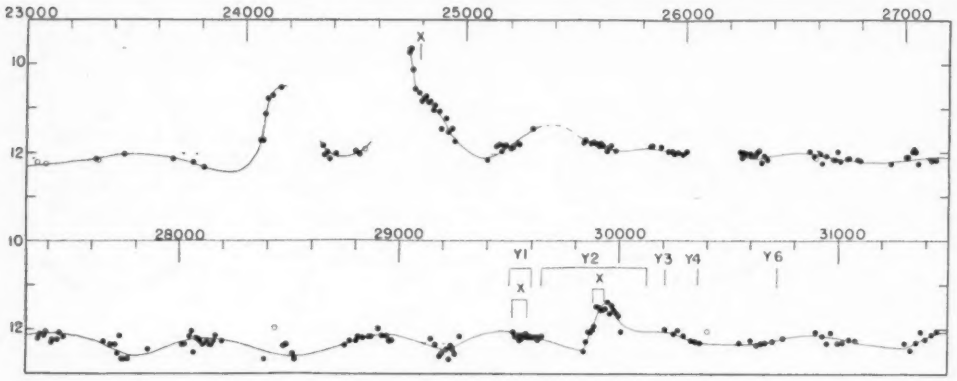

FIG. 2.—Photographic light-curve of AX Persei. Harvard spectra are marked by symbol *X*

TABLE 3

MAXIMA AND MINIMA OF Z ANDROMEDAE

JD Maxima	JD Minima	JD Maxima	JD Minima	JD Maxima	JD Minima	JD Maxima	JD Minima
15000	15350	19600:	20060	23440	23820	27840	28180
15740	16110	20460	20800	24200	24550	28600:	28830
16410	16810	20980	21270	24900	25400	29120	29370
17200	17540	21600	22100	25630	26000	29540	29970
18100	18400	22240	22670	26370	26700		
18750	19200:	22820	23380	27200	27460		

TABLE 4

MAXIMA AND MINIMA OF AX PERSEI

JD Maxima	JD Minima	JD Maxima	JD Minima	JD Maxima	JD Minima	JD Maxima	JD Minima
10600	12850	15250	25100	22750	.....	26900	.....
11900	13500	15750	25856	23500	.....	27350	.....
12550:	21756	16600:	27150	24150	.....	28100	.....
13100	23150	20700	27800	24750	.....	28900	.....
13850	23850	21450	28600	25350:	.....	29500	.....
14450:	24400	22100:	29250	26150:	.....		

[4] C. Payne-Gaposchkin and Constance Boyd, *Ap. J.*, **104**, 357, 1946.

The spectral variations of Z Andromedae and AX Persei are no less remarkable than their light-curves, and a concurrent study of the two types of data is necessary for an understanding of the systems.

Z Andromedae has been studied, notably by H. H. Plaskett, by P. W. Merrill, and at the Yerkes Observatory. A summary of the salient features of the spectra is given in Table 6. The times at which the various spectra were obtained are indicated in Figures 1 and 3, by the symbols given (in parentheses) in the bibliography that follows Table 6.

TABLE 5

DETERMINATION OF LENGTH OF CYCLE

	Z ANDROMEDAE		AX PERSEI	
	Length of Cycle (Days)	No. of Cycles	Length of Cycle (Days)	No. of Cycles
Median cycle	714±82 (p.e.)	42	685±79 (p.e.)	28
Maxima	JD 15000–29540	.....	JD 11900–16600	.....
Consecutive cycles	692 (mean)	21	671 (mean)	7
Maxima	.....	.....	JD 20700–28100	.....
Consecutive cycles	.....	.....	673 (mean)	11
Minima	JD 15350–29970	.....	JD 23150–25830	.....
Consecutive cycles	696 (mean)	21	670 (mean)	4
Minima	.....	.....	JD 27150–29250	.....
Consecutive cycles	.....	.....	700 (mean)	3
Average mean cycle	694	.....	675	.....

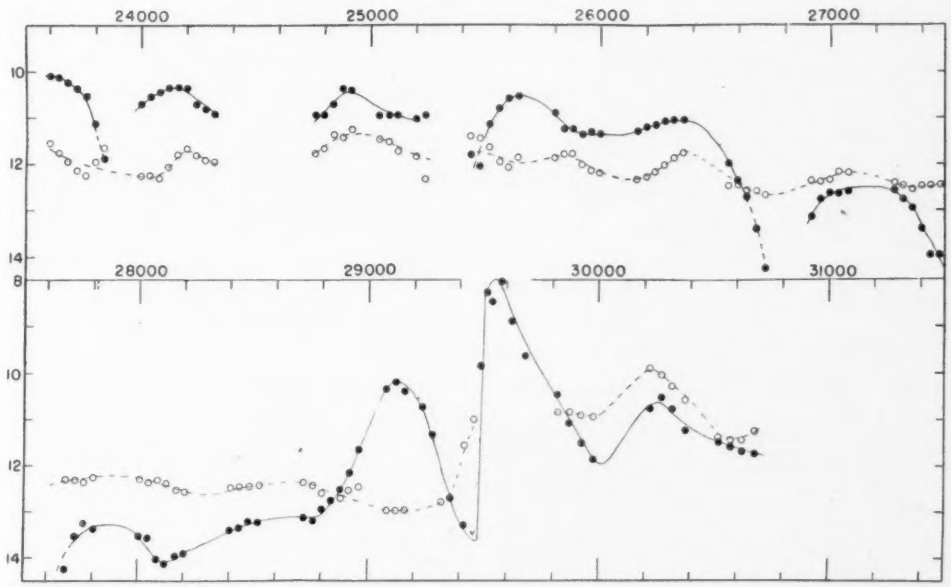

FIG. 3.—Resolution of light-curve of Z Andromedae into red (*circles*) and blue (*dots*) components

TABLE 6

SUMMARY OF SPECTRA OF Z ANDROMEDAE

JD or Year	Observer*	Description
23642–23678(10) 24122(1) 24396(1) 24761–24873(4) 25099–25105(2)	H. H. Plaskett	Emission spectrum representing a combination of "(1) a *stellar* part with lines due principally to *H*, *He* I, *Mg* II and *Fe* II, and (2) a *nebular* part with lines due to *He* II, *N* III and [nebulium]" These two spectra were used for a spectrophotometric study, which led to a color temperature of 5200° ± 900° K
23693	P. W. Merrill	Spectrum as described by Plaskett
23662, 23674	F. S. Hogg, I	*TiO* bands detected on Plaskett's spectra of these dates
1932–1933	F. S. Hogg, II	"Twelve spectrograms obtained during the last two years show that the *TiO* bands strengthened as the star faded. The emission lines have weakened relative to the continuous spectrum . . . ."
29475	P. Wellmann	*He* II, *N* III present, with weak violet absorption; *TiO* still present
29523–29603	Yerkes I	P Cygni spectrum with Plaskett's "nebular" spectrum missing; *TiO*, *He* II, *N* III, *O* III, have disappeared; emissions of *H*, *Fe* II, *Ti* II remain with violet absorption borders; forbidden lines weak; during the interval, absorption increases, emission decreases slightly
29541–29560	P. W. Merrill	Shell-type spectrum; 4686 absent
29649	P. W. Merrill	4686 barely visible
29762–29867	Yerkes I*a*	Spectrum like Plaskett's; also a P Cygni spectrum ascribed to expanding shell; 4363 relatively strong; some evidence of late component
29779	P. W. Merrill	Shell spectrum disappearing
29831	P. W. Merrill	Only traces of shell spectrum remain
29867–29995	Yerkes II	Increased intensity ratio, nebular/auroral lines of [*O* III]; P Cygni absorption disappears; Balmer continuum appears in emission: spectrum has post-nova character
30000–30215	Yerkes III	Increased intensity ratios: $\frac{Fe\ \text{II}}{N\ \text{III}, C\ \text{III}, C\ \text{IV}}$, $\frac{O\ \text{III fluorescent}}{[N\ \text{V}]}$, $\frac{He\ \text{I}}{[Ne\ \text{III}]}$, $\frac{Fe\ \text{II}}{He\ \text{I}, [O\ \text{III}]}$, $\frac{Si\ \text{II}, Mg\ \text{II}}{\text{Continuum}}$ No variation in structure of nuclear features, but weaker; decrease of [*O* III], [*Ne* III], [*Ne* V]; slow decrease of $\frac{\text{auroral}}{\text{nebular}}$ [*O* III] since 1940; strong Balmer continuum in emission; new shell, still near photospheric surface
30360–30400	Yerkes IV	[*Ne* III] increased; now as in August, 1940
30556–30664	Yerkes V	Strong [*Fe* VII], also [*Fe* V]; peak excitation on JD 30500; hardly any absorption, but evidence of late spectrum in visual region
30664–30725	Yerkes VI	Slow decline in excitation; [*Fe* VII] and [*Fe* V] still present (30725) but weaker than on 30541 or even than on 30664
31029	Yerkes VI*a*	Increase of excitation
31225–31369	Yerkes VII	Increase of [*Fe* VII] and [*Ne* V]. *Fe* I very weak; *Fe* II decreasing; [*Fe* II] increasing

* *Authors and symbols:*
H. H. Plaskett, *Pub. Dom. Ap. Obs.*, Vol. **4**, No. 10, 1928 (P).
P. W. Merrill, *Ap. J.*, **99**, 15, 1944 (M).
F. S. Hogg, I, *Pub. A.S.P.*, **44**, 328, 1932 (H).
F. S. Hogg, II, *Pub. A.A.S.*, **8**, 14, 1934 (H).
P. Wellmann, *Beob. zirk.*, **21**, 105, 1939; *V.J.S.*, **75**, 53, 1940 (W).
Yerkes I: P. Swings and O. Struve, *Ap. J.*, **91**, 601, 1940 (Y1).
Yerkes I*a*: P. Swings and O. Struve, *Ibid.*, **93**, 356, 1941 (Y1*a*).
Yerkes II: P. Swings and O. Struve, *Ibid.*, **94**, 296, 1941 (Y2).
Yerkes III: P. Swings and O. Struve, *Ibid.*, **95**, 152, 1942 (Y3).
Yerkes IV: P. Swings and O. Struve, *Ibid.*, **96**, 257, 1942 (Y4).
Yerkes V: P. Swings and O. Struve, *Ibid.*, **97**, 194, 1943 (Y5).
Yerkes VI: P. Swings and O. Struve, *Ibid.*, **98**, 93, 1943 (Y6).
Yerkes VI*a*: O. Struve, *Ap. J.*, **99**, 209, 1944 (Y6*a*).
Yerkes VII: P. Swings and O. Struve, *Ap. J.*, **101**, 230, 1945 (Y7).

Nineteen short-dispersion spectra of Z Andromedae, taken at Harvard with the 8-inch Draper telescope and one or two objective prisms provide some additional information, which is given in Table 7. Successive columns give the (hitherto unpublished) comments of Miss Cannon, Mrs. Mayall, and the writer. The two last spectra in the list were taken by Mrs. Mayall, who has kindly made them available.

The Harvard spectra are somewhat scattered in time, and the first six fall in an interval in which the course of the light-curve is uncertain. The remainder are collected in Table 8, which relates position on the light-curve to general spectroscopic behavior.

The information pieced together for Z Andromedae from light-curves and spectra may be summarized as follows:

Both "components" vary together with the 690-day cycle. The blue "component" has an observed range of about 6 mag.; the red "component" varies by $2\frac{1}{2}$ mag. at most.

At the highest maxima of the blue component, the spectrum is that of a minor nova outburst, which is followed, as the star declines, by the typical spectral development of a slow nova.

TABLE 7

HARVARD SPECTRA OF Z ANDROMEDAE

JD	Miss Cannon	Mrs. Mayall	Mrs. Payne-Gaposchkin
13914	Poor; bright lines seen	4686=3; $H\gamma=1$	4686; $H\gamma$ weaker
13925	Spectrum seen, no bright lines distinctly seen	Very poor, but bright lines in red	Too poor
13926	.....	4686=2, $H\gamma=1$	4686; $H\gamma$ weaker
13980	Only a faint blotch, no lines or bands	.....	.....
14546	.....	$H\beta=1$, 4686=3, $H\gamma=2$	$H\beta$, $H\gamma$, $H\delta$, 4686
14874	.....	$H\beta=2$, 4686=3, $H\gamma=3$, $H\delta=1$	$H\beta$, $H\gamma$, $H\delta$, decreasing intensity, 4686
15310	$H\beta$, 4686; $H\gamma$, $H\delta$, $H\epsilon$; $H\gamma=4686$; $H\beta$ fainter	$H\beta=4$, 4686=5, $H\gamma=5$, $H\delta=1$, $H\epsilon=1$	$H\beta$, $H\gamma$, $H\delta$, $H\epsilon$
16142	Bright lines seen; too near edge	$H\beta=2$, 4686=4, $H\gamma=4$, $H\delta=3$	$H\beta$, 4686, $H\gamma$, $H\delta$; very poor
16462	$H\beta$, $H\gamma$, $H\delta$, 4686 distinctly seen; $H\epsilon$?	$H\beta=4$, 4686=5, $H\gamma=5$, $H\delta=3$	$H\beta$, 4686, $H\gamma$, $H\delta$; weak continuum; good
16467	$H\beta$, 4686, $H\gamma$, $H\delta$, $H\epsilon$ seen; all bright, $H\gamma$ perhaps the strongest	$H\beta=3$, 4686=4, $H\gamma=5$, $H\delta=2$	$H\beta$, 4686, $H\gamma$, $H\delta$; $H\gamma$ is very strong; medium continuum
16485	$H\beta$, 4686, $H\gamma$, $H\delta$; all are bright	$H\beta=3$, 4686=3, $H\gamma=3$, $H\delta=2$	$H\beta$, 4686, $H\gamma$, $H\delta$; 4686=$H\gamma$
16787	Too faint, barely seen	4686=1	Continuum just seen; if bright lines, they are very faint
17849	.....	$H\gamma=1$	Continuum just seen; if bright lines they are very faint
18299	.....	$H\gamma=1$	Faint continuum, no bright lines
20072	.....	$H\beta=2$, 4686=1; no background	Two bright lines
20072	.....	4686=2; single bright line	Single bright line
20449	.....	Very bright; spectrum burned out, but $H\beta$ appears to be bright=1	Continuum very strong, bright $H\beta$, $H\gamma$?
29613	.....	$H\beta=3$, $H\gamma=2$, $H\delta=1$, $H\epsilon=1$	$H\beta$, $H\gamma$; medium continuum
29849	.....	$H\beta=3$, 4686=3, $H\gamma=2$, $H\delta=1$	$H\beta$, 4686 (=$H\beta$), $H\gamma$, $H\delta$; medium continuum

Titanium oxide is recorded during the intervals when the red component is relatively bright (JD 23600 on; JD 27000 [strengthened]; JD 29475; JD 30600); it disappears during high maxima.

The color temperature of 5200°, determined by Plaskett, is consistent with the color index of +0.8 observed at that time.

The successive appearance of *He* II 4686 as the star declines and of [*O* III] 4363, followed by the nebular lines, which increase in intensity relative to the auroral line, all seem (in the light of Table 6) to be part of a regularly recurrent pattern.

TABLE 8

SUMMARY OF INFORMATION FROM EARLY SPECTRA

Position on Light-Curve	Dates (JD)	Description
Faint	17849 18299	Faint continuum; *H* (? 4363) seen
Faint, just before rise	20072	No continuum; *H*, 4686 seen on one plate, 4686 alone on another; spectrum apparently varying rapidly
Rising to maximum	14874	Balmer lines bright; 4686 strong; ? 4363 present
Bright maximum	20449 29613	Strong continuum; Balmer lines bright; no other bright lines seen
Decline from bright maximum	29849	Medium continuum; Balmer lines bright; 4686 strong; no evidence of 4363
Decline from intermediate maximum	16462 16467 16485	Weak continuum; Balmer lines bright; 4686 strong; evidence of 4363
Intermediate minimum	15310 16142	Balmer lines; 4686; 4363?
Decline to faint minimum	16787	Continuum barely seen; bright lines very faint; 4686 seen

TABLE 9

YERKES SPECTRA OF AX PERSEI

JD	References*	Remarks
29500–600	Yerkes I	Weak continuum, corresponding to gM3e; very high excitation; strong Balmer continuum in emission; bright *H*, *He* I, *He* II, [*Fe* VII], [*Ne* V], [*Fe* X]?
29660–30000	Yerkes II	[*Fe* VII], [*Fe* VI] disappeared; N_1, N_2 decreased relative to 4363; [*Ne* III]/*H*, 3888/[*Ne* III]
30005–145	.....	[*Ne* III] weaker than 3888; 4472 strengthened relative to 4640; N_1, N_2 decreased; no [*Fe* VII]
30209–215	Yerkes III	[*Fe* VII], [*Ne* V] again strong; decreased *He* I, *N* III, *C* III, [*O* III], [*Ne* III]; excitation has increased since JD 30000
30360	Yerkes IV	[*O* II] fairly strong; [*Fe* VII] weaker; auroral/nebular [*O* III] decreased; [*Fe* V], [*Fe* VI] strong
30720	Yerkes VI	Again increasing in excitation; [*Fe* VII] as on JD 30300 [*Ne* III] weaker; [*Fe* V] still present, weakened

* *References:*
Yerkes I: P. Swings and O. Struve, *Ap. J.*, **91**, 607, 1940.
Yerkes II: P. Swings and O. Struve, *ibid.*, **94**, 299, 1941.
Yerkes III: P. Swings and O. Struve, *ibid.*, **95**, 152, 1942.
Yerkes IV: P. Swings and O. Struve, *ibid.*, **96**, 254, 1942.
Yerkes VI: P. Swings and O. Struve, *ibid.*, **98**, 93, 1940.

Spectroscopic material for AX Persei is summarized in Tables 9 and 10. The information complements that for Z Andromedae, which, for the most part, covers bright, disturbed intervals. For AX Persei the information begins during the faint, quiescent period and covers one outburst of intermediate intensity. Only two of the Harvard plates, taken in 1914 during a high maximum, show appreciable blue continuum.

TABLE 10

HARVARD SPECTRA OF AX PERSEI

JD	Mrs. Mayall	Mrs. Gaposchkin
24796.....	$H\beta=2$, $H\gamma=2$, $H\delta=1$	Medium continuum, runs far to violet; $H\beta=2?$, $H\gamma=1?$, $H\delta?$
24798.....	$H\beta=1?$	Medium continuum; bright lines?
29515.....	$H\beta=3$, $H\gamma=1$, $H\delta=1$	$H\beta=2$, $H\gamma=1$, $H\delta=1$
29517.....	$H\beta=1$	$H\beta=1$, $H\gamma?$
29518.....	$H\beta=2$, $H\gamma=1$, $H\delta=1$	$H\beta=1$, $H\gamma=\frac{1}{2}$
29518.....	$H\beta=3$, $H\gamma=1$	$H\beta=2$, $H\gamma=1$
29522.....	$H\beta=3$, $H\gamma=1$, $H\delta?$	$H\beta=2$, $H\gamma=1$, $H\delta=\frac{1}{2}$
29524.....	$H\beta=4$, 4686=1, $H\gamma=3$, $H\delta=1$	$H\beta=2$, 4686=1, $H\gamma=2$, $H\delta=1$
29524.....	$H\beta=5$, $H\gamma=3$, $H\delta=1$	$H\beta=2$, $H\gamma=1$, $H\delta=1$
29525.....	$H\beta=4$, 4686=1, $H\gamma=3$, $H\delta=1$	$H\beta=3$, 4686=1, $H\gamma=2$, $H\delta=1$
29577.....	$H\beta=5$, 4686=1, $H\gamma=3$, $H\delta=2$, $H\epsilon=1$	$H\beta=4$, 4686?, $H\gamma=2$, $H\delta=1$, $H\epsilon=\frac{1}{2}$
29579.....	$H\beta=5$, 4686=1, $H\gamma=3$, $H\delta=2$, $H\epsilon=1$	$H\beta=3$, 4686=$\frac{1}{2}$, $H\gamma=2$, $H\delta=2$
29583.....	$H\beta=2$, $H\gamma=1$	$H\beta=1$, $H\gamma=\frac{1}{2}$
29612.....	$H\beta=5$, no 4686, $H\gamma=4$, $H\delta=2$, $H\epsilon=1$	$H\beta=4$, no 4686, $H\gamma=3$, $H\delta=2$, $H\epsilon=1$
29878.....	$H\beta=2$, $H\gamma=1$	$H\beta=1$, $H\gamma=\frac{1}{2}$
29931.....	$H\beta=3$, 4686=3, 4640=1, $H\gamma=2$, $H\delta=1$	$H\beta=2$, 4686=2, 4640=$\frac{1}{2}$, $H\gamma=1$, $H\delta=\frac{1}{2}$
29934.....	$H\beta=4$, 4686=3, 4640=1, $H\gamma=1$, $H\delta=1$	$H\beta=2$, 4686=2, 4640?, $H\gamma=1$
29934.....	$H\beta=3$, 4686=3, $H\gamma=1$, $H\delta=1$	$H\beta=2$, 4686=2, 4640?, $H\gamma=1$

During the low maximum at 29500, the Harvard plates show the bright Balmer lines strong and 4686 weak or missing. During the rise to the intermediate maximum at 29930, the Balmer lines and 4686 were strong, the *N* III lines at 4640 were present but weak. This behavior is similar to that described in Table 8 for Z Andromedae, but the excitation is higher throughout.

THE ECLIPSING SYSTEM UV LEONIS

SERGEI GAPOSCHKIN
Harvard College Observatory
Received August 3, 1946

ABSTRACT

The eclipsing system UV Leonis has been studied on 18 spectrograms made at the McDonald Observatory and on 562 photographic Harvard patrol plates. The spectrum outside eclipse shows two components of spectral class G0 and G2. Orbital velocities of both components were obtained. The spectroscopic elements are: $K_1 = 165$ km/sec; $K_2 = 180$ km/sec; $(a_1 + a_2) \sin i = 2.85 \times 10^6$ km $= 4.10\ \odot$; $(m_1 + m_2) \sin^3 i = 2.56\ \odot$. The photometric elements are: Min. $= 2425672^d722 + 0^d60008582E$; Max. $= 8^m48$; min.$_1 = 9^m28$; min.$_2 = 9^m22$ (not rectified); $k = 0.96$ ($a = 1.0$); $i = 90°$; $a_2 = 0.41$; $b_2 = 0.39$; $a_1 = 0.43$; $b_1 = 0.41$; $z = 0.10$; $\gamma = 1.06$; $L_2 = .049$; and $L_1 = 0.51$. The combination of spectroscopic and photometric elements makes the system UV Leonis a well-determined one. The absolute dimensions are: $R_2 = 1.12\ \odot$; $R_1 = 1.17\ \odot$; $m_2 = 1.34\ \odot$; $m_1 = 1.22\ \odot$; $Sp_2 =$ G0; $Sp_1 =$ G2; $Mvis_2 = 4^m74$; $Mvis_1 = 4^m91$, the two latter being computed from R's and adopted temperatures of 5750° and 5510° C, respectively. A striking difference between the less massive component of this system and that of RT Andromedae (of the same period) is indicated.

I. SPECTROSCOPIC OBSERVATIONS

At the McDonald Observatory, in December, 1944, I obtained 18 spectrograms with the 82-inch mirror for the eclipsing system UV Leonis. All the spectrograms appeared to be of good quality. The spectrum on 10 of them shows double lines. Both spectra are of good quality and of G type; the classification based on the metallic lines is adopted as G0 and G2. Nine metallic lines, chiefly of iron, together with $H\gamma$ and $H\delta$, were measured. Each plate was measured once by the writer; the reduction was performed by Mrs. C. Payne-Gaposchkin. The distribution of the spectra over the phases is favorable. Table 1 gives the spectroscopic observations with additional information (see also Fig. 1).

The plotting of the radial velocities against the phase shows a satisfactory agreement between photometric and spectroscopic observations. Though the number of spectrograms is not large, they seem to indicate a small eccentricity of the orbit. The method of Lehmann-Filhés has been used, and the results are given in Table 2.

II. PHOTOMETRIC INVESTIGATION

The 562 photographic plates used have been measured twice at different times. The field is not rich in stars, and the number of comparison stars is limited. Three were selected, as given in Table 3; their magnitudes were obtained by the author from an unpublished sequence at Harvard and by comparison with the neighboring Harvard Standard Region C6. The scale and color were also investigated on Harvard yellow plates and visually at the McDonald Observatory.

The period has been discussed by means of twenty-five times of primary and thirteen times of secondary minima over an interval of forty years. A new period was found; the elements are Min. $= 2425672.722 + 0^d60008582$. Since the period is short and the exposure time of the plates is long, the observed brightness on a given plate may be in error. The error may be large not only where the change of brightness is rapid but also where the light-curve has greater curvature, e.g., at second and third contact and on the shoulders of the light-curve. Since there is no method of evaluating rigorously the necessary correction to magnitude, a simple graphical procedure, involving the determination of the "center of gravity" of the exposure-time effect, has been used. First, a light-curve was obtained from the original observations, and the shift of the center of gravity of a number of points on this curve was determined for different exposure times. The uncor-

TABLE 1

VELOCITIES OF UV LEONIS IN KM/SEC

JD	φ_0	Exposure Time (Minutes)	Velocity (All but H)	All
2431440.015	0.531	50	−221 (8)	−215 (11)
			+ 87 (7)	82 (8)
31440.982	.142	45	+ 32 (6)	+ 32 (6)
			−172 (8)	− 92 (11)
31441.883	.644	40	− 55 (6)	− 56 (8)
			+ 30 (2)	30 (2)
31442.905	.347	37	−135 (7)	−132 (9)
			+ 79 (5)	+ 70 (7)
31443.906	.015	38	+132 (6)	+123 (8)
			−178 (8)	−167 (10)
31444.028	.218	40	− 46 (9)	− 50 (11)
31444.915	.697	35	− 24 (10)	− 27 (12)
31445.028	.307	41	−154 (7)	−145 (9)
			+ 86 (6)	+ 84 (7)
31445.922	.374	40	−188 (8)	−200 (10)
			+104 (8)	+ 98 (10)
31446.029	.553	40	−189 (4)	−165 (7)
			+ 92 (3)	+ 81 (6)
31446.937	.066	40	+ 81 (6)	+ 81 (6)
			−183 (4)	−165 (7)
31447.015	.196	40	− 58 (8)	− 48 (10)
31447.911	.689	40	− 48 (8)	− 46 (10)
31447.985	.812	35	− 60 (7)	− 54 (9)
31448.906	.347	40	−134 (4)	−133 (6)
			+ 84 (3)	+ 69 (5)
31456.876	.629	45	−120 (6)	− 91 (8)
			+ 26 (6)	+ 26 (6)
31456.909	.683	45	− 47 (7)	− 47 (8)
31456.940	0.735	45	− 49 (6)	− 46 (10)

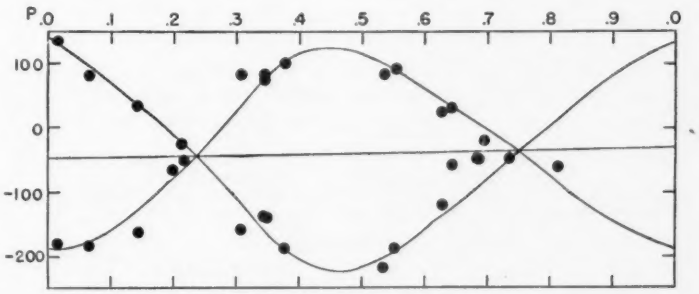

FIG. 1.—Velocity-curves of UV Leonis

TABLE 2

SPECTROSCOPIC ELEMENTS OF UV LEONIS

$K_1 = 165$ km/sec
$K_2 = 180$ km/sec
Ratio of masses = 1.09

$(a_1 + a_2) \sin i = 2.85 \times 10^6$ km $= 4.1\odot$
$(m_1 + m_2) \sin^3 i = 2.56\odot$

rected light-curve shows a considerable ellipticity, $z = 0.20$, with the two ranges $0^m.68$ and $0^m.62$. After correction for exposure-time effect, the ellipticity was reduced, $z = 0.10$, and the minima were deeper, $0^m.80$ and $0^m.74$. As an illustration, a part of the correction table is given in Table 4; tabulated quantities are hundredths of a magnitude.

The rectification of the light-curve has been made graphically by plotting l^2 against $\cos 2\theta$; the deduced value of z is 0.10. The application of the method of least squares to the formula $l = a + b \cos\theta + c \cos^2\theta$ has led to $z = 0.0905 \pm 0.0203$; y (coefficient of reflection effect) $= 0.0236 \pm 0.0088$; and $x = 0.9999 \pm 0.0191$. There is a slight indication that the minima are separated by not exactly half the period; the phases of the minima being $0^P.755$ and $0^P.245$, respectively. However, in obtaining the dimensions of the system, this small eccentricity has been neglected. The rectified light-curve is given in Table 5.

The maximum has been adopted from observations outside the eclipse as $8^m.48$; the ranges then are $0^m.74$ and $0^m.68$. From these values there is very little latitude for a and

TABLE 3

COMPARISON STARS FOR UV LEONIS

Designation	BD	IPg
a	14°2277 (8.5)	$8^m.10$
b	14 2271 (9.1)	9.11
c	14 2274 (9.1)	9.30

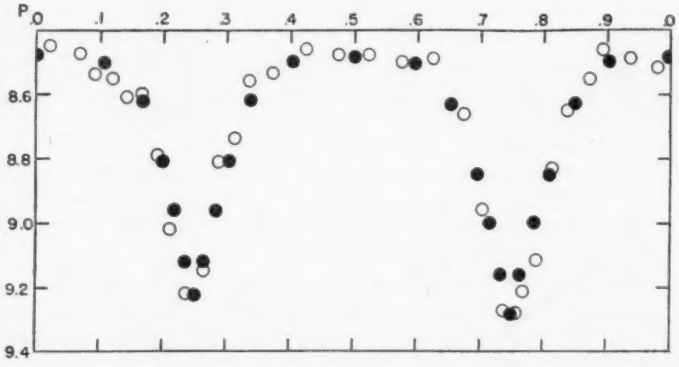

FIG. 2.—Light-curve of UV Leonis. Circles, observed normals; dots, computed uniform curve

TABLE 4

CORRECTION FOR EXPOSURE TIME

Exposure Time (Minutes)	Phase								
	$0^P.00$	$0^P.10$	$0^P.20$	$0^P.25$	$0^P.35$	$0^P.50$	$0^P.65$	$0^P.75$	$0^P.90$
60	0	0	+0	+ 9	− 1	0	− 1	+ 8	−2
80	0	−2	0	13	4	0	4	16	4
120	0	−7	+2	+28	−12	0	−12	+34	−8

k; the latter must lie between 1.00 and 0.96. In order to use the secondary minimum, together with the primary, in investigating the elements, the magnitudes of the secondary minimum were reduced to the amplitude of the primary; the numbers are given in parentheses in Table 5. The errors of the normal points of Table 5 cannot be greater than $0^m.04$.

The light-curve (the ascending and descending branches) is more consistent with assumption of a total eclipse and the ratio of radii 0.96 than with $k = 1.00$ and $k = 0.96$. The run of observations is, indeed, such that it favors a still smaller value of k, in violation of the limits set by the depth of the secondary minimum. This is well illustrated

TABLE 5

RECTIFIED LIGHT-CURVE OF UV LEONIS

Phase	IPg	Phase	IPg	Phase	IPg	Phase	IPg
0.0070*.....	9.22	0.2273.....	8.52	0.4612.....	8.97(9.01)	0.7239.....	8.48
.0178.....	9.15	.2711.....	8.45	.4869.....	9.16(.22)	.7738.....	8.48
.0393.....	9.06	.3190.....	8.46	.5128.....	9.09(.15)	.8264.....	8.48
.0615.....	8.78	.3400.....	8.52	.5373.....	8.76(.80)	.8768.....	8.47
.0860.....	8.61	.3681.....	8.52(.53)	.5627.....	8.69(.73)	.9212.....	8.62
.1200.....	8.52	.3895.....	8.58(.60)	.5822.....	8.51(.54)	.9530.....	8.91
.1421.....	8.44	.4153.....	8.56(.58)	.6247.....	8.49(.50)	0.9874.....	9.21
0.1841.....	8.49	0.4401.....	8.74(.77)	0.6748.....	8.45(.46)		

* Adopting the middle of the primary minimum, $\varphi = 0^d.750$.

TABLE 6

ELEMENTS OF UV LEONIS

$a = 1.00$	$a_1 = 0.43$
$k = 0.96$	$a_2 = 0.41$
$i = 90°$	$b_1 = 0.41$
$\gamma = 1.06$	$b_2 = 0.39$
$L_2 = 0.49$	$s = 0.10$
$L_1 = 0.51$	$b/a = 0.95$

by plotting the intensity (l) against $\sin^2 \varphi$. The solution of the light-curve is given in Table 6, for uniform solution, using S. Scharbe's method.[1] The computed light-curve, given in the figure, shows a systematic deviation at the bottom of the minimum.

III. ABSOLUTE DIMENSIONS AND DISCUSSION

The system of UV Leonis is one of the very few eclipsing variables of short period and late spectrum for which adequate data exist to obtain masses and radii. Both components have well-defined orbital velocities, and the minima are so deep that the ratio of radii is practically uniquely determined. The combination of the spectroscopic with the photometric elements leads to the absolute dimensions given in Table 7.

It is of interest to compare these values with those for stars of similar character. Table 8 gives all known G stars, other than the sun, for which masses have been determined. Except for those indicated otherwise, all values are taken from the compilation by the author.[2] There is a striking similarity in masses for UV Leonis and systems like AR Lacertae, WZ Ophiuchi, and RT Andromedae, the first two of which are determined

[1] *Poulkovo Bull.*, **94**, 31, 1923.

[2] *Harvard Reprints*, No. 201, 1940.

TABLE 7

ABSOLUTE DIMENSIONS OF UV LEONIS

Major axes	1.15⊙	1.20⊙
Minor axes	1.10⊙	1.15⊙
Mean radii	1.12⊙	1.17⊙
Masses	1.34⊙	1.22⊙
M (visual)	4^m74*	4^m91*
Spectra	G0	G2

* Computed with the temperature of 5750° and 5510°C, respectively.

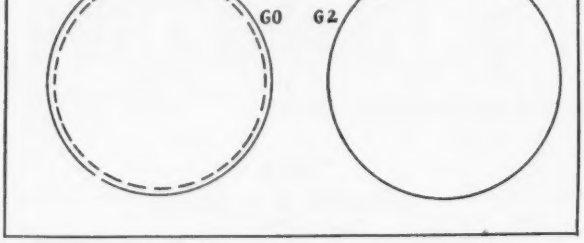

FIG. 3.—Relative dimensions of UV Leonis

TABLE 8

MASSES OF G STARS

Star	Spectrum	Mass	Period	Star	Spectrum	Mass	Period
RT And*	G0	1.50⊙	0^d63	AR Lac	G2	1.41⊙	1^d90
WZ Oph	G0	1.41	4.16	U Sge	G2	2.03	3.38
WZ Oph	G0	1.35	.....	AR Lac	G3	1.42	1.90
UV Leo	G0	1.34	0.60	RS CVn	G8	1.74	4.80
UV Leo	G2	1.22	.....	U Cep	G8	1.1;	2.49
W UMa	G0	0.64	0.33	RT Lac	G9	1.0	5.07
ER Ori†	G1	0.50	0.41	RT And*	G8:	0.99	0.63

* C. Payne-Gaposchkin, *Ap. J.*, **103**, 291, 1946.

† S. Gaposchkin, *Pub. A.S.P.*, **56**, 199, 1944.

with very high accuracy. Even more interesting is a sharp difference between the masses of short-period systems, like W Ursae Majoris and ER Orionis, and those of the rest of the group. This may be partly due to the fact that the former have periods of less than half a day, that their components are close to each other, and that the reflection effect on the radial velocities (making the amplitude smaller) is considerable, which will lead to a falsification of the masses.

Another point of interest is the comparison between the system of RT Andromedae and the present one. They have similar periods (0.6 days), about the same ellipticity, and the primaries are of about the same spectral class; but the secondary spectrum of the system RT Andromedae is of definitely later type than that of UV Leonis. There is, however, a great difference in photometric elements, exemplified in the different light-curves. RT Andromedae represents a combination of a main-sequence star and a subgiant instead of a pair of similar stars, as with UV Leonis. To understand why they are so different in one respect and so similar in another involves a knowledge of the origin and evolution of double stars.

The writer wishes to express his appreciation of the hospitality of Dr. Struve during his stay at the McDonald Observatory, which made possible the securing of the spectrograms used in the present investigation, and of the generous permission of Dr. Shapley to make this visit.

THE ECLIPSING SYSTEM RX GEMINORUM

SERGEI GAPOSCHKIN
Harvard College Observatory
Received August 3, 1946

ABSTRACT

The system has been studied on 19 spectrograms of the McDonald Observatory and on 1376 photographic patrol plates of the Harvard Observatory, supplemented by 239 visual estimates by Enebo. Outside the eclipse the spectrum shows but one component, of spectral class A4. Orbital velocities were obtained only for this component. At minimum—a constant brightness of short duration—the spectrum is practically unchanged. No trace of a secondary spectrum was observed. The spectroscopic elements are $V_0 = +33.5$ km/sec; $K = 25.5$ km/sec; $e = 0.295$; $\omega = 21°.7$; $f = 0.018\ \odot$; $a_2 \sin i = 4.07 \times 10^6$ km $= 5.85\ \odot$. The photographic light-curve exhibits a small reflection effect, slight asymmetry of the primary minimum (fall is slower than rise), and a constant phase of small duration at the bottom of the minimum. The photographic elements for (*D*) solution are: Max. $= 9^m.20$, $A_1 = 2^m.02$, $A_2 = 0^m.02$, $k = 0.40$, $r_1 = 0.188$, $r_2 = 0.075$, $i = 83°.9$, $L_2 = 0.84$, and $\gamma = 30.9$; the computed spectrum of the invisible component is K0. The visual light-curve is less well determined than the photographic one. Its relative elements for (*U*) solution are: Max. $= 9^m.25$, $A_1 = 1^m.76$, $k = 0.38$, $r_1 = 0.198$, $r_2 = 0.075$, $i = 83°.0$, $L_2 = 0.82$, $\gamma = 31.5$; the color index during the total minimum is $0^m.21$, at maximum, $0^m.05$. The spectroscopic and photographic observations indicate that RX Geminorum is a typical system, consisting of a main-sequence star and a subgiant. The approximate dimensions of the components are: masses, 3.1 ⊙ and 0.62 ⊙; radii, 2.20 ⊙ and 5.5 ⊙; absolute visual magnitudes, 1.1 and 2.7; and spectra A4 and K0p. The observed spectrum at primary minimum is, however, of class A.

I. SPECTROSCOPIC WORK

During my stay at McDonald Observatory I obtained 19 spectrograms of RX Geminorum with the Cassegrain spectrograph of the 82-inch reflector. The spectrum is simple, with well-developed hydrogen lines. Some fainter lines at λλ 4172–4178 and λλ 3900–3913 indicate that the star is, if not a supergiant, at least not a normal main-sequence star. Only one spectrum (A4) was measurable. All measurements were made by the author and all reductions by Mrs. Cecilia Payne-Gaposchkin. The radial velocities from hydrogen, calcium, and iron lines are given in Table 1. The distribution of the plates is favorable, though their number is too small for detailed discussion of such spectroscopic phenomena as the rotation effect, which is probably present in the spectrum of this system.

II. SPECTROSCOPIC ORBIT

Though the plates are not numerous, the general trend of the radial velocity-curve of the brighter component (A4) is unmistakable; the orbit is eccentric. Using the Lehmann-Filhés method, we obtain the spectroscopic elements for all lines as shown in Table 2.

I have only one plate on the descending branch of the minimum close to totality. There is definite indication that the minima came earlier in 1944–1945 than predicted by the ephemeris, so that the plate is taken, if not entirely during the totality, at least during a part of it. A simultaneous visual estimation at that phase was easily made, for there is a very close companion star at 11.0 mag. The visual magnitude of RX Geminorum was only 0.1 brighter than this companion—that is, 10.9—at JD 30435.959. Our spectrum shows at this phase the K line unchanged and sharp. On this basis, therefore, the spectral class would be about A5. Wyse, who classified the star at minimum on spectrograms of small dispersion, has given it as A3p. But on our spectrum there is a definite indication of the presence of λ 4227, which is not visible on any of the other spectra. The hydrogen lines are definitely present. The primary presents no difficulties for classification; it is about A4 in the Morgan system. The distribution of energy in the spectrum suggests a

TABLE 1

VELOCITIES OF RX GEMINORUM IN KM/SEC

JD	Phase	All Lines	*H*	*Fe* II	*Ca* II
31428.889	0.306	+17: (4)	+50:	−22:	− 11:
431.903	.554	10.1 (5)	6.5	+ 8.5	+ 11
432.807	.628	26.4 (5)	33	+44	+ 38
432.840	.631	30.8 (6)	37.5	+27	+ 34
433.940	.720	51.8 (5)	59	+44	+ 57
435.959	.886*	27.2 (4)	29	+29	+ 22
437.838	.040	18 (5)	15	+25	+ 10
439.855	.205	25 (4)	20	.....	+ 13
440.775	.280	4 (4)	1	.....	+ 13
441.718	.358	20.2 (5)	18.5	+21	+ 22
442.795	.446	25.8 (5)	24	+24.5	+ 32
443.848	.532	14.8 (5)	10	+11	+ 32
444.869	.616	37.2 (5)	38.5	+22.5	+ 44
445.832	.694	61 (5)	53.5	+65	+ 68
446.881	.780	65 (5)	65	+48	+100
447.879	.862	66 (5)	63	+66	+ 72
448.877	.944	50.8 (4)	38.5	+51	+ 75
456.842	.596	45.8 (4)	48	+40	+ 47
458.656	0.745	+66 (5)	+70.5	+44.5	+100:

* In minimum, faint.

TABLE 2

SPECTROSCOPIC ELEMENTS OF RX GEMINORUM

$K_A = 25.5$ km/sec
$f = 0.018$
$e = 0.295$
$\omega = 21°.7$
$V_0 = 33.5$ km/sec
$a_A \sin i = 4.07 \times 10^6$ km $= 5.86\odot$
$P = 12^d.209$*

* From the photometric work.

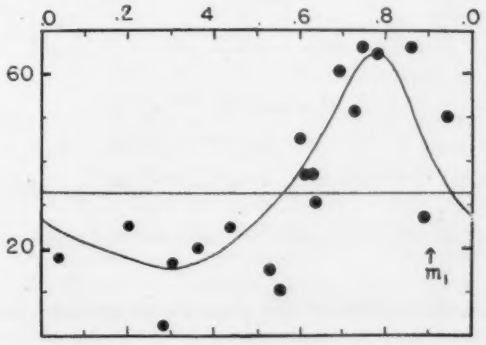

FIG. 1.—Velocity-curve for RX Geminorum; ordinates are radial velocities (km/sec), abscissæ are phases in units of the period.

lower temperature, in conformity with the surface brightness. The velocity-curve shows a possible rotation effect. No doubt the star deserves more attention spectroscopically.

III. PHOTOMETRIC OBSERVATIONS

The photographic observations (1376) will be discussed first. The comparison stars were determined with reference to Selected Area 50, with the stars of 8.55, 10.34, 11.99, 12.00, and 12.08 mag. Eight plates with different exposure time from 60 to 120 minutes were used, and the magnitudes are given in Table 3. The star *x* is the one very close to the

TABLE 3

COMPARISON STARS FOR RX GEMINORUM

Star	Scale	BD	I Pg	Vis
a′	+ 8	34°1458 (9.1)	8.62 ±0.03	8.95
a	+ 4	33°1412 (8.8)	9.00: ± .12	9.26
c	− 6	33°1413 (9.3)	9.96 ± .02	9.51
d	−15	33°1416 (9.3)	10.63 ± .02	9.95
x	−23	.....	11.86 ±0.03	10.98

variable. Some other comparison stars of intermediate brightness were used, which, however, have no BD numbers. The visual magnitudes were determined in reference to the photovisual magnitude given by C. Wirtanen and A. N. Vyssotsky[1] for their field 35°11, together with other sequences.

I have used over twenty minima to investigate the possible correction of the period, over an interval of forty years. The period seems to have been constant until JD 2428000, when it shortened slightly (see Fig. 2).

IV. THE PHOTOGRAPHIC LIGHT-CURVE

All photographic estimations were combined into fifty-one normal points; the light-curve is given in Table 4. The phases φ_0 and φ are the original (referred to JD 2400000),

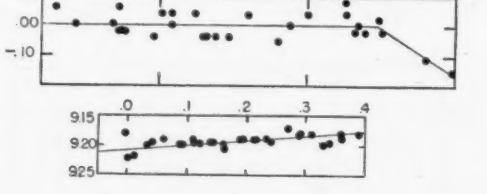

FIG. 2.—Phase of minimum of RX Geminorum (referred to primary minimum of mean light-curve) as a function of Julian Day.

FIG. 3.—Reflection effect for RX Geminorum; ordinates are photographic magnitudes; abscissae are phases.

and the one reduced to the middle of the primary minimum ($\varphi_0 = 0.902$) as the zero point.

There is a definite indication of a reflection effect (see Fig. 3); the correction for the reflection effect has been made with the formula $\Delta m = 0^m.01 \cos \varphi$. The minimum seems to be slightly asymmetrical, the descending branch the steeper.

[1] *Ap. J.*, 101, 141, 1945.

Solutions based on the method of Scharbe[2] for uniform and total darkening were carried out. Both represent the observations well within the observed uncertainty. The probable (or mean) errors can be inferred from the fact that the probable error of a single estimate is between $0^m.09$ and $0^m.12$.

V. VISUAL OBSERVATIONS

The visual observations of eclipsing binaries have until recently been progressively neglected, owing to the efficiency of the photographic observations. But an investigation of thick atmospheres requires independent work in several wave lengths. The system of

TABLE 4

PHOTOGRAPHIC LIGHT-CURVE FOR RX GEMINORUM

φ_0	n	I Pg	φ	φ_0	n	I Pg	φ
$0^p.010$	30	$9^m.21$	$0^p.108$	0.661	34	$9^m.18$	$0^p.759$
.030	38	9.20	.128	.688	30	9.21	.786
.058	43	9.19	.156	.711	24	9.18	.809
.089	29	9.20	.187	.733	42	9.19	.831
.111	29	9.19	.209	.764	45	9.20	.862
.137	41	9.19	.235	.787	40	9.19	.885
.161	33	9.20	.259	.812	27	9.19	.910
.190	31	9.18	.288	.837	36	9.22	.935
.212	30	9.18	.310	.853	17	9.23	.951
.234	24	9.18	.332	.861	14	9.25	.959
.256	31	9.17	.354	.870	16	9.44	.968
.286	32	9.18	.384	.879	12	9.73	.977
.308	44	9.18	.406	.883	12	10.50	.981
.334	35	9.20	.432	.888	11	10.90	.986
.360	54	9.19	.458	.895	8	11.10	.993
.384	32	9.20	.482	.902	10	11.22	.000
.415	36	9.22	.513	.906	8	11.22	.004
.437	29	9.21	.535	.911	7	11.07	.009
.462	32	9.18	.560	.916	7	10.68	.014
.490	59	9.18	.588	.923	7	10.27	.021
.513	22	9.20	.611	.928	12	9.68	.026
.540	30	9.16	.638	.934	16	9.35	.032
.561	28	9.18	.659	.945	13	9.21	.043
.585	26	9.16	.683	.962	21	9.18	.060
.608	41	9.19	.706	0.988	24	9.16	0.086
0.640	24	9.18	0.738				

RX Geminorum consists of an A star and a component of later spectral class. It has a well-defined totality, and the period is 12 days; we might expect a thick atmosphere effect, though not a large one. It is unfortunate that there is no well-observed visual light-curve to be compared with the photographic curve. All that I have are 239 visual observations of Enebo, made more than thirty years ago.[3] The distribution of the observations is rather unfavorable, for the observer had the object of determining the period of the star rather than a reliable light-curve. Since the magnitude scale of comparison stars used by Enebo was not on the international scale, I have determined magnitudes for the reduction of his observations. The reduction has been made with the help of the following relations:

$$S.G. = 9^m.10 + 0.83\ (\text{Enebo} - 8^m.5)$$

[2] *Poulkovo Bull.*, **94**, 31, 1923.

[3] Ark. f. Math. och Naturvidensk. B, Vol. **33**, No. 8, 1913.

to $m = 10^m.18$ and after $m = 10.18$

$$S.G. = 10^m.50 + 1.11\ (\text{Enebo} - 10^m.18)\ .$$

The visual light-curve of RX Geminorum is given in Table 5.

TABLE 5

VISUAL LIGHT-CURVE OF RX GEMINORUM

φ	n	I Pg	φ	n	I Pg	φ	n	I Pg
$0^p.003$.....	5	$11^m.01$	$0^p.323$.....	6	$9^m.22$	$0^p.828$.....	6	$9^m.22$
.007.....	5	10.78	.353.....	6	9.21	.882.....	6	9.20
.012.....	5	10.55	.409.....	6	9.25	.909.....	7	9.30
.026.....	5	10.19	.443.....	6	9.29	.945.....	5	9.32
.031.....	5	9.32	.476.....	6	9.23	.959.....	5	9.26
.036.....	5	9.24	.522.....	7	9.23	.965.....	5	9.34
.046.....	5	9.24	.551.....	7	9.31	.969.....	5	9.50
.079.....	10	9.25	.598.....	6	9.23	.974.....	5	9.75
.123.....	2	9.32	.634.....	6	9.25	.977.....	5	10.09
.158.....	9	9.21	.673.....	9	9.27	.979.....	5	10.16
.192.....	9	9.24	.714.....	8	9.21	.982.....	5	10.24
.227.....	9	9.28	.754.....	7	9.26	.986.....	5	10.51
0.270.....	10	9.22	0.806.....	8	9.23	0.993.....	5	10.71

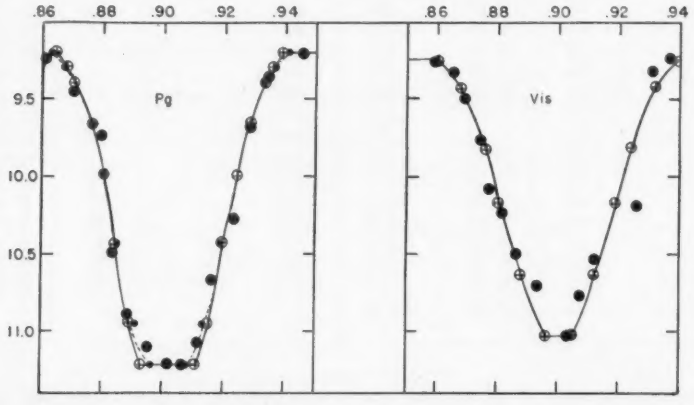

FIG. 4.—Primary minima of RX Geminorum. Large dots represent normals, small dots, computed (*D*) curve; circled crosses, computed (*U*) curves.

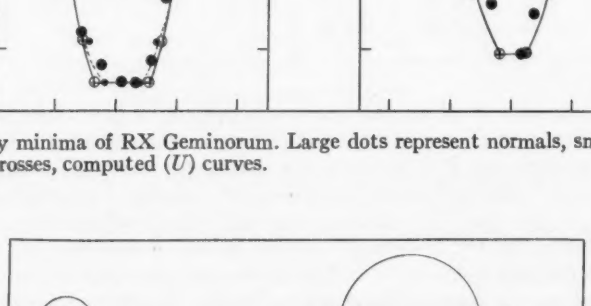

FIG. 5.—Relative dimensions for the system of RX Geminorum

A uniform solution was carried out for this light-curve, exactly as for the photographic light-curve. The results for the several solutions are summarized in Table 6.

VI. DISCUSSION

The system RX Geminorum is a normal one in respect to period, range, and photometric and spectroscopic elements. In order to see the whole interplay of the components we must consider the absolute dimensions. By applying the mass-luminosity relation, together with the relative elements for (*D*) solution, we find a mass for the A4 component equal to 3.1⊙; radius, 2.9⊙; and the visual absolute magnitude, +1.1. We find the spectral class of the larger component by using the ratio of the surface brightness (γ = 30.9) and the arbitrarily adopted photographic surface brightness $3^m.4$ for the brighter component. The deduced spectrum is K0. With this spectral class and with the relative radius we can find the mass and radius of this component. But similar dimensions can be found from the A4 component and relative elements and from the mass function, by

TABLE 6

PHOTOGRAPHIC AND VISUAL ELEMENTS OF RX GEMINORUM

	PHOTOGRAPHIC (1376 OBSERV.)		VISUAL (239 OBSERV.)
	U	*D*	*U*
Ratio of radii	0.34	0.40	0.38
Radius of A star	0.065	0.075	0.075
Radius of K star	0.192	0.188	0.198
Light of A star	0.84	0.84	0.82
Light of K star	0.16	0.16	0.18
Ratio of surface brightness	46.1	30.9	30.9
Inclination	83.5	83.9	83.0
Spectrum of the smaller star	A4	A4	A4
Spectrum of the larger star	K4*	K4*	K4*
Maximum brightness	$9^m.20$	$9^m.20$	$9^m.25$
Minimum brightness	11.22	11.22	11.01
Eclipse	Total	Total	Total

* From surface brightness.

adopting a mass of 3.1⊙ for the A4 component. Table 7 gives the intercomparison of the results.

According to Table 7, the system is a combination of two stars, of which one is on the main sequence in every respect—spectrum, A4; mass, 3.1⊙; radius, 2.5⊙; and luminosity, $+1^m.1$; the other is a typical subgiant of spectral class K0 with a radius of 5.5⊙ and luminosity $+2^m.7$ but with mass probably less than that of the sun. The large red star totally eclipses the smaller one for 3.4 hours; but the spectrum remains practically the same as at maximum, A4. The color index $0^m.21$ at the minimum indicates also that the spectral class is near A. This system is not the first one for which such a discrepancy (A5 observed and K0 predicted) has been found, but it is one of the most conspicuous. Wyse,[4] who first called attention to the fact that the spectrum during primary minimum is of class A, suggested tentatively the presence of a third body. Wyse's spectrum was taken entirely within totality: our spectrum, centered at phase 0.886, is still within the partial phase but at a time when 0.878 of the brighter component is covered. If the luminosity found in our solution is adopted, the "K component" is found to be half a magni-

[4] *Lick Obs. Bull.*, No 464, 1934.

tude brighter than the uneclipsed portion of the A component at this time. The photographic magnitude at the phase in question is 10.60.

An alternative explanation, which must be explored, is that the eclipse is annular and not total. An annular eclipse seems, however, to be ruled out by the photographic light-curve; and Enebo's visual light-curve is not good enough to carry much weight. From the observed duration of eclipse and totality, we find, for an annular eclipse, $k = 0.81$.

TABLE 7

ABSOLUTE DIMENSIONS OF RX GEMINORUM

	A4 Component	K0 Component
Mass	3.1 ⊙*	2.4 ⊙* 0.8 ⊙†
Radius	2.9 ⊙* 2.20⊙†	6.6 ⊙* 7.2 ⊙‡ 5.50⊙†
Absolute visual magnitude	+1.1*	+2.1 * +2.7
Ratio of masses	.....	0.20§

* From mass luminosity and the light-curve.
† From mass function and k.
‡ From mass function, radius of A4, and k.
§ From mass of A4 (3.1) and mass function (0.018).

From the depths of the two minima for the annular case, $k = 0.93$ (secondary minimum of depth 0^m02) or $k = 0.92$ (secondary minimum inappreciable). The shape of the minimum is incompatible with such a high value of k; the largest value that can be deduced is 0.72. This value is impossible because it leads to a negative inclination. For the darkened solution the matter is even worse. In other words, the system remains a puzzle.

The writer extends his thanks to Dr. Struve for the opportunity to work at the McDonald Observatory in December, 1944.

THE ECLIPSING SYSTEM RY GEMINORUM

SERGEI GAPOSCHKIN
Harvard College Observatory
Received August 3, 1946

ABSTRACT

The eclipsing system RY Geminorum has been studied from 13 spectrograms of the McDonald Observatory, 1667 photographic patrol plates of the Harvard College Observatory, and 73 visual observations of Beyer. Outside eclipse the spectrum shows only one component, of class A2. During the total minimum the spectrum of the fainter, larger, and less massive is K2. Orbital velocities were obtained only for the brighter component (A2); the spectroscopic elements are: $V_0 = +9.0$ km/sec; $K = 30.0$ km/sec; $a \sin i = 4.0 \times 10^6$ km $= 5.75 \odot$; and $f = 0.022 \odot$. The photographic elements for the (*D*) solution are: Max. $= 8^m52$; $A_1 = 2^m80$; $A_2 = ?$; $k = 0.42$; $r_A = 0.086$; $r_K = 0.205$; $i = 85°.0$; $\gamma = 64.6$; $L_A = 0.92$; $L_K = 0.08$; Sp_K = K2 (predicted); and $P = 9^d30090$. The visual light-curve is less well determined, but the minmum is fully covered with observations. Its elements are: Max. $= 8^m45$; $A_1 = 2^m00$; $A_2 = ?$; $k = 0.35$; $r_A = 0.079$; $r_K = 0.225$; $i = 80°.4$; $L_A = 0.84$; $L_K = 0.16$; $\gamma = 42.5$ for (*U*); and the color index during the totality is 0^m87. The comparison between the spectroscopic and the photometric observations indicates a satisfactory agreement. There is a definite eccentricity of the spectroscopic orbit. The comparison between the visual and the photographic dimensions (*U*) indicates the possibility of a thick atmosphere. Like RX Geminorum, this system consists of a main-sequence and a subgiant star.

I. SPECTROSCOPIC OBSERVATIONS

At the McDonald Observatory in December, 1944, I obtained 13 spectrograms of the eclipsing system RY Geminorum, of period 9 days.

The spectrum of the brighter component presents a beautiful series of hydrogen lines and metallic lines, which are sharp and indicate giant characteristics. The spectrograms were measured by the author and reduced by Mrs. Payne-Gaposchkin. The velocities are given in Table 1. The number of the plates is not large, but they are well distributed over the whole period of the variation. One plate is taken at the time of totality. The blue end of the spectrum has weakened greatly, and some new metallic lines appear in the red

TABLE 1

RADIAL VELOCITIES OF RY GEMINORUM IN KM/SEC

JD	Phase	Mean (Km/Sec)	*H*	*Fe* II	*Ti* II	*Ca* II
31431.014	0.349	−24.4	− 3.5	−34	−30	−30
439.948	.310	−12.1	−12.5	−32	+ 3.5	−11
440.017	.425	− 3.5	− 5.5	+ 1	−12	+ 1
441.917	.522	+10.0	− 3	+11	+ 3	+22
442.874	.625	+23.0	+20.0	+12	+18	+41
443.876	.732	+50.4	+38	+43	+43	+60
444.963	.849	+32.7	+40	+37	+32	+66
445.912	.951*	−20.3	−21	.....	.....	.....
446.908	.058	+ 0.5	− 1.5	+11	−17	+16
448.836	.266	− 9.8	− 6	−14	−32	−11
455.871	.022	+ 6.4	− 3.5	+ 4	− 6.5	+13
456.810	.123	− 0.6	+ 3.0	−16.5	+ 1	+10
458.726	0.329	−24.1	−16.5	−38	−32	−14

* At minimum.

end. The spectrum is definitely of late type; my estimate is K2. The spectroscopic elements are almost a copy of those of the system RX Geminorum, with which RY Geminorum shows great similarity. They were derived by the method of Lehmann-Filhés (see Table 2).

II. PHOTOGRAPHIC OBSERVATIONS

The 1667 photographic estimations were obtained on the Harvard patrol plates, covering an interval of forty-five years. The estimations of minima have been used to check

TABLE 2

SPECTROSCOPIC ELEMENTS FOR RY GEMINORUM

$a \sin i$	$= 4.00 \cdot 10^6$ km	V_0	$= +\ 9.0$ km/sec
f	$= 0.022$	K_2	$=\ 30.0$ km/sec
Spectrum	$=$ A2 + K2	P	$= 9^d30090$

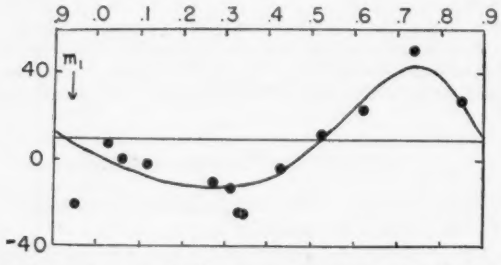

FIG. 1.—Velocities of RY Geminorum. Ordinates are radial velocities in km/sec, abscissae are phases in units of period.

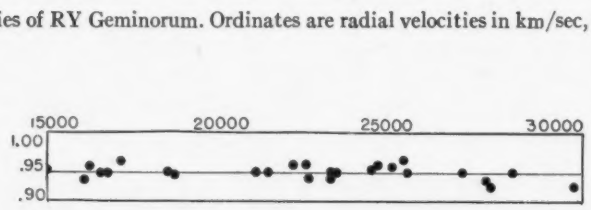

FIG. 2.—Phase of minimum of RY Geminorum as a function of Julian Day

the period of 9^d30090. As is seen from Figure 2, no correction is needed. The photographic light-curve reduced with the above period is given in Table 3.

The magnitudes are on the International scale and were obtained by comparison with Harvard Standard Region C4. The comparison stars are given in Table 4.

The photographic light-curve exhibits one of the largest ranges known. No secondary minimum is indicated by observations. Primary minimum is total. The solutions for this light-curve, using Scharbe's method,[1] are given in Table 6. At the bottom of the minimum the (*D*) solution is better than the (*U*) (see Fig. 3).

III. VISUAL OBSERVATIONS

A system like RY Geminorum, with two widely different components and a rather long period, may furnish a good case for the study of a thick atmosphere, by comparing the relative dimensions obtained in the photographic and the visual wave lengths. Unfortunately, as with RX Geminorum, there is no well-observed visual light-curve.

[1] S. Scharbe, *Poulkovo Bull.*, **94**, 31, 1923.

We have 73 visual observations by Beyer,[2] of which 63 are within a minimum. I have investigated the visual magnitudes of Beyer and found that they are close to the International scale: $8^m.35$ of Beyer corresponding to $8^m.45$ of Gaposchkin, and 10.35 of Beyer corresponding to $10^m.45$ of Gaposchkin. The visual solutions were carried out with the same method as the photographic solutions.

TABLE 3

PHOTOGRAPHIC LIGHT-CURVE OF RY GEMINORUM

Phase	No. Obs.	I Pg	Phase	No. Obs.	I Pg	Phase	No. Obs.	I Pg
$0^p.015$*	40	$8^m.52$	$0^p.462$	27	$8^m.53$	$0^p.902$	11	$8^m.68$
.034	48	8.53	.490	54	8.53	.907	10	8.93
.060	63	8.52	.512	47	8.52	.911	8	9.53
.086	31	8.52	.538	36	8.52	.917	7	9.94
.110	34	8.50	.563	38	8.53	.922	10	10.37
.133	49	8.50	.586	37	8.52	.926	9	11.13
.163	32	8.50	.612	31	8.54	.932	4	11.21
.187	41	8.50	.636	41	8.53	.937	8	11.33
.210	47	8.50	.660	45	8.53	.942	6	11.32
.237	39	8.53	.686	49	8.53	.947	4	11.33
.263	42	8.50	.710	36	8.49	.953	4	10.95
.284	41	8.50	.734	53	8.52	.957	7	10.81
.312	44	8.54	.761	33	8.52	.962	7	10.12
.336	52	8.50	.784	45	8.50	.970	4	9.53
.362	37	8.54	.812	51	8.53	.971	3	8.96
.387	47	8.52	.841	39	8.53	.974	6	8.71
.413	54	8.52	.863	42	8.53	0.987	23	8.57
0.438	40	8.52	0.888	45	8.57			

* Computed with $\varphi_0 = 1/P$ (JD -2400000).

TABLE 4

COMPARISON STARS (PHOTOGRAPHIC)

Star	I Pg	P.E.	Star	I Pg	P.E.
a	$8^m.39$	± 0.05	d	$10^m.17$	± 0.03
b	8.68	$\pm$ .03	e	10.65	$\pm$ .02
c	9.25	± 0.06	f	11.41	± 0.04

TABLE 5

VISUAL LIGHT-CURVE OF RY GEMINORUM

Phase	Mag.	No.	Phase	Mag.	No.	Phase	Mag.	No.
$0^p.883$	$8^m.45$	1	$0^p.935$	$10^m.50$	6	$0^p.967$	$9^m.56$	4
.892	8.58	2	.942	10.42	12	.974	8.99	3
.906	8.89	6	.950	10.43	8	0.982	8.54	2
.918	9.76	3	.954	10.37	5			
0.928	10.29	5	0.959	10.09	6			

[2] *A.N.*, **234**, 88, 1928.

IV. THE RELATIVE DIMENSIONS

Comparing, now, the photographic dimensions with those from the visual light-curve, we find a small difference, as in the case of the very similar system RX Geminorum. The difference is of the same amount (4 or 5 per cent) for the two systems and in the same direction. It is small, and future photometric observations will be required to confirm its reality (see Table 6).

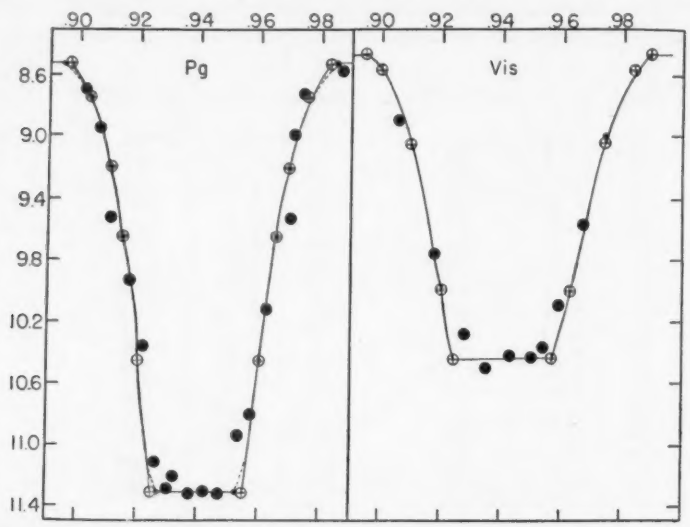

FIG. 3.—Primary minima of RY Geminorum. Large dots represent normals; small dots, *D* solution; circled crosses, uniform solution. Ordinates are I Pg and I Pv; abscissae are phases.

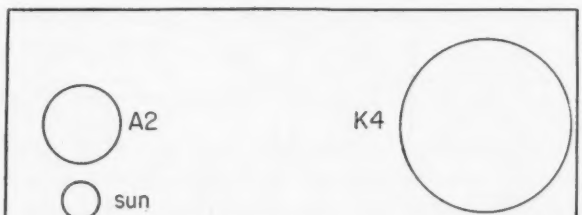

FIG. 4.—Relative dimensions in the system RY Geminorum

V. DISCUSSION

The system RY Geminorum is a twin of the system of RX Geminorum. Both consist of widely different components: a main-sequence star and a subgiant, revolving around each other in about the same period. The similarity of the two systems can be seen from Table 7. Both systems show large ranges of light-variation: $2^{m}.02$ for RX Geminorum and $2^{m}.80$ for RY Geminorum, with total eclipses. Also both have shown some indications that point to the existence of thick atmosphere. But there is one marked difference—the fact that, while the observed spectrum during the totality of RY Geminorum is in full

agreement with the color class, predicted from the ratio of surface brightness and the color index (k2 and K2), this is not the case for RX Geminorum (a5 and K0). The observed radial velocities of the centers of gravity of the systems are +9.0 for RY Geminorum and +33.5 for RX Geminorum.

If we compare these two systems with that of AS Eridani[3] period of 2^d.66, we see a great similarity in the spectrum, mass, radius, and luminosity of the brighter component (A); but, in respect to the fainter one, a conspicuous difference exists. Both fainter components in RX and RY Geminorum are of intermediate luminosity between giant and main sequence, while that of AS Eridani is on the main sequence.

TABLE 6

RELATIVE DIMENSIONS OF RY GEMINORUM

	PHOTOGRAPHIC		VISUAL		PHOTOGRAPHIC		VISUAL
	U	*D*	*U*		*U*	*D*	*U*
r_1	0.211	0.205	0.225	L_2	0.92	0.92	0.84
r_2	0.074	0.086	0.079	L_1	0.08	0.08	0.16
k	0.35	0.42	0.35	i	84.2	85.0	84.4
γ	93.9	64.6	42.9	Spectrum$_1$	K5	K2	.....

TABLE 7

COMPARISON OF RX AND RY GEMINORUM

	RX Gem	RY Gem		RX Gem	RY Gem
Period	12^d.21	9^d.30	$a \sin i$	$4.07 \cdot 10^6$ km	$4.00 \cdot 10^6$ km
Spectra	A4, K0	A2, K2	Masses	3.1, 0.62⊙	3.5, 0.70⊙
Mass function	0.018⊙	0.022⊙	Radii	2.2, 5.5⊙	2.7, 6.4⊙

The writer extends his thanks to Dr. Struve for the privilege of working for a month at the McDonald observatory.

NOTE.—Since the paper was sent to the printer I have received a letter from Dr. McKellar at the Dominion Observatory (Victoria, B.C., Canada) in which he gives the following radial velocities of the star:

JD	Phase	Velocity
28199.877	0.934	+23 km/sec
209.844	.010	− 2
486.944	.802	+56
533.885	.846	+32.7
815.029	.077	+ 7.0
966.787	.393	− 1.6
982.775	.112	− 3.0
29550.015	0.099	− 6.5

Though the distribution of the velocities over the period is less favorable than my own, they confirm my results. An interesting plate is at phase 0.934 (during totality), 1^{h}20^m before the middle of the eclipse. My plate at the phase 0.951 was taken 2^{h}20^m after the middle of the eclipse. The respective velocities are +23 and −20.3 km/sec.

[3] S. Gaposchkin, *Harvard Bull.* (in press).

SOME RADIAL-VELOCITY AND LINE-INTENSITY MEASURES IN THE SPECTRUM OF β CANIS MAJORIS*

ANNE B. UNDERHILL
Yerkes and McDonald Observatories
Received August 8, 1946

ABSTRACT

Coudé plates of β Canis Majoris taken in February and March, 1942, have been measured for radial velocity. The observations of February 13 and March 4 cover the 6-hour period nearly completely. The amplitude of the velocity-curve and γ velocity vary, being 20 and 26.8 km/sec, respectively, on February 13, and 7 and about 31 km/sec on March 4. A variable amplitude is in accord with previous observations. A variable γ velocity is consistent with Henroteau's observations of 1922. A period of 0.252809 day connects the present velocity-curves and that obtained by Struve and Swings in 1941. The times of maximum and minimum radial velocity agree with those predicted by Meyer's formula. The line-quality changes follow the previously established period of 0.2513015 day. The line-sharpness period and the radial-velocity period are distinct.

The central absorptions and equivalent widths of the *O* II and *H* lines vary slightly over the 6-hour cycle, being largest at times of sharpest lines. The variation in the *He* I lines is less conspicuous, being of the order of the probable errors of the measurements. Curves of growth show that the *O* II ions and *He* I atoms have zero or very small turbulent velocity. The populations of the *He* I levels and the *O* II levels investigated are close to the values found by Unsöld for the B0 dwarf, τ Scorpii.

The star β Canis Majoris is known[1] to show radial-velocity changes of varying amplitude with a period of about 6 hours. The quality of the spectral lines changes periodically also, the lines being sharp and deep at times and quite diffuse at other times. A variation of 0.03 mag. in light in about 6 hours has been found by Fath.[2]

The purpose of this investigation is to ascertain whether the period of the line sharpness and the period of the velocity changes are identical and to obtain an estimate of the turbulent velocity from curves of growth. The lines show considerable turbulent broadening.

This investigation is a sequel to the work of Struve and Swings,[3] which was based on a series of coudé spectrograms taken at the McDonald Observatory in January, 1941. Further plates of β Canis Majoris were taken by Swings and Struve at McDonald with the coudé spectrograph, series of plates, each extending over practically the full 6-hour period, being taken on February 13 and March 4, 1942. These plates form the basis of the following discussion.

I. RADIAL-VELOCITY MEASUREMENTS

All the plates were measured for radial velocity. Since the plates are too long to be accommodated all at once in the measuring engine, the plates were taken in sections, three regions on each plate being measured and reduced separately, and then a mean velocity for the plate was derived from the mean velocity of each region. To obtain the mean velocity of the plate, the mean velocity of each section was weighted according to the number of lines measured in that section. The velocities from each section agreed within their probable error.

Table 1 gives details regarding the regions measured. Most of the lines used were *O* II and *He* I lines. The hydrogen lines were not used for determining the mean velocity

* *Contributions from the McDonald Observatory, University of Texas*, No. 128.

[1] Henroteau, *Lick Obs. Bull.*, **9**, 157, 1918; *Pub. Dom. Obs.*, **8**, 31, 1922; Meyer, *Pub. A.S.P.*, **46**, 202, 1934.

[2] *Lick Obs. Bull.*, **17**, 116, 1935.

[3] *Ap. J.*, **94**, 99, 1941.

TABLE 1

REGIONS MEASURED FOR RADIAL VELOCITY

Region	Wave-Length Range	Dispersion (A/Mm)	Source of Stellar Wave Lengths
I.....	3950–4036	At Hϵ, 2.01	Kühlborn, *Veröff. Univ. Sternw. Berlin-Babelsberg*, Vol. 12, No. 1, 1938
II.....	4068–4188	At Hδ, 2.51	Struve and Swings, *Ap. J.*, **94**, 99, 1941
III.....	4337–4529	At Hγ, 3.52	*Ibid.*

TABLE 2

RADIAL-VELOCITY MEASURES

Plate Cd	Date 1942	U.T. (Days)	No. of Lines	Velocity (Km/Sec)	Phase ($P = 0^d.252809$)	Line Quality
193.....	February	13.049	43	+25.2	0.000	3
194.....		13.088	47	32.8	0.154	3
195.....		13.123	51	35.6	0.292	5
196.....		13.150	56	36.6	0.399	2
197.....		13.169	44	30.6	0.474	2
198.....		13.190	45	27.1	0.557	1
199.....		13.207	41	23.4	0.624	1
200.....		13.228	42	17.0	0.707	2
201.....		13.257	50	17.0	0.855	2
219.....	March	4.097	54	33.7	75.345	3
220.....		4.123	47	31.5	75.448	4
221.....		4.149	56	28.9	75.551	4
222.....		4.168	56	28.0	75.626	5
223.....		4.201	53	28.9	75.756	4
224.....		4.239	37	27.8	75.906	1
227.....		5.059	53	31.7	79.151	2
228.....		5.077	49	32.5	79.222	3
233.....		6.056	50	33.5	83.094	3
234.....		6.077	45	+32.5	83.177	2
	Struve and Swings's Measures					
	1941					
65.....	January	24.104	68	+38.17	−1522.671	.....
66.....		24.137	62	35.39	1522.541	.....
67.....		24.168	54	29.85	1522.418	.....
68.....		24.203	53	25.74	1522.270	.....
69.....		24.235	47	25.55	1522.144	.....
70.....		24.264	49	28.64	1522.029	.....
71.....		24.287	51	30.83	1521.938	.....
72.....		24.313	51	31.99	1521.835	.....
73.....		24.342	51	+34.83	−1521.720	.....

ERRATA

Owing to an error in the reductions, the velocities obtained from plates Cd 193–201, inclusive, should be increased by 2.8 km/sec; those from plates Cd 219–228, inclusive, should be increased by 1.4 km/sec; and those from Cd 233 and 234 should be increased by 1.3 km/sec. The γ velocities are now +29.6 km/sec on February 13, 1942, and +32.4 km/sec on March 4, 1942. Agreement is still not obtained with the Lick observations of a constant γ velocity of +34 km/sec for the system β Canis Majoris.

of each section. An attempt was made to measure all the lines listed by Kühlborn[4] or by Struve and Swings[3] for each section; but the number of lines measured varies from plate to plate quite considerably, as the line quality changes over the 6-hour cycle. This variation of line quality was noted by the previous investigators and is quite conspicuous on the present plates, since it is possible to measure many more lines at epochs of sharpest lines than at epochs of very diffuse lines.

Table 2 gives the radial-velocity measures reduced to the sun. The γ velocities obtained from these short-period radial-velocity changes are +26.8 km/sec on February 13, 1942; +31 km/sec on March 4, 1942; and +31 km/sec on January 24, 1941. Struve and Swings's measures are reproduced here, as they will be used to supplement the new material. The observations of January 24, 1941, and March 4, 1942, do not extend over quite a whole cycle, hence the γ velocity is estimated from the appearance of the section of velocity-curve available.

A varying γ is in accord with Henroteau's[1] observations of 1922, which indicate that there is a short-period velocity variation of changing amplitude superimposed over a systemic velocity, which changes with a 42-day period. If the γ velocity from Struve and Swings's measures is put on the descending branch of Henroteau's curve for γ velocity, the more recent measures fall on the curve pretty well. There is not sufficient evidence to define the curve any better than Henroteau has done. The present observations are not consistent with a constant γ velocity of 34 km/sec, as reported by Meyer[1] from a study of the plates obtained at the Lick Observatory.

It was found that a period of 0.252809 day satisfactorily connects the short-period velocity-curves over about 1600 cycles, which is the scope of the observations discussed here. Time, t_0, is taken arbitrarily at 1942, February 13.049, U.T., and the phase of each plate for a period of 0.252809 day is given in the sixth column of Table 2. Figure 1 shows a plot of the three most nearly complete series of measures. Maximum velocity occurs at phase 0.335. The long-period change in amplitude and γ velocity of these short-period velocity-curves is evident. According to Meyer, the amplitude changes with a period of 49.1 days.

In the seventh column of Table 2 are given visual estimates of the line quality. These estimates are based on a scale of 5, the value 1 being given for broad, diffuse lines, which show no central core; 5 to lines which have a sharp, narrow core and very small wings. Value 3 is halfway between 1 and 5, the lines showing some core, but also fairly diffuse wings. Values 2 and 4 are intermediate between 1 and 3, and 3 and 5, respectively. No definite asymmetries were noticed in the lines.

Small arrows in Figure 1 indicate the epochs of sharpest lines. These times are consistent with the period of 0.2513015 day, which was established by the Lick[1] observations. The times of sharpest lines are not in phase with the epochs of maximum velocity. Plate XIV shows the group of *O* II lines near $H\gamma$ and illustrates the change in appearance of the lines. On February 13, sharpest lines occurred at phase 0.292 near maximum velocity, whereas the lines are very diffuse at phase 0.624, intermediate to low velocity. On March 4—19 days later—the situation is reversed, sharpest lines occurring at a time of low velocity and quite diffuse lines occurring at the highest velocity measured. This evidence shows that the short-velocity period and the line-width period are distinct, thus confirming the work of Henroteau and that of Meyer.

Figure 2 shows the observed short-period velocity-curves and the curves computed from the formula developed by Meyer[1] to represent the short-period variations. In order to make the comparison as convenient as possible, the calculated velocities have been plotted around the observed γ-axis in each case rather than around the constant γ-axis of 34 km/sec found by Meyer. It is seen that Meyer's formula predicts time of maximum and minimum very well in these three cases, though the fit in the intermediate part of the

[4] *Veröff. Univ. Sternw. Berlin-Babelsberg*, Vol. 12, No. 1, 1938.

PLATE XIV

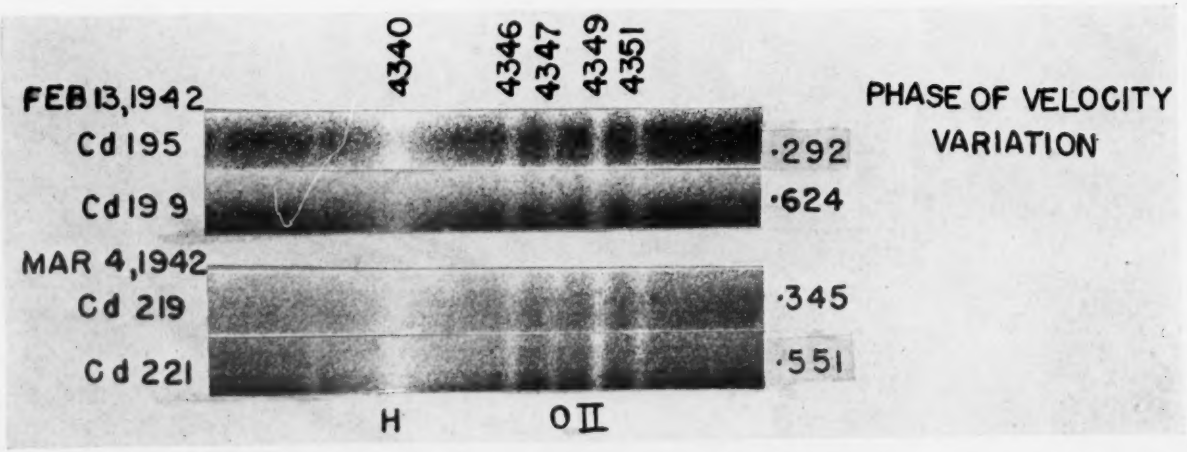

LINE-WIDTH CHANGES IN THE SPECTRUM OF β CANIS MAJORIS

curves is not quite so good and the amplitudes are not quite right. Neither of the periods of 0.2513015 day and 0.2500222 day, which are combined by Meyer, will fit the radial-velocity observations when used singly.

The radial-velocity measurements suggest that β Canis Majoris is a pulsating star of short period. Upon these variations is superimposed a velocity variation of period of about 42 days, which could be interpreted as binary motion around an invisible companion but also might be similar to the long-period radial-velocity variation shown in some RR Lyrae-type stars to be superimposed over the short-period fluctuations. It

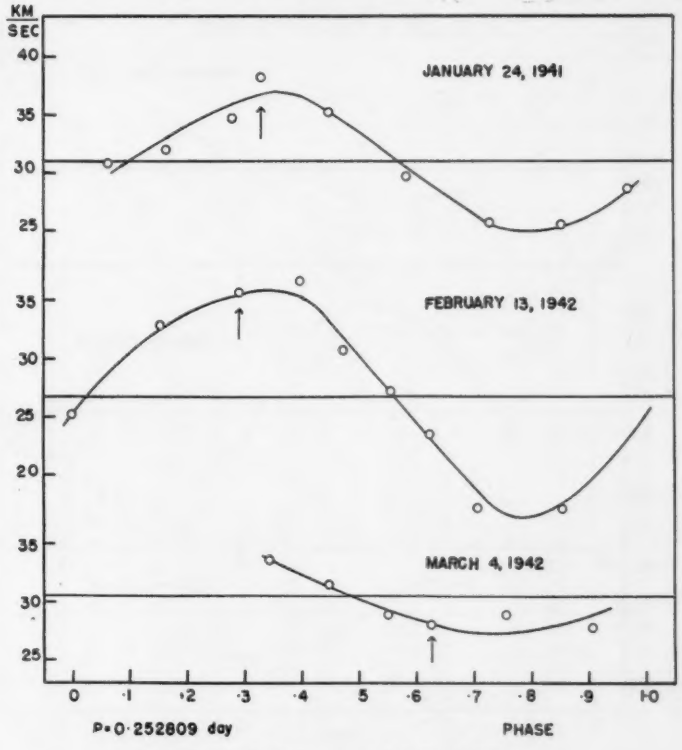

FIG. 1.—Velocity-curves of β Canis Majoris

seems likely that the difference in period between the radial-velocity changes and the changes in line shape, as well as the varying amplitude of the radial-velocity-curves, is connected with the long-period variation.

II. EQUIVALENT-WIDTH MEASUREMENTS

Equivalent widths of the *He* I lines, the *H* lines, and the lines of the 3s — 3p transition array of *O* II were derived from the most suitable plates. The equivalent widths of the *O* II and the *H* lines are greatest at the times of sharpest lines. The change in equivalent widths of the *He* lines is indeterminate, being of the order of the probable error of the measures. The measured central absorptions of the lines were found to vary over the cycle, being greatest at epochs of sharpest lines. The effect is most noticeable for the *O* II lines and less conspicuous for the *He* I and *H* lines.

The individual measures of equivalent width and central absorption are given in Table 3. The equivalent widths are given in milliangstroms and the central absorptions

in percentages. No attempt has been made to correct these central absorptions for instrumental profile; however, for any given line they are indicative of the true change in central intensity, though direct comparison of lines of widely different wave length and total absorption would be hazardous. The equivalent width measure is W; the central absorption is A_c. The *O* II lines are arranged in multiplets of the 3s — 3p transition array;[5] and the *He* I lines are arranged according to series. The measures for plates Cd 221 and 195 are put side by side, since the lines are sharp in these cases. The lines are visually quite diffuse on the other plates, Cd 196, 197, 200. The last two columns of the table

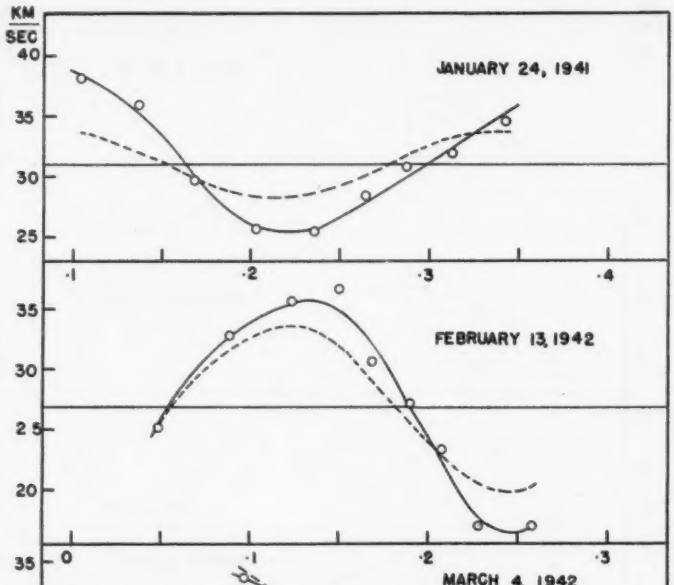

FIG. 2.—Comparison of observed velocity-curves and those predicted by Meyer's formula. The calculated values have been plotted around the observed γ axis, instead of around $\gamma = 34$ km/sec, as given by Meyer.

give, respectively, the mean of the Cd 195 and 221 measures, and the mean of the measures from plates Cd 196, 197, 200.

The measures for the *O* II line λ 4367 are very uncertain, as this line was very weak, and are not used in constructing the curve of growth. The measures for the *He* I line λ 3965 and the *O* II line λ 3973 are also rather uncertain, as these lines lie in the wings of $H\epsilon$ and most of the plates were rather thin in this region. When a line fell in the wing of a *H* line, the wing was taken as the continuum for that line. A correction for the blending effect of hydrogen was not attempted. The lines λ 3965 and λ 3973 were used in constructing curves of growth; but, in placing the theoretical curve, little weight was given to them.

[5] *Zs. f. Ap.*, 21, 22, 1942; *Revised Multiplet Table*, p. 8, 1945.

These line-intensity observations are directly comparable with those obtained by R. M. Petrie[6] in a study of HD 199140, a β Canis Majoris star, and confirm his conclusions about the variation in central intensity and slight change in equivalent width of the lines over the short period. No conclusion can be drawn from the present observations as to the reality of a change in spectral class. Furthermore, the present data show that the period of line-quality change is distinct from that of the short-period velocity changes in β Canis Majoris, although a similar difference does not appear to be reported for HD 199140.

TABLE 3

EQUIVALENT-WIDTH MEASURES

λ	Element	Individual Values										Mean Values			
		Cd 221		Cd 195		Cd 196		Cd 197		Cd 200		Sharp Lines		Diffuse Lines	
		W	A_c	*W*	A_c	*W*	A_c	*W*	A_c	*W*	A_c	*W*	A_c	*W*	A_c
3973....	*O* II	85	17	91	15	.....	.....	88	17	117	16	88	16	102	16.5
3983....		63	14	51	10.5	.....	.....	54	10	53	10	57	12	54	10
4317....		210	28	181	29	122	19	126	20	142	22	195	28.5	130	20
4320....		178	30	176	29	146	21.5	162	21	139	22	177	29.5	149	21.5
4326....		59	13	109	15	56	10.5	96	12	67	10.5	84	14	73	11
4337....		65	10	93	15	67	11	78	8	71	9	79	12.5	72	9
4346....		166	25.5	160	25.5	108	21	179	28	123	15	163	25.5	137	21
4349....		277	38	290	40	258	32	290	33	227	29	284	39	258	31
4367....		44	7	29	12	.....	.....	65	8	27	4	36	7	46	6
4347....		128	16	174	23.5	101	14	124	16	149	18	151	20	141	18
4351....		169	25	174	31	156	19	141	19	156	21	171	28	156	30
4415....		246	36	273	39.5	224	27.5	304	33	237	28	260	38	255	29.5
4417....		208	34	190	34.5	182	25.5	241	27	200	22	199	34	208	25
4452....		124	15	127	17	84	14	93	11	72	11	126	16	83	12
4026....	*He* I	546	33.5	610	36	662	41	738	37.5	493	31.5	578	34.5	631	36.5
4471....		754	57	929	56	718	44	770	52	689	46	842	56.5	726	47
4009....		265	19	260	21.5	200	20	216	18	184	16	262	20	200	18
4144....		297	28	333	31.5	398	30	358	28	366	29.5	315	30	374	29
4388....		.....	.....	543	42	470	34	544	39.5	487	36	543	42	500	36.5
3965....		113	21	113	18	.....	.....	112	14.5	133	21	113	19.5	122	18
4169....		97	14	116	15	114	14	94	12	141	14.5	107	14.5	116	13.5
4437....		137	23.5	112	17	102	14	97	14	116	15	124	20	105	14
3970....	*H*	1649	40	1725	41	.....	.....	1822	43	1471	38	1687	40.5	1646	40.5
4101....		.....	.....	2610	52	2310	48	2124	45	1925	43	2610	52	2120	45
4340....		3057	54	2980	57	2522	48	3434	50	2198	48	3018	56	2718	49

Curves of growth were constructed from the *O* II lines (Fig. 3, *a*) and the *He* I lines (Fig. 3, *b*) by plotting $\log W/\lambda$ against $\log g_i f\lambda - (5040/T)\chi_i$. Here g_i is the statistical weight of the lower level of the line, χ_i the excitation potential of that level, and T the temperature. A temperature of 25,200° is assumed. The solid curve is the theoretical curve of growth computed in each case from the approximate equations quoted by Goldberg.[7] Mean equivalent widths from plates when the lines are sharp and from plates when the lines are diffuse have been plotted separately. The theoretical curves can be fitted to the observations without any vertical shift, thus indicating that the *O* II and *He* I atoms have small turbulent velocities.

[6] *Pub. A.S.P.*, **9**, 53, 1939; *J.R.A.S. Canada*, **40**, 149, 1946.

[7] *Ap. J.*, **89**, 623, 1939.

The total width in angstroms of the *O* lines was measured on the profiles, at a depth equal to half the central absorption. The mean width at half-absorption of all the lines corresponds to a velocity range of 45 km/sec. The width is slightly more when the lines are diffuse and slightly less when the lines are sharp; but the accuracy of the measurements is not sufficient to warrant treating the two cases separately. Greenstein[8] has shown that the effective resolving-power of the coudé spectrograph is about 35,000, corresponding to a $\Delta\lambda$ of 9 km/sec at 4300 A. The thermal velocity of the *O* II ions is

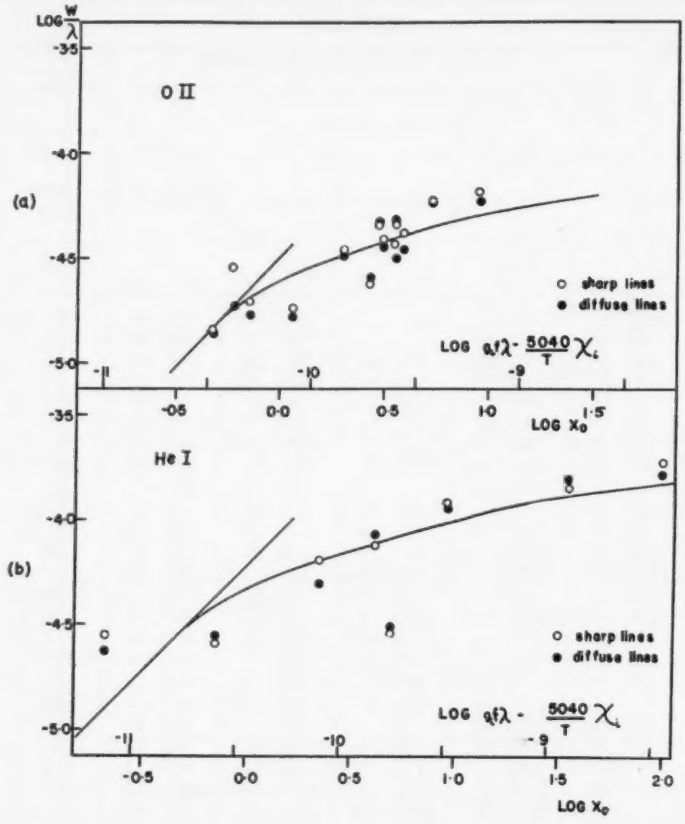

FIG. 3.—Curves of growth: *a*, 3s—3p transition array of *O* II; *b*, all available *He* I lines

5.1 km/sec at 25,200°. Thus some other broadening agent beyond thermal motion and finite resolving-power of the spectrograph must be found to account for the observed width of the lines. It is suggested that motion of optically thick sections of the atmosphere causes the broadening which is observed. The intensity of the line is not affected by these mass motions, since, within the range of depth in the atmosphere in which the line is formed, the atoms have only thermal motions. However, when the integrated starlight from all over the disk is observed, the parts of the line formed in each element of atmosphere are seen displaced to the violet or to the red according to whether the element in which the line was formed was expanding or contracting, and hence a broadened profile is obtained. The curve of growth is not affected, since the absorption coefficient of

[8] *Ap. J.*, 95, 194, 1942.

the atoms is not affected by these superimposed motions, any more than it is when the star is in rotation.

Horizontal displacements of the curve of growth give

$$\log \frac{N_a}{b\,(T)} \frac{\pi e^2}{m c} \frac{1}{\sqrt{\pi}} \frac{1}{v} = \log X_0 - \log g_i f \lambda + \frac{5040}{T} \chi_i$$

and thus enable us to estimate the population of the lower levels of the lines. The quality N_a is the number of atoms in the requisite state of ionization; $b(T)$ is the partition function; and v is the thermal velocity of the atoms. The results are given in Table 4. The

TABLE 4

POPULATION OF LEVELS

He I		*O* II	
Level	log *N*	Level	log Nf_{3s-3p}
2^3P.....	15.00	$3s(^3P)^2P$	13.79
2^1P.....	14.59	$3s(^3P)^4P$	14.18
.....	.....	$3s(^1D)^2P$	13.57

total f-value of the 3s − 3p transition array of *O* II is not known, hence only log Nf_{3s-3p} can be determined. It seems likely that f_{3s-3p} is close to 1.

These populations are comparable to those found by Unsöld[5] for τ Scorpii. He found log N = 14.95 for the 2^3P level of *He* I, and log Nf_{3s-3p} = 14.26 for *O* II.

This investigation was undertaken at the suggestion of Dr. O. Struve and owes much to his guidance. The author is grateful for many stimulating discussions with Dr. Struve and with Dr. J. L. Greenstein of problems arising in the course of the investigation and expresses her thanks for their help.

SPECTROGRAPHIC OBSERVATIONS OF RY PERSEI AND RZ OPHIUCHI*

W. A. HILTNER
Yerkes and McDonald Observatories
Received August 5, 1946

ABSTRACT

The eclipsing variables RY Per and RZ Oph have been investigated spectrographically. The velocity-curves for hydrogen and helium in RY Per are not identical. Helium gives a rotational velocity approximately twice that of hydrogen. Satellite lines of hydrogen before first contact suggest that a stream of hydrogen gas flows from the F5 star to the smaller B4 star. RZ Oph shows hydrogen emission at all phases. The emission has its origin in a gaseous ring around the smaller F8 primary star. A significant velocity-curve was not obtained; however, an approximate upper limit for the semi-amplitude has been established.

RY PERSEI

The variable star RY Persei is an eclipsing binary with a period of approximately 1 week. Its variability was discovered by Mme Ceraski in 1906. A number of investigators have observed the light-curve; Nijland[1] established a period of 6.863571 days, and Shapley[2] and Fetlaar[3] have made solutions based on Nijland's observations. Recently Walbach and Gaposchkin[4] published a solution based on a light-curve obtained from estimates on patrol plates. The photographic range observed by them is 2.01 mag. at primary minimum, and a secondary minimum was reported with a depth of 0.01 mag. These observers also noted a periodic change in the period; a sine curve with a semi-amplitude

TABLE 1

WAVE LENGTHS OF STAR LINES FOR RY PERSEI

B4 Star		F5 Star	
H13	3734.37	*Fe* I	4045.79
H12	3750.15	*Fe* I	4063.57
H11	3770.63	*Sr* II	4077.72
H10	3797.90	*Hδ*	4101.75
H9	3835.39	*Fe* I blend	4143.69
H8	3889.05	*Ca* I	4226.95
Hδ	4101.75	*Cr* I+*Ti* II	4289.95
Hγ	4340.48	*Fe* I+*Sc* II	4325.76
Hβ	4861.34	*Hγ*	4340.47
He I	3819.61	*Fe* II+*Cr* I+*Mg* I	4351.84
He I	4026.19	*Fe* I	4384.18
He I	4143.76	*Hβ*	4861.34
He I	4387.93		
He I	4471.48		

* *Contributions from the McDonald Observatory, University of Texas*, No. 129.

[1] *A.N.*, **176**, 172, 1907; **183**, 281, 1910; **231**, 207, 1927; *B.A.N.*, **2**, 231, 1924.

[2] *Contr. Princeton U. Obs.*, No. **3**, 1913.

[3] *B.A.N.*, **3**, 195, 1926.

[4] *Pub. A.A.S.*, **10**, 72, 1940; see also *Harvard Bull.*, No. 915, 1941.

TABLE 2

RADIAL VELOCITIES OF RY PERSEI

PLATE	DATE	U.T.	PHASE (IN DAYS)	RADIAL VELOCITIES (IN KM/SEC)			
				H	*He* I	F Star	*Ca* II K
G*f*/2 6705	1945 Oct.	16.308	0.028	.....	.....	+ 0.4	.....
6706		16.353	0.073	.....	.....	+ 2.6	.....
6707		16.387	0.107	.....	.....	+ 3.8	.....
6708		16.419	0.139	.....	.....	+10.3	.....
6709		16.446	0.147	−39.6	−117.2	.....	.....
6710		16.468	0.169	−39.4	−130.8	.....	.....
6711		16.487	0.188	−43.2	−111.5	.....	− 7.9
6712		16.505	0.206	−43.8	−115.6	.....	+ 0.8
5318	Feb.	25.156	0.218	−51.3	−121.8	.....	−27.1
5366	Mar.	4.079	0.277	−36.2	− 73.6	.....	−11.7
5367		4.091	0.289	−22.4	− 70.5	.....	−11.7
5368		4.107	0.305	−28.8	− 59.0	.....	− 7.9
5468		11.070	0.405	− 1.0	− 17.6	.....	− 6.7
5469		11.082	0.417	+12.3	− 2.4	.....	−25.0
5470		11.097	0.432	− 3.9	− 45.5	.....	− 2.9
5471		11.111	0.446	+ 2.0	− 28.0	.....	− 6.7
CQ 4037	1944 Dec.	5.089	0.514	−12.9	− 97.7	.....	−16.5
G*f*/2 5374	1945 Mar.	5.071	1.269	+13.8	− 67.1	.....	−15.4
5375		5.090	1.288	− 6.1	− 29.6	.....	−19.3
5487		12.070	1.405	− 8.3	− 49.8	.....	−10.3
5488		12.081	1.416	−11.0	− 49.8	.....	−10.3
5489		12.092	1.427	−19.3	− 38.9	.....	−10.3
5490		12.102	1.437	−20.2	− 35.4	.....	−14.1
CQ 4043	1944 Dec.	6.384	1.809	− 0.8	− 72.6	.....	−20.1
G*f*/2 5502	1945 Mar.	13.095	2.430	−10.9	− 70.5	.....	−20.8
CQ 4047	1944 Dec.	7.033	2.458	−20.3	− 43.4	.....	−11.3
4051		7.184	2.609	−17.1	− 54.4	.....	−17.4
G*f*/2 5330	1945 Feb.	28.135	3.197	−15.1	− 40.4	.....	−12.2
5331		28.156	3.218	−14.0	− 37.7	.....	−12.2
5332		28.174	3.236	− 9.9	− 45.7	.....	− 4.6
5396	Mar.	7.106	3.304	−16.4	− 20.0	.....	+ 0.2
5397		7.136	3.334	− 8.3	− 34.6	.....	+ 0.2
CQ 4353	Feb.	22.072	3.998	− 1.7	− 21.6	.....	− 9.0
4354		22.102	4.028	+10.9	− 22.9	.....	− 9.0
G*f*/2 5334	Mar.	1.166	4.228	− 3.2	+ 6.8	.....	−12.1
5406		8.069	4.267	− 5.2	+ 8.4	.....	− 7.2
5407		8.079	4.277	+ 2.8	− 18.5	.....	− 7.2
5408		8.090	4.288	+15.2	+ 60.6	.....	− 3.5
5409		8.100	4.298	+13.0	.....	.....	−11.1
CQ 3403	1944 July	4.462	4.749	+13.3	− 3.6	.....	−13.3
4359	1945 Feb.	23.068	4.994	+36.2	+ 42.9	.....	− 9.0
4360		23.092	5.018	+32.4	+ 46.2	.....	− 6.0
G*f*/2 5424	Mar.	9.071	5.269	+39.0	+ 15.6	.....	−10.9
5426		9.094	5.292	+34.1	+ 0.4	.....	− 7.1
CQ 4031	1944 Dec.	3.204	5.492	+26.2	+ 22.2	.....	− 3.5
4369	1945 Feb.	24.069	5.995	+20.9	+ 1.1	.....	− 8.9
4370		24.094	6.020	+32.0	+ 2.8	.....	− 5.9
4372		24.201	6.127	+32.3	− 1.4	.....	−18.1
G*f*/2 5342	1945 Mar.	3.069	6.131	+ 8.8	− 33.5	.....	−11.9
5343		3.088	6.150	+43.8	− 31.8	.....	− 8.1
5344		3.113	6.175	+46.3	− 10.9	.....	− 4.3
5448		10.071	6.269	+39.0	− 46.6	.....	−14.5
5449		10.083	6.281	+56.8	+ 6.0	.....	−14.5
5450		10.095	6.293	+56.0	− 36.4	.....	− 6.9

TABLE 2—*Continued*

Plate	Date	U.T.	Phase (In Days)	Radial Velocities (In Km/Sec)			
				H	*He* I	F Star	*Ca* II K
CQ 4033.....	1944 Dec.	4.099	6.387	+36.5	− 24.3	.....	− 7.0
4034.....		4.124	6.412	+31.5	− 19.0	.....	− 0.9
G*f*/2 6617.....	1945 Sept.	25.434	6.589	+62.5	+ 81.3	.....	+ 6.7
6618.....		25.455	6.610	+74.6	+ 85.0	.....	− 1.0
6619.....		25.472	6.627	+57.2	+ 84.6	.....	+ 6.7
6702.....	Oct.	16.185	6.749	.....	.....	− 8.0	.....
6703.....		16.217	6.801	.....	.....	− 8.8	.....
6704.....		16.258	6.842	.....	.....	−13.6	.....

of 0.5 hour and a period of 19 years agreed with the observations. The following relative elements of the system were obtained:

$$L_1 = 0.157\ ,^{5} \qquad r_2 = 0.122\ A\ ,$$
$$r_1 = 0.197\ A\ , \qquad i = 89\overset{\circ}{.}0.$$
$$L_2 = 0.843\ ,$$

RY Per was placed on the observing program of the 82-inch reflector of the McDonald Observatory in July, 1944, and 62 spectrograms were obtained from July 4, 1944, to October 16, 1945. Two arrangements of the Cassegrain spectrograph were employed: two quartz prisms and a 500-mm camera (designated "CQ"), giving a dispersion of 55 A/mm at $H\gamma$, and two glass prisms and a 180-mm Schmidt camera (designated "G*f*/2"), giving a dispersion of 75 A/mm at $H\gamma$ (see Table 2).

The spectrum of RY Per at maximum light is B4 with moderately diffuse lines (see Pl. XV). The helium lines probably appear more diffuse than the hydrogen lines, but the comparison is difficult. On the spectrograms taken with the quartz prisms the hydrogen lines were usually measured for radial velocity to $H13$, beginning with $H\gamma$, while the spectrograms obtained with the glass prisms were frequently measured to $H10$, beginning with $H\beta$. The line $H\epsilon$ was always excluded because of a strong interstellar *Ca* II H line. Four helium lines were normally measured. The wave lengths employed for determining radial velocities are listed in Table 1.

Table 2 gives the observed radial velocities. The phases reckoned from primary minimum were computed by the formula

$$\text{Primary minimum} = \text{JD}2418216.701 + 6.863571E\ ,$$

given by Nijland.[6] The velocities for hydrogen and helium are listed in separate columns. The observed radial velocities are plotted in Figures 1 and 2. It is clearly shown that the two velocity-curves are not in agreement. Graphical solutions of the two velocity-curves yielded the results shown in the tabulation on facing page.

The radial velocity of the secondary component, observable at primary minimum, has been measured on seven spectrograms. Its spectral class is F5, with giant characteristics; the λ 4077 line of *Sr* II is rather strong relative to *Fe* I 4063. The assumed wave lengths are also listed in Table 1 and the observed radial velocities are recorded in Table 2 and plotted in Figures 1 and 2.

[5] The subscript 1 refers to the star in front at primary minimum.

[6] *A.N.*, **231**, 207, 1927.

PLATE XV

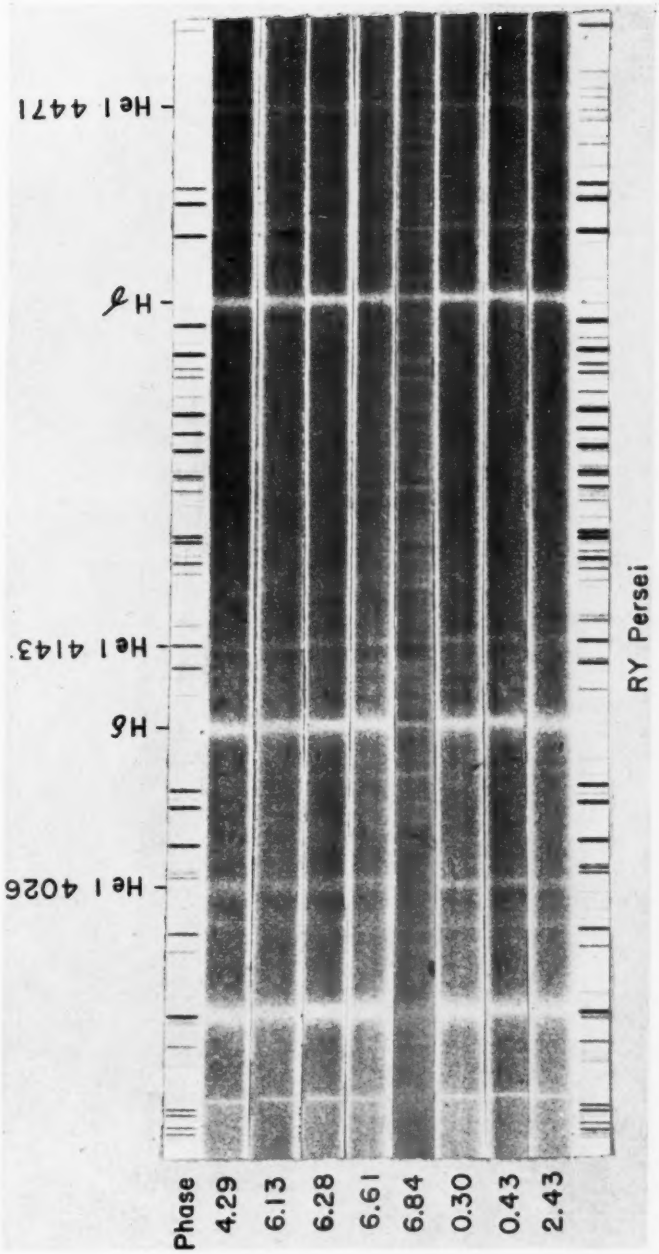
He I 4471
Hε
He I 4143
Hδ
He I 4026
Phase
4.29
6.13
6.28
6.61
6.84
0.30
0.43
2.43
RY Persei

PLATE XVI

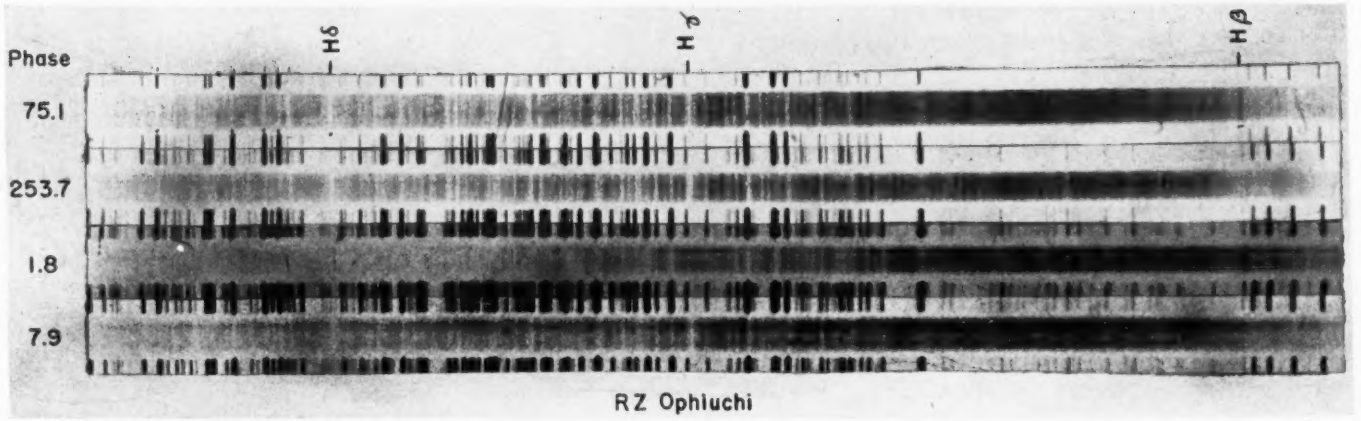

There are several interesting features in the spectrum and the velocity-curves of RY Per. First, the rotational effect of hydrogen and helium is different, with the latter element showing nearly twice the rotational velocity. A similar phenomenon was observed in RZ Scuti by Neubauer and Struve.[7] In RZ Sct the range for helium was 250 km/sec and that for hydrogen, 100 km/sec; and in RY Per helium and hydrogen show rotational velocities of approximately 200 km/sec and 110 km/sec, respectively. In RY Per, as in RZ Sct, it is probable that hydrogen forms a slowly rotating envelope about the reversing layer of the star. Second, the hydrogen velocity-curve from phase 6.15 to phase 6.5 is anomalous. The observed radial velocities are systematically large. A similar phenomenon was also observed in RZ Sct, but in that case hydrogen and helium

	Hydrogen	Helium
P	6.863571 (assumed)	6.863571 (assumed)
γ	+4.5 km/sec	−26 km/sec
K	27 km/sec	36 km/sec
e	0.22	0.21
ω	334°	14°
$a \sin i$	2.6×10^6 km	3.4×10^6 km
$f(m)$	0.015⊙	0.033⊙

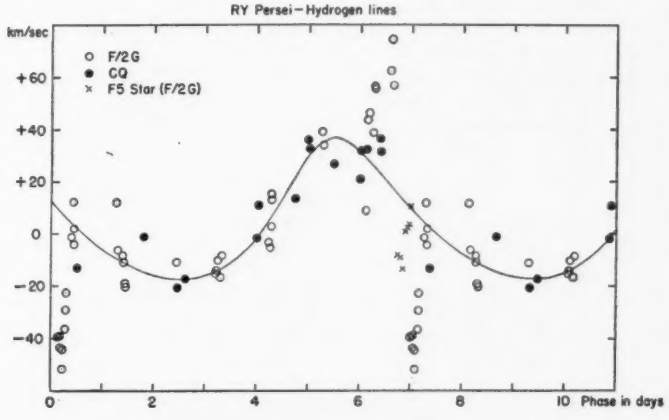

FIG. 1.—Velocity-curve of RY Persei from the *H* lines

were similar. In RY Per it is clear that the two velocity-curves are different at this phase. Third, the velocity-curves for the two elements are different in amplitude, and still more pronounced is the difference in γ velocities. It is well established that the hydrogen-curve normally falls above the helium-curve. This same phenomenon was observed by Deutsch[8] in BD + 55°616. He found that the γ velocity for hydrogen was 14 km/sec more positive than that of *He* I and that the semi-amplitude for hydrogen was 38.4 km/sec, in contrast to 65.6 km/sec for that of *He* I. It is also observed that in RY Per and BD + 55°616 the velocity-curves for the two elements in question are similar when the brighter components are receding from the observer. To interpret the discrepancies in the observed velocity-curves it appears necessary to assume that the brighter, smaller component is surrounded by an asymmetrical envelope and is approach-

[7] *Ap. J.*, **101**, 240, 1945.

[8] *Ap. J.*, **102**, 496, 1945.

ing the star with respect to the *He* I atoms. That some such mechanism is present in the case of RY Per is substantiated by three spectrograms obtained on March 10, 1945, which suggest that a stream of hydrogen flows from the F5 star to the B4 star. On the above date, between phases 6.27 and 6.29 (0.10 days before first contact), the hydrogen lines showed a second component displaced to the red, resembling the satellite lines observed in β Lyr,[9] which were interpreted in that case in terms of a flow of material from the smaller F star to the larger B9 star. The interstellar K line has a velocity of -9.4 km/sec.

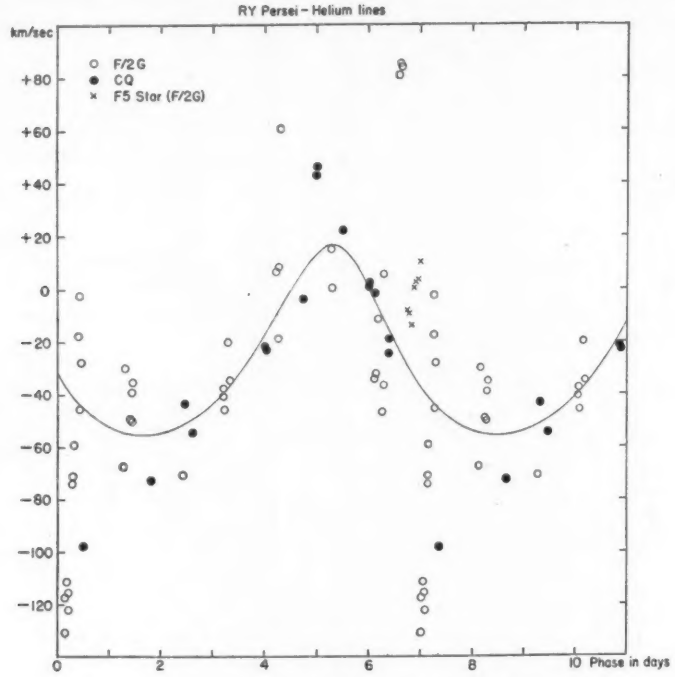

FIG. 2.—Velocity-curve of RY Persei from the *He* I lines

RZ OPHIUCHI

The variability of RZ Oph was also discovered by Mme Ceraski, in 1905. A period of 261.9 days was established by Beyer[10] and others. The depth of the total primary minimum is 0.80 mag. The eclipse lasts 16 days, or 0.061 P, and totality lasts 8 days, or 0.031 P. Outside of eclipse, mag. 10.0, the spectrum is that of an F8 supergiant, similar to γ Cyg. At primary eclipse the spectrum closely resembles that of ξ Cyg, a K5 supergiant. In full light hydrogen emission at $H\beta$ is present as a double line, with a separation of the components of 284 km/sec. This emission undergoes an eclipse similar to that in some other eclipsing binaries with hydrogen emission. The behavior of $H\beta$ emission near and during primary eclipse is given in Table 3. The spectrograms were obtained at the McDonald Observatory with the Cassegrain spectrograph and have a dispersion of 120 A/mm at $H\beta$. This dispersion is sufficient easily to resolve the components on Eastman 103*a*-O emulsion (see Pl. XVI).

The observations of the eclipse of the ring suggest that the inner radius of the ring

[9] See O. Struve, *Ap. J.*, **93**, 104, 1941.

[10] *A.N.*, **234**, 94, 1928.

is approximately equal to the radius of the secondary star and that the outer radius is about 50 per cent greater.

A total of thirty-seven spectrograms of RZ Oph were obtained during one cycle, of which all but seven were outside of eclipse. In addition to estimating the character of $H\beta$ emission, the spectrograms were measured for radial velocities. The pertinent data concerning the spectrograms are given in Table 4, along with the measured radial velocities. The phases were computed by the formula given by Beyer.[10]

$$\text{Primary minimum} = \text{JD}2418630.65 + 261.943E\,.$$

TABLE 3

Hβ EMISSION IN RZ OPHIUCHI

Computed Phase	Character of Hβ Emission
−14.14	Both components present
−11.08	Only red component present
− 9.20	Only red component present
− 8.21	Only red component present
− 6.14	Only red component present
− 5.18	Red component much stronger
− 4.19	Red component much stronger
− 2.20	Red component much stronger
− 1.20	Components about equal
+ 1.82	Violet component stronger
+ 7.87	Only violet component present
+12.79	Only violet component present
+13.77	Violet component present and possibly the red component
+14.81	Both components present

TABLE 4

RADIAL VELOCITIES OF RZ OPHIUCHI

Plate (G f/2)	Date (1945)	U.T.	Phase (In Days)	Radial Velocity (In Km/Sec)	Plate (G f/2)	Date (1945)	U.T.	Phase (In Days)	Radial Velocity (In Km/Sec)
5365	Mar.	3.500	52.14	+ 9.6	6518	Sept.	20.101	252.74	+ 1.7
5423		8.489	57.13	+ 2.0	6539		21.091	253.73	+ 0.1
5549		17.494	66.14	− 5.7	6562		22.252	254.90	− 7.5
5660		26.469	75.11	+ 3.7	6577		23.155	255.80	+ 4.8
5703		30.462	79.10	+ 0.9	6588		24.122	256.76	−13.2
5714	May	30.414	140.06	− 6.1	6599		25.103	257.75	− 6.6
5737	June	12.394	153.04	− 2.5	6624		27.094	259.74	+ 4.9
5744		17.279	157.92	− 1.7	6630		28.097	260.74	+ 2.6
5746		21.408	162.05	+ 2.2	6645	Oct.	1.122	1.82	+ 6.9
5753	July	18.356	189.00	− 3.7	6666		7.169	7.87	− 4.3
5789		21.207	191.85	+ 0.3	6673		12.088	12.79	− 5.4
5919		31.272	201.92	− 5.3	6676		13.065	13.77	+13.6
6091	Aug.	13.262	214.90	+ 5.9	6689		14.107	14.81	+ 8.8
6107		14.246	215.89	0.0	6697		15.093	15.79	+ 0.4
6138		16.292	217.94	− 1.7	6700		16.075	16.77	− 0.5
6261		30.208	231.85	− 4.8	6736		18.076	18.77	− 6.3
6321	Sept.	7.215	239.86	+ 6.7	6789		23.075	23.77	+14.5
6411		15.154	247.80	+ 1.6	6824		26.055	26.75	− 0.8
6476		18.213	250.86	+10.6					

Although the spectrum has exceptionally sharp lines, the resulting measurements are disappointing as can be seen in Figure 3. It is obvious that we have no information concerning the velocity-curve except that an approximate upper limit can be established for the semi-amplitude. However, if no orbital motion is assumed, the resulting probable error of a single observation is ± 3.8 km/sec, which is very similar to the value ± 3.3 km/sec that Struve[11] obtained from a series of spectrograms of α Per with the same spectrograph.

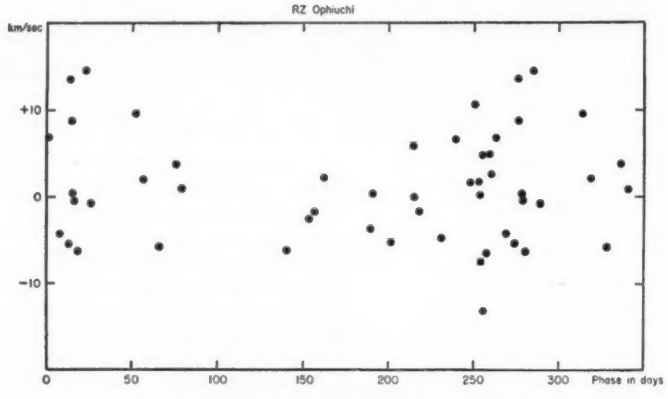

FIG. 3.—Radial velocities of RZ Ophiuchi

This suggests that the semi-amplitude is certainly not greater than 5 km/sec. The upper limits of $a \sin i$ and $f(m)$ then take on the values 18×10^6 km and $0.003\odot$, respectively.

A discussion of eclipsing binary systems with gaseous hydrogen rings was recently published by Struve,[12] and RZ Oph was among the stars discussed.

It is a pleasure to thank Drs. Struve, Sahade, and Edmondson for obtaining some of the spectrograms.

[11] *Ap. J.*, **102**, 125, 1945.

[12] *Ap. J.*, **103**, 95, 1946; *Observatory*, **66**, 208, 1946.

THE RATIO OF INTERSTELLAR ABSORPTION TO REDDENING

JESSE L. GREENSTEIN
Yerkes Observatory
Received July 31, 1946

ABSTRACT

The wide-base-line photoelectric six-color photometry of Stebbins and Whitford provides a new determination of the variation of space reddening with wave length; the derived variation is near $1/\lambda^{0.56}$. The ratio of photographic absorption to short-base-line photoelectric colors (C_1 scale) lies between 10 and 15. The curvature of the energy-curves of the reddened B stars with respect to unreddened B stars may produce an underestimation of the reddening if measured in color classes; longer-base-line color scales, such as the Greenwich gradients, and the V−I scale show larger reddenings. An observational technique for the discovery of reddened stars is based on the apparent discrepancy between long- and short-base-line colors. The present absorption law is interpreted with reference to the theory of absorption and scattering by small particles; a direct determination of the ratio of absorption to reddening may permit a decision as to whether the particles are dominantly metals or dielectrics—the latter now seeming more probable.

The photoelectric six-color photometry[1,2] by Stebbins and Whitford provides a major forward step in the determination of the ratio of interstellar absorption to reddening. The large wave-length range covered provides, in itself, a definite minimum value. Extrapolating observed absorptions for estimation of the absorption at infinite wave length now involves smaller uncertainty. Certain difficulties arising in the use of short-base-line color excesses are also clarified. In their first paper,[1] Stebbins and Whitford derive the variation of interstellar absorption with wave length. Since, to a first approximation, this variation is nearly proportional to $1/\lambda$, they compute the deviation of the

TABLE 1

POINTS MEASURED IN SIX-COLOR PHOTOMETRY

	U	V	B	G	R	I
λ.....	3530	4220	4880	5700	7190	10300 A
$1/\lambda$.....	2.83	2.37	2.05	1.75	1.39	0.97 μ^{-1}

observed energy-curves of reddened stars from those expected on the basis of the $1/\lambda$ relation. They compare a reddened and an unreddened B star by forming the differences between the observed magnitudes at six colors. Their six effective wave lengths are given in Table 1. The stars observed are of spectral types O5–B3; many of the reddened stars are supergiants. Their reductions involve the use of colors measured at the ultraviolet point, U. Since U may be affected by the Balmer absorption (or emission) lines and continuum, I have reinvestigated the reddening as derived from the points V to I, inclusive. The Paschen lines and continuum should be substantially weaker than the Balmer lines, and there is little reason to expect effects at point I. There are no other lines strong enough to affect materially the measured energy of the star within the wide filter bands employed. Absolute-magnitude effects should be small, although not absolutely excluded, in the range V − I.

The reduction of the data on the V − I base line follows directly the method used by Stebbins and Whitford[1] in their Table 5. The magnitude differences between the red-

[1] *Ap. J.*, **98**, 20, 1943. [2] *Ibid.*, **102**, 318, 1945.

dened and the unreddened star are reduced by a scale factor to the values that they would have had if the reddening (and possible temperature difference) had been such as to give a V − I color difference of 1.00 mag. (This assumes a proportionality of the absorptions, or the existence of a single functional form for the reddening law.) The expected differences, if the reddening varied as $1/\lambda$, are then subtracted and the residuals, D, tabulated. The mean residuals, grouped by spectral type, are given in Table 2, which gives the number (N) of reddened stars; the mean observed color excesses $E(C_1)$ on the short-base-line photoelectric scale;[3] the actual mean observed $\delta(V-I)$ for each group; and the values of D, the deviation from the $1/\lambda$ law, as reduced to the case $\delta(V-I) = 1.00$

TABLE 2

DEVIATIONS OF THE REDDENING FROM THE $1/\lambda$ RELATION

Type	N	$\overline{E(C_1)}$	$\delta(\overline{V-I})$	D				
				V	B	G	R	I
O8	7	+0m19	+1m03	0m000	+0m035	+0m033	+0m035	0m000
B0	8	+0.34	+2.06	0.000	+0.044	+0.055	+0.041	0.000
B1	6	+0.28	+1.61	0.000	+0.046	+0.066	+0.012*	0.000
B2	6	+0.30	+1.78	0.000	+0.061	+0.054	+0.032	0.000
Mean D†				0m000	+0m046	+0m049	+0m031*	0m000
Reddening for $1/\lambda$				1.000	0.771	0.557	0.300	0.000
Observed reddening for V−I=1.00				1.000	0.817	0.606	0.331*	0.000

* Two B1 stars have discrepant measures at point R, which reduce the value of D far below the mean. If these stars are omitted, D for B1 stars at point R becomes +0m032, and the mean D for all stars becomes +0m036. This change would make the curve for the variation of D with $1/\lambda$ considerably smoother.

† The method of choosing pairs of stars is somewhat arbitrary and may be criticized because it involves a comparison of stars of high and low luminosity. Since it is theoretically possible that the energy distribution in a supergiant may show intrinsic differences (and curvature) when compared to that in a dwarf, a part of the observed curvature might not be due to space reddening. To investigate this possibility, six relatively slightly reddened supergiants of types B1 and B2 were selected as well as four highly reddened supergiants. The luminosity classifications were from unpublished data by Dr. W. W. Morgan. The mean V−I color of the first group was −1.78 mag. and of the second group +0.94 mag. The reduction to determine the law of reddening was then carried through as before, and the deviations, D, from the $1/\lambda$ law were reduced to a reddening $\delta(V-I) = 1.00$ mag. The results were as follows:

Point	V	B	G	R	I
D	0m000	+0m054	+0m066	+0m055	0m000

The new values of D are similar to those found in Table 2, being larger by an amount slightly in excess of their probable error. Any intrinsic curvature of the energy-curves of the supergiants should cancel out in this comparison. We may therefore safely exclude absolute-magnitude effects as the source of the observed curvature.

mag. The ratio of $(V-I)/E(C_1)$ is found to be 5.8; this is an underestimate because of the systematic errors introduced by the method of selection of the pairs of stars.

The observed deviations in Table 2 are similar to those found by Stebbins and Whitford,[1] but on a smaller scale because of the reduced wave-length range covered. The agreement shows that the Balmer absorption has little systematic effect on the six-color photometry of the early B stars. The reddening law is one which varies less rapidly than $1/\lambda$. The observed mean absorptions for a star whose V − I reddening is 1 mag. are plotted in Figure 1, together with extrapolations to infinite wave length. An approximate fit to the observed values of δm can be obtained. Assume that the variation of $\delta m(\lambda)$ is to be represented by an interpolation formula of the form

$$\delta m\,(n, \lambda) = c_n\,(1/\lambda^n - 1/\lambda_I^n)\,, \qquad (1)$$

[3] Stebbins, Huffer, and Whitford, *Ap. J.*, **91**, 20, 1940.

where λ_I is the effective wave length of the infrared photoelectric measure. Then form the difference

$$D(n, \lambda) = \delta m(n, \lambda) - \delta m(1, \lambda), \quad (2)$$

in order to obtain the predicted deviations from the $1/\lambda$ relation,

$$D(n, \lambda) = c_n(1/\lambda^n - 1/\lambda_I^n) - c_1(1/\lambda - 1/\lambda_I). \quad (3)$$

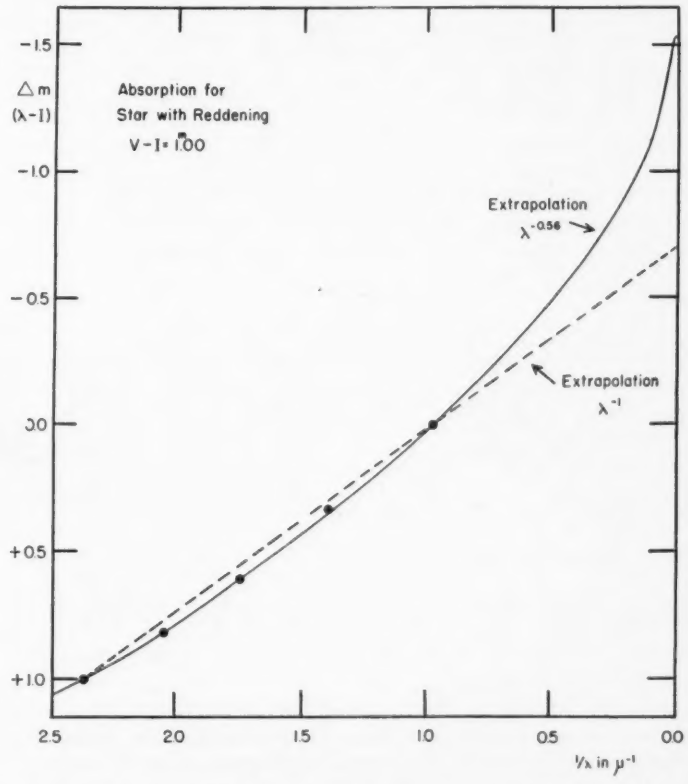

FIG. 1.—The observed mean values of the reddening for a star with V − I = 1.0 mag. are plotted. The dotted line represents the expected values if the $1/\lambda$ relation is valid. The solid curve represents the values of the reddening if the $\lambda^{-0.56}$ relation is valid. The zero point of the magnitude scale of reddenings should be the value for $1/\lambda = 0.0$, i.e., if the $1/\lambda$ relation were valid, $\delta m(\lambda)$ would be +1.69 mag. for the point V; if the $\lambda^{-0.56}$ extrapolation is adopted, $\delta m(\lambda) = +2.54$ mag. for point V.

We can then compute $D(n, \lambda)$ for the desired values of n and λ. The results of such computations are given in Table 3 and compared with the observed values of D. Auxiliary quantities tabulated are the constants c_n; δm (I − ∞), the extrapolation of our interpolation formula to infinite wave length to obtain the absorption at point I on the assumption that there is zero nonselective absorption; $E(C_1)$ is the predicted reddening on the short-base-line photoelectric scale (1332 B stars); A(pg) is the absorption at the photographic effective wave length, taken for reddened stars to be 4400 A.

It can be seen that δm(I − ∞) increases strongly with decreasing n. In Table 3 a minimum value of $A(\text{pg})/E(C_1)$ is given in the last line, based on the following assump-

tions. Beyond the point I, let us assume that the absorption decreases as $1/\lambda$; let us also assume that there is no nonselective absorption. Then,

$$A\ (\mathrm{pg}) = c_n\,(1/\lambda_{\mathrm{pg}}^n - 1/\lambda_{\mathrm{I}}^n) + c_1/\lambda_{\mathrm{I}}\,, \tag{4}$$

$$A\ (\mathrm{pg}) = c_n\,(1/\lambda_{\mathrm{pg}}^n - 1/\lambda_{\mathrm{I}}^n) + 0^{\mathrm{m}}.69\,. \tag{5}$$

Comparison of the observed and predicted D in Table 3 shows that the index in the law of reddening is close to 0.56; a value of 0.75 seems definitely too large. Then the ratio of absorption to C_1 reddening is 14:1, by extrapolating $n = 0.56$ to infinite wave length; the "minimum" value, using the $1/\lambda$ extrapolation is 9:1. The extrapolation of the observed absorptions over the V − I region to infinite wave length is sensitive to n, particularly when $n < 1$. This can be seen in Figure 1, where the upward curvature ob-

TABLE 3

COMPUTED VALUES OF THE DEVIATIONS FROM $1/\lambda$

Color	Obs. D	Computed $D(n, \lambda)$				
		$n = 1.0$	0.75	0.62	0.56	0.50
V	0m000	0m000	0m000	0m000	0m000	0m000
B	0.046	0.000	0.024	0.039	0.043	0.050
G	0.049	0.000	0.026	0.041	0.046	0.052
R	0.031	0.000	0.017	0.028	0.031	0.034
I	0.000	0.000	0.000	0.000	0.000	0.000
c_n	.....	0m714	1m073	1m377	1m567	1m802
$\delta m(\mathrm{I}-\infty)$	.....	0.69	1.05	1.35	1.54	1.77
$E(C_1)$	.....	0.207	0.191	0.182	0.179	0.175
$(\mathrm{V}-\mathrm{I})/E(C_1)$	.....	4.83	5.24	5.49	5.59	5.71
$A(\mathrm{pg})/(\mathrm{V}-\mathrm{I})$	.....	1.63	1.99	2.30	2.49	2.72
$A(\mathrm{pg})/E(C_1)$	.....	7.87	10.4	12.6	13.9	15.5
Minimum $A(\mathrm{pg})/E(C_1)$	.....	7.87	8.54	8.98	9.13	9.35

tained with $n = 0.56$ results in an absorption difference between I and ∞ of 1.54 mag. This may possibly be an overestimation. If we extrapolate, using the $1/\lambda$ relation, $\delta m(\mathrm{I} - \infty)$ is only 0.69 mag. The small curvature of 0.049 mag. in the V − I region results in 0.85 mag. increase in $\delta m(\mathrm{I} - \infty)$. The true value of $\delta m(\mathrm{I} - \infty)$ may lie between the two estimates; we shall later discuss the possibility that the extrapolation might yield less than 0.69 mag. Nonselective absorption, free-free absorption in interstellar hydrogen, and electron scattering produce some small absorption in the infrared and are all neglected in this investigation. The "minimum" value of $A(\mathrm{pg})/E(C_1) = 9:1$ may be taken as a relatively conservative one at present.

These conclusions confirm early spectrophotometric determinations, such as that of Greenstein,[4] in which an index $n = 0.8$ was suggested by an upward curvature of energy-curves of reddened B stars. The investigation by Greenstein and Henyey,[5] based on the C_1 scale of photoelectric color excesses, involved completely different assumptions than those made in spectrophotometric work and seemed to indicate that the nonselective component of the reddening is small; a ratio of about 9:1 was also found for $A(\mathrm{pg})/E(C_1)$.

[4] *Ap. J.*, **87**, 151, 1938.

[5] *Ap. J.*, **93**, 327, 1941.

THE RELATION BETWEEN COLOR-INDEX SCALES

The new photoelectric material on wide-base-line colors helps to clarify a complex and neglected problem in the photometry of reddened stars. There is now little doubt that the energy-curves of the reddened B stars deviate from the black-body-curves (assuming that the unreddened B stars radiate like black bodies). The stars of later spectral type may also have small deviations from a black body, caused by spectral lines or by different types of variation of opacity with wave length. A single linear reduction from one short-base-line color-index scale to another may not be possible. The existence of different reduction-curves for space-reddened B stars and for late-type stars (which I will call "temperature-reddened stars") is well shown in a detailed comparison by the Greenwich observers[6] of Greenwich gradients[7] with various color systems. In their Figures 1, 3, and 4, gradients are compared with three photoelectric scales. Gradients are measured from λ 4200 to λ 6300, while the photoelectric scales have short base lines within the region λλ 3800–4800. Photoelectric colors (for example, the C_1 scale), in a certain sense, underestimate the reddening; the deviations from black-body radiation now found in the B stars will explain, at least qualitatively, the fact that the reddened B stars show the C_1 scale to be relatively compressed in comparison with gradients. Another demonstration of this phenomenon is found in a comparison by Sherman and Morgan[8]

TABLE 4

COLOR CLASSES OF REDDENED B STARS

Star	Grad.	V−I	C_1	Becker	Bottlinger
P Cyg	f8	f5	a9	a2	.....
55 Cyg	f7	f5	a8	a3	a2
χ^2 Ori	f2	.....	a3	a3	a0
σ Cyg	a7	.....	.....	b9	b9
ν Cep	g0	.....	.....	f0	f2

of color classes of reddened stars, as determined on the spectrophotometric broad base line and on three photoelectric systems. Their Table 4 is reproduced, in part, in my Table 4, with the addition of color classes determined on the V − I base line and with the use of the color classes based on the Greenwich gradients ("Grad."). The colors of main-sequence, unreddened, later-type stars were used to establish the relation, in each color system, between intrinsic color and spectral type; the color class of a reddened star was then determined from its observed color. (W. W. Morgan has also demonstrated the existence of this effect in several unpublished investigations of the relation between spectral type and color.) The Greenwich gradient scale and the V − I scale are both sufficiently long to give accordant measures of the reddening suffered by these stars; the short-base-line colors underestimate the reddening by roughly one-half. The C_1 scale of color excesses is extremely useful in all investigations of space reddening; nevertheless, the new V − I colors are the most sensitive means of discovery of reddened stars. The V − I scale also permits an accurate calibration of the absorption corresponding to a given C_1 reddening. A similar calibration remains to be made for the International scale; it is probable that the relation between V − I and International colors will not be the same for late-type stars as for very highly reddened stars. The ratio of absorption to International color excess is not accurately known at present and may be best determined, not from effective wave lengths, but from direct observations of International color excesses of stars with known reddenings on the V − I scale, using highly reddened B stars.

[6] *M.N.*, **100**, 196, 1940. [7] *Ibid.*, **100**, 189, 1940. [8] *Ap. J.*, **89**, 516, 1939.

The usefulness of broad-base-line colors is clearly demonstrated in Figures 2 and 3. In Figure 2 are plotted the observed values of V − I and C_1 for the North Polar Sequence stars, and for stars of types B3 and earlier (space reddened but with substantially similar intrinsic colors). The two groups define clearly separated relations between the color systems; a certain nonlinearity is present in both groups. For simplicity, a linear relation was fitted to each by least squares (star NPS 2r was omitted from the NPS group):

$$\text{Temperature-reddened NPS stars}, \quad C_1 = 0^{m}.40 + 0^{m}.269\,(V-I), \tag{6}$$

$$\text{Space-reddened B stars}, \quad C_1 = 0^{m}.16 + 0^{m}.159\,(V-I). \tag{7}$$

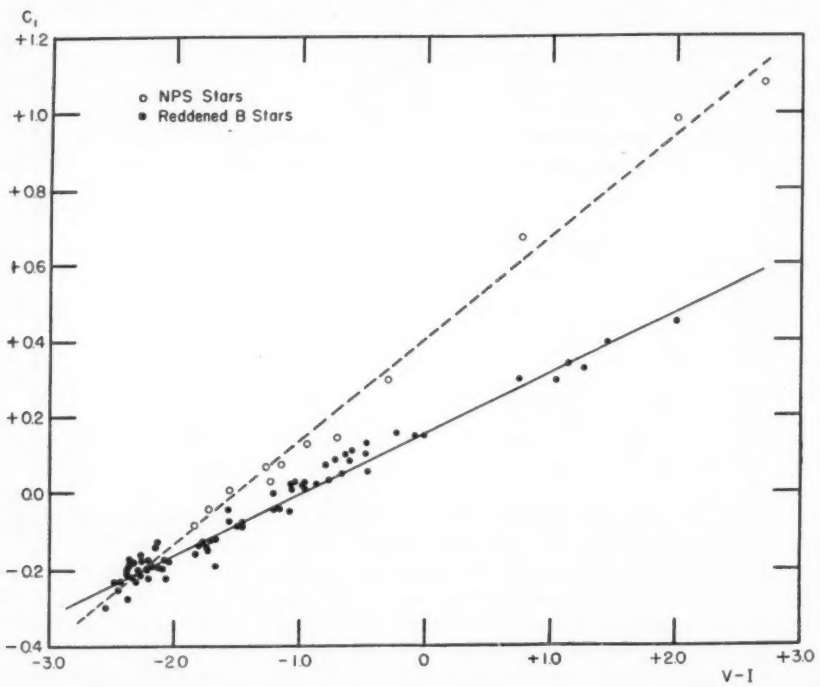

FIG. 2.—The plotted points represent stars for which C_1 and V − I are known. The least-squares solutions are plotted.

There is a large difference in slope between the two groups. In equation (7) the scale coefficient is also definitely lower than the value 0.173 derived in Table 2 and also lower than any predicted value of $E(C_1)/V - I$ in Table 3, even with $n = 0.56$. This difference of slope may be affected by the method of selection for the data in Table 2 or by the nonlinearity of the relation between the scales of colors. It does not seem profitable to refine the analysis further; the uncertainty and possible variability with color of the effective wave lengths of the C_1 scale will affect the predicted value of $E(C_1)$. The value of $(V-I)/C_1 = 1/0.159 = 6.3$, in agreement with Stebbins and Whitford,[1,2] will be adopted. The result is an increase of the ratio $A(pg)/E(C_1)$, for $n = 0.56$, to 15.6, and of the "minimum" value to 10.3.

In Figure 3 the Greenwich gradients are plotted against V − I for temperature-

reddened stars (types B6 or later) and for early B stars separately. The least-squares solutions give

$$\text{Temperature-reddened stars}, \quad \text{Grad.} = 1.30 + 0.677\,(V-I), \tag{8}$$

$$\text{Space-reddened B stars}, \quad \text{Grad.} = 1.45 + 0.682\,(V-I). \tag{9}$$

In these two sets of long-base-line colors there is negligible difference of scale and a small zero-point shift. The wave-length range of the gradients, about 0.9 μ^{-1}, seems sufficient to give a measure of the reddening (in color classes) similar to the longer V − I base line. This supposition is confirmed by the rather scanty data in Table 4; here the gradi-

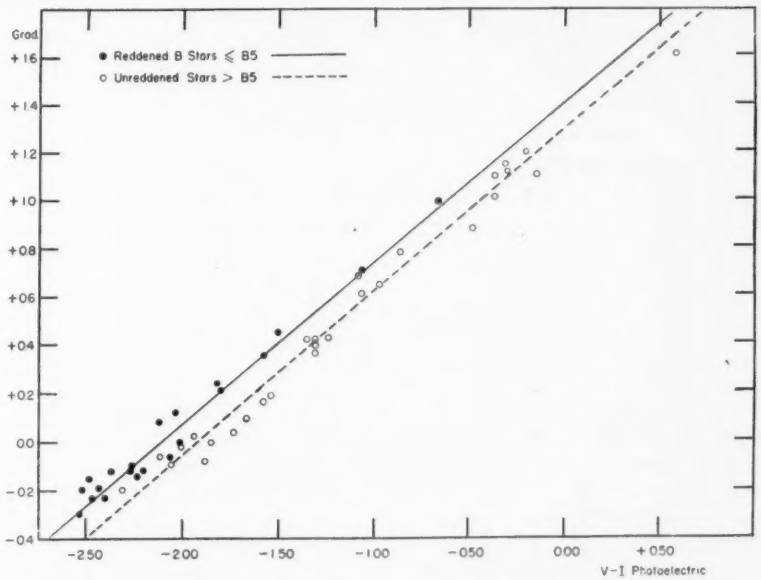

FIG. 3.—The plotted points represent stars common to the lists of V − I and the Greenwich gradients. The least-squares solutions are plotted.

ents and V − I measures give accordant reddenings, in color classes, which are larger than those determined by the short-base-line photoelectric measures.

A similar phenomenon has been discovered observationally in several unpublished investigations by Dr. W. W. Morgan at the Yerkes Observatory. Photographs have been taken in the galactic plane, using the Tikhoff method; the color-curve of the refracting telescope provides a separation of radiation in the different colors. An illustration of a plate obtained in such a way is given by Münch and Terrazas;[9] red and blue light appear as separate extrafocal rings. When panchromatic plates are used, the base line for colors is approximately 4500–6000 A. Faint reddened B stars have been found with color classes in the late K's; the photoelectric excesses correspond to considerably earlier color classes. It is obvious that our knowledge of B stars fainter than apparent magnitude +10 is very incomplete; if such stars are in the galactic plane, they will be highly reddened. Consider, now, a B star with a large reddening, for example, HD 169034, a cB0 star. According to Stebbins and Whitford,[1] this star has a V − I color of +2.01 mag. and a C_1 color of +0.45 mag. A near-by unreddened B star like HD 204172 has V − I = −2.18 mag. and C_1 = −0.19 mag. The color difference on the V − I scale is +4.19

[9] *Ap. J.*, **103**, 371, 1946.

mag., and on the C_1 scale +0.64 mag. On the other hand, the star NPS 3r (HD 114282), type gK2, has V − I = +2.00 mag. and C_1 = +0.98 mag. When compared with HD 204172 the color difference on the V − I scale is +4.18 mag. and on the C_1 scale +1.17 mag. If we form the differences of colors between the highly reddened B star and the temperature-reddened gK2 star, we obtain:

$$\delta\,(V-I)\,, \qquad \text{HD } 169034 - \text{HD } 114282 = +0.01 \text{ mag}\,.$$

$$\delta C_1\,, \qquad \text{HD } 169034 - \text{HD } 114282 = -0.53 \text{ mag}\,.$$

The B star has nearly the same V − I color as the gK2 star but is − 0.53 mag. bluer on the C_1 scale. We can derive a statistical mean value of this expected color difference on the C_1 scale between a space-reddened and a temperature-reddened star for which V − I colors are the same by subtracting equation (6) from equation (7):

$$\delta C_1 = -0^{m}.24 - 0.110\,(V-I)\,. \tag{10}$$

The particular case of HD 169034, referred to above, would give a predicted value of $\delta C_1 = -0.46$ mag., in fair agreement with the observed −0.53 mag.

Consequently, it may be suggested that new faint reddened stars can be selected as follows: A wide-field telescope is used to obtain short-dispersion objective-prism (or -grating) spectra in the galactic plane. An infrared emulsion of type I-N (or further to the infrared) should be used. The spectra can be broken into three wave-length regions by means of suitable filters. Interference-type filters or gelatin filters can be used. Two successive exposures could be made, one with a Wratten 45 filter, which would isolate bands near 8500 and 4800 A, and then with a Wratten 35, which gives a band at 4200 A. Possible better sets of filters may be developed to obtain three regions simultaneously. The three images would possess an extrafocal quality, because of their appreciable wavelength range and would permit accurate visual estimates of color classes on a short base line in the blue-violet and on a long base line from violet to infrared. Such a classification would reveal reddened B stars as objects of large, broad-base-line color and relatively small, short-base-line color. For a star like HD 169034, the point at 4800 A would be about 0.5 mag. brighter than in normal late-type stars. A spectral classification of suspected stars might be required to eliminate late-type stars with distorted energy-curves from the reddened B stars. A three-ring Tikhoff exposure method or a three-color direct photograph could also be used in the discovery of highly reddened stars.

It is even more striking to compare the long-base-line colors of two stars with the same C_1 color. From equations (6) and (7) we obtain the difference of V − I color of space and temperature-reddened stars of the same C_1:

$$\delta\,(V-I) = 2.54C_1 + 0.49 \text{ mag}\,. \tag{11}$$

The coefficients in equation (11) are not accurately determined by the present data. However, we can compare HD 169034, the cB0 star, with the stars of the North Polar Sequence. We find that Polaris, HD 8890 (cF7), has C_1 = +0.49, and V − I = −0.30. Consequently, δ(V − I) is +2.31 mag. for approximately equal C_1, between the space-reddened and the temperature-reddened star. The value given by equation (11) is +1.63 mag., which is probably within the accuracy to be expected. (In all these discussions no consideration has been taken of statistical effects to be expected when the actual regression-curves are replaced by simple linear least-squares relations.) In any case, stars with as much space reddening as HD 169034 would show excess brightnesses of more than 2 mag. in the infrared, when compared with late-type stars of the same C_1 color.

THE NATURE OF THE INTERSTELLAR PARTICLES

Of the 28 stars now observed by Stebbins and Whitford, only θ^1 Ori, the Trapezium group, shows an obviously different type of reddening law. The upward curvature of the energy in the blue and violet regions in θ^1 Ori is much greater than is shown by the mean D's tabulated. This observation agrees with that of Baade and Minkowski.[10] The exceptional type of reddening may be connected with the fact that most of the reddening is produced close to hot O stars in the dark and bright nebulosity of the Orion nebula. It may be suggested that (1) radiation pressure alters the frequency distribution of particle sizes[11] in the dust cloud and thus changes the integrated absorption coefficient; (2) high-temperature ultraviolet radiation changes the optical properties of the material; or (3) the high-energy density of radiation in the nebula causes particles of certain ranges of size and composition to evaporate. Since many stars have large parts of their reddening produced in dense dark nebulae in which the stars are immersed, an observational discrimination may be possible. It should be remarked that there exists another peculiarity of the absorption in the Orion nebula. The diffuse interstellar band at 4430 A is known to be unexpectedly weak in θ^1 Ori, according to W. W. Morgan;[12] on the other hand, I find the band very strong in HD 147889, a B2 star deeply immersed and reddened in a dark nebula, in which there is also a strong reflection bright nebula. The presence of the hotter stars or the emission lines in the nebula seems to be associated with the difference between λ 4430 in θ^1 Ori and HD 147889. (An investigation of λ 4430 in bright nebulae is now in progress.) Another suggestive observation is that by Joy,[13] of T Tauri variables in dense dark nebulosities; here the presence of emission lines suggests possible evaporation of gaseous material from the interstellar particles close to the stars.

Excluding θ^1 Ori, there is a remarkable uniformity in the reddening law; possible differences of particle sizes or frequency distributions between thick, dark nebulosities and general interstellar space seem to have little effect. The observed reddening law covers a very large range of wave lengths; certain types of particles may be searched for which would give the observed law. It has been shown[11] that, with a properly chosen frequency distribution of particle sizes, either metals or dielectrics would give almost any desired law of interstellar reddening. If, however, we assume that particles of only one size are present, the observed reddening law and the ratio $A(\mathrm{pg})/E(C_1)$ (determined independently) would decide between metallic and dielectric particles.

Let us assume that particles of one size are present. Let the radius of the particle be a, and let us define $\alpha = 2\pi a/\lambda$. Define the efficiency factor $Q(\alpha)$, such that

$$\text{Extinction} = Q(\alpha)\,\pi a^2 . \qquad (12)$$

The quantity $Q(\alpha)$ is an effective cross-section of the particle and is given by the Mie theory for spherical particles; it is a function of the refractive index of the particle N and of α. The absorption in magnitudes is proportional to Q; Greenstein[11] gives values of $Q(\alpha)$ for various metals and dielectrics; new computations and a résumé of older data are given by van de Hulst.[14] In all cases, $Q(\alpha)$ has a maximum value[14] near $\alpha(N-1) = 2$; for small α it drops, roughly proportional to α^4 for dielectrics and to α for metals; for larger α, $Q(\alpha)$ rises and falls, asymptotically approaching a limit, $Q(\infty) = 2$. If we are to explain the absorption by a single particle size, we must find a section of these curves sufficiently large to cover a change in α by a factor of about 3 (since $1/\lambda$ varies from 1 to 2.8 in the photoelectric measures) and such that the slope of the curves is compatible with the observed law of interstellar reddening. Particles with α greater than that at which

[10] *Ap. J.*, **86**, 123, 1937.

[11] *Harvard Circ.*, No. 422, 1937.

[12] *A.J.*, **51**, 21, 1944.

[13] *Ap. J.*, **102**, 168, 1945.

[14] *Optics of Spherical Particles*, Thesis, Amsterdam, 1946.

the first maximum of $Q(a)$ occurs are excluded, since they would make the stars appear bluer rather than redder, and even at point U the interstellar absorption is still observed to increase with increasing $1/\lambda$. The interpretation of these curves in terms of the interstellar absorption is further complicated by the fact that most real substances have a refractive index which varies with wave length; in general, the refractive index increases toward the ultraviolet and causes the actual $Q(a)$ to increase more rapidly with decreasing wave length than is shown in any of the plotted extinction-curves. For example, it is known that small metallic particles ($a << 1$) have an extinction coefficient of the form

$$\delta m\ (\lambda) = \text{constant} \times 1/\lambda \times \text{imaginary part} \left(\frac{1 - N^2}{N^2 + 2}\right); \tag{13}$$

where the imaginary part of the complex refractive index yields a coefficient[11,15] to be multiplied into $1/\lambda$ to obtain the final total extinction. For *Fe* particles the net result is a variation near $1/\lambda^2$; for *Ni* particles, near $1/\lambda^3$. Consequently, the observed interstellar absorption-curve cannot be explained by very small metallic particles and, of course, also cannot be explained by very small dielectric particles. The increase of the refractive index in both metals and dielectrics toward the ultraviolet is a quite general phenomenon, connected with the existence of absorption bands in the far ultraviolet.

We must therefore determine whether particles of one size, near the maximum of the $Q(a)$ curves, can explain the observed interstellar absorption-curve. The total extinction per gram of dust particles of this size is about the same[11] for metals and for dielectrics and is about 10^4–10^5. For purposes of simplicity, let us neglect the variation of refractive index with wave length. Assume that the particle radius, a, is such that $Q(a)$ has its maximum value somewhere in the near ultraviolet, say at point U ($1/\lambda = 2.83$). Then at point I, ($1/\lambda = 0.97$), $a(\text{I}) = 0.342\ a(\text{U})$. An investigation of the form of the curves[11,14] for the behavior of dielectric particles was then made; the results are attended with considerable uncertainty, since the form of the $Q(a)$ curves is rather poorly defined by the available computations near $a = 1$. If we measure the slope, γ, of the curve $\log Q(a) = f(\log a)$, the interstellar reddening will vary as

$$\delta m\ (\lambda) = \text{constant} \times\ (1/\lambda)^{\gamma} \tag{14}$$

in the range of wave length at which the slope γ is measured. For a dielectric with $N = \frac{4}{3}$, if we take $a(\text{U}) = 5$, the slopes γ are 0.59 at point U, 1.2 at point V, 1.9 at point B, 2.7 at point R, and 3.1 at point I. This very rapid change of the shape of the $\delta m(\lambda)$ curve is not compatible with the observations. If the index N is greater than $\frac{4}{3}$, the variation of γ is even steeper. In the case of metallic particles, Schalén has shown[15] that a rather more satisfactory fit is obtained; the better fit arises because the limiting value of γ is unity, if the variation of refractive index with wave length is neglected, when $a << 1$. The recent work of van de Hulst,[14] however, indicates that the rate of variation of the slope with wave length will be slower if we use a lower index of refraction for dielectric particles. Curves for dielectrics with different indices, N, are similar if $Q(a)$ is plotted against $(N - 1)a$. It may be estimated that if N were between 1.1 and 1.2, the variation of γ with wave length would be compatible with the observations.

While the interpretation of the absorption as due to dielectric particles of a certain size meets with certain difficulties, there is a possibility of distinguishing between metals and dielectrics which may eventually require us to assume that the particles are dielectric. For very long wave lengths, $a \to 0$; for metals the absorption will vary roughly as $1/\lambda$ in this range, and for dielectrics as $1/\lambda^4$. Consequently, the absorption between point I and infinite wave length will be smaller for dielectrics than for metals. The re-

[15] Schalén, *Uppsala Ann.*, Vol. 1, No. 2, 1939.

sult will be that $A(\text{pg})/E(C_1)$ will be smaller for dielectrics. We have shown that if the absorption for $1/\lambda$ less than 0.97 (i.e., in the far infrared) varies as $1/\lambda$, $A(\text{pg})/E(C_1)$ will have the "minimum" value of 10.3. It is quite possible that this value is too large to be compatible with other direct observational determinations of the ratio of absorption to reddening. If this should prove to be true, the absorption beyond point I must vary more rapidly than $1/\lambda$; the dielectric particles would then be a more satisfactory source of such absorption. The observed interpolation formula, $1/\lambda^{0.56}$ must break down in the fairly near infrared, since it gives a value of $A(\text{pg})/E(C_1)$ of 15.6, which is almost certainly incompatible with direct observations of this ratio. Observations of reddened B stars at wave lengths near 20,000 A could be decisive.

The entire set of arguments can be carried through similarly in case a mixture of particles of different sizes are present in space; the effects would be less pronounced, and there would be no difficulty fitting the observed law of reddening by the $Q(a)$ curves of dielectric particles even with high index. If an upper limit to the particle size present in space should exist, there would still remain a possibility of distinguishing between metals and dielectrics by the behavior of the absorption-curve in the far infrared.

CONTINUOUS EMISSION IN THE ORION NEBULA*

JESSE L. GREENSTEIN
Yerkes and McDonald Observatories
Received August 17, 1946

ABSTRACT

Short-dispersion slit spectra of the central part of the Orion nebula have been measured spectrophotometrically. The energy distribution in the continuum is determined with respect to θ^1 Ori C; the adopted stellar color temperature is based on gradients and photoelectric colors. The nebular continuum has a color temperature of 12,000° on both sides of the Balmer limit; the Balmer emission discontinuity is 1.6 mag. If the energy distribution in the Balmer continuum is interpreted as recombination emission, its electron temperature is about 65,000°. This excessively high value can be replaced by a more reasonable value near 12,000° if we assume that the optical thickness of the nebula in the Balmer continuum is appreciable. Suggested observational tests of this hypothesis include the predicted absence of filamentary structure in direct photographs taken in ultraviolet light. The complex effects of radiation scattered by dust particles in the nebula and of particle reddening are considered. The intensity of the hydrogen lines indicates an electron temperature near 9,000°; lines near the series limit reveal a peculiarly rapid rise in intensity for high quantum numbers, as they approach the intensity at the series limit. The density and size of the nebula are estimated to be sufficient to give appreciable self-absorption.

THE OBSERVATIONS

The Orion nebula, NGC 1976, has high surface brightness and a large angular diameter. The excitation and illumination have been ascribed dominantly to the stars of the Trapezium group, θ^1 Ori, of spectral types O7–B1. While a large part of the nebular radiation is in the emission lines, there exists a strong continuous spectrum. Spectrophotometric investigations of the continuum have been made by Greenstein and Henyey[1] and by Barbier,[2] who measured both the emission discontinuity at the Balmer series limit and the color temperature, T_c, of the continuous emission. Greenstein and Henyey used the McDonald nebular spectrograph, and their results refer to the outer parts of the nebula, between 3′ and 8′ from the Trapezium; they found an emission discontinuity of −0.4 mag. and a gradient of the nebular continuum in the range λλ 3920–6060 of +0.85, making the nebula slightly bluer than θ^1 Ori. Barbier[2] used a conventional slit spectrograph of higher resolution and studied the inner and brighter part of the nebula, about 1′ distant from θ^1 Ori. He finds an emission discontinuity of −1.6 mag. and a gradient of +2.14, in the range λλ 4180–4670, making the nebula very much redder than the star.

The resolution of the McDonald nebular spectrograph is about 30 A; Barbier's spectra seem to resolve about 8 A. The great strength of the emission lines and their confluence near the series limit require the highest possible resolution. While Swings and Struve[3] obtained a spectrum with the $f/2$ camera of the McDonald Cassegrain spectrograph, the long exposures required make photometry difficult. Consequently, I have re-observed the central part of the nebula with the two-prism (quartz) $f/1$ camera at McDonald; the exposures are 20 minutes on 103*a*-O film with a slit width projected on the plate of 0.02 mm. The dispersion is 200 A/mm at λ 3727, and the observed resolution is about 4A. The line *H*19 is the last hydrogen line resolved on the plate. Microphotometer tracings of high and low magnification are shown in Figure 1; the resolution seems to be considerably higher than in the tracing reproduced by Barbier.[2] A reproduction of a typical spectrogram is given in Plate XVII. There was no star brighter than 13 mag. on the slit; a long slit was used, running in the east-west direction, and the nebula was kept in a fixed position

* *Contributions from the McDonald Observatory, University of Texas*, No. 130.

[1] *Ap. J.*, **89**, 647, 1939. [2] *Ann. d'ap.*, **7**, 80, 1944. [3] *Ap. J.*, **96**, 310, 1942.

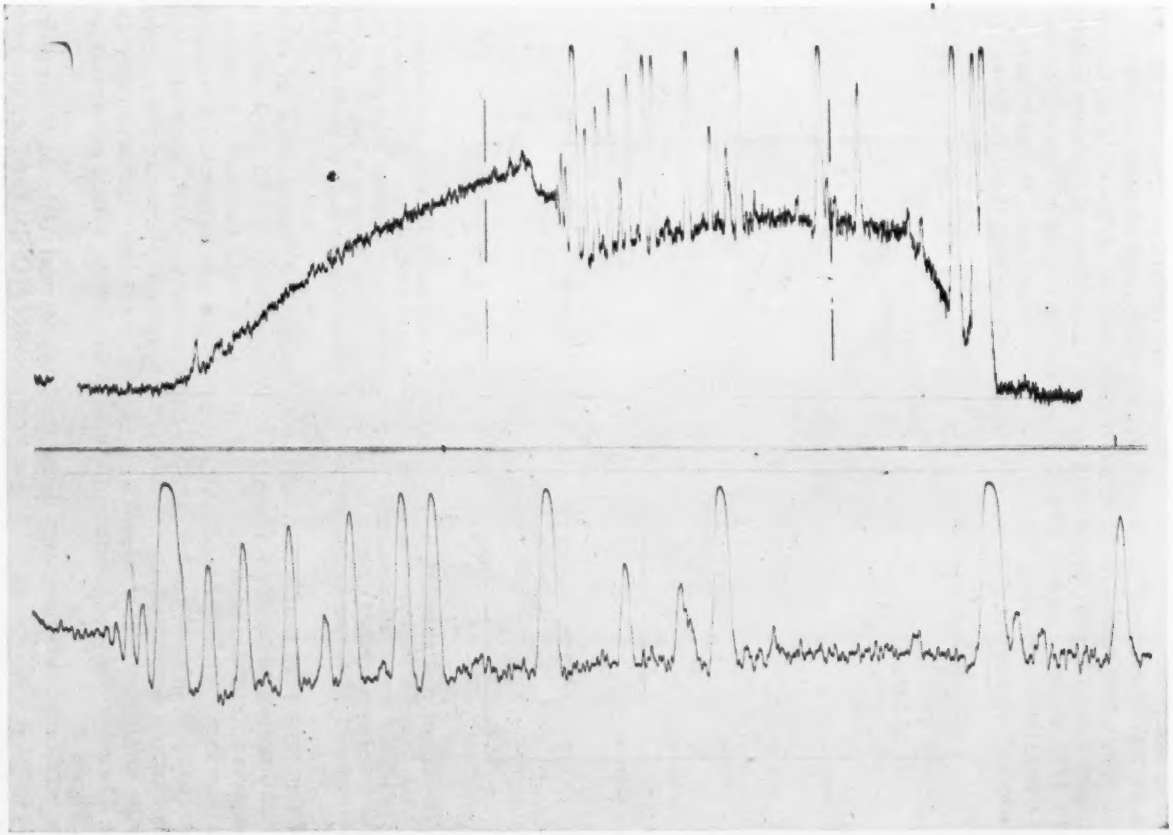

FIG. 1.—Microphotometer tracings of the spectrum of the Orion nebula. The upper tracing shows the region from λ 3188 to λ 5007, at low magnification. The lower tracing, taken at three times the magnification, runs from λ 3660 to λ 4472; it shows the relatively high resolving-power obtained. Note the weakness of λ 4363 with reference to *N*1 and *N*2.

during the exposure. Spectrophotometric comparison was made with the star θ^1 Ori C; the star was reduced about 5 mag. in brightness by means of a rapidly rotating sector. Calibration was provided by a tube photometer with ultraviolet, blue, and green filters. One exposure of the nebula was obtained through a rotating sector to reduce the brightness by 2.5 mag. and permit comparison of the nebular continuum and the strong emission lines. Three normal exposures of the nebula and five of the star were also obtained.

The mean energy distribution in the nebula was determined on three plates; the continuous emission can be located on the tracings with a fair degree of certainty between λ 4000 and λ 4750, as can be seen in the high-magnification tracing in Figure 1; between λ 3640 and λ 4000 the overlapping of the hydrogen lines is significant. Points to be measured were selected to be as free as possible from weak nebular lines listed by Wyse;[4] the

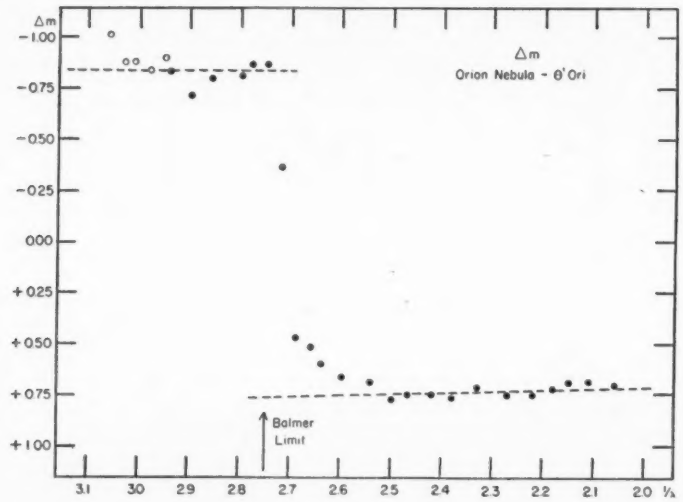

FIG. 2.—The differences of magnitude between the Orion nebula and θ^1 Ori C are plotted against $1/\lambda$ in μ^{-1}. In this figure the measures near the Balmer limit are smoothed, and the emission lines not shown. Open circles are uncertain points in the far ultraviolet, where less than three plates were measured. The dotted lines represent the adopted relative energy-curves. Please note that the point at $1/\lambda = 2.90$ has been plotted 0.10 mag. too low; when plotted correctly, it falls exactly on the dotted line.

location of the continuum near strong lines could be fairly well established by extrapolation from undisturbed regions of the spectrum. Near $H\beta$ and N1, N2, the location of the continuum is uncertain; and in the far ultraviolet the ozone bands and the weakness of the spectrum introduce larger accidental errors. The internal agreement of measures in the three nebular spectra and in the five stellar spectra was excellent. Spectrophotometry was particularly simple because the nebular continuum, in the mean, had the same density as the star (differences of magnitude ranged from +0.8 to −0.8) and almost the same color. The mean observed differences of magnitude, $\delta m(\lambda)$, nebula *minus* star, are plotted in Figure 2.

It is now established that the energy distribution in a normal reddened B star differs slightly from that of a black body.[5,6,7] In the single case of θ^1 Ori, it has been shown[5,6,8] that the reddening is of an abnormal character. I have plotted the measured differences

[4] *Ap. J.*, **95**, 356, 1942.

[5] Stebbins and Whitford, *Ap. J.*, **98**, 20, 1943.

[6] *Ibid.*, **102**, 318, 1945.

[7] Greenstein, *Ap. J.*, **104**, 403, 1946.

[8] Baade and Minkowski, *Ap. J.*, **86**, 123, 1937.

PLATE XVII

ENLARGEMENT (20×) OF THE SPECTRUM OF THE ORION NEBULA, SHOWING EMISSION LINES AND CONTINUUM; EXPOSURE 20 MINUTES, DISPERSION 200 A/MM at λ 3727

For maximum visibility of the Balmer discontinuity, hold the plate at arm's length. Note the strength of the continuum between λλ 3646–3700 compared to that to the red of λ 3727.

of brightness given by Stebbins and Whitford[6] between the Trapezium group and the mean of δ, ϵ, and ζ Ori, over the range from their point U ($1/\lambda = 2.83\ \mu^{-1}$) to point I ($1/\lambda = 0.97\ \mu^{-1}$), in Figure 3. The reddening of θ^1 Ori is +1.29 mag. on the U − I scale of colors. I have also plotted the values of $\delta m(\lambda)$ expected if the reddening were like that of the normal reddened B stars as well as those expected if the reddening followed the $1/\lambda$ relation (which is the expected form if the radiation is that of a black body). The deviation from the $1/\lambda$ relation is large for θ^1 Ori. The present range of wave length ($2.06 < 1/\lambda < 3.06$) is sufficiently small, however, that we can approximate the observed energy distribution by a black body. If we use the last three measured points (B, V, U), we can approximate by a straight line of slope +0.40, with deviations of only ±0.02 mag. The relative spectrophotometric gradient, $\delta\varphi$, of θ^1 Ori with respect to δ, ϵ, and ζ Ori is +0.37.

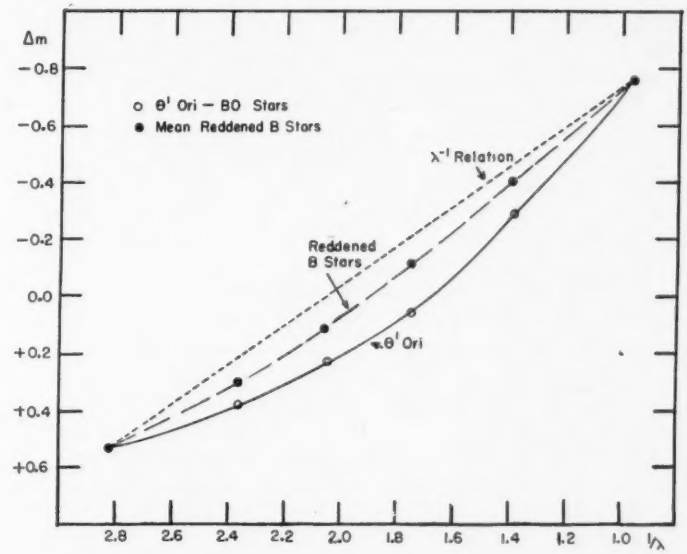

FIG. 3.—The photoelectric observations of the difference in magnitude between θ^1 Ori and δ, ϵ, and ζ Ori are shown as open circles. The solid dots represent the mean values observed for normal reddened B stars, and the dotted line, the black-body curve (or $1/\lambda$ reddening).

The Greenwich color temperature measures[9] for δ and ϵ Ori give their mean gradient as −0.16 with respect to the mean A0 star; if we adopt 14,000° for the color temperature of the mean A0 star, we obtain φ (δ, ϵ Ori) = 0.87, or $T_c = 23{,}000°$. Then $\varphi(\theta^1$ Ori) = 1.24, or $T_c = 12{,}500°$. The value of T_c for δ and ϵ Ori is approximately confirmed by Stebbins and Whitford's measures[6] of the V − I long-base-line colors. They adopt $T_c = 5500°$ for the standard dG6 stars; then $T_c = 20{,}400°$ for δ, ϵ, and ζ Ori, or $\varphi = 0.94$. On their scale, however, the mean A0 star has $T_c = 11{,}300°$, which may be rather low. A slight upward revision of T_c for the standard dG6 stars would bring both the A0- and the B-star temperatures into agreement with the Greenwich values. The uncertainty of T_c for θ^1 Ori is probably less than 2000°, and the adopted value of 12,500° may possibly be considered slightly high.[10]

[9] *M.N.*, **100**, 189, 1940.

[10] In all these discussions it is assumed that the intrinsic colors of the four stars of the Trapezium are the same; it is also assumed that there is no appreciable difference in the intrinsic colors of δ, ϵ, and ζ Ori.

PROPERTIES OF THE NEBULAR CONTINUUM

By inspection of Figure 2 we see that the nebula may be slightly redder than θ^1 Ori C; the dotted line at the right represents the observations well and has a slope corresponding to $\delta\varphi = +0.07$, for $1/\lambda < 2.5$. For $1/\lambda > 2.75$, $\delta\varphi = 0$ fits the observations. Consequently, φ (neb) = 1.31 and $T_c = 11{,}500°$ in the blue. In the violet, φ (neb) = 1.24 and $T_c = 12{,}000°$. The value of the discontinuity at the series limit, D, is 1.60 in mag. or 0.64 in $\log_{10} I$, in good agreement with Barbier,[2] who finds 0.56. However, Barbier gives $T_c = 6950°$ in the region λλ 4190–4685, and $T_c = 10{,}300°$ to the violet of the series limit. The differences between the results of the present investigation and those of Barbier are significant in the blue region. His resolving-power is relatively low, apparently, since he chooses only three points, at λλ 4685, 4567, 4190, as substantially unaffected by emission lines and determines the gradient in the nebula from those points. I believe that the results of the present investigation, using a larger number of points, determine the energy distribution more accurately. Inspection of the present plates shows that line blending is not serious for λ > 4000 A. In the ultraviolet region Barbier uses the energy beyond the Balmer limit in β Ori and α CMa as a standard. He adopts $\varphi_2 = 1.48$, which gives $T_c = 9800°$ in α CMa; however, the mean A0 star in the French color-temperature work has $\varphi_2 = 1.39$. The use of this higher T_c for his standard star would bring the color temperature in the Balmer emission into close agreement with the new value of 12,000°. However, his value of $T_c = 6950°$ in the blue is, I believe, definitely too low.

The bright O9 star, θ^2 Ori is only 2′ distant from θ^1 Ori; however, it is bluer by −0.14 mag. on the C_1 scale of photoelectric colors.[11] We may conclude that θ^2 Ori is well in front of the nebula and also less luminous than θ^1 Ori. It probably contributes relatively little to the excitation and illumination of the nebula. We shall assume that θ^2 Ori can be neglected in further discussions of the source of the nebular continuum. It is not probable that θ^1 Ori is completely behind the dark and bright nebulosity that makes up the Orion nebula, since the nebulosity seems substantially opaque for radiation of fainter and more distant stars.

The known possible sources of the continuum are: (1) recombination of ionized hydrogen atoms, (2) scattering and reflection by dust particles, (3) free-free emission, and (4) electron-scattering. It is improbable that process (2) would show a discontinuity at the Balmer-series limit; therefore, for λ < 3646, it is apparent that bound-free transitions in hydrogen constitute the main source of the intensity. In the region between λ 4000 and λ 4700 the emission may be of complex origin. Process (2) may be operative, and Paschen emission (Pac) similar to the Balmer continuum (Bac) may exist. The ratio of Paschen to Balmer emission can be computed theoretically. Since θ^1 Ori is reddened (and the reddening seems to be substantial even in the short distance between θ^1 and θ^2 Ori), it is possible that there is scattering and reflection of starlight by the reddening particles. We shall call this diffused continuum C and assume that it is similar to that observed in reflection nebulae. The discontinuity in intensity at the Balmer limit will be measured by D, where

$$D = \log_{10} \frac{I\,(\lambda < 3646)}{I\,(\lambda > 3646)} = \log_{10} \frac{C + \text{Bac} + \Sigma\,\text{Pac}}{C + \Sigma\,\text{Pac}}. \qquad (1)$$

We will include the Paschen and higher-series continua and the free-free transitions in Σ Pac. Barbier[2] has used the observed value of D to find the electron temperature, T_e, of the hydrogen gas; as T_e increases, D decreases. If $C \neq 0$, T_e will always be overestimated. Electron-scattering also reduces D; however, the optical thickness of the nebula due to free electrons is probably small. Barbier gives D as a function of T_e from computa-

[11] Stebbins, Huffer, and Whitford, *Ap. J.*, **91**, 20, 1940.

tions based on the theoretical work of Cillié.[12,13] After enlarging his computations, I give in Table 1 the theoretical values of D for various values of C/Bac. The value of D when $C = 0$ is given by

$$D = \log_{10} \frac{\sum_{n=2}^{\infty} \frac{1}{n^3} e^{(\chi_n - h\nu)/kT_e} + \frac{h^2 k T_e}{4\pi^2 e^4 m} e^{-h\nu/kT_e}}{\sum_{n=3}^{\infty} \frac{1}{n^3} e^{(\chi_n - h\nu)/kT_e} + \frac{h^2 k T_e}{4\pi^2 e^4 m} e^{-h\nu/kT_e}}, \tag{2}$$

TABLE 1

THE BALMER DISCONTINUITY, D

T_e	C/Bac				T_e	C/Bac			
	0	0.1	0.2	0.3		0	0.1	0.2	0.3
5,000°....	2.34	1.02	0.77	0.63	20,000°...	0.72	0.58	0.49	0.42
7,500....	1.68	.96	.73	.61	25,000....	.60	.49	.42	.37
10,000....	1.31	.87	.68	.57	30,000....	.51	.41	.36	.32
15,000....	0.93	0.70	0.57	0.49	40,000....	0.38	0.33	0.29	0.26

where χ_n is the energy required to ionize hydrogen from the nth level. At the Balmer limit, $h\nu = \chi_2$; and we obtain

$$D = \log_{10} \frac{\frac{1}{8} + \sum_{n=3}^{\infty} \frac{1}{n^3} e^{(\chi_n - \chi_2)/kT_e} + \frac{h^2 k T_e}{4\pi^2 e^4 m} e^{-\chi_2/kT_e}}{\sum_{n=3}^{\infty} \frac{1}{n^3} e^{(\chi_n - \chi_2)/kT_e} + \frac{h^2 k T_e}{4\pi^2 e^4 m} e^{-\chi_2/kT_e}}. \tag{3}$$

The last term in numerator and denominator of equation (3) measures the free-free emission, negligible at low T_e; when $T_e < 7500°$, terms with $n > 4$ are also negligible.

The observed value of $D = 0.64$ (Fig. 2) gives $T_e = 22{,}000°$ if we assume $C = 0$. On the other hand, if $C \neq 0$, the value of T_e can be quite low. For example, if $C/\text{Bac} = 0.2$, then $T_e = 12{,}000°$, in agreement with the color temperature. Such a value of C/Bac corresponds to $C/\Sigma\,\text{Pac} = 2.7$; about 70 per cent of the nebular continuum for $\lambda > 3646$ would be diffused stellar radiation rather than Paschen emission.

Beyond the Balmer limit, both Σ Pac and C are small compared to Bac. If we neglect C for $\lambda < 3646$, we get another estimate of T_e—one which we should theoretically expect to be the most direct and reliable. Essentially as a consequence of the assumed Maxwellian velocity distribution in the electron gas, the sum of the Balmer and higher continua gives an intensity I_ν (neb):

$$I_\nu\,(\text{neb})\, d\nu = C_1 N_i N_e e^{-h\nu/kT_e} d\nu\,. \tag{4}$$

[12] *M.N.*, **92**, 820, 1932.

[13] *Ibid.*, **96**, 771, 1936.

Let us compare this intensity with that in a black body at temperature T_c. Then the ratio is

$$\frac{I_\nu(\text{neb})\,d\nu}{I_\nu(*)\,d\nu} = \frac{1}{\nu^3}\, e^{-h\nu/kT_e}\left(e^{h\nu/kT_c} - 1\right). \tag{5}$$

If we express this ratio in stellar-magnitude differences δm, nebula *minus* star, and differentiate with respect to frequency, we can write equation (5) in a form similar to that used in the determination of spectrophotometric gradients. If we use as units $1/\lambda$ in μ^{-1}, we obtain

$$\frac{d(\delta m)}{d(1/\lambda)} = 1.086\left[\frac{14{,}300}{T_e} - \varphi + 3\lambda\right], \tag{6}$$

where φ is the usual stellar gradient. Our observations (Fig. 2) show that there is a zero slope of the δm-curve in the region beyond the Balmer limit. Thus,

$$\frac{14{,}300}{T_e} = \varphi - 3\lambda\,. \tag{7}$$

The mean wave length is about 0.34 μ, and $\varphi = 1.24$ for θ^1 Ori; then equation (7) gives $T_e = 65{,}000°$. If we assume that the total uncertainty of the gradient of θ^1 Ori and of the comparison of the nebula and the star gives a possible error of about ± 0.15 in the quantities to be inserted in equation (6), we can estimate a rough uncertainty of T_e near $\pm 20{,}000°$. Barbier obtained $T_e = 33{,}000°$, using the same method. While the two determinations differ, they are essentially in accord in indicating an enormously high electron temperature; at these high temperatures a small difference in the assumed color temperature of the comparison star makes a very large difference in the electron temperature of the nebula. (The same difficulty is encountered in determining accurate color temperatures of hot stars.) What seems definite is that the energy in the Bac decreases only slowly toward the ultraviolet. If interpreted as a simple recombination spectrum, this strong ultraviolet emission gives an electron temperature which can be conservatively estimated as larger than 40,000°. Such a value seems incompatible with all other determinations of T_e in planetary or diffuse nebulae and with other methods which can be applied to the Orion nebula.

This surprising phenomenon in the Bac region may be related to the anomalous continuous emission observed in the Crab nebula and in planetaries. Let us discard the assumption made as to the transparency of the nebula to its own radiations and consider the effects of self-reversal in the Balmer continuous emission. It should be remembered that the $2s^2S$ level of hydrogen is highly metastable and that the hydrogen absorption lines are observed in various astronomical sources under conditions of high dilution. We consider the effect of self-absorption within the Bac as follows. Let the only source of nebular emission in the Bac region be the recombination of ions; neglect the stimulated emission because of the high dilution. The ionization is governed by the exciting star and by the diffuse nebular radiation in the far ultraviolet. The electron temperature, T_e, is constant through the nebula; the nebula is considered to be a homogeneous plane-parallel slab, with x the depth measured from the front surface and x_0 the thickness. Let the only source of absorption be the bound-free transitions of hydrogen (although the free-free transitions are formally included). The emergent intensity of nebular radiation is given by

$$I_\nu d\nu = d\nu \int_0^{x_0} \epsilon_\nu \exp\left(-\int_0^x k_\nu dx\right) dx\,, \tag{8}$$

where ϵ_ν is the emission per unit volume, and k_ν the absorption per unit length. In the case of hydrogen we have

$$\epsilon_\nu = C_1 N_i N_e e^{-h\nu/kT_e} \tag{9}$$

$$k_\nu = C_2 N_2 \nu^{-3}\,. \tag{10}$$

The absorption coefficient involves the number of atoms of hydrogen in the second level, N_2; and we cannot compute it explicitly if the metastability of the $2s^2S$ level is appreciable. It is also not directly possible to give T_e in terms of the temperature of the exciting star without considering the problem of collisional excitation of the forbidden lines of other elements. From equation (8) we obtain

$$I_\nu d\nu = C_1 N_i N_e e^{-h\nu/kT_e} d\nu \int_0^{x_0} e^{-C_2 N_2 \nu^{-3} x} dx \,. \tag{11}$$

Introducing the optical depth

$$\tau_\nu = k_\nu x \,, \tag{12}$$

and integrating, we obtain

$$I_\nu d\nu = \frac{C_1 N_i N_e}{C_2 N_2} \nu^3 e^{-h\nu/kT_e} d\nu \,(1 - e^{-\tau_\nu(0)}) \,. \tag{13}$$

Equation (13) includes two correct formulae for limiting cases:

$$I_\nu d\nu = N_i N_e C_1 x_0 e^{-h\nu/kT_e} d\nu \,, \qquad \text{as} \qquad \tau_\nu(0) \to 0 \,, \tag{14}$$

$$I_\nu d\nu = \frac{C_1 N_i N_e}{C_2 N_2} \nu^3 e^{-h\nu/kT_e} d\nu \qquad \text{as} \qquad \tau_\nu(0) \to \infty \,. \tag{15}$$

In equation (14) we have the energy distribution and intensity predicted by the recombination formula (9) in a thin layer; and in equation (15) we have essentially the black-body formula in the absence of stimulated emission. The form of equation (15) is to be expected, since in the limit an opaque mass radiates like a black body at its boundary temperature, which is T_e. If we use equation (15) to compute the electron temperature from the color temperature of the observed Bac, we of course obtain $T_e = T_c$, instead of the value given by equation (7). If $\tau_\nu(0) = 3$ at the Balmer limit, the energy distribution given by equation (13) differs by only 10 per cent from the black-body distribution in equation (15), within the short range of wave lengths observed. In the far ultraviolet the energy in Bac should eventually correspond to a lower T_c than near the Balmer limit. However, if $\tau_\nu(0)$ is larger than 3, the color and electron temperatures will agree well.

If strong self-absorption exists within the Bac, it is not necessarily true that similar self-absorption exists within the Paschen continuum, since there is no metastable level above $2s^2S$. Consequently, the ratio of continuous absorption coefficients will have a strong discontinuity near the Balmer limit. The emission lines may also show self-reversal, depending on their Doppler width; the theory of the Balmer decrement might require some revision. The discontinuity in absorption coefficient near the series limit would be partly masked by the increase of the mean line-absorption coefficient.[14] A general depression in the ultraviolet energy distribution of stars seen through the nebula might be expected. (Such a depression is not visible in the spectra of the Trapezium stars.) Another observational test involves the filamentary structure of emission nebulae. In photographs taken at $\lambda < 3646$, sharp features, such as bright filaments, would be weakened and diffuse in appearance if they are behind most of the nebular gaseous absorption. On the other hand, photographs taken by the light of forbidden lines (in which no line self-absorption exists) at $\lambda > 3646$ could show sharp filamentary structure, diffused only by the dust-particle absorption. Remarkable photographs by Baade[15] of the Crab nebula show in general that the filamentary structure is very pronounced in the [*N* II] lines and much weaker in the blue and violet where continuous emission dominates; (the Crab nebula is not directly comparable with the Orion nebula because of the absence of hydro-

[14] By continuity, the large absorption coefficient in the Bac requires that the line-absorption coefficient in the higher series members also be large.

[15] *Ap. J.*, **96**, 188, 1942.

gen lines in the former). It would be interesting to determine whether photographs of the Orion nebula, taken at $\lambda < 3646$, reveal a more amorphous structure than those taken in the blue, green, or red. In many nebulae the emission lines are influenced by general expansion. If the line *He* I, λ 3188 ($2^3S-4^3P^o$) could be observed with sufficiently high dispersion to be seen as double, then the longer-wave component should be relatively weakened in comparison to the longer-wave component of λ 3888 ($2^3S-3^3P^o$).

The hypothesis of strong self-absorption within the Bac is novel and untested; it is apparently required by the anomalously high T_e given by the energy distribution in the Bac, using equation (14). A value of T_e much higher than 10,000° is probably excluded by our knowledge of the spectra of planetary nebulae. In spite of their higher excitation and ionization and their hotter exciting stars, electron temperatures[16] seldom exceed 10,000.° Aller[17] has pointed out that the low intensity of λ 4363, the more highly excited forbidden line of [*O* III], corresponds to $T_e = 10{,}500°$. In spectra of stars seen partly through the Orion nebula, O. C. Wilson[18] found the absorption line λ 3888 of *He* I, direct evidence for the population of a highly excited metastable state. We shall temporarily adopt $T_e = T_c = 12{,}000°$ for the Bac emission; then we obtain a consistent group of measures of T_e in the nebula. The Bac yields 12,000°; the small Balmer discontinuity can be explained by the existence of some reflection spectrum; the forbidden-line emission spectrum is about that expected at this T_e. If no Balmer continuous absorption exists, the energy distribution in Bac gives T_e between 65,000° and 33,000° (Barbier's value); the Balmer discontinuity, without any reflection spectrum, gives 22,000°; the forbidden line spectrum, 10,500°.

THE REFLECTION CONTINUUM AND THE EFFECT OF REDDENING

An observational distinction between the reflection continuum and the recombination hydrogen continuum in the blue is difficult. Polarization measurements in the spectrum may be possible, but polarization is not always present in reflection nebulae. The Paschen discontinuity is relatively small and badly distorted by terrestrial absorption bands. (If we define a quantity like D in eq. [1] for the Paschen limit, it is 0.48 for $T_e = 10{,}000°$ and 0.20 for $T_e = 25{,}000°$.) A reflection continuum may be expected from the general theory of reflection nebulae, unless the dust particles in the Orion nebula are very different from those near later-type stars in the Orion region. A rough value of the intensity of the continuum, C, may be computed. Consider the illumination by the Trapezium stars at a distance r of a part of the nebula lying in the celestial sphere; let R be the distance of the stars from the earth and m their apparent magnitude as seen at the earth. An observer at r will see the Trapezium as of magnitude m', where

$$m' = m - t_1 + 2.5 \log_{10}\left(\frac{r}{R}\right)^2 . \qquad (16)$$

The absorption in the line of sight to the earth is t_1. Express the angular separation of the point in the nebula from the star, in radians, as α; then

$$m' = m - t_1 + 5 \log_{10}\alpha . \qquad (17)$$

If interstellar dust exists at that point, with total optical thickness t_2, diffusing starlight uniformly in all directions with albedo γ, the first-order diffused intensity is, per unit solid angle,

$$\frac{\gamma}{4\pi} t_2 e^{-t_2} \qquad (18)$$

[16] Menzel, Aller, and Hebb, *Ap. J.*, **93**, 230, 1941.

[17] *Pub. A.S.P.*, **58**, 165, 1946.

[18] *Pub. A.A.S.*, **9**, 274, 1939.

in units of the incident intensity. Convert to surface brightness, $M(n)$, of the nebula in magnitudes per square degree at a distance α' in minutes of arc:

$$M(n) = m + t_2 - t_1 + 5 \log_{10}\alpha' - 2.5 \log_{10}(\gamma t_2) - 6.1 . \quad (19)$$

This formula is similar to Hubble's relation. Assume that the optical depth is about unity, $t_1 = t_2 = 1$, and that $\gamma = 0.5$. Then at one minute of arc from the Trapezium, $M(n) = +0.05$ mag. per square degree in the visual range of the spectrum (since $m = 5.4$ for the Trapezium refers to the visual range). This is an extremely high surface brightness, greater than that of most planetary nebulae, but evidence is not available to prove it sufficient to account for the observed continuum.

There exists some reddening material in front of θ^1 Ori; if this material produces the continuous spectrum, C, and is also located in the region where hydrogen emission occurs, the problem of color effects in the nebula is very complex. Certain simple models describing the effect of the dust on the hydrogen emission may be considered; we wish to consider the effect of the reddening on the color temperature of the continuum.

1. If the dark material lies completely in front of both θ^1 Ori and the nebular emission, the nebular emission is reddened as much as the light of θ^1 Ori. Then we correct φ (θ^1 Ori) to give a color temperature equal to its effective temperature. The value of T_c for $\lambda < 3646$ is then about 20,000°. There is no expected continuum, C.

2. Let the hydrogen and dust particles be well mixed throughout the nebula, and let the nebular particles have zero albedo. There will be no expected continuum, C, caused by diffused starlight. Model reflection nebulae have been investigated by Henyey and Greenstein,[19] but in these the fluorescence process was neglected. Let the rate of emission of Bac be proportional to ϵ per unit volume and let the absorption coefficient of light by the dust be k' (omitting the effect of hydrogen absorption within Bac). The equation of transfer can be derived as follows:

$$dI = -k'I\,ds + \epsilon\,ds . \quad (20)$$

The solution is of the form

$$I e^{\tau_1} = \int_0^{\tau_1} \frac{\epsilon}{k'} e^{\tau} d\tau . \quad (21)$$

The optical thickness of the dust is τ_1. From the reddening-curve of θ^1 Ori in Figure 3 it is apparent that τ_1 is very large; therefore let $\tau_1 \to \infty$. The surface brightness of the nebula, then, is

$$I = \frac{\epsilon}{k'} . \quad (22)$$

Consider two wave lengths, with $\lambda_2 < \lambda_1$,

$$\frac{I_1}{\epsilon_1} = \frac{\text{constant}}{k_1'} , \quad (23)$$

$$\frac{I_2}{\epsilon_2} = \frac{\text{constant}}{k_2'} . \quad (24)$$

The reddening of the Bac by dust absorption is measured by the color excess, E, as follows:

$$E = -2.5 \left(\log_{10} \frac{I_2}{\epsilon_2} - \log_{10} \frac{I_1}{\epsilon_1} \right) , \quad (25)$$

$$E = 2.5 \log_{10} \frac{k_2'}{k_1'} . \quad (26)$$

[19] *Ap. J.*, **88**, 580, 1938.

If k' varied as $1/\lambda^n$, then

$$E = 2.5n \log_{10} \frac{\lambda_1}{\lambda_2}. \tag{27}$$

While equation (27) could be used with normally reddened B stars, in the case of θ^1 Ori it seems best to use the observed reddening law. From Figure 3, $n < 1$. The absorption at point I ($1/\lambda = 0.97$) is unknown but may be estimated at 1 mag. Then at $\lambda_2 = 4000$ A, $k'_2 = 2.18$; and at $\lambda_1 = 4800$ A, $k'_1 = 1.99$. Inserting these values in equation (26), we find the reddening of the nebular emission to be $E = 0.10$ mag. If we correct the nebular continuum in the region $4000 < \lambda < 4800$ for this reddening, we obtain a correction, $\delta\varphi = -0.17$. Then the true nebular continuum has $\varphi(\text{neb}) = 1.07$, or $T_c = 16{,}000°$ in the blue. In the ultraviolet the nature of the reddening-curve is not known accurately, but for $\lambda < 3646$ we may estimate $T_c = 14{,}500°$.

3. In models (1) and (2) we have neglected the diffused stellar radiation completely. Since the albedo of the dust may be high, one limiting model is that with $\gamma = 1$. The particles scatter radiation without absorption. Since energy is conserved, all radiation emitted by the nebula escapes at the same rate as it is emitted. The observed and initial intensity distributions of the nebular radiation are the same, and no correction is required to the color temperatures, except for the reddening in front of the nebula. In model (3), T_e is about 12,000° in the Bac region, if we assume, as before, that the nebula is optically thick in hydrogen absorption beyond the series limit. In case $\gamma = 1$, the diffused stellar radiation in the blue would be large and the Pac emission relatively unimportant. The energy distribution in C then could be studied according to the theory of reflection nebulae.[19] However, since the variation of absorption with wave length is abnormally slow in θ^1 Ori, it is improbable that the color of the nebula and that of the star would differ appreciably.[20]

In summary, we may estimate that the dust absorption may change the color temperature of the nebular emission and that $12{,}000° < T_c < 20{,}000°$. Part of the continuum for $\lambda > 4000$ probably originates by diffusion by small particles in the nebula. The intensity of this reflection continuum lies between 10 and 20 per cent of that in the Balmer continuous emission. It is suggestive that the Balmer jump observed in the outer part of the Orion nebula[1] was smaller than that measured in the present investigation. It is possible that the reflection continuum, C, is relatively more important in the outer parts of the nebula, thus reducing the observed D. A relative decrease of C in the inner part of the nebula could be caused by radiation pressure, which reduces the density of interstellar dust near θ^1 Ori, or by the alteration of the optical properties of the dust particles in a region of relatively high radiation density.

THE LINE SPECTRUM

One spectrogram was obtained with a rotating sector to reduce the intensity of the emission lines by a factor of 10. The exposure time was the same as for the normal nebular exposures. The photometry of the lines, unfortunately, is not accurate, since a narrow slit was used. Further, $H\beta$ is in a region where the plate sensitivity is decreasing rapidly. The accuracy of line intensities for $H\beta$, $H\gamma$, and $H\delta$ may be rather low. The lines $H9$, $H10$, and $H11$ are measurable on all the nebular spectra. The other hydrogen lines have blending features, mainly *He* I and [*Ne* III]. The intensity of the lines was expressed in units of the energy within one wave-number of the stellar spectrum; the energy at λ 3646 (in the Bac) was measured also with respect to the star. Since we know the color temperature of θ^1 Ori, we can determine the ratio of the intensity in a line to that in one wave-number at the series limit. The lines of *He* I at the series limit do not offer any serious problem. The results are given in Table 2. The assumptions involved in the computation

[20] *Ibid.*, eqs. 12 and 13′, and Figs. 1 and 4.

of T_e are that the lines are produced by recombination without self-reversal; the theory is that of Cillié[12,13] and the more complete theoretical investigation by Baker and Menzel.[21] On assumption *B* of Baker and Menzel, it is found that the weighted mean value of T_e indicated by the observed line intensities is about 6500°; if we use the theory of Cillié, $T_e = 9000°$. The effect of reddening by dust within the nebula is to make the true value of I_n/Bac smaller than the observed, thus lowering the value of T_e deduced from Table 2. It is quite possible that the assumption of simple recombination in the production of the Balmer lines is not correct; the rather low value of T_e here derived is not of great weight.

TABLE 2

LINE INTENSITIES COMPARED TO CONTINUOUS EMISSION

Line	$\text{Log}_{10} I_n/\text{Bac}$	Line	$\text{Log}_{10} I_n/\text{Bac}$
$H\beta$.....	+3.15::	$H9$.....	+2.04
$H\gamma$.....	2.65:	$H10$.....	1.93
$H\delta$.....	+2.34:	$H11$.....	+1.81

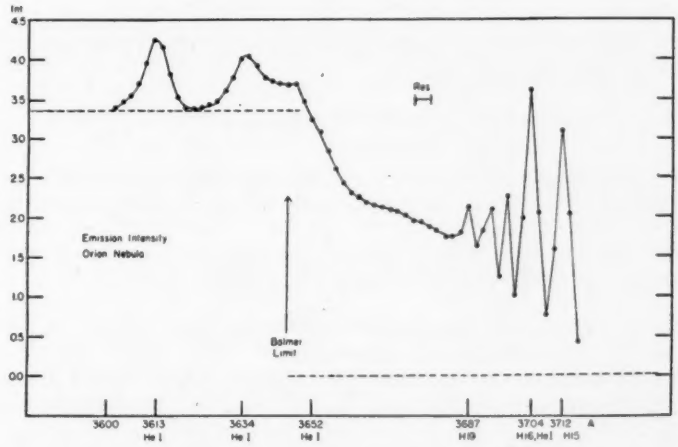

FIG. 4.—Intensity in the hydrogen emission near the series limit. The dotted line at the lower right is the unit of intensity, the extrapolated value of the emission for $4000 < \lambda < 4700$. The dotted line at the upper left is the ultimate value of the Balmer emission at $\lambda < 3646$. The dots are the observed intensities. Note that *He* I lines blend with *H* 16 and disturb the region near the Balmer limit. The bar labeled *Res.* shows the estimated resolving-power.

THE BALMER DISCONTINUITY

The intensity of the hydrogen lines may be correlated with the peculiar nature of the Balmer emission near the series limit. The microphotometer tracings in Figures 1 and 2 and the detailed emission intensities in Figure 4 show clearly the presence of a new phenomenon. In Figure 4, I plot the intensities of the lines $H15$–$H19$, the intensity in the region of overlapping lines, and the series limit itself. The underlying emission of Σ Pac and *C* is subtracted, and the intensity plotted is that of the hydrogen emission lines and the Balmer continuum. The unit of intensity is the intensity in Σ Pac and *C*, extrapolated to λ 3646. The microphotometer tracings were measured every millimeter (corresponding to every 2 A). Individual lines disappear just beyond $H19$, the point at which the expected resolution, 4 A, becomes insufficient to separate the lines. From $H19$

[21] *Ap. J.*, 88, 52, 1938.

on, over a range of 40 A to the series limit, the intensities rise, becoming constant at the series limit (except for the *He* I lines). According to the correspondence principle, in thermodynamic equilibrium the mean intensity of the emission lines lying within a frequency range $\delta\nu$ near the series limit should be continuous with the intensity in the continuum, per $\delta\nu$. This is certainly not true for lines as high as *H*19 in Figure 4. The line *H*16 is blended with *He* I; taking the average intensity in *H*15, *H*17, *H*18, and *H*19, we find a mean intensity of $I = 1.7$. At $\lambda < 3646$, however, the Bac clearly gives $I = 3.4$, as does the region far to the ultraviolet (see Fig. 2). The appearance of the very rapid increase in intensity of high series members is unusual. In chromospheric and prominence spectra[22] there is a clear continuity of the higher series members with the continuum. Other nebulae have not yet been studied in detail. The ratio of mean line emission to Bac for the lines *H*9, *H*10, and *H*11 is 0.37 and for *H*15–*H*19, 0.50. Obviously, for large principal quantum numbers the ratio is 1.

We must consider in more detail the behavior of the expected line emission near the series limit. Menzel and Aller[23] give the intensity in the continuum at the head of the Balmer series as

$$I_{k2}d\nu = \tfrac{1}{8} N_i N_e K h T_e^{-3/2} g_{k2} d\nu \,. \tag{28}$$

In equation (28) Kh is a numerical constant, and g_{k2} is the Gaunt factor (0.88 at the Balmer limit). For a hydrogen line, they give

$$I_{n2} = \tfrac{1}{8} N_i N_e K h T_e^{-3/2} g_{n2} b_n \frac{2R}{n^3} e^{hR/n^2kT_e} , \tag{29}$$

where b_n is a dimensionless factor representing the departure from thermodynamic equilibrium (in which $b = 1$). We obtain the ratio of line to continuum as follows:

$$\frac{I_{n2}}{I_{k2}d\nu} = \frac{b_n g_{n2} 2R}{d\nu g_{k2} n^3} e^{hR/n^2kT_e} . \tag{30}$$

The interval in frequency between successive Balmer lines approaches $2R/n^3$ as n becomes large; also as n becomes large, for reasonable values of T_e, the exponent of e in equation (30) approaches zero. Call the mean intensity when a given line is spread out over the interval between successive lines, $\bar{I}_{n2}$. We find that equation (30) becomes

$$\frac{\bar{I}_{n2}}{I_{k2}} \to b_n \frac{g_{n2}}{g_{k2}}, \qquad \text{as} \qquad n \to \infty \,. \tag{31}$$

The ratio of the Gaunt factors, g, becomes of the order of unity, and the variation of mean line intensity with n is merely that of b_n. In the limit, as $n \to \infty$, $b_n \to 1$. If we examine the values of b_n tabulated by Baker and Menzel[21] in their computation of the intensities of the Balmer lines, we find that b_n lies well below unity, even when $n = 30$, unless T_e is very high. Adopting their model *B*, the nebula optically thick in the Lyman region, a value of b_{17} near 0.5 (the observed value for the lines *H*15–*H*19) requires that T_e be less than 10,000°. An electron temperature as high as 28,000°, suggested as the mean value by Barbier,[2] gives $b_{17} = 0.75$ and seems to be excluded. The accuracy of the observational determination of b_{17} is actually quite high; only small differences of intensity and wave length are involved, and the effects of interstellar absorption are negligible. Therefore, we may view the value of b_n, for high values of n, as perhaps the most reliable method of determining T_e. We obtain $T_e = 9000°$. The correction of the observed in-

[22] See, e.g., microphotometer tracings by Dimitroff and Menzel in *Harvard Ann.*, **105**, 99, 1937, Pl. II. In the chromosphere, T_e is lower than in the Orion nebula; if the phenomenon involved only T_e, it should be even more pronounced in the chromosphere. However, it is the deviations from thermodynamic equilibrium that must be responsible for the difference.

[23] *Ap. J.*, **93**, 195, 1941.

tensity distribution just to the red of the series limit for the effect of instrumental resolving-power would provide a detailed comparison of the observations with the theory of the asymptotic value of b_n for very large n; the present dispersion is too low for such an attempt. A more rigorous use of equation (30) confirms the general argument based on equation (31).

Near the series limit we can also neglect the effect of self-absorption, because of the continuity of the absorption coefficients in the lines and in the continuum. However, it would be an interesting theoretical problem to obtain b_n, the deviation from thermodynamic equilibrium, in the presence of partial self-absorption. If the nebula is opaque at certain wave lengths, effects due to the stratification of the elements may also be of importance.

IONIZATION, EXCITATION, AND ABUNDANCE OF HYDROGEN

The absolute intensities of the lines and continua can be used to obtain an estimate of the number of atoms of hydrogen in the nebula. In this investigation no new data on absolute surface brightnesses were obtained. Some approximate quantitative considerations may be of interest.

In the nebula the electron density is high and the energy density of radiation also high, compared to conditions in interstellar space. If hydrogen, in relatively high density, exists near the Trapezium group, there will be an inner region where the hydrogen is mainly ionized and an outer region in which it becomes mainly neutral. Bengt Strömgren[24] has considered the problem of the extinction of the ultraviolet ionizing radiation of the O stars in a hydrogen cloud in space and has computed a distance, s_0, at which the transition from ionized to neutral hydrogen occurs. It is tempting to consider that the bright nebulosity has a size roughly measured by this s_0, since at greater distances the hydrogen is mainly neutral and the recombination process will not operate. I shall assume that the stellar radiation is that from a black body at $T = 35{,}000°$ (color temperature); the electron temperature is taken as 10,000°, and the radius of the star as four times the solar radius. Then

$$s_0 = 20N^{-2/3} \text{ parsecs}, \tag{32}$$

where N is the total number of hydrogen atoms per cm³ (ionized N_i *plus* neutral N_0). In planetary nebulae, $N_e = N_i = N$ is of the order of 10^4. The value of s_0 then is 0.043 psc, which seems too small. The Orion nebula is at a distance of about 400 psc, and the inner bright region is about 4′ in radius, or 0.47 psc. Such a value is obtained if $N = 300$ per cm³. The approximation involved is the neglect of the problem of radiative transfer of the Lyman continuum and lines in Strömgren's treatment.

At such low electron densities in most of the bright nebula and in the surrounding neutral hydrogen region, there will be a strong tendency for the level $2s^2S$ of hydrogen to become strongly overpopulated with respect to the $2p^2P^o$ levels. The metastability of the 2s level is nearly complete. Breit and Teller[25] find that the mixing of the 2s and the 2p states by random electric fields of passing electrons gives a transition probability 2s − 2p of about 5×10^{-2} sec^{-1}, at $T_e = 10{,}000°$ and with N_e near 10^3. The simultaneous emission of two photons results in transitions from 2s to 2p with a probability of about 8 sec^{-1}. Since this lifetime is similar to that of the upper levels of many observed forbidden lines, the de-excitation of 2s by ionization or collision is probably also rare. Consequently, we may expect that the Boltzmann distribution will give the number of excited atoms as follows:

$$\frac{N(2s)}{N(1s)} = \frac{N(2s)}{N_0} = 10^{-5040\chi_2/T_e}. \tag{33}$$

[24] *Ap. J.*, 89, 526, 1939. [25] *Ap. J.*, 91, 215, 1940.

Then $N(2s)$ is about $10^{-4}\, N_0$, for $T_e = 12{,}000°$. Now if we compute the absorption coefficient per atom in state 2s, at the Balmer series limit, we find that k_ν (atom) is near 10^{-17}. If we have a column of neutral hydrogen, x_0 cm thick, the optical depth will be

$$\tau_\nu(0) = x_0 N_0 1 0^{-4} 1 0^{-17} . \tag{34}$$

If we wish $\tau_\nu(0)$ to be unity, $x_0 N_0 = 10^{21}$. Now, outside the ionized region we can take $N_0 = 10^3$, so $x_0 = 10^{18}$, or about 0.33 psc. To obtain opacity within the Balmer continuum we thus require a region of neutral hydrogen of the same density and about the same size as the observed bright nebula.

A rough numerical check is obtained from Ambarzumian's evaluation[26] of the number of excited atoms in the Orion nebula from the observed surface brightness of the nebula in $H\beta$ and $H\gamma$. He found that there were about 10^4 atoms in each state ($n = 4$ and 5) per cm^2 column through the nebula (assuming no self-absorption within the lines). Since there is no appreciable effect of metastability for these levels, their population is reduced from the Boltzmann value by the dilution W. (We neglect a possible more complete discussion based on the work of Baker and Menzel[21]). Then

$$x_0 N_n = x_0 N_0 W \frac{\varpi_n}{\varpi_0}\, e^{-\chi_n/kT} . \tag{35}$$

If we could estimate W exactly, equation (35) would give the number of neutral atoms. However, the exciting radiation is variable through the nebula, and the excitation cannot be described by the Boltzmann formula. For a rough approximation we take the value of $W = 10^{-14}$ (at the edge of the ionized region) and use the electron temperature $T_e = 12{,}000°$. Then Ambarzumian's observed populations yield $x_0 N_0 = 10^{22}$ and the value of $\tau_\nu(0)$ is 10. While preliminary, these attempts to determine the opacity in the Balmer continuum suggest an appreciable order of magnitude. The total mass of hydrogen in the nebula is about ten times the solar mass.

ADDENDUM

In private correspondence Dr. Donald H. Menzel of the Harvard Observatory has pointed out some theoretical difficulties in the derivation of equation (15). I am deeply indebted to him for discussion of some of these points. I attempted to show that T_e becomes equal to T_c for a nebula optically thick in the Balmer continuum. In such a nebula it would be necessary to consider theoretically in detail the energy transfer in the Lyman continuum as well and derive the variation of T_e with distance from the exciting star. Further, I assumed that the hydrogen is partly ionized and partly neutral in the same volume of space. This volume must be large enough to contain a sufficient number of ionized (recombining and emitting) atoms, as well as neutral (absorbing) atoms to produce opacity. In the discussion of Strömgren's theory in the last section, we see that the ionized and neutral regions may be mainly separated in space. It is possible to compute the energy distribution in an emitting nebula surrounded by an absorbing hydrogen cloud. The emergent energy is then quite different from that of a black body. Instead of equation (15) we find that

$$I_\nu d\nu = I_0 d\nu \exp\left[-h\nu/kT_e - \tau_\nu(0)(\nu_0/\nu)^3\right], \tag{36}$$

where ν_0 is the frequency at the Balmer limit. The last term depends on the variation of the hydrogen absorption with frequency. The exciting stars, if seen through this neutral hydrogen absorbing material, would show a Balmer absorption discontinuity. If $\tau_\nu(0) = 1$, $T_c = T_e$ at the series limit as in our first model, but there would be appreciable change of color temperature with wave length. If $\tau_\nu(0)$ is large, T_c would be high, and the series limit would appear as an absorption discontinuity. If such more complex phenomena should be observed in nebulae, we may have to consider this second model.

[26] *Zs. f. Ap.*, **6**, 107, 1933.

The theoretical situation is incompletely investigated at present. It would be profitable to consider the emission intensities to be expected in a nebula in which the second level of hydrogen is treated separately for the 2s and the 2p states. Even in an optically thin nebula, the values of b_n might be changed. Dr. Menzel further points out that if the nebula is opaque, b_n might approach unity even for small values of n. For example, in the chromosphere and probably in Be stars the observations indicate that b is close to unity. The total amount of hydrogen per unit area in a Be star may well be of the same order as in the Orion nebula. The dilution is very much greater in the nebula, however.

The full explanation of the observations must wait on a more complete theory of the recombination emission of hydrogen. If, in fact, high opacity does require b_n near unity, the observation that $b_{17} = 0.5$ may indicate that the nebula is not opaque. Unfortunately, the low observed value of b_{17} indicates a low T_e, while the energy distribution in the Balmer continuum requires a high T_e. In such a new theory it would be desirable to re-evaluate also the expected Balmer emission discontinuity, which may be affected by the self-absorption from the 2s level. In a planetary nebula, where the complications arising from the reflection continuum do not exist, the theoretical predictions of the Balmer discontinuity, the values of b_n, and the energy distributions in Pac and Bac can all be compared with observation.

ON THE CONTINUOUS ABSORPTION COEFFICIENT OF THE NEGATIVE HYDROGEN ION. III

S. CHANDRASEKHAR AND FRANCES HERMAN BREEN
Yerkes Observatory
Received August 14, 1946

ABSTRACT

In this paper the contribution to the continuous absorption coefficient of the negative hydrogen ion by the free-free transitions is evaluated in terms of the matrix elements of the acceleration in the Hartree field of a hydrogen atom. The new coefficients are larger than the earlier determinations by factors exceeding 10 over the entire range of wave lengths of astrophysical interest.

Tables of the continuous absorption coefficient of H^-, including both the bound-free and the free-free transitions for various temperatures ($2520° \leqslant T \leqslant 10{,}080°$) and wave lengths ($\lambda > 4000$ A) are also provided. It is further shown that the new coefficients are sufficient to account for the solar continuous spectrum from λ 4000 A to λ 25,000 A.

1. *Introduction.*—In two earlier papers[1] the continuous absorption coefficient of the negative hydrogen ion has been considered, and its cross-sections for the radiative processes leading to its ionization have been determined with some degree of definitiveness. And recent astrophysical discussions[2] relating to the continuous spectrum of the sun have shown that the cross-sections which were derived for these "bound-free" transitions of H^- are adequate to account for the continuous absorption in the solar atmosphere between λ 4000 A and λ 10,000 A. Beyond λ 10,000 A, however, there appears to be an additional source of absorption, which it would be natural to suppose is due to the radiative transitions of free electrons in the field of neutral hydrogen atoms.[3] But the existing evaluations[4] of these "free-free" transitions make them insufficient to account for the observed amount of absorption beyond λ 10,000 A by factors exceeding 10. Indeed, on the strength of this discrepancy, the existence of a hitherto "unknown source of absorption" has been concluded.[5] However, as similar conclusions relating to the bound-free transitions have proved premature in the past, we have examined the earlier evaluations of the free-free transitions of H^- and have found, as we shall presently explain, that there are ample grounds for mistrusting them, even as to giving the correct orders of magnitude. We have, accordingly, made some further calculations to obtain estimates of the free-free transitions, on which at least some reliance could be placed. It is the object of this paper to present the results of such calculations and to show that these newly determined cross-sections for the free-free transitions, together with the cross-sections for the bound-free transitions given in Paper II, are sufficient to account for the continuous absorption in the solar and in the stellar atmospheres of neighboring spectral types in a manner which dispels any remaining belief in an "unknown source of absorption."

2. *The inadequacy of the Born approximation for the evaluation of the free-free transitions of* H^-.—The essential approximation which underlies all the earlier evaluations[4] is that of Born's for describing the motion of an electron in the field of a hydrogen atom.

[1] S. Chandrasekhar, *Ap. J.*, **102**, 223, 395, 1945. These papers will be referred to as Papers I and II, respectively.

[2] G. Münch, *Ap. J.*, **102**, 385, 1945; D. Chalonge and V. Kourganoff, *Ann. d' ap.* (in press).

[3] The possible astrophysical importance of this process was first suggested by A. Pannekoek, *M.N.*, **91**, 162, 1931.

[4] L. Nedelsky, *Phys. Rev.*, **42**, 641, 1932; D. H. Menzel and C. L. Pekeris, *M.N.*, **96**, 77, 1935; J. A. Wheeler and R. Wildt, *Ap. J.*, **95**, 281, 1942.

[5] See particularly the discussion of Chalonge and Kourganoff (*op. cit.*).

This is apparent, for example, from the agreement of the calculations of Menzel and Pekeris with those of Wheeler and Wildt, in which the Born approximation is explicitly made. However, on consideration it appears that for the range of energies which occur in stellar atmospheres the Born approximation for incident s-electrons must be a very bad one; for, as the mean energy of the electrons in a Maxwellian distribution at temperature T is

$$\tfrac{1}{2}\bar{k}^2 = 0.0243\left(\frac{T}{5040}\right) \tag{1}$$

when expressed in atomic units, it is evident that it is only electrons with $k^2 < 0.05$ that will principally contribute to the continuous absorption. And for s-electrons with as small energies as these, the Born approximation must fail. This is indeed well known from the work of P. M. Morse and W. P. Allis.[6] But it may be useful to illustrate this failure in a manner which will emphasize the magnitude of the errors to which the Born approximation may lead in the cross-sections for radiative transitions. For this purpose, we have compared in Figure 1 the radial s-waves

$$\chi_0\,(\text{Born}) = \sin k r \tag{2}$$

on the Born approximation with the properly normalized s-spherical waves in the Hartree field of a hydrogen atom, which the authors have recently tabulated.[7] It is seen that for $r < 2$ the Hartree waves have amplitudes which are larger than χ_0 (Born) by factors which, on the average, exceed 3. However, similar comparisons between the p-waves

$$\chi_1\,(\text{Born}) = \frac{\sin k r}{k r} - \cos k r \tag{3}$$

on the Born approximation and the corresponding Hartree waves show that equation (3) provides a satisfactory approximation for the energies in which we are interested. Remembering that, in the evaluation of the matrix elements of the acceleration, the wave functions for $r < 2$ are all that matters (cf. Fig. 2, in which we have plotted the acceleration $\ddot{r}$ in the static field of a hydrogen atom) and, further, that the contribution to the absorption coefficient arising from the $s \rightarrow p$ and $p \rightarrow s$ transitions must far outweigh all the others, it is apparent that in the Hartree approximation we shall obtain cross-sections which will be larger by ten or more times the values obtained with the Born approximation. In other words, we may expect a correct evaluation of the free-free transitions of H^- to bring about an agreement between physical theory and the demands of astrophysical data without the need of postulating a still unknown source of continuous absorption.

3. *Formula for the evaluation of the cross-sections for the free-free transitions of* H^- *on the Hartree approximation.*—Our remarks in the preceding section have shown the inadequacy of the Born approximation for the evaluation of the free-free transitions of H^-. The use of the Hartree approximation suggests itself as the next best, though the effects of exchange and polarization may very well be appreciable for the very slow s-electrons in which we are primarily interested. But it may be hoped that these latter effects will not, at any rate, affect the orders of magnitude of the derived quantities! In any case, to improve on the Hartree approximation would require an amount of numerical work which will be several fold; and the task is immense even as it is.[8] These considerations, to-

[6] *Phys. Rev.*, **44**, 269, 1933.

[7] S. Chandrasekhar and F. H. Breen, *Ap. J.*, **103**, 41, 1946.

[8] For example, the present work has required the numerical integration of 63 radial functions and the evaluation of 523 infinite integrals, not to mention the computation of numerous auxiliary functions and tables. (All this work was done with a Marchant.)

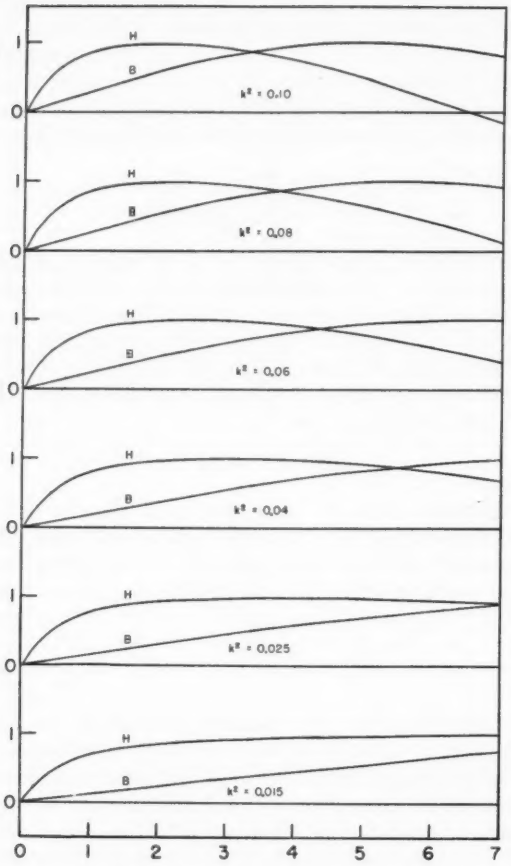

FIG. 1.—A comparison of the radial wave functions of s-electrons in the field of a hydrogen atom on the Born (B) and the Hartree (H) approximations for various energies of astrophysical interest. (The abscissa measures the distance from the center in units of the Bohr radius).

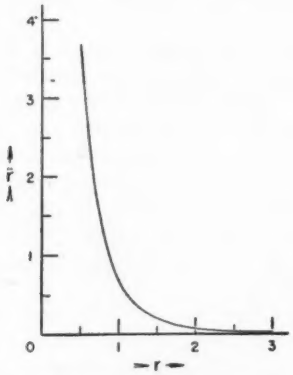

FIG. 2.—The acceleration $\ddot{r} = [r^{-2} + 2(1 + r^{-1})]e^{-2r}$ of an electron in the Hartree field of a hydrogen atom.

gether with the urgency of the astrophysical needs, have prompted us to undertake in some detail the evaluation of the cross-sections for the free-free transitions of H^-, using the *s*- and the *p*-spherical waves in the Hartree field of the hydrogen atom which we have tabulated in an earlier paper.[7]

Now, in the Hartree approximation a wave function representing a plane wave at infinity is given by

$$\Psi = \sum_{l=0}^{\infty} \frac{i^l\,(2l+1)}{k\,r} P_l\,(\mu)\,\chi_l\,(r;\,k^2)\,, \tag{4}$$

where the radial functions $\chi_l(r;\,k)$ are solutions of the equation

$$\frac{d^2\chi_l}{d\,r^2} + \left\{k^2 - \frac{l\,(l+1)}{r^2} + 2\left(1+\frac{1}{r}\right)e^{-2r}\right\}\chi_l = 0\,, \tag{5}$$

which have unit amplitude at infinity. (In the foregoing equations we have adopted the atomic system of units). For wave functions of the form (4) the standard formula in the quantum theory, which gives the cross-section for a transition in which a free electron with an initial momentum k_0 (in atomic units) becomes an electron with a momentum k_1 by the absorption of a quantum of appropriate energy from an incident beam of unit specific intensity, can be written in the form[9]

$$\left.\begin{aligned} a\,(k_0^2;\,\Delta k^2) &= \frac{256\pi^2}{3}\left(\frac{2\pi e^2}{h\,c}\right)\left(\frac{h^2}{4\pi^2 m\,e^2}\right)^5 \frac{1}{k_0^2 k_1\,(\Delta k^2)^3} \\ &\times \sum_{l=1}^{\infty} l\{\,|\,(l,\,k_0^2\,|\,\ddot{r}\,|\,l-1,\,k_1^2)\,|^2 + |\,(l-1,\,k_0^2\,|\,\ddot{r}\,|\,l,\,k_1^2)\,|^2\}\,\mathrm{cm}^5\,, \end{aligned}\right\} \tag{6}$$

where the various matrix elements $(l,\,k_1^2|\ddot{r}|l-1,\,k_2^2)$ have to be evaluated in atomic units and

$$\Delta k^2 = k_1^2 - k_0^2\,. \tag{7}$$

Equation (6) gives the cross-section for a single hydrogen atom in the ground state for the transition in question when there is one electron with momentum k_0 in unit volume. Moreover, the wave length, λ, of the radiation for which formula (6) gives the atomic absorption coefficient is

$$\lambda\,(\Delta k^2) = \frac{911.3}{\Delta k^2}\,A\,. \tag{8}$$

In the Hartree field of a hydrogen atom the acceleration is given by

$$\ddot{r} = \left[\frac{1}{r^2} + 2\left(1+\frac{1}{r}\right)\right]e^{-2r}\,, \tag{9}$$

and the matrix elements which have to be evaluated are of the type

$$(l,\,k_0^2\,|\,\ddot{r}\,|\,l-1,\,k_1^2) = \int_0^{\infty} \chi_l\,(r;\,k_0^2)\left[\frac{1}{r^2} + 2\left(1+\frac{1}{r}\right)\right]e^{-2r}\chi_{l-1}\,(r;\,k_1^2)\,d\,r\,. \tag{10}$$

To obtain the absorption coefficients appropriate for an assembly in which we have a Maxwellian distribution of electrons corresponding to a temperature T, we must average $a(k_0^2;\,\Delta k^2)$ over all initial k_0^2 (and for a fixed Δk^2) with the weight function

$$197.8\,\theta^{3/2} k_0\,e^{-31.326 k_0^2} \tag{11}$$

[9] Cf. J. A. Gaunt, *Phil. Trans. R. Soc., London*, A, **229**, 163, 1930; see particularly formula (5.24) on p. 194; also Wheeler and Wildt, *op. cit.*, eq. (6) on p. 284.

where

$$\theta = \frac{5040}{T}. \tag{12}$$

In astrophysical applications it is convenient to express the free-free atomic absorption coefficients as per unit electron pressure. If we denote by $\kappa(\Delta k^2)$ the corresponding atomic absorption coefficient after averaging over a Maxwell distribution of initial velocities, we find that we can write our basic formula in the form

$$\left.\begin{aligned}\kappa(\Delta k^2) = {} & \frac{7.251\times 10^{-29}\theta^{5/2}}{(\Delta k^2)^3}\int_0^\infty d(k_0^2)\,\frac{f(k_0^2)}{k_0^2 k_1} \\ & \times \sum_{l=1}^{\infty} l\{|(l, k_0^2|\ddot{r}|l-1, k_1^2)|^2 + |(l-1, k_0^2|\ddot{r}|l, k_1^2)|^2\}\frac{\text{cm}^4}{\text{dyne}},\end{aligned}\right\} \tag{13}$$

where

$$f(k_0^2) = 100 k_0 e^{-31.32\theta k_0^2}. \tag{14}$$

4. *Details of the evaluation: tables of the necessary matrix elements.*—The problem of numerically evaluating absorption coefficients for free-free transitions is a specially troublesome one, since for each wave length the coefficients must be computed for a range of initial velocities sufficient to allow for the averaging over Maxwell distributions for various temperatures. If the matrix elements for all the necessary values of k_0^2 and Δk^2 must be individually evaluated, then the number of wave functions which would be needed will be so many as to make the problem an impracticable one on this score alone. It may, therefore, be useful to place on record the details of our procedure in this instance.

First, we may observe that the infinite series in equation (13) is so rapidly convergent that we may ignore all terms except the first one. This may be verified in the following manner:

We have already indicated in § 2 that for $l \geqslant 1$ we can use the Born approximation without any serious error. We may therefore write

$$\chi_l(r; k^2) = \left(\frac{\pi k r}{2}\right)^{1/2} J_{l+\frac{1}{2}}(kr). \tag{15}$$

Accordingly, for $l \geqslant 2$,

$$\left.\begin{aligned}(l, k_1^2|\ddot{r}|l-1, k_2^2) = {} & \tfrac{1}{2}\pi (k_1 k_2)^{1/2}\int_0^\infty r J_{l+\frac{1}{2}}(k_1 r) J_{l-\frac{1}{2}}(k_2 r) \\ & \times\left[\frac{1}{r^2} + 2\left(1+\frac{1}{r}\right)\right] e^{-2r} dr.\end{aligned}\right\} \tag{16}$$

Writing equation (16) in the form

$$\left.\begin{aligned}(l, k_1^2|\ddot{r}|l-1, k_2^2) = {} & -\tfrac{1}{2}\pi k_1 k_2\int_0^\infty r J_{l+\frac{1}{2}}(k_1 r) J_{l-\frac{1}{2}}(k_2 r) \\ & \times\frac{d}{dr}\left[\left(1+\frac{1}{r}\right)e^{-2r}\right] dr\end{aligned}\right\} \tag{17}$$

and integrating by parts, we find after some further reductions that

$$\left.\begin{aligned}(l, k_1^2|\ddot{r}|l-1, k_2^2) = {} & \tfrac{1}{2}\pi (k_1 k_2)^{1/2}\int_0^\infty (1+r)\, e^{-2r}[k_1 J_{l-\frac{1}{2}}(k_1 r) J_{l-\frac{1}{2}}(k_2 r) \\ & - k_2 J_{l+\frac{1}{2}}(k_1 r) J_{l+\frac{1}{2}}(k_2 r)]\, dr.\end{aligned}\right\} \tag{18}$$

The integrals over the Bessel functions which occur in the foregoing equation can be expressed in terms of the Legendre functions of the second kind, $Q_l(x)$, and their derivatives, $Q_l'(x)$.[10] We find

$$(l, k_1^2|\ \ddot{r}\ |l-1, k_2^2) = \tfrac{1}{2}k_1 Q_{l-1}(x) - \tfrac{1}{2}k_2 Q_l(x) - \frac{1}{k_2}Q_{l-1}'(x) + \frac{1}{k_1}Q_l'(x), \quad (19)$$

where the argument for the Legendre functions is

$$x = \frac{k_1^2 + k_2^2 + 4}{2k_1k_2}. \quad (20)$$

Using equation (19), we can readily verify the fact that all transitions in which the incident electron is characterized by an l greater than 1 contribute less than a fraction of 1 per cent to the sum in equation (13). It is therefore sufficient to consider only the matrix elements $(0, k_0^2|\ddot{r}|1, k_1^2)$ and $(1, k_0^2|\ddot{r}|0, k_1^2)$. In evaluating these matrix elements it was found convenient to distinguish three cases, discussed below.

i) $k_0^2 < 0.015$ *and* $k_1^2 > 0.015$.—It has been shown[7] that, when $k^2 < 0.015$, the radial functions $\chi_0(r; k^2)$ and $\chi_1(r; k^2)$ can be expressed with sufficient accuracy in the form

$$\chi_0(r; k^2) = \frac{1}{A_0(k)}[X_0(r) - k^2 Y_0(r)] \quad (21)$$

and

$$\chi_1(r; k^2) = \frac{1}{A_1(k)}[X_1(r) - k^2 Y_1(r)], \quad (22)$$

where $A_0(k)$ and $A_1(k)$ are the factors which normalize the functions in brackets to unit amplitude at infinity and X_0, Y_0, X_1, and Y_1 are certain functions which have been tabulated. With this representation of the wave functions, the matrix element $(0, k_0^2|\ddot{r}|1, k_1^2)$ can be expressed in the form

$$\left.\begin{aligned}(0, k_0^2|\ \ddot{r}\ |1, k_1^2) = \frac{1}{A_0(k_0)\,A_1(k_1)}\Big[&\int_0^\infty X_0X_1\ddot{r}\,dr - k_0^2\int_0^\infty Y_0X_1\ddot{r}\,dr \\ &- k_1^2\int_0^\infty X_0Y_1\ddot{r}\,dr + k_0^2k_1^2\int_0^\infty Y_0Y_1\ddot{r}\,dr\Big].\end{aligned}\right\} \quad (23)$$

The corresponding expression for $(1, k_0^2|\ddot{r}|0, k_1^2)$ can be obtained from equation (23) by simply interchanging k_0 and k_1.

Thus, when k_0^2 and k_1^2 are both less than 0.015, the necessary matrix elements can all be evaluated in terms of four definite integrals which are listed in Table 1.

TABLE 1

INTEGRALS FOR COMPUTING THE MATRIX ELEMENTS WHEN k_0^2 AND k_1^2 ARE BOTH LESS THAN 0.015

$\int_0^\infty X_0X_1\ddot{r}dr$ 0.40044	$\int_0^\infty Y_0X_1\ddot{r}dr$ 0.22641
$\int_0^\infty Y_0Y_1\ddot{r}dr$ 0.16669	$\int_0^\infty X_0Y_1\ddot{r}dr$ 0.09076

ii) $k_0^2 < 0.015$ *and* $k_1^2 \geqslant 0.015$.—In this case we can use the representation (20) or (21) only for the radial function describing the incident electron, and the required matrix elements can be expressed in the forms

$$(0, k_0^2|\ \ddot{r}\ |1, k_1^2) = \frac{1}{A_0(k_0)}\left[\int_0^\infty X_0\chi_1(r; k_1)\ \ddot{r}\,dr - k_0^2\int_0^\infty Y_0\chi_1(r; k_1)\ \ddot{r}\,dr\right] \quad (24)$$

[10] Cf. G. N. Watson, *Theory of Bessel Functions*, p. 389, Cambridge University Press, 1944.

and

$$(1, k_0^2 \mid \ddot{r} \mid 0, k_1^2) = \frac{1}{A_1(k_0)} \left[\int_0^\infty X_1\chi_0(r; k_1)\, \ddot{r}\, dr - k_0^2 \int_0^\infty Y_1\chi_0(r; k_1)\, \ddot{r}\, dr \right]. \quad (25)$$

The integrals which occur on the right-hand side of equations (24) and (25) have been evaluated for various values of $k_1^2 \geqslant 0.015$ and are listed in Table 2; for these values of k_1^2 and for all $k_0^2 < 0.015$, the required matrix elements can be found without further numerical integrations according to equations (24) and (25).

iii) $k_0^2 \geqslant 0.015$ *and* $k_1^2 \geqslant 0.015$.—In this case there is no short cut to the evaluation of the matrix elements, and the integrals must all be evaluated individually. However, for this purpose we have only the radial functions tabulated in the paper by Chandrasekhar and Breen.

Our procedure, then, for determining the various matrix elements with assigned k_0^2 and Δk^2 was as follows:

TABLE 2

INTEGRALS FOR COMPUTING THE MATRIX ELEMENTS WHEN $k_0^2 < 0.015$

k_1^2	$\int_0^\infty X_1\chi_0(r; k_1^2)\ddot{r}dr$	$\int_0^\infty Y_1\chi_0(r; k_1^2)\ddot{r}dr$	$\int_0^\infty X_0\chi_1(r; k_1^2)\ddot{r}dr$	$\int_0^\infty Y_0\chi_1(r; k_1^2)\ddot{r}dr$
0.015	0.64185	0.14271	0.0033763	0.0018942
.030	.71329	.15557	.0067421	.0037565
.045	.74163	.15863	.0101066	.0055872
.060	.75618	.15858	.013458	.0073854
.080	.76622	.15650	.017920	.0097336
.100	.77079	.15328	.022366	.012025
.125	.77307	.14861	.027895	.014809
.150	.77310	.14360	.033392	.017504
.175	.77164	.13840	.038851	.020113
.200	.76954	.13170	.044272	.022636
0.250	0.76357	0.12293	0.054972	0.027421

First, the matrix elements listed in Table 3 were computed with the known radial functions. (This table also includes the matrix elements computed according to eqs. [23], [24], or [25]). The values given in Table 3 show sufficiently smooth differences with both arguments to enable satisfactory interpolation for any intermediate value. Using these directly computed values, we next found, by interpolation, all the matrix elements which were needed for the evaluation of $\kappa(\Delta k^2)$ according to equation (13); the matrix elements found in this manner are given in Table 4, which was then the basis for our further calculations.

5. *The continuous absorption coefficient of* H^-.—Even with as complete a table of matrix elements as Table 4, the evaluation of the continuous absorption coefficient for free-free transitions is a tiresome matter, since, for each wave length and temperature for which the coefficient is desired, a numerical integration must be performed. The coefficients tabulated in Table 5 were determined in this manner according to equation (13).

In Table 5 we have also entered the absorption coefficients due to the bound-free transitions for $\lambda < 16{,}500$ A. These latter coefficients were obtained by multiplying the cross-sections derived from those given in Paper II (Table 3) by the factor

$$\phi(\theta) = 4.158 \times 10^{-10} \theta^{5/2} e^{1.726\theta}, \quad (26)$$

which gives the number of H^- ions present per neutral hydrogen atom and unit electron pressure. The contributions to the continuous absorption coefficient of H^- by the

TABLE 3

THE MATRIX ELEMENTS $(0, k_0^2|r|1, k_1^2)$ AND $(1, k_0^2|r|0, k_1^2)$ EVALUATED BY EXACT NUMERICAL INTEGRATIONS

k^2	$(0, 0.0025\|r\|1, k^2)$	$(1, 0.0025\|r\|0, k^2)$	$(0, 0.005\|r\|1, k^2)$	$(1, 0.005\|r\|0, k^2)$	$(0, 0.0075\|r\|1, k^2)$	$(1, 0.0075\|r\|0, k^2)$
0.0025	0.0005256	0.0005257	.....	.....	.....	.....
.0050	.0010513	.0006778	0.001356	0.001356	.....	.....
.0075	.001577	.0007681	.002033	.001536	0.002304	0.002304
.0100	.002103	.0008293	.002711	.001659	.003073	.002488
.0125	.002629	.0008738	.003390	.001747	.003842	.002621
.0150	.003153	.0009022	.004066	.001804	.004608	.002707
.0300	.006297	.001003	.008119	.002005	.009201	.003008
.0450	.009439	.001043	.01217	.002085	.01379	.003128
.060	.01257	.001063	.01621	.002126	.01837	.003189
.080	.01674	.001077	.02158	.002154	.02446	.003232
.100	.02089	.001084	.02694	.002167	.03053	.003251
.125	.02605	.001087	.03360	.002174	.03808	.003261
.150	.03119	.001087	.04022	.002174	.04558	.003261
.175	.03629	.001085	.04680	.002170	.05304	.003255
.200	.04135	.001082	.05333	.002164	.06044	.003246
0.250	0.05135	0.001074	0.06622	0.002147	0.07506	0.003221

k^2	$(0, 0.01\|r\|1, k^2)$	$(1, 0.01\|r\|0, k^2)$	$(0, 0.0125\|r\|1, k^2)$	$(1, 0.0125\|r\|0, k^2)$	$(0, 0.015\|r\|1, k^2)$	$(1, 0.015\|r\|0, k^2)$
0.010	0.003318	0.003318	.....	.....	.....	.....
.0125	.004148	.003495	.....	.....	.....	.....
.015	.004975	.003609	0.005241	0.004513	0.005412	0.005412
.030	.009935	.004011	.010467	.005015	.010808	.006015
.045	.01489	.004171	.01569	.005215	.01620	.006254
.060	.01983	.004253	.02090	.005317	.02158	.006377
.080	.02641	.004309	.02783	.005388	.02873	.006463
.100	.03296	.004335	.03473	.005421	.03586	.006502
.125	.04112	.004348	.04332	.005437	.04473	.006522
.150	.04922	.004349	.05186	.005438	.05355	.006523
.175	.05727	.004341	.06035	.005428	.06232	.006516
.200	.06527	.004329	.06877	.005414	.07102	.006494
0.250	0.08105	0.004296	0.08541	0.005372	0.08820	0.006445

k^2	$(0, 0.02\|r\|1, k^2)$	$(1, 0.02\|r\|0, k^2)$	$(0, 0.025\|r\|1, k^2)$	$(1, 0.025\|r\|0, k^2)$	$(0, 0.03\|r\|1, k^2)$	$(1, 0.03\|r\|0, k^2)$
0.02	0.007594	0.007593	0.007842	0.009471	0.008021	0.01135
.04	.01517	.008260	.01567	.010303	.01603	.01237
.06	.02270	.008506	.02345	.010609	.02398	.01274
.08	.03023	.008619	.03123	.01075	.03194	.01291
.10	.03773	.008672	.03898	.01082	.03987	.01299
.125	.04707	.008699	.04862	.01085	.04974	.01303
.150	.05635	.008701	.05821	.01085	.05955	.01303
.175	.06557	.008685	.06774	.01083	.06930	.01301
.200	.07473	.008663	.07721	.01081	.07899	.01298
0.250	0.09277	0.008597	0.09590	0.01072	0.09811	0.01288

TABLE 3—*Continued*

k^2	(0, 0.035|$\vec{r}$| 1, k^2)	(1, 0.035|$\vec{r}$| 0, k^2)	(0, 0.04|$\vec{r}$| 1, k^2)	(1, 0.04|$\vec{r}$| 0, k^2)	(0, 0.06|$\vec{r}$| 1, k^2)	(1, 0.06|$\vec{r}$| 0, k^2)
0.04	0.01630	0.01444	0.01650	0.01651	.....	.....
.06	.02440	.01487	.02470	.01700	0.02544	0.02544
.08	.03249	.01507	.03290	.01723	.03388	.02578
.100	.04056	.01516	.04107	.01733	.04230	.02595
.125	.05060	.01521	.05123	.01739	.05279	.02603
.150	.06058	.01521	.06135	.01740	.06321	.02605
.175	.07050	.01519	.07139	.01737	.07357	.02600
.200	.08036	.01515	.08137	.01732	.08387	.02594
.250	0.09982	0.01504	0.10109	0.01720	.10422	.02576
0.350	.....	.....	.....	.....	0.1440	0.02528

k^2	(0, 0.08|$\vec{r}$| 1, k^2)	(1, 0.08|$\vec{r}$| 0, k^2)	(0, 0.1|$\vec{r}$| 1, k^2)	(1, 0.1|$\vec{r}$| 0, k^2)	(0, 0.125|$\vec{r}$| 1, k^2)	(1, 0.125|$\vec{r}$| 0, k^2)
0.080	0.03435	0.03435	.....	.....	.....	.....
.100	.04289	.03457	0.04317	0.04317	.....	.....
.125	.05352	.03469	.05388	.04332	0.05408	0.05408
.150	.06410	.03471	.06453	.04339	.06478	.05417
.175	.07462	.03466	.07513	.04330	.07543	.05406
.200	.08507	.03458	.08566	.04321	.08602	.05395
.250	.1057	.03434	.1065	.04292	.1070	.05361
.350	0.1461	0.03372	.1472	.04216	.1480	.05270
.450	.....	.....	.1866	.04130	0.1876	0.05165
.50	.....	.....	.2057	.04086	.....	.....
.60	.....	.....	.2427	.03996	.....	.....
.70	.....	.....	.2783	.03906	.....	.....
0.80	.....	.....	0.3123	0.03818	.....	.....

k^2	(0, 0.15|$\vec{r}$| 1, k^2)	(1, 0.15|$\vec{r}$| 0, k^2)	(0, 0.175|$\vec{r}$| 1, k^2)	(1, 0.175|$\vec{r}$| 0, k^2)	(0, 0.2|$\vec{r}$| 1, k^2)	(1, 0.2|$\vec{r}$| 0, k^2)
0.150	0.06485	0.06485	0.06478	0.07552	0.06467	0.08614
.175	.07552	.06478	.....	.....	.....	.....
.200	.08614	.06467	.08607	.07533	.....	.....
.250	.1071	.06428	.1071	.07490	.1070	.08547
.350	.1483	.06321	.1483	.07369	.1482	.08414
.450	.1881	.06198	0.1882	0.07230	.1882	.08259
.50	.2074	.06134	.....	.....	.2076	.08177
.60	.2451	.06005	.....	.....	.2455	.08010
.70	0.2812	0.05874	.....	.....	.2819	.07835
0.80	.....	.....	.....	.....	0.3169	0.07676

k^2	(0, 0.25|$\vec{r}$| 1, k^2)	(1, 0.25|$\vec{r}$| 0, k^2)	(0, 0.35|$\vec{r}$| 1, k^2)	(1, 0.35|$\vec{r}$| 0, k^2)	(0, 0.45|$\vec{r}$| 1, k^2)	(1, 0.45|$\vec{r}$| 0, k^2)
0.25	0.1064	0.1064	.....	.....	.....	.....
.35	.1476	.1049	0.1457	0.1457	.....	.....
.40	.1678	.1040	.1658	.1446	.....	.....
.45	.1876	.1030	.1856	.1434	0.1829	0.1829
.50	.2071	.1021	.2050	.1422	.2023	.1815
.60	.2451	.1001	.2430	.1396	.2402	.1785
.70	.2817	.09809	.2798	.1370	.2769	.1754
0.80	0.3169	0.09603	0.3152	0.1344	0.3124	0.1722

TABLE 3—*Continued*

k^2	$(0, 0.5\|P\|1, k^2)$	$(1, 0.5\|P\|0, k^2)$	$(0, 0.6\|P\|1, k^2)$	$(1, 0.6\|P\|0, k^2)$
0.50	0.2008	0.2008	.....	.....
.60	.2385	.1976	0.2351	0.2351
.70	.2752	.1942	.2716	.2314
0.80	0.3107	0.1909	0.3070	0.2277

bound-free and free-free transitions can thus be brought together in the same system (cm^4/dyne).

In Figure 3 we have illustrated the results of Table 5 for $T = 6300°$ ($\theta = 0.8$). For comparison we have also included the earlier evaluations.

In Table 6 the coefficients given in Table 5 have been reduced by the stimulated emission factor

$$(1 - e^{-31.326\,\Delta k^2}) \ , \tag{27}$$

which is quite appreciable in the infrared. The values given in Table 6 are such as to enable satisfactory interpolation for most astrophysical applications.

Finally, in Table 7 we give the net absorption coefficient of H^-, including both the bound-free and the free-free transitions.

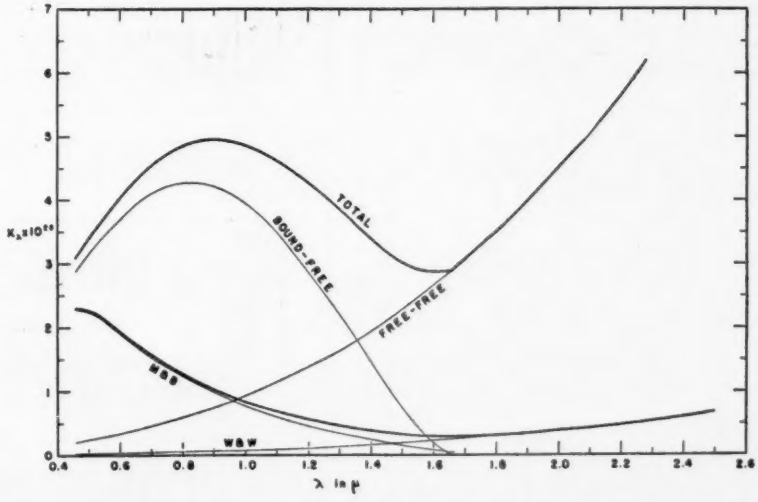

FIG. 3.—The continuous absorption coefficient of H^- per neutral hydrogen atom and per unit electron pressure for a temperature of 6300° K. The results of earlier determinations of the same quantities are included for comparison. The curve *M & B* is derived from the cross-sections of Massey and Bates for the bound-free transitions, and the curve *W & W* corresponds to the results of Wheeler and Wildt.

TABLE 4

THE MATRIX ELEMENTS $(0, k_0^2|\ddot{r}|1, k_0^2+\Delta k^2=k_1^2)$ AND $(1, k_0^2|\ddot{r}|0, k_0^2+\Delta k^2=k_1^2)$ FOR VARIOUS VALUES OF k_0^2 AND Δk^2 DERIVED BY INTERPOLATION FROM TABLE 3

Δk^2	$k_0^2=0.0025$		$k_0^2=0.0050$		$k_0^2=0.0075$		$k_0^2=0.0100$		$k_0^2=0.0125$		$k_0^2=0.0150$		$k_0^2=0.020$	
	$(0,k_0^2\|\ddot{r}\|1,k_1^2)$	$(1,k_0^2\|\ddot{r}\|0,k_1^2)$	$(0,k_0^2\|\ddot{r}\|1,k_1^2)$	$(1,k_0^2\|\ddot{r}\|0,k_1^2)$	$(0,k_0^2\|\ddot{r}\|1,k_1^2)$	$(1,k_0^2\|\ddot{r}\|0,k_1^2)$	$(0,k_0^2\|\ddot{r}\|1,k_1^2)$	$(1,k_0^2\|\ddot{r}\|0,k_1^2)$	$(0,k_0^2\|\ddot{r}\|1,k_1^2)$	$(1,k_0^2\|\ddot{r}\|0,k_1^2)$	$(0,k_0^2\|\ddot{r}\|1,k_1^2)$	$(1,k_0^2\|\ddot{r}\|0,k_1^2)$	$(0,k_0^2\|\ddot{r}\|1,k_1^2)$	$(1,k_0^2\|\ddot{r}\|0,k_1^2)$
0......	0.000526	0.000526	0.001356	0.001356	0.002304	0.002304	0.003318	0.003318	0.004370	0.004370	0.005412	0.005412	0.007594	0.007594
0.005....	.001577	.000768	.002711	.001659	.003842	.002621	.004975	.003609	.006112	.004626	.007209	.005668	.009496	.007820
.010....	.002629	.000874	.004069	.001815	.005373	.002774	.006628	.003780	.007854	.004814	.009008	.005866	.01139	.008003
.015....	.003677	.000924	.005417	.001893	.006904	.002887	.008281	.003912	.009596	.004958	.010808	.006015	.01328	.008148
.020....	.004725	.000961	.006769	.001958	.008436	.002974	.009935	.004011	.01134	.005064	.01261	.006123	.01517	.008260
.025....	.005773	.000991	.008119	.002005	.009967	.003037	.01159	.004083	.01308	.005140	.01441	.006200	.01706	.008350
.030....	.006821	.001012	.009470	.002041	.01150	.003083	.01324	.004134	.01482	.005194	.01620	.006254	.01894	.008418
.040....	.008916	.001038	.01217	.002085	.01456	.003140	.01654	.004203	.01830	.005272	.01979	.006342	.02270	.008506
.050....	.011006	.001054	.01487	.002114	.01761	.003180	.01983	.004253	.02176	.005328	.02337	.006400	.02647	.008575
.060....	.01309	.001065	.01755	.002134	.02066	.003208	.02312	.004286	.02523	.005367	.02695	.006444	.03023	.008619
.070....	.01518	.001073	.02024	.002148	.02370	.003228	.02641	.004309	.02869	.005393	.03052	.006473	.03399	.008649
.080....	.01726	.001078	.02292	.002159	.02674	.003241	.02969	.004324	.03214	.005410	.03408	.006493	.03773	.008672
.090....	.01933	.001082	.02560	.002166	.02977	.003249	.03296	.004335	.03559	.005423	.03764	.006507	.04147	.008686
.100....	.02141	.001084	.02827	.002169	.03280	.003255	.03623	.004342	.03903	.005431	.04119	.006516	.04521	.008696
.120....	.02554	.001087	.03360	.002174	.03883	.003261	.04274	.004349	.04589	.005439	.04827	.006524	.05265	.008703
.140....	.02965	.001087	.03890	.002174	.04483	.003261	.04922	.004349	.05271	.005437	.05531	.006522	.06005	.008696
.160....	.03374	.001086	.04417	.002172	.05081	.003257	.05566	.004343	.05950	.005429	.06232	.006516	.06741	.008681
.180....	.03781	.001084	.04941	.002169	.05675	.003251	.06207	.004334	.06625	.005418	.06928	.006500	.07473	.008663
.200....	.04186	.001082	.05463	.002162	.06265	.003243	.06844	.004323	.07296	.005404	.07621	.006480	.08200	.008638
0.225....	0.04687	0.001078	0.06110	0.002154	0.06997	0.003231	0.07634	0.004307	0.08128	0.005383	0.08479	0.006455	0.09098	0.008604

Δk^2	$k_0^2=0.025$		$k_0^2=0.030$		$k_0^2=0.035$		$k_0^2=0.040$		$k_0^2=0.045$		$k_0^2=0.050$		$k_0^2=0.055$	
	$(0,k_0^2\|\ddot{r}\|1,k_1^2)$	$(1,k_0^2\|\ddot{r}\|0,k_1^2)$	$(0,k_0^2\|\ddot{r}\|1,k_1^2)$	$(1,k_0^2\|\ddot{r}\|0,k_1^2)$	$(0,k_0^2\|\ddot{r}\|1,k_1^2)$	$(1,k_0^2\|\ddot{r}\|0,k_1^2)$	$(0,k_0^2\|\ddot{r}\|1,k_1^2)$	$(1,k_0^2\|\ddot{r}\|0,k_1^2)$	$(0,k_0^2\|\ddot{r}\|1,k_1^2)$	$(1,k_0^2\|\ddot{r}\|0,k_1^2)$	$(0,k_0^2\|\ddot{r}\|1,k_1^2)$	$(1,k_0^2\|\ddot{r}\|0,k_1^2)$	$(0,k_0^2\|\ddot{r}\|1,k_1^2)$	$(1,k_0^2\|\ddot{r}\|0,k_1^2)$
0......	0.009805	0.009805	0.01204	0.01204	0.01428	0.01428	0.01651	0.01651	0.01874	0.01874	0.02097	0.02097	0.02321	0.02321
0.005....	.01176	.009989	.01404	.01221	.01630	.01444	.01856	.01666	.02081	.01888	.02306	.02110	.02531	.02333
.010....	.01372	.01017	.01603	.01237	.01833	.01458	.02060	.01679	.02288	.01900	.02515	.02121	.02741	.02343
.015....	.01567	.01030	.01802	.01251	.02035	.01469	.02265	.01690	.02495	.01911	.02724	.02131	.02951	.02351
.020....	.01762	.01042	.02000	.01261	.02237	.01479	.02470	.01700	.02702	.01919	.02932	.02139	.03161	.02359
.025....	.01956	.01050	.02199	.01268	.02440	.01487	.02675	.01708	.02909	.01926	.03141	.02145	.03371	.02364
.030....	.02151	.01056	.02398	.01274	.02642	.01494	.02880	.01714	.03117	.01932	.03350	.02151	.03581	.02369
.040....	.02540	.01066	.02796	.01284	.03047	.01503	.03290	.01723	.03530	.01941	.03767	.02159	.04000	.02377
.050....	.02929	.01073	.03194	.01291	.03451	.01510	.03699	.01729	.03944	.01947	.04183	.02164	.04418	.02382
.060....	.03317	.01077	.03591	.01295	.03854	.01514	.04107	.01734	.04356	.01951	.04598	.02168	.04836	.02385
.070....	.03704	.01080	.03987	.01299	.04257	.01518	.04514	.01736	.04767	.01953	.05013	.02170	.05253	.02387
.080....	.04091	.01083	.04382	.01301	.04659	.01520	.04920	.01738	.05178	.01955	.05426	.02172	.05668	.02389
.090....	.04477	.01084	.04777	.01302	.05060	.01521	.05326	.01739	.05587	.01956	.05839	.02173	.06083	.02389
.100....	.04862	.01085	.05171	.01303	.05460	.01522	.05731	.01740	.05996	.01956	.06251	.02172	.06497	.02388
.120....	.05630	.01085	.05955	.01303	.06257	.01521	.06537	.01739	.06811	.01954	.07071	.02170	.07321	.02384
.140....	.06394	.01084	.06736	.01302	.07050	.01519	.07339	.01736	.07621	.01951	.07887	.02166	.08142	.02380
.160....	.07153	.01082	.07512	.01299	.07839	.01516	.08137	.01732	.08427	.01947	.08699	.02161	.08957	.02374
.180....	.07909	.01080	.08284	.01296	.08623	.01512	.08930	.01728	.09227	.01941	.09504	.02155	.09767	.02367
.200....	.08659	.01077	.09050	.01292	.09402	.01507	.09718	.01722	.10022	.01935	.10305	.02148	.10571	.02360
0.225....	0.09590	0.01073	0.10001	0.01287	0.10367	0.01502	0.10694	0.01716	0.11008	0.01928	0.11299	0.02139	0.11570	0.02350

TABLE 4—*Continued*

Δk^2	$k_0^2=0.06$		$k_0^2=0.07$		$k_0^2=0.08$		$k_0^2=0.09$		$k_0^2=0.100$		$k_0^2=0.125$		$k_0^2=0.150$	
	$(0,k_0^2\|\ddot{r}\|1,k_1^2)$	$(1,k_0^2\|\ddot{r}\|0,k_1^2)$	$(0,k_0^2\|\ddot{r}\|1,k_1^2)$	$(1,k_0^2\|\ddot{r}\|0,k_1^2)$	$(0,k_0^2\|\ddot{r}\|1,k_1^2)$	$(1,k_0^2\|\ddot{r}\|0,k_1^2)$	$(0,k_0^2\|\ddot{r}\|1,k_1^2)$	$(1,k_0^2\|\ddot{r}\|0,k_1^2)$	$(0,k_0^2\|\ddot{r}\|1,k_1^2)$	$(1,k_0^2\|\ddot{r}\|0,k_1^2)$	$(0,k_0^2\|\ddot{r}\|1,k_1^2)$	$(1,k_0^2\|\ddot{r}\|0,k_1^2)$	$(0,k_0^2\|\ddot{r}\|1,k_1^2)$	$(1,k_0^2\|\ddot{r}\|0,k_1^2)$
0......	0.02544	0.02544	0.02990	0.02990	0.03435	0.03435	0.03876	0.03876	0.04317	0.04317	0.05408	0.05408	0.06485	0.06485
0.005....	.02755	.02555	.03203	.02998	.03648	.03440	.04091	.03881	.04531	.04320	.05622	.05411	.06699	.06484
.010....	.02966	.02564	.03416	.03005	.03862	.03446	.04305	.03885	.04746	.04323	.05837	.05413	.06912	.06483
.015....	.03177	.02572	.03628	.03012	.04076	.03451	.04519	.03889	.04960	.04326	.06051	.05415	.07126	.06482
.020....	.03388	.02578	.03841	.03018	.04289	.03457	.04733	.03893	.05174	.04329	.06265	.05416	.07339	.06480
.025....	.03599	.02583	.04053	.03022	.04502	.03460	.04947	.03896	.05388	.04332	.06478	.05417	.07552	.06478
.030....	.03810	.02588	.04265	.03026	.04715	.03463	.05160	.03899	.05601	.04334	.06692	.05416	.07766	.06476
.040....	.04230	.02595	.04689	.03031	.05140	.03467	.05586	.03903	.06028	.04338	.07118	.05411	.08190	.06472
.050....	.04650	.02599	.05111	.03035	.05564	.03470	.06011	.03905	.06453	.04339	.07543	.05406	.08614	.06467
.060....	.05069	.02602	.05533	.03037	.05988	.03471	.06435	.03905	.06878	.04336	.07968	.05400	.09036	.06460
.070....	.05488	.02604	.05954	.03038	.06410	.03471	.06859	.03902	.07301	.04332	.08391	.05396	.09457	.06453
.080....	.05905	.02605	.06374	.03038	.06831	.03469	.07281	.03899	.07724	.04327	.08812	.05392	.09877	.06445
.090....	.06321	.02605	.06793	.03036	.07252	.03467	.07703	.03896	.08146	.04323	.09233	.05386	.1030	.06437
.100....	.06736	.02603	.07211	.03034	.07672	.03464	.08123	.03894	.08566	.04321	.09653	.05379	.1071	.06428
.120....	.07564	.02599	.08044	.03029	.08507	.03458	.08959	.03884	.09402	.04310	.1049	.05365	.1155	.06409
.140....	.08387	.02594	.08872	.03022	.09337	.03448	.09791	.03874	.1023	.04298	.1132	.05349	.1238	.06389
.160....	.09205	.02587	.09694	.03014	.10163	.03439	.1062	.03863	.1106	.04285	.1215	.05332	.1320	.06368
.180....	.10017	.02580	.1051	.03005	.1098	.03429	.1144	.03851	.1189	.04271	.1297	.05314	.1402	.06345
.200....	.10825	.02572	.1132	.02996	.1180	.03418	.1226	.03838	.1270	.04256	.1379	.05295	.1483	.06321
.225....	.11827	.02561	0.1233	0.02984	.1281	.03405	0.1327	0.03821	.1372	.04237	.1480	.05270	.1584	.06291
.250....	.12821	.02549	....	....	0.1381	0.03387	....	....	.1472	.04216	.1580	.05244	.1684	.06261
0.300....	0.14786	0.02525	....	....	....	....	....	....	0.1671	0.04174	0.1778	0.05192	0.1881	0.06198

Δk^2	$k_0^2=0.175$		$k_0^2=0.20$		$k_0^2=0.25$		$k_0^2=0.35$		$k_0^2=0.45$		$k_0^2=0.50$	
	$(0,k_0^2\|\ddot{r}\|1,k_1^2)$	$(1,k_0^2\|\ddot{r}\|0,k_1^2)$	$(0,k_0^2\|\ddot{r}\|1,k_1^2)$	$(1,k_0^2\|\ddot{r}\|0,k_1^2)$	$(0,k_0^2\|\ddot{r}\|1,k_1^2)$	$(1,k_0^2\|\ddot{r}\|0,k_1^2)$	$(0,k_0^2\|\ddot{r}\|1,k_1^2)$	$(1,k_0^2\|\ddot{r}\|0,k_1^2)$	$(0,k_0^2\|\ddot{r}\|1,k_1^2)$	$(1,k_0^2\|\ddot{r}\|0,k_1^2)$	$(0,k_0^2\|\ddot{r}\|1,k_1^2)$	$(1,k_0^2\|\ddot{r}\|0,k_1^2)$
0......	0.07546	0.07546	0.08594	0.08593	0.1064	0.1064	0.1457	0.1457	0.1829	0.1829	0.2008	0.2008
0.005....	.07759	.07544	.08805	.08589	.1085	.1064	.1478	.1456	.1849	.1828	.2027	.2006
.010....	.07971	.07541	.09016	.08586	.1106	.1063	.1498	.1455	.1868	.1826	.2046	.2004
.015....	.08183	.07539	.09227	.08582	.1127	.1062	.1518	.1454	.1888	.1825	.2065	.2003
.020....	.08395	.07536	.09438	.08577	.1148	.1062	.1538	.1453	.1907	.1824	.2084	.2001
.025....	.08607	.07533	.09648	.08573	.1168	.1061	.1558	.1452	.1926	.1822	.2103	.2000
.030....	.08818	.07529	.09858	.08568	.1189	.1060	.1578	.1451	.1946	.1821	.2122	.1998
.040....	.09240	.07522	.1028	.08558	.1230	.1059	.1618	.1449	.1984	.1818	.2160	.1995
.050....	.09661	.07514	.1070	.08547	.1272	.1057	.1658	.1446	.2023	.1815	.2198	.1992
.060....	.10081	.07504	.1111	.08536	.1313	.1056	.1698	.1444	.2061	.1812	.2236	.1989
.070....	.1050	.07495	.1153	.08524	.1354	.1054	.1737	.1442	.2099	.1809	.2273	.1986
.080....	.1092	.07485	.1195	.08512	.1395	.1052	.1777	.1439	.2138	.1806	.2311	.1982
.090....	.1134	.07474	.1236	.08499	.1436	.1051	.1816	.1437	.2176	.1803	.2348	.1979
.100....	.1175	.07463	.1277	.08486	.1476	.1049	.1856	.1434	.2214	.1800	.2385	.1976
.120....	.1258	.07440	.1360	.08458	.1557	.1045	.1934	.1430	.2289	.1794	.2460	.1969
.140....	.1340	.07415	.1441	.08429	.1638	.1042	.2011	.1425	.2364	.1788	.2533	.1963
.160....	.1422	.07389	.1523	.08399	.1718	.1038	.2089	.1420	.2439	.1782	.2607	.1956
.180....	.1503	.07362	.1603	.08369	.1797	.1034	.2166	.1415	.2513	.1776	.2680	.1949
.200....	.1584	.07335	.1684	.08338	.1876	.1030	.2242	.1410	.2587	.1769	.2752	.1942
.225....	.1684	.07301	.1783	.08299	.1974	.1026	.2336	.1403	.2678	.1761	.2842	.1934
.250....	0.1784	0.07266	.1882	.08259	.2071	.1021	.2430	.1396	.2769	.1754	.2931	.1926
0.300....	....	....	0.2076	0.08177	0.2262	0.1011	0.2616	0.1383	0.2948	0.1738	0.3107	0.1909

TABLE 5*

THE CONTINUOUS ABSORPTION COEFFICIENT OF THE NEGATIVE HYDROGEN ION PER NEUTRAL HYDROGEN ATOM AND PER UNIT ELECTRON PRESSURE FOR VARIOUS TEMPERATURES ($\theta = 5040/T$) AND WAVE LENGTHS

Δk^2	λA	$\theta=0.5$	$\theta=0.6$	$\theta=0.7$	$\theta=0.8$	$\theta=0.9$	$\theta=1.0$	$\theta=1.2$	$\theta=1.4$	$\theta=1.6$	$\theta=1.8$	$\theta=2.0$
†.....	.....	1.86 (−30)	2.03 (−30)	2.17 (−30)	2.29 (−30)	2.40(−30)	2.49(−30)	2.66(−30)	2.79 (−30)	2.91(−30)	3.01(−30)	3.09(−30)
0.005....	182300	1.55 (−23)	1.70 (−23)	1.84 (−23)	1.95 (−23)	2.06(−23)	2.16(−23)	2.34(−23)	2.50 (−23)	2.64(−23)	2.77(−23)	2.89(−23)
.010....	91130	2.02 (−24)	2.24 (−24)	2.44 (−24)	2.61 (−24)	2.78(−24)	2.94(−24)	3.23(−24)	3.50 (−24)	3.76(−24)	4.00(−24)	4.23(−24)
.015....	60750	6.27 (−25)	7.00 (−25)	7.67 (−25)	8.30 (−25)	8.89(−25)	9.48(−25)	1.06(−24)	1.16 (−24)	1.27(−24)	1.37(−24)	1.46(−24)
.020....	45560	2.77 (−25)	3.12 (−25)	3.45 (−25)	3.76 (−25)	4.06(−25)	4.36(−25)	4.93(−25)	5.49 (−25)	6.05(−25)	6.60(−25)	7.14(−25)
.025....	36450	1.49 (−25)	1.69 (−25)	1.88 (−25)	2.06 (−25)	2.25(−25)	2.43(−25)	2.78(−25)	3.14 (−25)	3.49(−25)	3.84(−25)	4.20(−25)
.030....	30380	9.00 (−26)	1.03 (−25)	1.16 (−25)	1.28 (−25)	1.40(−25)	1.52(−25)	1.77(−25)	2.01 (−25)	2.26(−25)	2.51(−25)	2.77(−25)
.040....	22780	4.17 (−26)	4.84 (−26)	5.51 (−26)	6.18 (−26)	6.86(−26)	7.54(−26)	8.92(−26)	1.03 (−25)	1.18(−25)	1.33(−25)	1.48(−25)
.050....	18230	2.34 (−26)	2.76 (−26)	3.18 (−26)	3.60 (−26)	4.03(−26)	4.48(−26)	5.38(−26)	6.32 (−26)	7.29(−26)	8.29(−26)	9.31(−26)
.060....	15190	1.48 (−26) 0.117(−26)	1.77 (−26) 0.219(−26)	2.06 (−26) 0.382(−26)	2.36 (−26) 0.634(−26)	2.66(−26) 1.01(−26)	2.98(−26) 1.56(−26)	3.63(−26) 3.48(−26)	4.30 (−26) 0.723(−25)	5.01(−26) 1.43(−25)	5.74(−26) 2.70(−25)	6.48(−26) 4.97(−25)
.070....	13020	1.02 (−26) 0.398(−26)	1.23 (−26) 0.746(−26)	1.44 (−26) 1.30 (−26)	1.66 (−26) 2.16 (−26)	1.89(−26) 3.45(−26)	2.13(−26) 5.33(−26)	2.63(−26) 11.9 (−26)	3.14 (−26) 2.47 (−25)	3.69(−26) 4.87(−25)	4.25(−26) 9.22(−25)	4.82(−26) 17.0 (−25)
.080....	11390	7.41 (−27) 0.603(−26)	9.02 (−27) 1.13 (−26)	1.07 (−26) 1.97 (−26)	1.24 (−26) 3.28 (−26)	1.42(−26) 5.23(−26)	1.61(−26) 8.08(−26)	2.00(−26) 18.0 (−26)	2.41 (−26) 3.74 (−25)	2.85(−26) 7.37(−25)	3.29(−26) 14.0 (−25)	3.76(−26) 25.7 (−25)
.090....	10130	5.64 (−27) 0.719(−26)	6.93 (−27) 1.35 (−26)	8.27 (−27) 2.36 (−26)	9.68 (−27) 3.91 (−26)	1.11(−26) 6.24(−26)	1.27(−26) 9.65(−26)	1.59(−26) 21.5 (−26)	1.92 (−26) 4.46 (−25)	2.28(−26) 8.80(−25)	2.65(−26) 16.7 (−25)	3.03(−26) 30.7 (−25)
.100....	9113	4.45 (−27) 0.774(−26)	5.50 (−27) 1.45 (−26)	6.61 (−27) 2.53 (−26)	7.78 (−27) 4.20 (−26)	8.99(−27) 6.71(−26)	1.03(−26) 10.4 (−26)	1.29(−26) 23.1 (−26)	1.58 (−26) 4.80 (−25)	1.87(−26) 9.46(−25)	2.18(−26) 17.9 (−25)	2.51(−26) 33.0 (−25)
.120....	7594	2.98 (−27) 0.778(−26)	3.73 (−27) 1.46 (−26)	4.53 (−27) 2.55 (−26)	5.38 (−27) 4.23 (−26)	6.27(−27) 6.75(−26)	7.20(−27) 10.4 (−26)	9.16(−27) 23.3 (−26)	1.13 (−26) 4.83 (−25)	1.35(−26) 9.52(−25)	1.58(−26) 18.1 (−25)	1.82(−26) 33.2 (−25)
.140....	6509	2.15 (−27) 0.725(−26)	2.72 (−27) 1.36 (−26)	3.33 (−27) 2.37 (−26)	3.98 (−27) 3.94 (−26)	4.66(−27) 6.28(−26)	5.38(−27) 9.72(−26)	6.89(−27) 21.6 (−26)	8.52 (−27) 4.49 (−25)	1.02(−26) 8.86(−25)	1.20(−26) 16.8 (−25)	1.39(−26) 30.9 (−25)
.160....	5695	1.63 (−27) 0.657(−26)	2.08 (−27) 1.23 (−26)	2.57 (−27) 2.15 (−26)	3.08 (−27) 3.57 (−26)	3.63(−27) 5.70(−26)	4.20(−27) 8.81(−26)	5.42(−27) 19.6 (−26)	6.72 (−27) 4.08 (−25)	8.10(−27) 8.04(−25)	9.55(−27) 15.2 (−25)	1.11(−26) 28.0 (−25)
.180....	5063	1.29 (−27) 0.591(−26)	1.65 (−27) 1.11 (−26)	2.05 (−27) 1.94 (−26)	2.47 (−27) 3.21 (−26)	2.92(−27) 5.13(−26)	3.39(−27) 7.93(−26)	4.39(−27) 17.7 (−26)	5.47 (−27) 3.67 (−25)	6.61(−27) 7.23(−25)	7.81(−27) 13.7 (−25)	9.06(−27) 25.2 (−25)
.200....	4556	1.04 (−27) 0.532(−26)	1.35 (−27) 0.997(−26)	1.68 (−27) 1.74 (−26)	2.03 (−27) 2.89 (−26)	2.41(−27) 4.61(−26)	2.81(−27) 7.13(−26)	3.65(−27) 15.9 (−26)	4.56 (−27) 3.30 (−25)	5.52(−27) 6.51(−25)	6.53(−27) 12.3 (−25)	7.59(−27) 22.7 (−25)
0.225....	4050	8.30 (−28) 0.468(−26)	1.08 (−27) 0.877(−26)	1.35 (−27) 1.53 (−26)	1.64 (−27) 2.54 (−26)	1.95(−27) 4.06(−26)	2.28(−27) 6.28(−26)	2.97(−27) 14.0 (−26)	3.72 (−27) 2.90 (−25)	4.52(−27) 5.73(−25)	5.60(−27) 10.9 (−25)	6.23 (−27) 20.0 (−25)

* The upper entries give the contributions to the absorption coefficients by the free-free transitions. The lower entries (for λ>16,500 A) give the corresponding contributions due to the bound-free transitions derived from the cross-sections given in *Ap. J.*, **102**, 395, 1945. The numbers in parentheses are the powers of 10, by which the corresponding entries should be multiplied to get the absorption coefficients in the unit CM^4/dyne.

† The entries in this line when divided by $(\Delta k^2)^2$ will give the corresponding absorption coefficients to sufficient accuracy for all $\Delta k^2 < 0.005$.

TABLE 6*

THE CONTINUOUS ABSORPTION COEFFICIENT OF THE NE

transitions derived from the cross-sections given in *Ap. J.*, **102**, 395, 1945. The numbers in parentheses are the powers of 10, by which the corresponding entries should be multiplied. The entries are the absorption coefficients in the unit $CM^4/dyne$.

† The entries in this line when divided by $(\Delta k^2)^{\frac{3}{2}}$ will give the corresponding absorption coefficients to sufficient accuracy for all $\Delta k^2 < 0.005$.

TABLE 6*

THE CONTINUOUS ABSORPTION COEFFICIENT OF THE NEGATIVE HYDROGEN ION PER NEUTRAL HYDROGEN ATOM AND PER UNIT ELECTRON PRESSURE FOR VARIOUS TEMPERATURES AND WAVE LENGTHS AFTER ALLOWING FOR THE STIMULATED EMISSION FACTOR $(1-e^{-h\nu/kT})$

Δk^2	λA	θ=0.5	θ=0.6	θ=0.7	θ=0.8	θ=0.9	θ=1.0	θ=1.2	θ=1.4	θ=1.6	θ=1.8	θ=2.0
†.....	.....	2.92 (−29)	3.81 (−29)	4.76 (−29)	5.74 (−29)	6.76 (−29)	7.81(−29)	9.98(−29)	1.22 (−28)	1.46(−28)	1.70(−28)	1.93(−28)
0.005...	182300	1.17 (−24)	1.53 (−24)	1.91 (−24)	2.30 (−24)	2.71 (−24)	3.13(−24)	4.01(−24)	4.91 (−24)	5.85(−24)	6.80(−24)	7.77(−24)
.010...	91130	2.93 (−25)	3.84 (−25)	4.80 (−25)	5.79 (−25)	6.83 (−25)	7.90(−25)	1.01(−24)	1.24 (−24)	1.48(−24)	1.72(−24)	1.97(−24)
.015...	60750	1.31 (−25)	1.72 (−25)	2.15 (−25)	2.60 (−25)	3.07 (−25)	3.55(−25)	4.56(−25)	5.61 (−25)	6.69(−25)	7.79(−25)	8.91(−25)
.020...	45560	7.45 (−26)	9.77 (−26)	1.22 (−25)	1.48 (−25)	1.75 (−25)	2.03(−25)	2.61(−25)	3.21 (−25)	3.83(−25)	4.46(−25)	5.10(−25)
.025...	36450	4.81 (−26)	6.32 (−26)	7.93 (−26)	9.61 (−26)	1.14 (−25)	1.32(−25)	1.69(−25)	2.09 (−25)	2.49(−25)	2.90(−25)	3.32(−25)
.030...	30380	3.38 (−26)	4.44 (−26)	5.57 (−26)	6.77 (−26)	8.01 (−26)	9.29(−26)	1.20(−25)	1.47 (−25)	1.76(−25)	2.05(−25)	2.34(−25)
.040...	22780	1.94 (−26)	2.56 (−26)	3.22 (−26)	3.91 (−26)	4.64 (−26)	5.38(−26)	6.94(−26)	8.54 (−26)	1.02(−25)	1.19(−25)	1.36(−25)
.050...	18230	1.27 (−26)	1.68 (−26)	2.11 (−26)	2.57 (−26)	3.05 (−26)	3.54(−26)	4.56(−26)	5.62 (−26)	6.70(−26)	7.79(−26)	8.91(−26)
.060...	15190	9.02 (−27) 0.0710(−26)	1.19 (−26) 0.148(−26)	1.50 (−26) 0.279(−26)	1.83 (−26) 0.493(−26)	2.17 (−26) 0.825(−26)	2.52(−26) 1.32(−26)	3.25(−26) 3.12(−26)	3.99 (−26) 0.671(−25)	4.76(−26) 1.36(−25)	5.54(−26) 2.61(−25)	6.33(−26) 4.86(−25)
.070...	13020	6.77 (−27) 0.265 (−26)	8.97 (−27) 0.545(−26)	1.13 (−26) 1.02 (−26)	1.38 (−26) 1.79 (−26)	1.63 (−26) 2.97 (−26)	1.89(−26) 4.74(−26)	2.44(−26) 11.0 (−26)	3.00 (−26) 2.35 (−25)	3.58(−26) 4.72(−25)	4.16(−26) 9.05(−25)	4.76(−26) 16.7 (−25)
.080...	11390	5.29 (−27) 0.431 (−26)	7.02 (−27) 0.879(−26)	8.84 (−27) 1.63 (−26)	1.08 (−26) 2.83 (−26)	1.27 (−26) 4.68 (−26)	1.48(−26) 7.42(−26)	1.90(−26) 17.1 (−26)	2.34 (−26) 3.63 (−25)	2.79(−26) 7.24(−25)	3.26(−26) 13.8 (−25)	3.73(−26) 25.5 (−25)
.090...	10130	4.27 (−27) 0.544 (−26)	5.65 (−27) 1.10 (−26)	7.12 (−27) 2.03 (−26)	8.66 (−27) 3.50 (−26)	1.03 (−26) 5.74 (−26)	1.19(−26) 9.07(−26)	1.53(−26) 20.8 (−26)	1.89 (−26) 4.38 (−25)	2.25(−26) 8.70(−25)	2.63(−26) 16.6 (−25)	3.02(−26) 30.6 (−25)
.100...	9113	3.52 (−27) 0.612 (−26)	4.66 (−27) 1.23 (−26)	5.87 (−27) 2.25 (−26)	7.14 (−27) 3.86 (−26)	8.46 (−27) 6.31 (−26)	9.81(−27) 9.92(−26)	1.26(−26) 22.6 (−26)	1.56 (−26) 4.74 (−25)	1.86(−26) 9.40(−25)	2.18(−26) 17.9 (−25)	2.50(−26) 32.9 (−25)
.120...	7594	2.52 (−27) 0.659 (−26)	3.34 (−27) 1.31 (−26)	4.21 (−27) 2.37 (−26)	5.11 (−27) 4.02 (−26)	6.06 (−27) 6.52 (−26)	7.03(−27) 10.2 (−26)	9.06(−27) 23.0 (−26)	1.12 (−26) 4.80 (−25)	1.34(−26) 9.50(−25)	1.57(−26) 18.0 (−25)	1.81(−26) 33.2 (−25)
.140...	6509	1.91 (−27) 0.644 (−26)	2.52 (−27) 1.26 (−26)	3.18 (−27) 2.26 (−26)	3.86 (−27) 3.82 (−26)	4.57 (−27) 6.16 (−26)	5.31(−27) 9.60(−26)	6.86(−27) 21.5 (−26)	8.50 (−27) 4.49 (−25)	1.02(−26) 8.86(−25)	1.20(−26) 16.8 (−25)	1.39(−26) 30.9 (−25)
.160...	5695	1.50 (−27) 0.603 (−26)	1.98 (−27) 1.17 (−26)	2.49 (−27) 2.09 (−26)	3.03 (−27) 3.51 (−26)	3.59 (−27) 5.63 (−26)	4.17(−27) 8.75(−26)	5.40(−27) 19.6 (−26)	6.72 (−27) 4.07 (−25)	8.10(−27) 8.04(−25)	9.55(−27) 15.2 (−25)	1.11(−26) 28.0 (−25)
.180...	5063	1.21 (−27) 0.556 (−26)	1.60 (−27) 1.07 (−26)	2.01 (−27) 1.90 (−26)	2.44 (−27) 3.18 (−26)	2.90 (−27) 5.09 (−26)	3.38(−27) 7.90(−26)	4.39(−27) 17.6 (−26)	5.47 (−27) 3.67 (−25)	6.61(−27) 7.23(−25)	7.81(−27) 13.7 (−25)	9.06(−27) 25.2 (−25)
.200...	4556	9.98 (−28) 0.509 (−26)	1.32 (−27) 0.974(−26)	1.66 (−27) 1.72 (−26)	2.02 (−27) 2.87 (−26)	2.40 (−27) 4.60 (−26)	2.80(−27) 7.12(−26)	3.65(−27) 15.9 (−26)	4.56 (−27) 3.30 (−25)	5.52(−27) 6.51(−25)	6.53(−27) 12.3 (−25)	7.59(−27) 22.7 (−25)
0.225...	4050	8.05 (−28) 0.454 (−26)	1.06 (−27) 0.865(−26)	1.34 (−27) 1.52 (−26)	1.64 (−27) 2.53 (−26)	1.95 (−27) 4.05 (−26)	2.27(−27) 6.27(−26)	2.97(−27) 14.0 (−26)	3.72 (−27) 2.90 (−25)	4.52(−27) 5.73(−25)	5.60(−27) 10.9 (−25)	6.23(−27) 20.0 (−25)

* The arrangement of this table is the same as Table 5.

† The entries in this line when divided by $(\Delta k^2)^{\frac{3}{2}}$ will give the corresponding absorption coefficients to a sufficient accuracy for all $\Delta k^2 < 0.005$.

TABLE 7*

THE CONTINUOUS ABSORPTION COEFFICIENT OF THE NEGATIVE HYDROGEN ION DUE TO THE FREE-FREE AND THE BOUND-FREE TRANSITIONS FOR VARIOUS TEMPERATURES AND WAVE LENGTHS AFTER ALLOWING FOR THE STIMULATED EMISSION FACTOR $(1-e^{-h\nu/kT})$

Δk^2	λA	$\theta=0.5$	$\theta=0.6$	$\theta=0.7$	$\theta=0.8$	$\theta=0.9$	$\theta=1.0$	$\theta=1.2$	$\theta=1.4$	$\theta=1.6$	$\theta=1.8$	$\theta=2.0$
†	.....	3.513 (−29)	4.593 (−29)	5.730(−29)	6.915(−29)	8.140(−29)	9.404(−29)	1.202(−28)	1.474 (−28)	1.754 (−28)	2.042 (−28)	2.330 (−28)
0.005	182300	1.168 (−24)	1.528 (−24)	1.906(−24)	2.301(−24)	2.710(−24)	3.132(−24)	4.006(−24)	4.913 (−24)	5.846 (−24)	6.795 (−24)	7.765 (−24)
.010	91130	2.934 (−25)	3.840 (−25)	4.796(−25)	5.794(−25)	6.829(−25)	7.897(−25)	1.012(−24)	1.243 (−24)	1.481 (−24)	1.724 (−24)	1.971 (−24)
.015	60750	1.313 (−25)	1.720 (−25)	2.151(−25)	2.602(−25)	3.066(−25)	3.554(−25)	4.560(−25)	5.610 (−25)	6.688 (−25)	7.793 (−25)	8.907 (−25)
.020	45560	7.447 (−26)	9.771 (−26)	1.223(−25)	1.482(−25)	1.750(−25)	2.028(−25)	2.606(−25)	3.209 (−25)	3.829 (−25)	4.463 (−25)	5.102 (−25)
.025	36450	4.811 (−26)	6.320 (−26)	7.925(−26)	9.607(−26)	1.136(−25)	1.317(−25)	1.695(−25)	2.088 (−25)	2.493 (−25)	2.904 (−25)	3.321 (−25)
.030	30380	3.375 (−26)	4.440 (−26)	5.575(−26)	6.765(−26)	8.006(−26)	9.289(−26)	1.196(−25)	1.474 (−25)	1.759 (−25)	2.049 (−25)	2.343 (−25)
.040	22780	1.941 (−26)	2.560 (−26)	3.220(−26)	3.913(−26)	4.636(−26)	5.383(−26)	6.935(−26)	0.8544(−25)	1.019 (−25)	1.186 (−25)	1.356 (−25)
.050	18230	1.270 (−26)	1.679 (−26)	2.115(−26)	2.572(−26)	3.049(−26)	3.541(−26)	4.561(−26)	0.5617(−25)	0.6695(−25)	0.7792(−25)	0.8901(−25)
.060	15190	0.9733(−26)	1.342 (−26)	1.784(−26)	2.324(−26)	2.996(−26)	3.846(−26)	6.363(−26)	1.071 (−25)	1.832 (−25)	3.167 (−25)	5.488 (−25)
.070	13020	0.9423(−26)	1.443 (−26)	2.153(−26)	3.164(−26)	4.600(−26)	6.631(−26)	13.46 (−26)	2.652 (−25)	5.077 (−25)	9.462 (−25)	17.22 (−25)
.080	11390	0.9599(−26)	1.580 (−26)	2.517(−26)	3.910(−26)	5.953(−26)	8.902(−26)	19.02 (−26)	3.861 (−25)	7.519 (−25)	14.15 (−25)	25.90 (−25)
.090	10130	0.9701(−26)	1.665 (−26)	2.741(−26)	4.366(−26)	6.770(−26)	10.261(−26)	22.29 (−26)	4.565 (−25)	8.928 (−25)	16.84 (−25)	30.86 (−25)
.100	9113	0.9638(−26)	1.695 (−26)	2.838(−26)	4.575(−26)	7.152(−26)	10.901(−26)	23.83 (−26)	4.894 (−25)	9.586 (−25)	18.10 (−25)	33.16 (−25)
.120	7594	0.9118(−26)	1.640 (−26)	2.786(−26)	4.532(−26)	7.124(−26)	10.895(−26)	23.90 (−26)	4.915 (−25)	9.632 (−25)	18.19 (−25)	33.34 (−25)
.140	6509	0.8344(−26)	1.513 (−26)	2.581(−26)	4.206(−26)	6.618(−26)	10.126(−26)	22.22 (−26)	4.570 (−25)	8.959 (−25)	16.92 (−25)	31.02 (−25)
.160	5695	0.7531(−26)	1.369 (−26)	2.337(−26)	3.809(−26)	5.993(−26)	9.169(−26)	20.12 (−26)	4.140 (−25)	8.117 (−25)	15.33 (−25)	28.12 (−25)
.180	5063	0.6768(−26)	1.230 (−26)	2.100(−26)	3.423(−26)	5.385(−26)	8.238(−26)	18.08 (−26)	3.721 (−25)	7.298 (−25)	13.79 (−25)	25.30 (−25)
.200	4556	0.6086(−26)	1.1058(−26)	1.887(−26)	3.074(−26)	4.837(−26)	7.401(−26)	16.25 (−26)	3.346 (−25)	6.564 (−25)	12.41 (−25)	22.76 (−25)
0.225	4050	0.5347(−26)	0.9710(−26)	1.656(−26)	2.698(−26)	4.246(−26)	6.499(−26)	14.28 (−26)	2.941 (−25)	5.772 (−25)	10.91 (−25)	20.02 (−25)

* The coefficients are per neutral hydrogen atom and per unit electron pressure. The numbers in parentheses give the powers of 10 by which the corresponding entries should be multiplied to get the coefficients in the unit CM^4/dyne.

† The entries in this line when multiplied by $(\lambda\ A/1000)^2$ will give the absorption coefficients for the various θ-values for all wave lengths $\lambda > 180{,}000$ A.

6. *Concluding remarks.*—It is not our intention here to make detailed applications of our new absorption coefficients to various astrophysical problems. But one comparison is of interest. In Figure 4 we have compared the theoretical variation of the continuous absorption coefficient of H^- with wave length for $T = 6300°$ with that derived by Chalonge and Kourganoff in their recent discussion of the continuous spectrum of the sun for the same temperature. It is seen that the agreement is very satisfactory. In any event, there is no basis for the conclusion that the free-free transitions of H^- are not

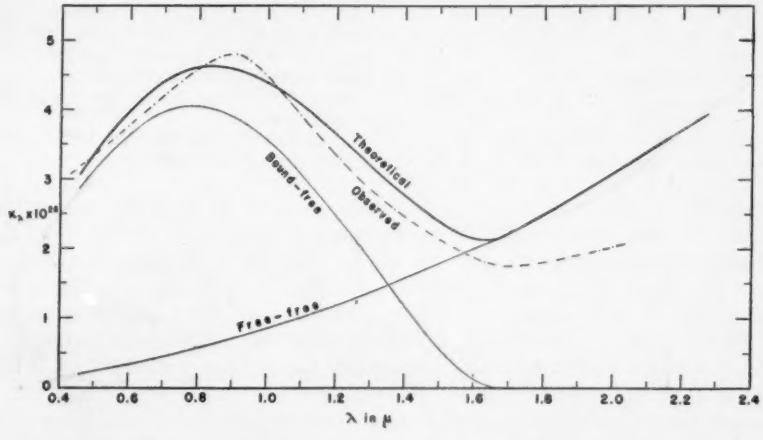

FIG. 4.—A comparison of the theoretical variation of the continuous absorption coefficient with wave length of H^- for $T = 6300°$, with the corresponding variation derived empirically from the solar continuous spectrum by Chalonge and Kourganoff.

adequate to account for the observed amount of absorption in the red beyond λ 10,000 A. Indeed, it would appear that the negative ion of hydrogen by itself is able to account quantitatively for the entire continuous spectrum of the sun over the range of wave lengths λλ 4000 A to 25,000 A.

On the physical side we should, however, emphasize that, while our new coefficients for the free-free transitions of H^- are probably to be trusted generally, the importance of exchange and polarization for the slow *s*-electrons may lead to further changes. It is likely that these effects will have a tendency to reduce our coefficients somewhat. We hope to return to these questions in the near future.

THE CONTINUOUS SPECTRUM OF THE SUN AND THE STARS

S. CHANDRASEKHAR AND GUIDO MÜNCH[1]
Yerkes Observatory
Received September 5, 1946

Using the recent determination of the continuous absorption coefficient of H^- by Chandrasekhar and Breen, we have shown that the dependence of the continuous absorption coefficient with wave length in the range 4000–24,000 A, which can be inferred from the intensity distribution in the continuous spectrum of the sun, can be quantitatively accounted for as due to H^-; and, further, that the color temperatures measured in the wave-length intervals 4100–6500 A (Greenwich) and 4000–4600 A (Barbier and Chalonge) for stars of the main sequence and of spectral types A0–G0 can also be interpreted in terms of the continuous absorption of H^- and neutral hydrogen atoms.

The problem of the discontinuities at the head of the Balmer and the Paschen series is also briefly considered on the revised physical theory of the continuous absorption coefficient.

1. *Introduction.*—The two principal problems in the theory of the continuous spectrum of the stars are, first, to identify the source of the continuous absorption in the solar atmosphere which will account for the intensity distribution in the continuous spectrum of the sun and the law of darkening in the different wave lengths and, second, to account for the observed relations between the color and the effective temperatures of the stars. In this paper we shall show that the major aspects of these two problems find their natural solution in terms of the continuous absorption coefficient of the negative hydrogen ion as recently determined by Chandrasekhar and Breen.[2] More particularly, we shall show that the dependence of the continuous absorption coefficient with wave length in the range 4000–24,000 A, which can be deduced from the solar data, can be quantitatively accounted for as due to H^-; and, further, that the color temperatures measured in the wave-length intervals 4100–6500 A (Greenwich[3]) and 4000–4600 A (Barbier and Chalonge[4]) for stars of the main sequence and of spectral types A0–G0 can also be interpreted in terms of the continuous absorption of H^- and neutral hydrogen.

In addition to the two problems we have mentioned, we shall also consider some related questions concerning the discontinuities at the head of the Balmer and the Paschen series.

2. *The mean absorption coefficients of* H^- *and* H.—As is well known, the character of the emergent continuous radiation from a stellar atmosphere is determined in terms of the temperature distribution in the atmosphere; and, as has recently been shown,[5] the temperature distribution in a nongray atmosphere will be given approximately by a formula of the standard type

$$T^4 = \tfrac{3}{4} T_e^4 \, (\tau + q[\tau]), \tag{1}$$

where T_e denotes the effective temperature and $q(\tau)$ a certain monotonic increasing function of the optical depth τ, provided that the mean absorption coefficient κ, in terms of which τ is measured, is defined as a straight average of the monochromatic absorption coefficient weighted according to the net flux $F_\nu^{(1)}$ of radiation of frequency ν in a gray

[1] Fellow of the John Simon Guggenheim Memorial Foundation at the Yerkes Observatory.

[2] *Ap. J.*, **104**, 430, 1946.

[3] Sir Frank Dyson, *Observations of Color-Temperatures of Stars, 1926–1932*, London, 1932; also *M.N.*, **100**, 189, 1940.

[4] *Ann. d'ap.*, **4**, 30, Table 4, 1941.

[5] S. Chandrasekhar, *Ap. J.*, **101**, 328, 1945. This paper will be referred to as "Radiative Equilibrium VII."

atmosphere and if, further, $\kappa_\nu/\bar{\kappa}$ is independent of depth. On this approximation, then, the emergent intensity in a given frequency and in a given direction will depend not only on the continuous absorption coefficient at the frequency under consideration but also on the mean absorption coefficient κ over all frequencies.

As the discussion in this paper will establish for the stellar atmospheres considered, the contributions to κ in the visible and the infrared regions of the spectrum are essentially from only two sources: H^- and the neutral hydrogen atoms. The cross-sections for the absorption by H^- for various temperatures and wave lengths have been tabulated by Chandrasekhar and Breen in Table 7 of their paper, while those for hydrogen can be found from the formulae of Kramers and Gaunt, standardized, for example, by B. Strömgren.[6] However, the evaluation of the mean absorption coefficient for wave lengths shorter than 4000 A is made uncertain on two accounts: First, there is the absorption by the metals and the excessive crowding of the absorption lines toward the violet, which is particularly serious for spectral types later than F0; and, second, there is the absorption in the Lyman continuum. On both these accounts the true values of $\bar{\kappa}$ will be larger than those determined by ignoring them. But the exact amount by which they will be larger will be difficult to predict without a detailed theory of "blanketing,"[7] on the one hand, and without going into a more exact theory[8] of radiative transfer than represented by the approximations leading to equation (1), on the other. However, since in this paper our primary object is to establish only the adequacy of H^- as the source of absorption in the solar atmosphere over the entire visible and infrared regions of the spectrum and the corresponding role of H^- and H for stellar atmospheres with spectral types A2–G0, it appeared best to ignore the refinements indicated and simply determine $\bar{\kappa}$ by weighting κ_ν due to H^- and H (without the Lyman absorption) at the conditions prevailing at $\tau = 0.6$ by the flux $F_\nu^{(1)}$ at this level.[9] For only in this way can we use the solution to the transfer problem in the form of equation (1) in a consistent manner. It should, however, be remembered that the effects we have ignored may easily increase $\bar{\kappa}$, determined in terms of H^- and H (without the absorption in the Lyman continuum) by factors of the order of 1.5 and probably not exceeding 2.[10]

Turning our attention, next, to the evaluation of $\bar{\kappa}$, we may first observe that, since our present method of averaging is a straight one, the contributions to κ_ν from different sources are simply additive. We may, accordingly, consider the mean absorption coefficient of H^- and H separately.

Now the absorption coefficient of H^-, including both the bound-free and the free-free transitions, is most conveniently expressed as per neutral hydrogen atom and per unit electron pressure in the unit cm^4/dyne. The monochromatic coefficients κ'_ν, after allowing for the stimulated emission factor $(1 - e^{-h\nu/kT})$, are tabulated in Chandrasekhar and Breen's paper for various values of $\theta(=5040/T)$. If we now denote by $a(H^-)$ the average

[6] "Tables of Model Stellar Atmospheres," *Publ. mind. Meddel. Kobenhavns Obs.*, No. 138, 1944.

[7] Cf. G. Münch, *Ap. J.*, **104**, 87, 1946.

[8] Such as, e.g., the (2, 2) approximation given in "Radiative Equilibrium VII," § 6.

[9] The choice of $\tau = 0.6$ for the "representative point" was made after some preliminary trials (cf. G. Münch, *Ap. J.*, **102**, 385, 1945, esp. Table 3), though it is evident on general grounds that a level such as $\tau = 0.6$, where the local temperature is approximately the same as the effective temperature, would be the correct one in the scheme of approximations leading to eq. (1).

[10] In all earlier evaluations of $\bar{\kappa}$ the absorption in the Lyman continuum did not, indeed, play any role. This was due to the manner in which $\bar{\kappa}$ was defined in those investigations as the Rosseland mean. But in "Radiative Equilibrium VII" it has been shown that there is no justification for taking the Rosseland means as they have been hitherto. Since the method of averaging, by which we have now replaced the Rosseland mean, is a straight one, it is no longer permissible simply to ignore the absorption in the Lyman continuum. At the same time, it is not possible to take it into account satisfactorily in the (2, 1) approximation leading to eq. (1). We should have to go at least to the (2, 2) approximation of "Radiative Equilibrium VII."

value of the coefficients κ'_ν, weighted according to the flux $F^{(1)}_\nu$ in a gray atmosphere at $\tau = 0.6$, where the temperature is approximately the effective temperature T_e, then the contribution $\bar{\kappa}(H^-)$ to the mass absorption coefficient $\bar{\kappa}$ by H^- is given by

$$\bar{\kappa}\,(H^-) = \frac{(1 - x_H)\, p_e}{m_H}\, a\,(H^-)\,, \tag{2}$$

where m_H is the mass of the hydrogen atom, p_e the electron pressure, and x_H the degree of ionization of hydrogen under the physical conditions represented by T_e and p_e.[11] The values of $a(H^-)$ found by graphical integration in accordance with the formula

$$a\,(H^-) = \frac{1}{F}\int_0^\infty \kappa'_\nu F^{(1)}\,(0.6)\,d\nu \tag{3}$$

for various values of $\theta = \theta_e$ are given in Table 1.

TABLE 1

THE MEAN ABSORPTION COEFFICIENTS $a(H^-)$ AND $a(H)$

θ	$a(H^-)$	$a(H)$	θ	$a(H^-)$	$a(H)$
0.5.....	0.563×10^{-26}	1.65×10^{-22}	0.9.....	6.08×10^{-26}	5.52×10^{-27}
0.6.....	1.145×10^{-26}	1.22×10^{-23}	1.0.....	9.32×10^{-26}	3.65×10^{-28}
0.7.....	2.25×10^{-26}	1.13×10^{-24}	1.2.....	2.00×10^{-25}	.....
0.8.....	3.88×10^{-26}	8.00×10^{-26}	1.4.....	3.89×10^{-25}	.....

Similarly, the contribution to $\bar{\kappa}$ by hydrogen can also be expressed in the form

$$\bar{\kappa}\,(H) = \frac{1 - x_H}{m_H}\, a\,(H)\,, \tag{4}$$

where

$$a\,(H) = \int_0^\infty \frac{fD}{a^3}\,(1 - e^{-a})\,\frac{F^{(1)}_a\,(0.6)}{F}\,da\,, \tag{5}$$

where $a = h\nu/kT_e$ and f and D are certain functions of temperature and frequency, respectively, which have been tabulated by Strömgren.[12] For reasons which we have already explained, we do not include the Lyman absorption in evaluating $a(H)$. The values of $a(H)$ for various temperatures are also listed in Table 1.

In terms of $a(H^-)$ and $a(H)$ given in Table 1, we can determine the combined mass absorption coefficient $\bar{\kappa}$ according to

$$\bar{\kappa} = \frac{1 - x_H}{m_H}\,[a\,(H^-)\,p_e + a\,(H)]\,. \tag{6}$$

Values of $\bar{\kappa}(H^-)$, $\bar{\kappa}(H)$, and $\bar{\kappa}$ determined in accordance with the foregoing equations for various temperatures and electron pressures are given in Table 2.

3. *The continuous absorption in the solar atmosphere*—As we have already stated in the introduction, one of the principal problems in the interpretation of the solar spectrum is the identification of the source of absorption which will predict the same dependence

[11] It will be noted that, in writing the mass absorption coefficient in the form (2), we have assumed the preponderant abundance of hydrogen in the stellar atmosphere.

[12] See the reference quoted in n. 6.

of the absorption coefficient with wave length in the range 4000–24,000 A, which can be inferred from the intensity distribution in the continuous spectrum and the law of darkening in the different wave lengths. While the amount and variation of the continuous absorption in the spectral region λλ 4000–24,000 A can be deduced in a variety of ways,[13] it appears that, for the purposes of the identification of the physical source of absorption, it is most direct to adopt the following procedure:

TABLE 2

THE MEAN MASS ABSORPTION COEFFICIENTS $\bar{\kappa}(H^-)$, $\bar{\kappa}(H)$, AND $\bar{\kappa}$ FOR VARIOUS TEMPERATURES AND ELECTRON PRESSURES

		$p_e=1$	$p_e=10$	$p_e=10^2$	$p_e=10^3$	$p_e=10^4$
$\theta_e=0.5$	$\bar{\kappa}(H^-)$	5.85×10^{-6}	3.70×10^{-4}	4.98×10^{-2}	2.12	32.1
	$\bar{\kappa}(H)$	1.71×10^{-1}	1.08	14.5	61.8	93.5
	$\bar{\kappa}$	1.71×10^{-1}	1.08	14.6	63.9	126
$\theta_e=0.6$	$\bar{\kappa}(H^-)$	3.93×10^{-4}	2.60×10^{-2}	5.82×10^{-1}	6.68	68.4
	$\bar{\kappa}(H)$	4.18×10^{-1}	2.76	6.19	7.10	7.27
	$\bar{\kappa}$	4.18×10^{-1}	2.79	6.77	13.8	75.7
$\theta_e=0.7$	$\bar{\kappa}(H^-)$	9.08×10^{-3}	1.28×10^{-1}	1.34	13.4	134
	$\bar{\kappa}(H)$	4.54×10^{-1}	6.41×10^{-1}	0.67	0.7	1
	$\bar{\kappa}$	4.63×10^{-1}	7.69×10^{-1}	2.01	14.1	135
$\theta_e=0.8$	$\bar{\kappa}(H^-)$	2.26×10^{-2}	2.32×10^{-1}	2.32	23.2	232
	$\bar{\kappa}(H)$	4.66×10^{-2}	0.48×10^{-1}	0.05	.....	.....
	$\bar{\kappa}$	6.92×10^{-2}	2.80×10^{-1}	2.37	23.2	232
$\theta_e=0.9$	$\bar{\kappa}(H^-)$	3.63×10^{-2}	3.63×10^{-1}	3.63	36.3	363
	$\bar{\kappa}(H)$	0.33×10^{-2}	0.03×10^{-1}	.....	.....	.....
	$\bar{\kappa}$	3.96×10^{-2}	3.66×10^{-1}	3.63	36.3	363
$\theta_e=1.0$	$\kappa(H^-)$	5.57×10^{-2}	5.57×10^{-1}	5.57	55.7	557
	$\bar{\kappa}(H)$	0.02×10^{-2}	.....	.....	.....	.....
	$\bar{\kappa}$	5.59×10^{-2}	5.57×10^{-1}	5.57	55.7	557
$\theta_e=1.2$	$\bar{\kappa}(H^-)$	1.20×10^{-1}	1.20	12.0	120	1200
$\theta_e=1.4$	$\bar{\kappa}(H^-)$	2.33×10^{-1}	2.33	23.3	233	2330

We compare the observed intensity distribution in the emergent solar flux F_λ (obs.) with the flux $F_\lambda^{(1)}$ (0) to be expected in a gray atmosphere.[14] It is evident that the *departures*,

$$\Delta \log F_\lambda = \log F_\lambda \text{ (obs.)} - \log F_\lambda^{(1)} (0) , \qquad (7)$$

must be related more or less directly with the dependence of the continuous absorption coefficient κ_ν' with wave length. Indeed, in the approximations leading to the temperature distribution (1) this relation must be one-one, since, with the adopted definition of $\bar{\kappa}$, the temperature distributions in the gray and the nongray atmospheres agree.[15] This suggests that, with the known value of κ_ν' due to H^-, we compare the predicted de-

[13] G. Mülders, *Zs. f. Ap.*, **11**, 132, 1935; G. Münch, *Ap. J.*, **102**, 385, 1945; D. Chalonge and V. Kourganoff, *Ann. d'ap.* (in press).

[14] The values of $F_\lambda^{(1)}$ (0) can be readily derived from the entries along the line $\tau = 0$ in Table 2 of "Radiative Equilibrium VII."

[15] Cf. the remarks in italics on p. 343 in "Radiative Equilibrium VII."

partures from $F_\lambda^{(1)}(0)$ with those observed. The only uncertainty in these predictions will be of the nature of a "zero-point" correction, since a value of $\bar{\kappa}$ different from the one adopted will lead to an approximately constant additive correction to $\Delta \log F_\lambda$.[16]

In order, then, to make the comparison suggested in the preceding paragraph, we need to determine $\Delta \log F_\lambda$ in terms of κ'_λ due to H^- and an adopted $\bar{\kappa}$. Assuming in the first instance that the contribution to $\bar{\kappa}$ is only H^-, we find that

$$a(H^-) = 5.62 \times 10^{-26} \text{ cm}^4/\text{dyne} \tag{8}$$

for an adopted value of

$$\theta_e = 0.8822 . \tag{9}$$

The value of κ'_λ for $\theta = 0.8822$ can be found by simple interpolation in Table 7 of Chandrasekhar and Breen's paper. The ratios $\kappa'_\lambda/a(H^-)$ derived in this manner are

TABLE 3

THE PREDICTED DEPARTURES [LOG F_λ (obs.) − LOG $F_\lambda^{(1)}(0)$] FROM GRAYNESS OF THE SOLAR ATMOSPHERE DUE TO THE ABSORPTION BY H^-

λA	$\frac{\kappa'_\lambda}{\bar{\kappa}(H^-)}$	$\frac{\kappa'_\lambda}{1.42\bar{\kappa}(H^-)}$	LOG F_λ (THEO.)		LOG $F_\lambda^{(1)}(0)$	Δ LOG F_λ	
			$\bar{\kappa}=\bar{\kappa}(H^-)$	$\bar{\kappa}=1.42\bar{\kappa}(H^-)$		$\bar{\kappa}=\bar{\kappa}(H^-)$	$=\bar{\kappa}1.42\bar{\kappa}(H^-)$
4000	0.686	0.483	14.489	14.532	14.358	+0.131	+0.174
4500	0.783	.551	14.468	.....	14.390	+ .078	.....
5000	0.881	.620	14.431	14.534	14.399	+ .032	+ .135
6000	1.029	.725	14.341	14.423	14.350	− .009	+ .073
7000	1.132	.797	14.259	14.329	14.285	− .026	+ .044
8000	1.188	.837	14.164	14.224	14.194	− .030	+ .030
9000	1.183	.833	14.070	14.128	14.098	− .028	+ .030
10,000	1.125	.792	13.982	14.034	13.999	− .017	+ .035
11,000	1.028	.724	13.897	13.946	13.901	− .004	+ .045
12,000	0.911	.642	13.817	13.862	13.805	+ .012	+ .057
13,000	0.788	.555	13.742	13.784	13.712	+ .030	+ .072
14,000	0.651	.458	13.674	13.713	13.624	+ .050	+ .089
15,000	0.523	.368	13.608	13.643	13.537	+ .071	+ .106
16,000	0.481	.339	13.532	13.566	13.454	+ .078	+ .112
17,000	0.486	.342	13.448	13.480	13.374	+ .074	+ .106
18,000	0.516	.363	13.362	13.395	13.297	+ .065	+ .098
19,000	0.562	.396	13.279	13.313	13.223	+ .056	+ .090
20,000	0.618	.435	13.197	13.230	13.152	+ .045	+ .078
21,000	0.679	.478	13.118	13.149	13.083	+ .035	+ .066
22,000	0.749	.527	13.042	13.073	13.016	+ .026	+ .057
23,000	0.820	0.577	12.971	13.003	13.952	+0.019	+0.051

given in Table 3 for various values of λ. With these values of $\kappa'_\lambda/a(H^-)$, the theoretical determination of $\Delta \log F_\lambda$ is straightforward with the help of the nomogram of Burkhardt's table,[17] which one of us has recently published.[18] The results of the determination are given in Table 3. In Figure 1 we have further compared the computed departures $\Delta \log F_\lambda$ with those observed.[19] It is seen that the predicted variation of the

[16] This is seen most directly in an approximation in which we expand the source function $B_\lambda(T)$ as a Taylor series about a suitable point and determine the emergent flux in terms of it (see, e.g., A. Unsöld, *Physik der Sternatmosphären*, p. 109. eq. [31.18], Berlin, 1938).

[17] *Zs. f. Ap.*, **13**, 56, 1936.

[18] G. Münch, *Ap. J.*, **102**, 385, Fig. 2, 1945.

[19] For λ > 9000 A the observed departures were obtained from a reduction of the solar data by M. Minnaert, *B.A.N.*, **2**, No. 51, 75, 1924; see also Unsöld, *op. cit.*, p. 32. For λ < 9000 A the reduction of G. Mülders (dissertation, Utrecht, 1934) was used.

departures runs remarkably parallel with the observed departures over the wavelength range 4000–20,000 A. (The observational data do not seem specially reliable for $\lambda > 20{,}000$ A.) However, the absolute values of the predicted departures are systematically less than the predicted departures by approximately a constant amount, indicating a zero-point correction in the sense that the adopted value of $\bar{\kappa}$ as due to H^- alone is somewhat too small. The calculations were accordingly repeated for other slightly larger values of $\bar{\kappa}$, and it was found that with $\bar{\kappa} = 1.42\ \kappa(H^-)$, the predicted and the observed departures agree entirely within the limits of the observational uncertainties over the whole region of the spectrum in which H^- contributes to the absorption. The

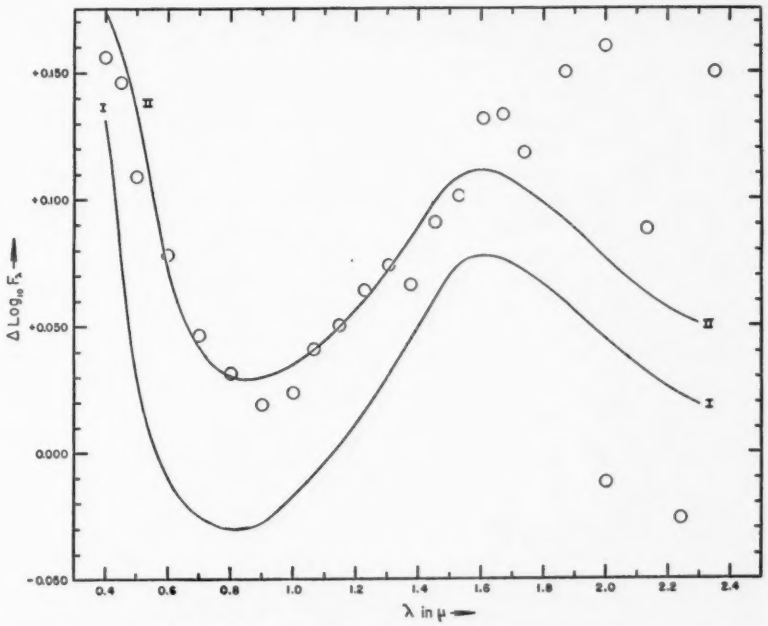

FIG. 1.—Comparison of the observed and the theoretically predicted departures [$\log F_\lambda - \log F^1_\lambda(0)$] from a gray atmosphere due to the absorption by H^-. The circles represent the observed departures of the solar emergent flux from that of a gray atmosphere, while Curves I and II are the theoretically derived departures on the two assumptions $\bar{\kappa} = \bar{\kappa}(H^-)$ and $\bar{\kappa} = 1.42\ \bar{\kappa}(H^-)$.

agreement is, in fact, so striking that we may say that H^- reveals its presence in the solar atmosphere by its absorption spectrum.

We may finally remark on the value of $\bar{\kappa} = 1.42\ \bar{\kappa}(H^-)$, indicated by the comparisons we have just made: it can, in fact, be deduced empirically from the solar data on the continuous spectrum that the absorption in the violet ($\lambda < 4000$ A) must increase the value of κ derived from the visible and the infrared regions of the spectrum by a factor of the order of 1.5.[20]

4. *The predicted color-effective temperature relations: comparison with observations.*—All earlier attempts[21] to predict the color temperatures in the region λλ 4000–6500 A for stars of spectral types A0–G0 in agreement with the observations have failed. This failure in the past has been due to the following circumstance: The observed relation between the color and the effective temperatures and, in particular, the fact that $T_c > T_e$

[20] Cf. G. Münch, *Ap. J.*, **102**, 385, 1945, esp. the remarks preceding eq. (19) on p. 394.

[21] R. Wildt, *Ap. J.*, **93**, 47, 1941, and *Observatory*, **64**, 195, 1942; R. E. Williamson, *Ap. J.*, **97**, 51, 1943.

implies that the continuous absorption coefficient is an increasing function of λ in the spectral region observed. But the physical theory on which the calculations were made placed the maximum of the absorption-curve in the region of λ 4500 A; this was incompatible with the observations and, moreover, predicted color temperatures less than the effective temperatures, contrary to all evidence. Indeed, on the strength of this discrepancy, it was concluded that H^- as a source of absorption was inadequate even in the region $\lambda\lambda$ 4500–6500 A, and the existence of an unknown source operative in this region was further inferred. However, later evaluations[22] of the bound-free transitions of H^- showed the unreliability of earlier determinations and placed the maximum of the absorption-curve in the neighborhood of λ 8500 A. The addition of the free-free transitions pushes this maximum only still further to the red. It is therefore evident that on the revised physical theory we should be able to remove the major discrepancies of the subject. We shall now show how complete the resolution of these past difficulties is.

From the point of view of establishing the adequacy of the physical theory in the region $\lambda\lambda$ 4000–6500 A, it is most instructive to consider the theoretical predictions for color temperatures which can be directly compared with the color determinations at Greenwich,[3] for the Greenwich measures are based on the mean gradients in the wave-length interval 4100–6500 A, and it is in the prediction of these colors that the earlier calculations were most discordant.[23]

Now, from the Planck formula in the form

$$i_\lambda = \frac{2hc^2}{\lambda^5}\frac{1}{e^{c_2/\lambda T}-1}, \tag{10}$$

it readily follows that

$$\frac{1}{i_\lambda}\frac{di_\lambda}{d\,(1/\lambda)} = 5\lambda - \frac{c_2}{T}\,(1 - e^{-c_2/\lambda T})^{-1}. \tag{11}$$

Defining the gradient

$$\phi = \frac{c_2}{T}\,(1 - e^{-c_2/\lambda T})^{-1} \tag{12}$$

in the usual manner, we can write

$$\frac{1}{M}\frac{d\log_{10} i_\lambda}{d\,(1/\lambda)} = 5\lambda - \phi \qquad \left(\frac{1}{M} = 2.303\right). \tag{13}$$

If F_{λ_1} and F_{λ_2} are the emergent fluxes at two wave lengths λ_1 and λ_2 and if ϕ is the mean gradient in this wave-length interval, then we can write, in accordance with equation (13)

$$\phi = 5\lambda_m - \frac{1}{M}\frac{\log_{10}(F_{\lambda_1}/F_{\lambda_2})}{\lambda_1^{-1} - \lambda_2^{-1}}, \tag{14}$$

where λ_m denotes an appropriate mean wave length for the interval to which the gradient ϕ refers. Equation (14) can be re-written in the following form:

$$\phi = 5\lambda_m - \frac{1}{M}\frac{\Delta\log_{10} F}{\Delta\,(1/\lambda)}. \tag{15}$$

According to equation (15), the theoretical determination of color temperatures will proceed by determining, first, the gradient ϕ from the values of F_λ at the end-points of the wave-length interval and then determining the temperature which will give this gradient.

[22] S. Chandrasekhar, *Ap. J.*, **102**, 223, 395, 1945

[23] Cf. Fig. 6 in Williamson's paper (*op. cit.*).

For the Greenwich measures $\lambda_m = 0.55\ \mu$, and equation (15) becomes

$$\phi\ (\text{Greenwich}) = 2.75 - 2.56 \log_{10}\left(\frac{F_{4100}}{F_{6500}}\right), \qquad (16)$$

provided that, in determining the gradients, wave lengths are measured in microns.[24]

In Table 4 we have listed the values of κ'_λ/κ for the wave lengths 4100 A and 6500 A for various values of θ_e and p_e. In terms of these values the determination of the fluxes at the two wave lengths 4100 A and 6500 A is straightforward with the help of Burkhardt's table. The gradient ϕ then follows according to equation (16) and, from that, the color temperature. The reciprocal color temperatures $\theta_c = 5040/T_c$ derived in this manner are given in Table 5. The resulting color–effective temperature relations are illustrated

TABLE 4

κ'_λ/κ IN MODEL STELLAR ATMOSPHERES

$5040/T_e$	λA	$p_e=10$	$p_e=10^2$	$p_e=10^3$	$p_e=10^4$
	λ 3647	.....	3.45	3.22	2.68
		.....	0.161	0.181	0.332
	λ 4000	0.210	0.212	0.238	0.397
$\theta=0.5$.....	λ 4600	0.316	0.318	0.346	0.513
	λ 6500	0.826	0.834	0.848	0.991
	λ 8203	.....	1.51	1.51	1.55
		.....	0.490	0.526	0.788
	λ 3647	.....	4.04	2.60	1.09
		.....	0.178	0.427	0.685
	λ 4000	0.148	0.205	0.481	0.770
$\theta=0.6$.....	λ 4600	0.221	0.278	0.585	0.901
	λ 6500	0.579	0.637	0.935	1.25
	λ 8203	.....	1.27	1.36	1.45
		.....	0.424	0.885	1.36
	λ 3647	6.06	2.82	0.961	0.684
		0.176	0.461	0.625	0.645
	λ 4000	0.208	0.521	0.695	0.725
$\theta=0.7$.....	λ 4600	0.276	0.617	0.810	0.848
	λ 6500	0.546	0.901	1.11	1.14
	λ 8203	0.889	1.105	1.22	1.24
		0.356	0.893	1.19	
	λ 3647	1.54	0.720	0.625	.....
		0.518	0.601	0.614	0.611
	λ 4000	0.582	0.671	0.685	0.685
$\theta=0.8$.....	λ 4600	0.681	0.781	0.800	0.800
	λ 6500	0.961	1.06	1.09	1.09
	λ 8203	1.11	1.178	1.19	1.19
		1.01	1.164		
	λ 3647	0.708	0.642	0.636	0.636
		0.631	0.636		
	λ 4000	0.690	0.690	0.690	0.690
$\theta=0.9$.....	λ 4600	0.800	0.800	0.800	0.800
	λ 6500	1.09	1.09	1.09	1.09
	λ 8203	1.16	1.16	1.16	1.16
		.....	.....	.....	.....

[24] The constant c_2 in eq. (12) then has the value 14,320.

in Figure 2. For comparison we have also plotted in this figure the Greenwich determinations for stars on the main sequence and of spectral types A0–G0 (reduced, however, to the Morgan, Keenan, and Kellman system of spectral classification). The color temperature of the sun for this wave-length interval is also plotted in Figure 1. It is seen from Figure 1 that the agreement between the observed and the theoretical color temperatures is entirely satisfactory, particularly when it is remembered that the earlier calculations failed even to predict the correct sign for $\theta_c - \theta_e$. It will, however, be noted that the observed values of θ_c for spectral types later than F0 are somewhat larger than the predicted values, though the agreement is as good as can be expected in the case of the sun. The reason for this must undoubtedly be the crowding of the absorption lines toward the violet in the later spectral types and the consequent depression of the continuous spectrum in this region. The correctness of this explanation is apparent when it is noted that in the case of the sun, in which allowance has been made for this effect of the lines on the continuum, the discordance is not present.

TABLE 5

THEORETICAL RECIPROCAL COLOR TEMPERATURES AND THE PREDICTED DISCONTINUITIES AT THE HEAD OF THE BALMER AND THE PASCHEN SERIES*

p_e		θ_e = 0.5	0.6	0.7	0.8	0.9	1.0
10	$\theta_c(G)$	.....	.....	.....	0.68	0.80	0.88
	$\theta_c(B \text{ and } C)$	.....	.....	.....	.61	.69	.75
	D_B	.....	.....	.....	.31	.015	.....
10^2	$\theta_c(G)$	.....	0.45	0.60	.73	.80	.88
	$\theta_c(B \text{ and } C)$	.....	.....	.47	.63	.69	.75
	D_B	.....	.....	[.50]	.07	.....	.....
	D_P	.....	.....	.030	.001	.....	.....
10^3	$\theta_c(G)$	[0.31]	.52	.65	.74	.80	.88
	$\theta_c(B \text{ and } C)$	.....	.42	.56	.64	.69	.75
	D_B	[.58]	[.34]	.13	.....	.....	.....
	D_P	.114	.051	.003	.....	.....	.....
10^4	$\theta_c(G)$	[.39]	.59	.66	.74	.80	.88
	$\theta_c(B \text{ and } C)$	[.34]	.50	.58	.64	.69	.75
	D_B	[.40]	.12	.018	.....	.....	.....
	D_P	[.071]	.006	.....	.....	.....	.....
Pure H^-	$\theta_c(G)$	.52	.59	.66	.74	.80	.88
	$\theta_c(B \text{ and } C)$	0.41	0.50	0.58	0.64	0.69	0.75

* $\theta_e(G)$ and $\theta_c(B \text{ and } C)$ are the reciprocal color temperatures, $5040/T_c$, appropriate for the wave-length intervals 4100–6500 A and 4000–4600 A, respectively; D_B and D_P, representing the logarithm of the ratio of the fluxes at the two sides of the series limits, are the expected Balmer and Paschen discontinuities, respectively.

Comparisons similar to those we have just made also can be made with the measurements of Barbier and Chalonge[4] on the color temperatures based on the observed gradients in the wave-length interval 4000–4600 A. The formula giving the theoretical gradient for this wave-length interval takes the form

$$\phi\,(B \text{ and } C) = 2.175 - 7.06 \log_{10}\left(\frac{F_{4000}}{F_{4600}}\right). \qquad (17)$$

The values of $\kappa'_\lambda/\bar{\kappa}$ at λ 4000 A and λ 4600 A are given in Table 4, and the reciprocal color temperatures derived from these in Table 5. The results are further illustrated in Figure 3, where the theoretical relations for various electron pressures are compared with the measures of Barbier and Chalonge (reduced also to the Morgan, Keenan, and Kellman system of spectral classification). It is seen that the general agreement is again good, though there are now somewhat larger differences between the computed and the observed color temperatures for spectral types later than F0 than were encountered in the comparison with the Greenwich colors. This must again be due to the crowding of the absorption lines toward the violet in the later spectral types and the further fact that

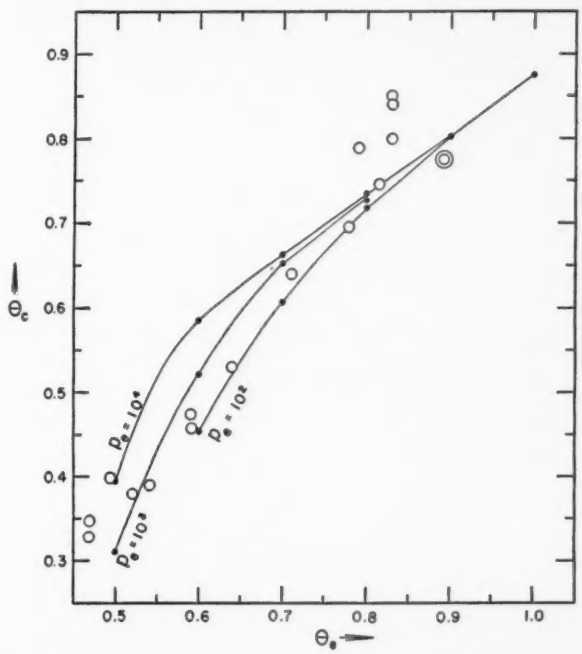

FIG. 2.—Comparison of the observed and the theoretical color effective-temperature relations for the wave-length interval 4100–6500 A. The ordinates denote the reciprocal color temperatures and the abscissae denote the reciprocal effective temperatures ($\theta = 5040/T$). The circles represent the Greenwich color determinations reduced to the Morgan, Keenan, and Kellman system of spectral classification. The double circle represents the sun.

the base line for the Barbier and Chalonge colors is much shorter than that for the Greenwich colors.

5. *The discontinuities at the head of the Balmer and the Paschen series.*—With the physical theory of the continuous absorption coefficient now available, we can also predict the extent of the discontinuities which we may expect at the head of the Balmer and the Paschen series of hydrogen. For this purpose the values of $\kappa'_\lambda/\bar{\kappa}$ on the two sides of the series limits are also given in Table 4. From these values it is a simple matter to estimate the discontinuities which will exist at the head of the Balmer and the Paschen series, and they are given in Table 5. The results for the Balmer discontinuities are further illustrated in Figure 4, in which the discontinuities measured by Barbier and Chalonge[4] for various stars are also plotted. The progressive increase of the electron pressure as we go from the later to the earlier spectral types is particularly apparent

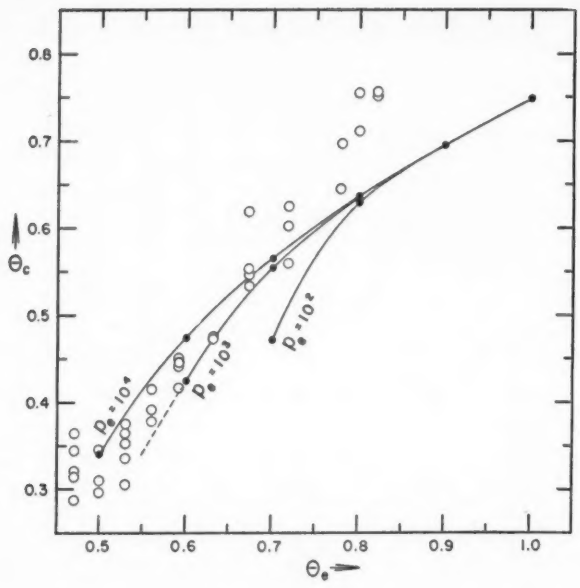

FIG. 3.—Comparison of the observed and the theoretical color effective-temperature relations for the wave-length interval 4000–4600 A. The ordinates denote the reciprocal color temperatures, and the abscissae denote the reciprocal effective temperatures $\theta = 5040/T$). The circles represent the color determinations of Barbier and Chalonge for the wave-length interval 4000–4600 A, reduced to the Morgan, Keenan, and Kellman system of spectral classification.

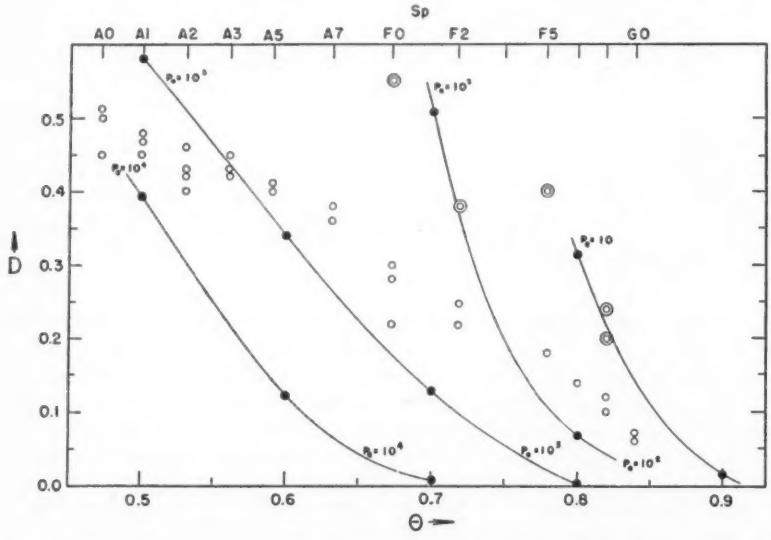

FIG. 4.—The predicted discontinuities (D) at the head of the Balmer series for various effective temperatures and electron pressures. The circles represent the discontinuities as measured by Barbier and Chalonge. (The double circles represent the observations for supergiants.)

from Figure 4; this progression is, moreover, in agreement with what is indicated by the color determinations (cf. Figs. 2 and 3). In Table 6 we give the electron pressures for the main-sequence stars of various spectral types estimated in this manner.

6. *Concluding remarks.*—While our discussion in the preceding sections has established the unique role which H^- plays in determining the character of the continuous spectrum of the sun and the stars, it should not be concluded that the various other

TABLE 6

ELECTRON PRESSURES FOR STARS ON THE MAIN SEQUENCE

Type	log p_e	Type	log p_e	Type	log p_e
A1	3.7	F0	2.4	F8	1.4
A2	3.3	F2	2.2	G0	1.2
A3	3.0	F4	2.0	G2	1.0
A5	2.8	F5	1.8		
A7	2.6	F6	1.6		

astrophysical elements of the theory are equally well established. Indeed, the theory of model stellar atmospheres as developed by Strömgren in recent years must not only be revised on the basis of the new absorption coefficients of H^- but also be advanced still further before we can be said to have a completely satisfactory account of all the classical problems of the theory of stellar atmospheres. But our discussion in this paper does give us the confidence that the continuous absorption by H^- discovered by Wildt must provide the key to the solution of many of these problems.

NOTES

LUMINOSITY CHARACTERISTICS ON LOW-DISPERSION SPECTRA OF STARS OF TYPES M0–M4

The luminosity classification of stars of spectral classes M0–M4 has usually been carried out with slit spectra by means of line ratios. On slitless spectra of low dispersion, however, Lindblad,[1] Vyssotsky,[2] and others have found the depression of the continuum on the red side of λ 4227 a useful criterion for distinguishing dwarfs from giants.

In examining the spectra of stars of classes M0–M4 taken with the 4° objective prism of the Warner and Swasey Observatory (dispersion at $H\gamma$ = 283 A/mm) it was observed that it is possible to extend the criteria in this spectral region to allow the recognition of supergiants.

Pl. XVIII shows two sets of three spectra, the first set representing stars of class M0, and the second stars of class M2. The luminosity decreases from top to bottom in each set and is indicated by the luminosity-class symbols[3] at the right of each spectrum. RW Cep has been assigned the symbol 0 because on spectrograms of all dispersions the criteria of high luminosity are much more strongly developed in this star than in Ia stars, such as μ Cep.

The following are the sensitive criteria:

1. *Intensity of Ca 4227.*—In dwarfs this line is the most conspicuous feature in the spectrum. It weakens progressively with increasing luminosity until in the more brilliant supergiants it is actually less intense than the neighboring absorption features to the violet.

2. *Continuous spectrum on both sides of λ 4227.*—In dwarfs the violet side is stronger than the red side. The two portions are of approximately equal intensity in giants, while in supergiants the violet side is definitely the weaker.

3. *G-band.*—The break in the spectrum at about λ 4308, corresponding to the red edge of the G-band, becomes steadily more pronounced with increasing luminosity. In supergiants the strengthening of λ 4290 (due mostly to *Cr*) gives rise to a conspicuous double line, λλ 4290–4308.

4. *Intensity of λ 4406.*—The strength of the blended line at λ 4406 increases with respect to the features on both sides of it in passing from dwarfs to giants. The lines in this region become indistinct in supergiants, but on slightly underexposed plates this criterion is useful in checking the distinction between giants and dwarfs.

It should be noted that the stars μ Cep and RW Cep are among the most brilliant supergiants known. For stars similar to α Ori or α Sco (luminosity class Ib) the supergiant characteristics are not so pronounced; but on good spectrograms these stars, too, can be readily picked out. As a test, two plates covering the field of the double cluster, h and χ Per, were examined, and the high luminosity of the four M-type supergiants known in this field was easily recognized. In addition, it was observed that HD 14826, BD+56°609 (m_v = 8.5) also has a supergiant spectrum. From these two plates the

[1] *Stockholms Obs. Ann.*, Vol. **12**, No. 2, 1935.

[2] *Ap. J.*, **97**, 381, 1943.

[3] Morgan, Keenan, and Kellman, *An Atlas of Stellar Spectra*, 1943.

PLATE XVIII

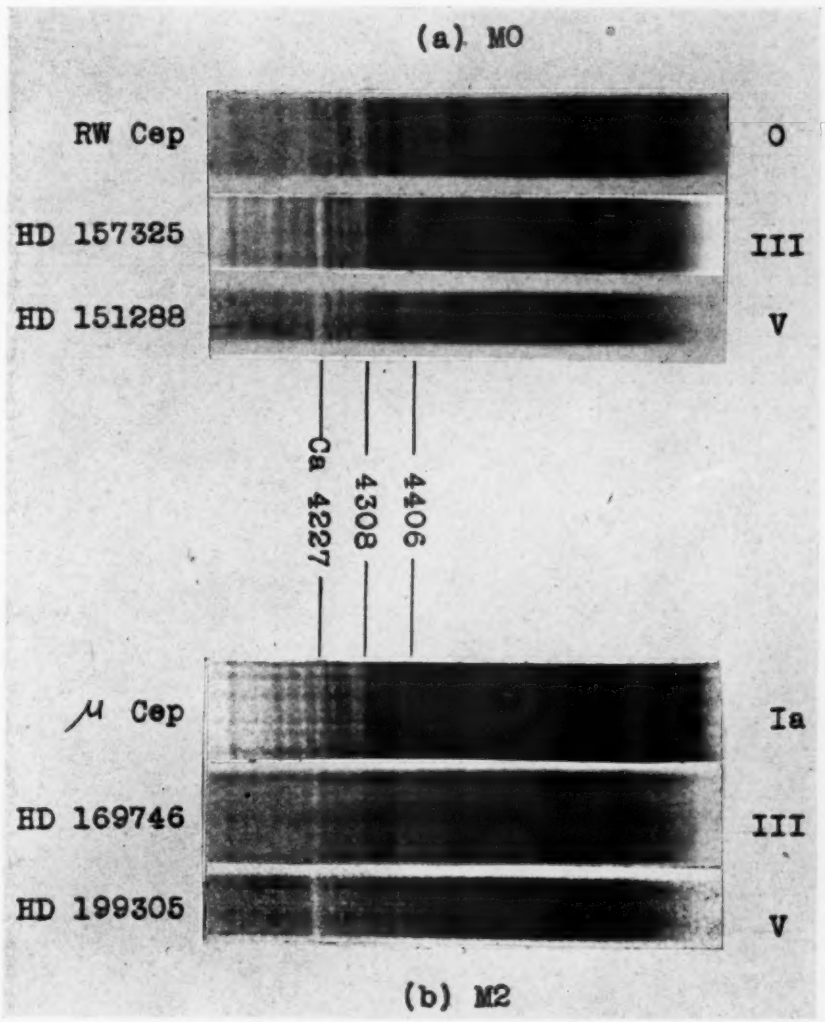

LUMINOSITY EFFECTS ON SMALL-SCALE SPECTROGRAMS OF M-TYPE STARS

spectrum was classified approximately as M2 Ib. Its known small proper motion ($\mu_\alpha = -0''.007$, $\mu_\delta = -0''.010$)[4] is consistent with assignment of the star to the extensive group of supergiants which are associated with the double cluster.

P. C KEENAN
J. J. NASSAU

PERKINS OBSERVATORY
AND
WARNER AND SWASEY OBSERVATORY
August 1946

THE RADIAL VELOCITY OF 27 CANIS MAJORIS

Table 1 contains the radial velocities of 27 Canis Majoris obtained at the Yerkes Observatory since October, 1943.[1] The velocity-curve in Figure 1 covers the entire range of our observations since 1925. The extraordinary character of this curve defies, at present, all attempts to explain

TABLE 1

RADIAL VELOCITIES OF 27 CANIS MAJORIS

Date	U.T.	Velocity (Km/Sec)	Date	U.T.	Velocity (Km/Sec)
1943 Oct. 7	11:15	− 8.8	1944 Oct. 27	9:53	−80.2
22	11:11	− 13.2	Nov. 8	9:47	−67.2
27	11:09	− 21.6	15	8:30	−74.8
Nov. 4	10:07	− 18.6	Dec. 1	8:35	−53.4
21	10:05	− 28.0	1	9:43	−43.4
28	8:39	− 16.2	2	7:59	−55.3
Dec. 5	8:22	− 10.0	26	6:52	−83.3
11	9:34	− 10.9	28	6:36	−79.0
20	8:50	− 33.0	1945 Mar. 8	1:24	−59.0
24	8:20	− 34.4	8	3:02	−62.8
26	7:24	− 24.2	10	1:31	−68.0
1944 Jan. 3	7:41	+ 0.8	10	2:52	−70.3
9	6:19	− 41.2	11	1:15	−67.6
9	7:55	− 22.5	11	2:37	−72.3
11	5:50	− 50.8	1946 Feb. 28	2:22	+28.1
18	4:42	− 46.7	Mar. 3	3:00	+27.3
23	5:13	− 31.4	3	3:20	+28.0
30	5:03	− 34.4	26	1:38	+67.4
Feb. 13	5:12	− 30.8	26	2:00	+62.6
19	3:54	− 39.8	27	1:21	+35.5
Mar. 24	2:25	− 70.8	27	1:44	+38.5
26	2:26	− 72.1	28	1:24	+53.0
Oct. 12	10:42	−110.7	28	1:44	+51.3
19	11:09	− 97.0	31	1:28	+49.3
20	11:28	− 78.7	31	1:54	+45.1
26	10:20	− 84.3			

[4] Van Maanen, *Mt. W. Contr.*, No. 205, 1921.

[1] See *Ap. J.*, **97**, 453, 1943.

the variations. During March, 1946, the spectrum showed faint but unmistakable absorption components on the violet sides of the strong hydrogen absorption lines. Such components were

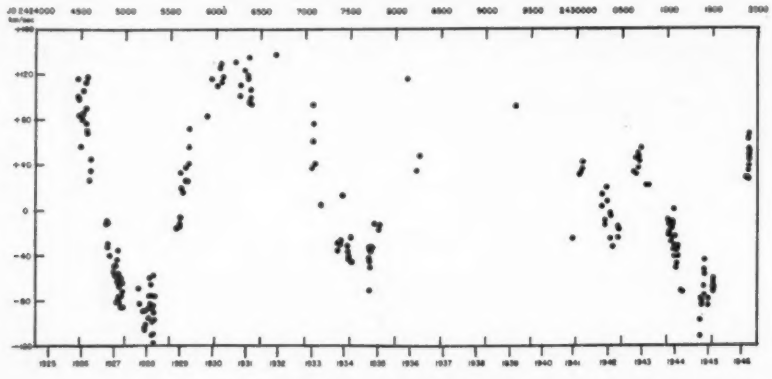

FIG. 1.—Radial velocities of 27 Canis Majoris

observed on previous occasions; they were not measured. I am indebted to several persons for the spectrograms of 1946 and to Mrs. Martha Carlson for part of the measurements.

O. STRUVE

August 1, 1946

ON THE POSSIBILITY OF TRACING POLARIZATION EFFECTS IN THE ROTATIONAL PROFILES OF EARLY-TYPE STARS

In connection with the interesting polarization effects in the continuous radiation of early-type stars recently predicted by Chandrasekhar[1] and established by Edith M. Janssen[2] for the eclipsing variable U Sagittae, the writer wants to call attention to the possibility of tracing effects of this kind in the rotational profiles of rapidly rotating early-type stars.

According to Chandrasekhar, the polarization of the continuous radiation increases from 0 at the center of the stellar disk to 0.11 at the limb, in consequence of a different law of darkening for the radial and for the tangential components. As different parts of the stellar disk give different displacements of the spectrum, faint effects of polarization should be expected in the rotational profiles of rapidly rotating stars.

Figure 1, for example, illustrates a favorable case. The upper curve gives the apparent rotational profile of the *unpolarized* radiation from the stellar disk. Superposed on this curve there will be profiles in *polarized light* from the regions (*2*) (vibration parallel to the axis of rotation) and from a fairly narrow central strip (*1*) (vibration perpendicular to the axis of rotation). For a spherical star the integrated polarized light will be the same for both vibrations, but, because of the Doppler shift, the two vibrations will appear with different intensity in an absorption line. In the center of the line a positive polarization will result (vibration parallel with the axis of rotation), whereas a negative polarization is to be expected in the wings of the absorption contour.

The writer has made an estimate of the effects which might appear in the favorable case outlined in Figure 1. By using Chandrasekhar's values of the intensity $i(r)$ and

[1] *Ap. J.*, **103**, 363, 1946.

[2] *Ap. J.*, **103**, 380, 1946.

degree of polarization $p(r)$ at different distances from the center of the stellar disk, the mean polarization p_a and the total intensity i_a of segment (*2*) have been calculated for different values of a, that is, the distance of the corresponding chord from the center. In fact, we have

$$p_a = \frac{\int_a p(r)\, i(r) \cos 2\vartheta \, d\sigma}{\int_a i(r)\, d\sigma}; \qquad (1)$$

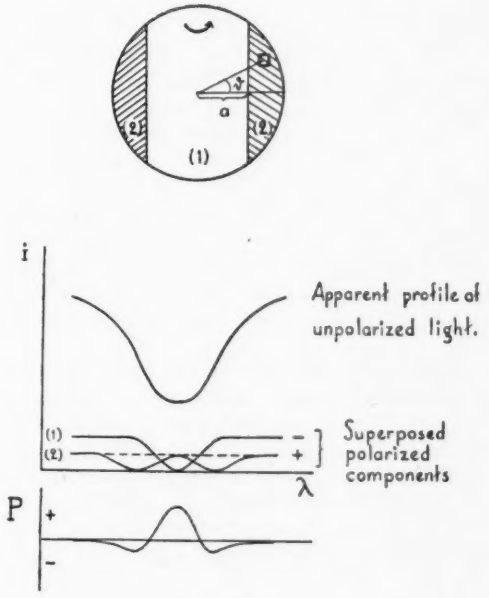

FIG. 1

TABLE 1

a	$\frac{i_a}{I}$	p_a	$p_a \frac{i_a}{I}$	P_+	P_-
0.8.....	0.04	0.030	0.0012	0.005	0.002
.7.....	.08	.022	.0017	.007	.002
.6.....	.12	.016	.0019	.008	.003
0.5.....	0.17	0.011	0.0019	0.008	0.003

where ϑ is the angle between the radius r and the normal a, and $d\sigma$ is the elemental area. By a graphical method of integration the values of Table 1 have been obtained, a being expressed in the stellar radius as unity and I being the intensity of the total light from the stellar disk.

The quantities P_+ and P_- in Table 1 are the polarization effects to be expected in a

line contour according to the favorable case outlined in Figure 1. Let us first consider P_+, which is the polarization appearing in the line center.

The unpolarized radiation has the intensity $I - 4\,p_s i_s$. Because of the line absorption (which is assumed to take place above the photosphere), the unpolarized light will assume the value $(1 - x)(I - 4p_s i_s)$ in the line center, x being the fraction absorbed. As the polarized component (*1*) is assumed to be absent in the line center, whereas the components (*2*) are supposed to have full intensity, we obtain the degree of polarization P_+ in the line center from

$$P_+ = \frac{2p_s i_s}{(1 - x)(I - 4p_s i_s) + 2p_s i_s}. \tag{2}$$

The values of Table 1 have been calculated on the assumption that $x = 0.5$.

A similar calculation can be made for P_-. The component (*1*) and one of the components (*2*) are here supposed to have full strength, whereas the other component (*2*) is supposed to be absent. We obtain

$$P_- = \frac{p_s i_s}{(1 - x')(I - 4p_s i_s) + 3p_s i_s}. \tag{3}$$

Assuming as a probable value $x' = 0.25$, we find the values given in Table 1.

The calculation has shown that a positive polarization, amounting to 8 promille, and a negative polarization of 3 promille can be expected in rotational profiles of early-type stars. In the case of flattened objects, somewhat stronger effects may possibly appear. With sensitive methods of observation, effects of this order of magnitude might be established.

From a considerable number of plates taken in 1934, the writer[3] was able to trace polarization in the $H\gamma$ absorption profile of β Lyrae. The effects were tentatively attributed to a superposed resonance radiation, but no satisfactory interpretation of the rather complicated effects could be given at that time. Perhaps the observed effects have something to do with a phenomenon of the kind proposed above.

In 1934 some other rapidly rotating stars were also observed by me, but no clear effects of polarization could be found in the absorption lines. It is to be remarked, however, that the objects in question have spectral types later than B.

YNGVE ÖHMAN

STOCKHOLM OBSERVATORY
September 6, 1946.

[3] *Nature*, **134**, 534, 1934; Stockholms Obs. Ann., **12**, No. 6, 16, 1936; Pop. Astr. Tidskr., **16**, 132, 1935; see also H. Zanstra, *M.N.*, **101**, 250, 1941.

REVIEWS

An Introduction to the Study of Eclipsing Variables. By ZDENĚK KOPAL. ("Harvard Observatory Monographs," No. 6.) Cambridge, 1946. Pp. x+220. $4.00.

The urgent need for advanced textbooks on astronomical subjects was recently pointed out by Struve in his review of a Russian book[1] with a similar title. The present book, however, is not an introduction to the complete field of the study of eclipsing variables but an exhaustive treatise of a limited part of the subject. The photometric and geometrical properties of the stars are fully treated and an up-to-date survey is given of the methods for analyzing their light-curves. However, the wealth of both elementary and advanced information from spectrographic observations is completely omitted.

Throughout the book the emphasis is laid on the mathematical analysis of the subject. As a result, the names of actual eclipsing binaries are rarely mentioned except in the Introduction and in some footnotes. Numerical examples or tables are not included. Among the 195 entries of the Index the name "Algol" is not found.

The organization of the book is clear. After an introductory chapter, it contains two parts. The first part, chapters ii–v, deals with spherically symmetrical stars, while the second part, chapters vi–ix, deals with distorted stars. Each part begins with a discussion of the photometric properties of single stars, proceeds with the computations of the total light for a given configuration, and ends with the methods for determining the orbits from the light-curves. The abbreviated titles of the chapters are: (i) "Introduction," (ii) "Nature of the Eclipses," (iii) "Determination of the Elements," (iv) "Improvement of the Elements," (v) "Orbital Eccentricity," (vi) "Distorted Stars," (vii) "Ellipticity and Reflection," (viii) "Light curves within Minima," (ix) "Elements of Distroted Systems." The bibliographical notes which conclude each chapter are excellent guides to the original papers.

The greater the mathematical requirements of a subject, the more careful an author should be in its presentation. Each superfluous coefficient or substitution should be omitted, and a strong effort should be made to choose clear and consistent notations. This is not only a great help to the reader but also a protection against mistakes. In this connection the reviewer wishes to comment upon three separate points.

1. A few minor errors have been noted. In equation (23), $\cos \sqrt{1 - r/r_1}$ is written instead of $\sqrt{1 - r^2/r_1^2}$; in equations (186), (342), and (333.1), the sign of Y_{rot} should be reversed; the expression (88) should be inverted; small errors in some other formulae are obvious. Wrong quotations of formulae, which may be traces of earlier drafts, are occasionally found. Furthermore, the author has not always been fortunate in the choice of his notations. For instance, on page 114 the potential Ψ determining the shape of a star, is written as

$$\Psi = U + V + W ;$$

now the consistent notations of the component terms of W would be W_T and W_{rot}. The notations used on pages 120–22, V_T and V_{rot}, are confusing. Finally, the book contains only two figures, one of which is poor.

2. The necessity of choosing concise notations is further illustrated by the first part of chapter viii. In the rectangular co-ordinate system $X'Y'Z'$ (p. 171), an arbitrary point can be given either by its rectangular co-ordinates X', Y', and Z' or by its radius vector r and the direction cosines, $L = X'/r$, $M = Y'/r$, and $N = Z'/r$. The direction cosines satisfy the equation (271):

$$L^2 + M^2 + N^2 = 1 .$$

Now Kopal defines by equation (266) a constant quantity r_1, introduced by equation (270) the new variables $z = Lr_1$, $y = Mr_1$, $x = Nr_1$, and "adopts x, y, and z as new independent

[1] D. J. Martinoff, *Eclipsing Variables.* Reviewed in *Ap. J.*, **101**, 380, 1945.

variables which should replace the polar coördinates r, θ, φ used formerly." This is evidently incorrect, since x, y, and z satisfy the identity

$$x^2 + y^2 + z^2 = r_1^2$$

and cannot be used as co-ordinates for an arbitrary point in space. But the author ignores this and infers from this identity that, "to the order of accuracy we are working," the intersection of the primary star with the x–y-plane "can still be considered a circle."

The full implications of this are not at once obvious. Chapter viii results in an expression for the loss of light $\Delta\mathcal{L}$ of a distorted star eclipsed by another distorted star. Distortion terms up to fourth-order spherical harmonics are taken into account. Since the fifth-order terms have the same magnitude as the squares of the second-order terms, the expression derived is the most general one as far as linear terms are concerned. The total number of terms in $\Delta\mathcal{L}$ is 146 (eqs. [282]–[289]). A preliminary examination suggests that the groups of terms denoted by α^U, α^D, f_*^U, f_*^D, f_2^U, and f_2^D are correct, whereas the groups of terms denoted by f_1^U and f_1^D probably need a revision.

Fortunately, the following chapter (ix) is hardly affected. It starts with a description of Russell's classical method of rectifiction of light-curves. The elaborate results of chapter viii are used only to demonstrate that Russell's procedure will give incorrect results as soon as third-order harmonics are involved.

Some remarks may be added to the discussion of the reflection effect in sections 60–63. Kopal denotes by $I(0, \mu)$ the intensity distribution of light emerging under different angles γ from a star's atmosphere and by $I^*(0, \mu)$ the distribution of "reflected" light. Until Chandrasekhar's recent investigations, these functions could hardly be computed. It is obvious, however, that they must satisfy the flux conditions:

$$2\pi \int_0^1 I(0, \mu)\, \mu d\mu = \pi F, \quad (1) \qquad 2\pi \int_0^1 I^*(0, \mu)\, \mu d\mu = \pi S \cos \alpha, \quad (2)$$

where $\mu = \cos \gamma$, πF = net flux radiated by 1 cm² of the star's surface, and $\pi S \cos \alpha$ = incident flux on 1 cm² of the star's surface. It should be noted that equation (1) is not satisfied by Chandrasekhar's approximations but only by the correct solution to which these approximations converge. The first approximation equation (230) gives a net flux which is only the fraction $(2 + \sqrt{3})/4 = 0.933$ of the correct flux, whereas the fourth approximation is still too small by 0.7 per cent.

Again the Hopf theorem, equation (225), by which I^* can be expressed in terms of I, is valid only in the case where the atmospheric particles re-emit or scatter the radiation isotropically. By applying the theorem to the approximate flux, equation (230), the error is doubled so that the values of $I^*(0, \mu)$ expressed in equation (231) give an emergent flux which is about $(0.933)^2 = 0.870$ times the incident flux.

It will therefore appear that, to get a useful approximation to the phase-function of a star for integrated light, the function $f(\epsilon)$ (p. 153) should be increased by 15 per cent, or the function $f^{IV}(\epsilon)$ by 1.4 per cent. In most applications, Kopal's statement that the phase-function nearly equals the phase-function $G(\epsilon)/\pi$, following from Lambert's law, will be useful.

Apart from these defects, which affect only certain parts, the book gives a reliable presentation of the subject of the theoretical interpretation of light-curves of eclipsing variables. The research worker or advanced student will find it a useful presentation of the classical methods and a guide to the discussion of more complicated effects. However, it cannot be recommended as an introductory volume for students, because its treatment does not stress sufficiently the interaction between theory and observations, which is vital for scientific progress.

H. C. VAN DE HULST

Yerkes Observatory

ERRATUM

On page 289, Volume **104,** the caption to Table 5 should read "Measured Equivalent Widths," not "Measured Equipment Widths."

INDEX TO VOLUME 104

INDEX TO SUBJECTS

INDEX TO AUTHORS